1979

Wind Field Analysis Around A Horizontal Axis Wind Turbine

B. C. Donner

R. H. Kirchhoff

PF67025F
UC-60
UM-WF-TR-79-5

WIND FIELD ANALYSIS
AROUND A HORIZONTAL AXIS WIND TURBINE

Technical Report

by

B.C. Donner and R.H. Kirchhoff

Energy Alternatives Program

University of Massachusetts

Amherst, Mass. 01003

December 1979

DISCLAIMER

PATENT STATUS

TECHNICAL STATUS

ABSTRACT

The dynamic interaction between the UMass 25 kW wind turbine, WF-1, and the local, turbulent wind field is investigated. The integral length scale for wind speed gusts is found to range from 40 to 200 m.

The system is seen to behave as a low pass filter with a cutoff frequency of 0.03 Hz. Power in the wind with gust frequencies below the cutoff frequency is available to the wind turbine. This represents approximately 70% of the total power in the turbulence, and about 5% of the total power in the wind. The power extraction is independent of the wind direction fluctuations when the nacelle yaw is damped.

TABLE OF CONTENTS

TABLE OF CONTENTS (Cont.)

TABLE OF SYMBOLS

SYMBOLS

A	Swept area of blade disc, m^2
Be	Bandwith, Hz
BMD02T	Biomedical Statcostical Package Time Series Analysis Program.
CS(n)	Cospectrum; real part of $S_{xy}(n)$
L_u	Integral length scale: downstream, m
L_v	Integral length scale; cross-stream, m
m	number of time lags
n	Frequency, Hz
n_p	Peak frequency, especially in power spectra, Hz
n_c	Cutoff (half-power) point, Hz
N	Number of sample points
Ny	Nyquist frequency, Hz
P_{ave}	Power available in the mean wind, kW
Pmax	Power available in the turbulent wind, kW
P_t	Power available to a real (inertial) machine, kW
PDF	Probability density function
PS(n)	Power spectra , dimensionless.
p	lag number, for discrete case analysis
$Q_x(\tau)$	Autocorrelation of variable x, dimensionless
$Q_{xy}(\tau)$	Cross-correlation of variables x and y, dimensionless
QS(n)	Quadrature spectrum; imaginary part of $S_{xy}(n)$
$R_x(\tau)$	Autocovariance of variable x
$R_{xy}(\tau)$	cross-covariance of variables x and y

TABLE OF SYMBOLS (Cont.)

SYMBOLS	
s^2	Variance
$S(n)$	Power spectral density
t	Time, s
T	Sampling period, s; integral time scale
T_u	Integral time scale; downstream, s
T_v	Integral time scale; cross-stream, s
$u(t)$	Instantaneous wind velocity; downstream.
$u'(t)$	Wind velocity fluctuations; downstream
U	Average wind velocity
$v(t)$	Instantaneous wind velocity; cross-stresm
$v'(t)$	Wind velocity fluctuations; cross-stream
$\overline{x}$	Mean of variable x
$\theta(t)$	Wind direction, variation from the mean
ρ	Air density, kg
τ	Time lag in correlation function, s
ψ^2	Mean square value
$H_{xy}(n)$, or	
$C(n)$	Coherence Squared
$H(n)$	Transfer Function

LIST OF FIGURES

LIST OF FIGURES (Continued)

LIST OF FIGURES (Continued)

LIST OF FIGURES (Continued)

LIST OF TABLES

CHAPTER I

INTRODUCTION

The dynamic interaction between the UMass 25 kilowatt wind furnace, WF-1, and the turbulent wind field was investigated. The relationships between the gustiness in the wind and the machine response were measured, and related by treating the wind turbine as a black-box system.

To quantify these relationships, WF-1 was instrumented by Murphy and Kirchhoff[1]. Wind speed and direction are measured at up to five places in the wind field with R.M. Young Gill type anemometers. These variables are recorded with rotor RPM, generator output current, and machine yaw angle on analog tape using an Ampex tape recorder. These data are digitized using an LSI/11 microprocessor and transmitted to the UMass Cyber System for processing. A schematic for this data acquisition system is shown in Fig. 1.

Data processing in preparation for statistical analysis is a two step process, detailed in Appendix A. The raw data, stored as alphanumeric characters, is edited to remove all colons which can appear as a carriage return command when the data file is read. Then the data is translated into base ten decimals, equivalent in value to the binary word stored in the LSI, and scaled to the original level of the measured variables.

The primary analysis of the discrete time series is then done using the Biomedical Statistical Package[2]. Preparation and transmission of the data for use with the statistical package is documented in Appendix A. Use of the Biomed program for time series analysis is demonstrated in Appendix B.

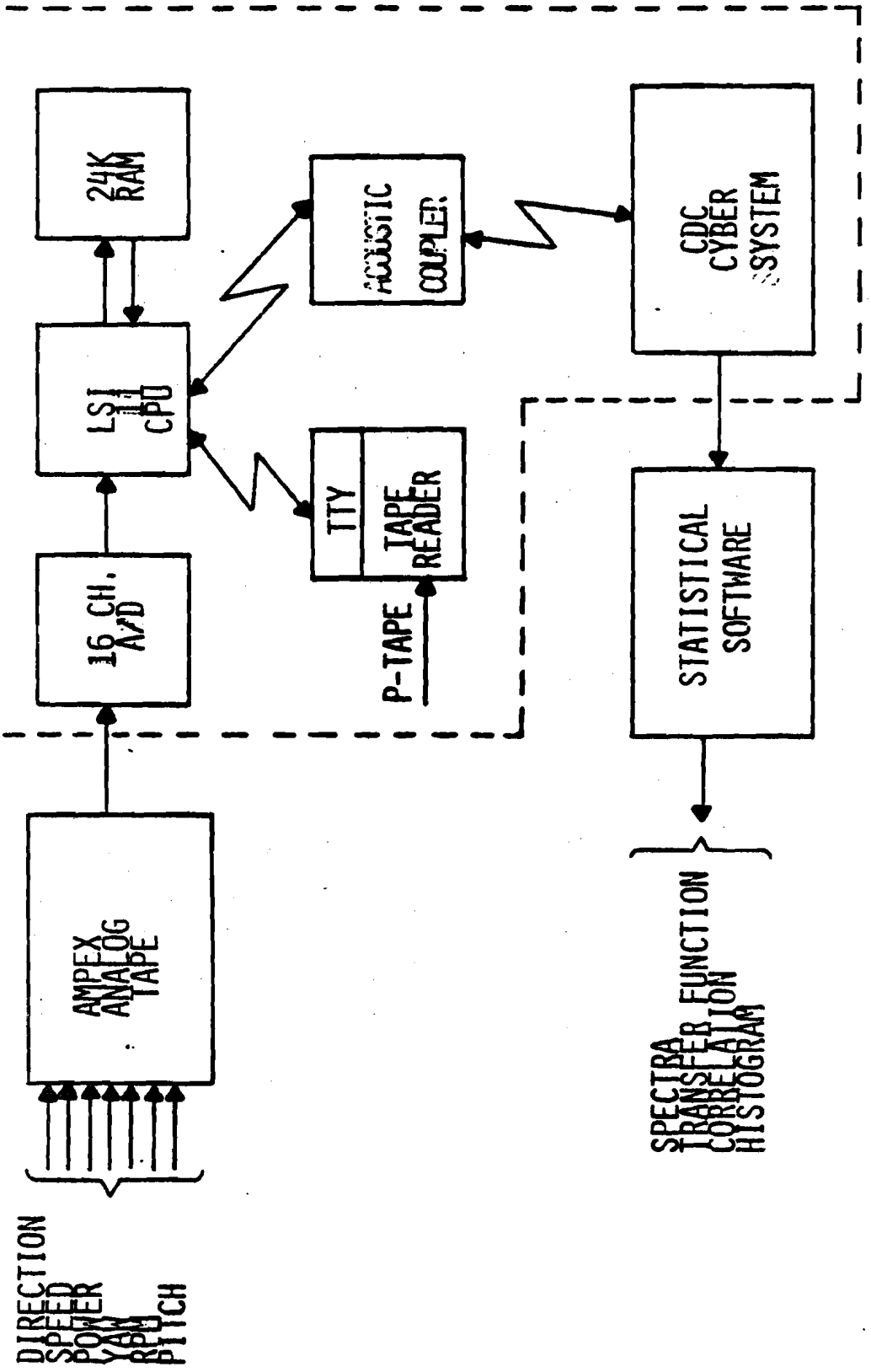

Figure 1. WIND FIELD ANALYSIS DATA SYSTEM

The response of such a wind turbine generator to turbulence in the wind field is not well known, primarily because of the stochastic nature of the turbulence. Since a significant amount of energy can be extracted from these random fluctuations by an appropriately designed machine, it is important to understand this response.

A wind machine will respond to turbulence primarily in two ways: variations in wind speed tend to change rotor RPM and output power, and variations in wind direction tend to change the yaw angle. These responses are not necessarily decoupled, since a machine must track the wind well in order to get a consistent response to wind speed gustiness. Conversely, the gyroscopic moments set up by the changing RPM of the blades tends to rotate the machine in yaw. The experimental evidence indicates that WF-1, with yaw damped, tracks the wind well enough to consider yaw angle and RPM or generator output current to be decoupled responses to the horizontal gustiness. This is discussed in Section 3.3.3.

The power in the turbulence is distributed with wind gust frequency, represented by the wind speed and wind direction power spectral density. Some of this power is available for extraction by the wind machine, and is in addition to the power extracted from the mean wind.

The maximum power which can be extracted from the turbulence by a wind turbine is dependent on how well the machine can respond to the highest frequency gusts. This is the dynamic or frequency response of the machine. The frequency at which half the power in the turbulence at that frequency is extracted is the half-power point or cut-off frequency. This is considered to be the highest frequency in the wind to which the machine will respond. A turbine with a higher cut-off frequency can extract more power from the turbulence.

The machine response can also be represented by the maximum gust length to which the machine can respond. The gust integral time scale and gust integral length scale are related through the mean wind speed, U:

$$U = L/T \tag{1}$$

Another important part of the wind field/wind turbine interaction is the influence which the nacelle and blade disc have on the local wind field upstream of the nacelle. To measure this effect, the five anemometers were located along a NNW line passing through the WF-1 centerline (Fig. 2). This is the direction of the prevailing winter winds, with four towers upstream and one downstream of the wind turbine. By measuring and recording wind speed signals from all five anemometers simultaneously, the influence of the nacelle and blade disc could be measured. The results are discussed in detail in Chapter IV.

The major emphasis of this work, then, is to quantify the response characteristics and to lay the groundwork by which designers in the wind power industry can optimize the extraction of energy from turbulence in the wind.

This work is by no means exhaustive. Additional work should be done in studying the effects of the machine in the near field upstream of the nacelle, and a more detailed assessment of the WF-I transfer function to include such factors as blade pitch, should be performed. However, the work now complete should provide a basis for making more detailed assessments of horizontal axis wind turbine designs in terms of wind power extraction potential.

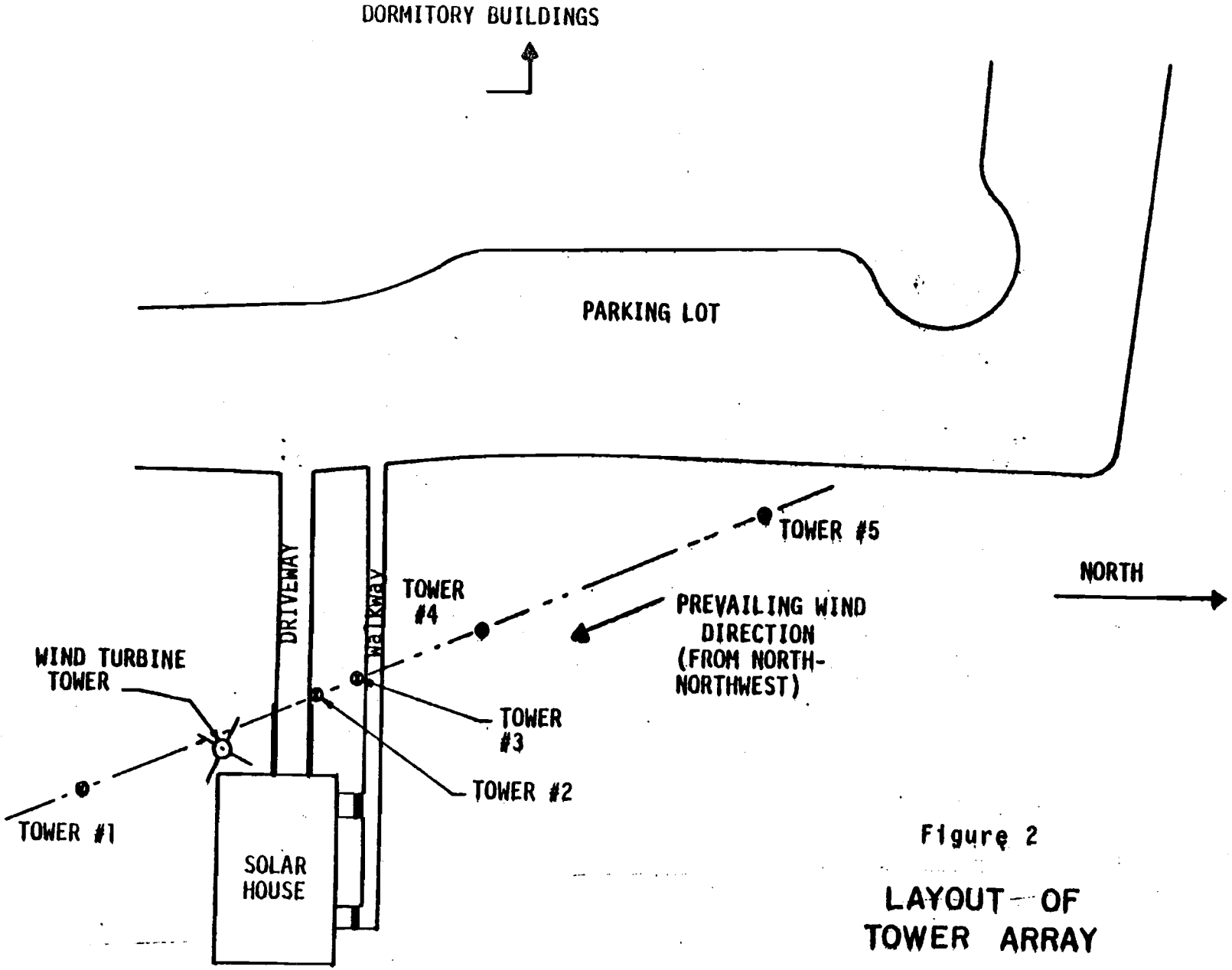

Figure 2

LAYOUT OF TOWER ARRAY

CHAPTER II

THEORY

2.1 Introduction

Fluctuations in wind speed and direction, and their associated machine responses, are random variables. These are coupled through the action of the "black-box" system. Since no explicit mathematical relationship can be used to describe the time history of these variables, statistical parameters are used to describe their characteristics. The relationship between the input and the response can then be calculated using these parameters.

Data for each of the system variables, both input and response, is considered to be stationary during the sampling period. This means that the statistical parameters of interest, such as the mean, variance, and integral scales of the turbulence, do not change significantly from one short interval to the next.

Discrete data records pose restrictions on the resolution of information about the variable in question. The highest frequency resolvable for a sampling time Δt is the Nyquist frequency, where:

$$Ny = \frac{1}{2\Delta t} \tag{2}$$

The minimum frequency and minimum frequency interval which can be resolved is the bandwidth. The bandwidth depends on Δt and the number of lags, m:

$$Be = \frac{1}{2m\Delta t} \tag{3}$$

The concept of time lags is discussed in Section 2.2.4 in conjunction with the autocovariance function.

Seemingly, any resolution could be obtained by increasing the number of lags. However, the results may become unstable if m is greater then 10% of the total number of data points. Since the total number of points comprising a data record is limited to 1000 by BMD02T, B_e is indirectly restricted by record length as well as Δt.

The following sections inroduce the statistical parameters used to characterize the system variables. For a more detailed description, refer to Bendat and Piersol[3] or Harris and Ledwidge[4].

2.2 Description of Statistical Parameters

2.2.1 Mean, Variance, and Mean Square Value

The mean of a data record consisting of N points is calculated using the following relations:

$$\bar{x} = \frac{1}{N} \sum_{i=1}^{N} x_i \tag{4}$$

where x_i is the ith data point.

The variance is the square of the fluctuations about the mean:

$$s^2 = \frac{1}{N} \sum_{i=1}^{N} (x_i - \bar{x})^2 \tag{5}$$

The positive square root of the variance is the standard deviation.

The mean square value of a random variable is the average of the square of each value in the time series:

$$\psi^2 = \frac{1}{N} \sum_{i=1}^{N} x_i^2 \tag{6}$$

The mean variance, and mean square value are related through:

$$\psi^2 = s^2 + \bar{x}^2 \tag{7}$$

As an example, consider that the power in the mean wind is proportional to U^3. However, "power" as it is used in signal theory, is proportional to the square of the variable. Using this definition, the power in the fluctuating wind speed, $u(t)$, is proportional to its mean square value, $u^2(t)$. The total power, by Eq. 7, is the sum of the power in the mean wind plus the power in the fluctuations:

$$u^2(t) = (u'(t))^2 + U^2 \tag{8}$$

2.2.2 Probability Density Function

The probability density function of a stochastic variable is a measure of the probability that the variable will fall in a particular range at a given instant of time. The data is presented as the number of times the variable falls within a specified range over the length of the data record.

2.2.3 Autocovariance and Autocorrelation

The autocovariance of a signal is a measure of the dependence the signal value has at one time on the value at a later time.

For non-deterministic (i.e., random) signals, a peak will occur in the autocovariance function at zero time lag. The autocorrelation function, $Q_x(\tau)$, is the autocovariance function normalized by $R_x(0)$,

so that the magnitude of the initial peak is unity. The autocorrelation function plays an important role in determining the integral length scales of the turbulence.

For a d.c. signal, whose value is independent of time, there is a perfect correlation between the values the signal has at any time lag. For a periodic signal, such as a sine wave, the autocorrelation is also periodic, having the form of the original signal. The superposition of noise on these signals alters their autocorrelations, as shown in Fig. 3. Comparison of these autocorrelations with those for experimental data provides useful insight into the process[5].

The calculation of the autocovariance for a continuous waveform, for each time lag, τ, uses the relation:

$$R_x(\tau) = \lim_{T\to\infty} \frac{1}{T} \int_0^T x(t)\, x(t+\tau)\, dt \qquad (9)$$

For each τ, $R_x(\tau)$ is the average of the product of $x(t)$ and $x(t + \tau)$. Since $x(t)$ can have the opposite sign to $x(t+\tau)$, the autocovariance function can be both positive and negative.

The largest magnitude for $R_x(\tau)$ will occur when $x(t)$ is always equal to $x(t + \tau)$ for all t, as is at $\tau = 0$. This means that the autocovariance:

$$|R_x(\tau)| \leq R_x(o) \qquad (10)$$

and for the autocorrelation:

$$-1 \leq Q_x(\tau) \leq 1 \qquad (11)$$

For a continuous stochastic variable, the autocovariance function, as τ approaches infinity, approaches the square of the mean:

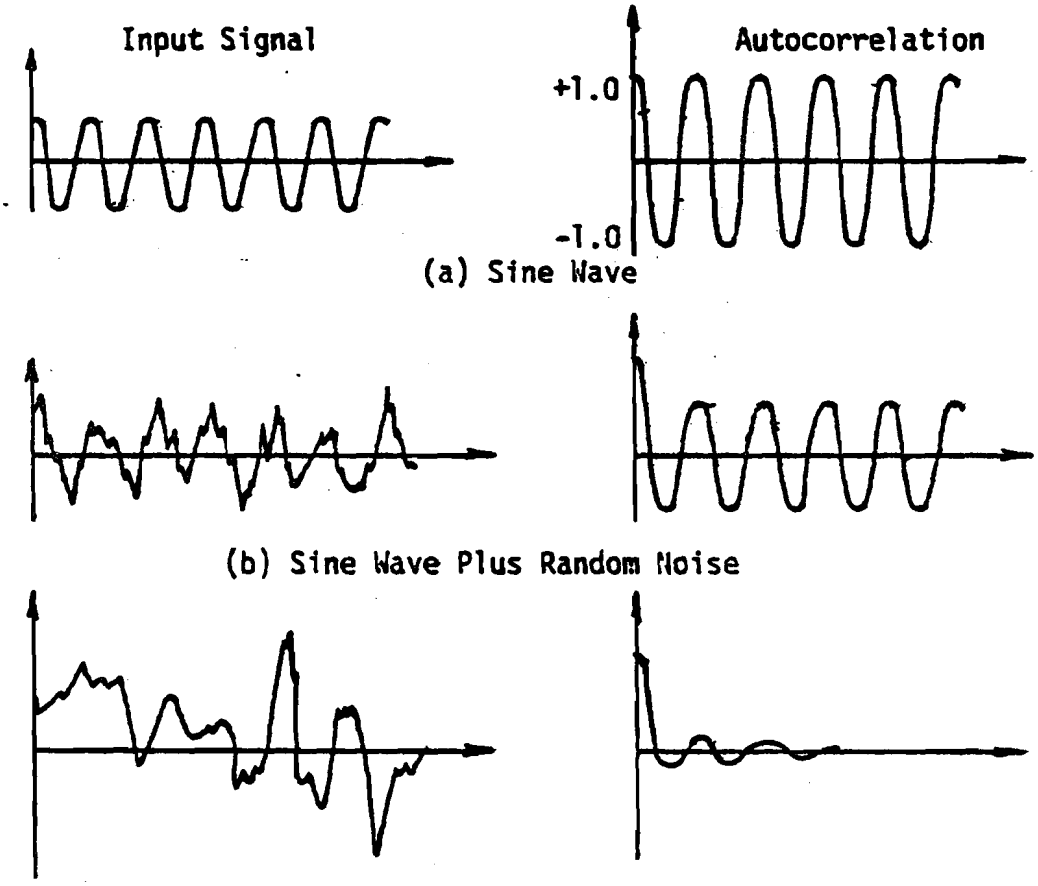

FIGURE 3. SOME PERIODIC AND RANDOM SIGNALS AND THEIR AUTOCORRELATION.

$$\lim_{\tau \to \infty} R_x(\tau) = \bar{x}^2 \qquad (12)$$

To simplify the interpretation of the autocovariance, the statistical program BMD02T permits the detrending of the data as an option. For this investigation, this option was selected for every analysis.

BMD02T calculates the autocovariance from the raw data as:

$$R_x(p) = \frac{1}{N-p} \sum_{i=1}^{N-p} x_i x_{i+p} \; ; \; p = 0, 1, 2 \ldots m \qquad (13)$$

where p is the lag number and m the number of lags. The autocovariance is then detrended, which is equivalent to extracting the mean and any linear trend in the raw data:

$$R_x(p)\Big|_{\text{detrended}} = R_x(p) - \bar{x}^2 - \frac{1}{12} \lambda(p) \alpha_x^2 \qquad (14)$$

where:

$$\alpha_x = \frac{1}{k \, \Delta t (N-k)} \left[\sum_{i=n-k+1}^{n} x_i - \sum_{i=1}^{k} x_i \right] \qquad (15)$$

$$k = \text{the integer part of } \frac{N+2}{3} \qquad (16)$$

$$\lambda(p) = (N \, \Delta t)^2 \left[1 - 2(p/N) - 2(p/N)^2 \right] \qquad (17)$$

and p is defined as before.

Since the program BMD02T extracts the mean of the data, it is expected that[6]:

$$\lim_{\tau \to \infty} R_x(\tau) \to 0 \qquad (18)$$

Similarly, for $\tau = 0$:

$$R_x(o) = \lim_{T \to \infty} \frac{1}{T} \int_0^T x^2(t) \, dt = \Psi^2 \qquad (19)$$

From this, using Eq. (8), an estimation of the square of the fluctuations, $(u'(t))^2$ can be obtained.

The Gill type anemometer measures wind speed, u(t), directly, but measures wind direction $\theta(t)$ and not the lateral fluctuations v(t). The relationship between these variables is shown in Fig. 4. Using the autocorrelation functions, a relationship between $\theta(t)$ and v(t) is found as follows:

$$Q_\theta(\tau) = \frac{\overline{\theta(t)\ \theta(t+\tau)}}{\overline{\theta(t)^2}} \tag{20}$$

$$\theta(t) = \frac{v(t)}{U + u(t)} \simeq \frac{v(t)}{U} \tag{21}$$

$$Q_\theta(\tau) = \frac{U^2\ \overline{v(t)\ v(t+\tau)}}{\overline{v^2(t)}\quad U^2} \tag{22}$$

$$= \frac{\overline{v(t)\ v(t+\tau)}}{\overline{v^2(t)}} \tag{23}$$

$$Q_\theta(\tau) \equiv Q_v(\tau) \tag{24}$$

Eq. (24) is not true for the autocovariance, since the relationship in Eq. (24) would then be different by a factor of $1/U^2$.

By Eq. (24), the integral length scale for the desired variable, v(t), is identical to the integral length scale of the measured variable $\theta(t)$.

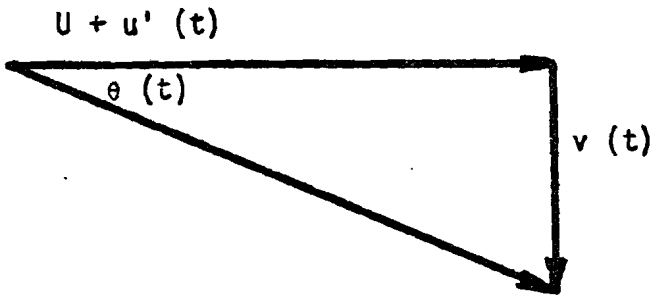

Note: $v'(t) \equiv v(t)$ if $\theta = 0$ is chosen as the average wind direction

FIGURE 4. VECTOR RELATIONSHIP BETWEEN THE LATERAL WIND VELOCITY COMPONENT V(t) AND THE WIND DIRECTION, $\theta(t)$.

2.2.4 Power Spectral Density and Power Spectra

The power spectral density function (P.S.D.) for discrete data is the signal power per unit bandwidth over the frequency range in question. The discrete bandwidth is defined by Eq. (3).

For stationary data, the PSD is related to the autocovariance through the Fourier Transform. The PSD contains the same information as the autocovariance, but transformed into the frequency domain. The difference in form, however, sometimes gives new insight into the nature of the process under investigation.

Based on the Fourier Transform for continuous data, the PSD is defined as:

$$S(n) = \int_{-\infty}^{\infty} R(\tau)\, e^{-j2\pi n\tau}\, dt \qquad (25)$$

For discrete data, the form of Eq. (25) is modified. The time series analysis program, BMD02T, actually computes the PSD from this modified form and the previously computed autocovariance. This relation is given below:

$$S\left(\frac{h\,\pi}{m\Delta t}\right) = \frac{2\Delta t}{\pi} \sum_{p=o}^{m} \varepsilon_p\, R_x^p \cos\left(\frac{h\pi p}{m}\right) \qquad (26)$$

where

$h = 0, 1, 2 \ldots m$

$p = 0, 1, 2 \ldots m$

$$\varepsilon_p = \begin{cases} 1 & o < p < m \\ 1/2 & p = o, m \end{cases}$$

Note that S is a function of discrete frequencies, $h\pi/m\Delta t$, which is expected because of the minimum resolvable bandwidth, Be. Once the

PSD is computed for each frequency interval, the PSD function is smoothed using Hamming's method.

The PSD is graphed as the natural log of the PSD versus the natural log of frequency. This form presents constant powers of n as straight lines with slope equal to the constant power. However, this does not give a realistic weight to higher frequencies[7]. For certain work the dimensionless form of the PSD, the power spectra, is frequently used in meteorological work.

The power spectra is graphed for this work as $nS(n)/U^2$ versus $\ln(n)$. This collapses the frequency range of interest to convenient size but perserves the area under the curve, since

$$nS(n)\ d(\ln(n)) = S(n)dn \tag{27}$$

Either circular or radian frequencies may be used in the computation of the power spectra, since the non-dimensional group $nS(n)/U^2$ remains unaffected.

2.2.5 Cross-covariance and Cross-correlation

The cross-covariance of two signals is a measure of the dependence of the value of one signal to the value of the other after some time lag, τ. In an analagous manner to the autocovariance, the cross-covariance is defined as:

$$R_{xy}(\tau) = \lim_{T\to\infty} \frac{1}{T} \int_0^T x(t)\ y(t+\tau)\ dt \tag{28}$$

$R_{xy}(\tau)$ can be either positive or negative, similar to the auto-covariance, and is bounded in magnitude by the relation[8]:

$$|R_{xy}(\tau)| \leq (R_x(o)\ R_y(o))^{1/2} \tag{29}$$

The peak in the cross-covariance may not be at $\tau = o$. For example, if a wind gust passes a point x in the wind field, and at a time T later passes a second point y in the wind field, unattenuated, the cross-covariance peak will occur at $\tau = T$.

The cross-correlation has the same form as the cross-covariance, but the peak is normalized in magnitude to unity. For the cross-correlation functions, Eq. (29) becomes:

$$|R_{xy}(\tau)| \leq 1 \tag{30}$$

One use that the cross-correlation function has in this work is in testing Taylor's Hypothesis. The Taylor Hypothesis is that the turbulent cells are carried along in the mean wind unchanged in character[9]. If this is so, then the peak in the cross-covariance function should occur at a time lag T, where T is the time it takes for the mass wind to travel from point x to point y in the field. In addition, the magnitude of the peak should be equal to $(R_x(o)\ R_y(o))^{1/2}$ based on Eq. (29). The results from this test are discussed in Chapter IV.

2.2.6 Cross-Spectral Density

The Fourier Transform of the cross-covariance function gives rise to the cross-spectral density (C.S.D.):

$$S_{xy}(n) = \int_{-\infty}^{\infty} R_{xy}(\tau) e^{-j2\pi n\tau}\ d\tau \tag{31}$$

The cross-spectral density measures the relationship, in phase and magnitude, of two variables in the frequency domain.

The magnitude relationship is the cospectrum, and calculated by BMD02T as:

$$CS_{xy}(h) = \frac{\Delta t}{\pi} \sum_{p=o}^{m} \varepsilon_p \, (R_{xy}(p) + R_{xy}(-p) \cos(\frac{h\pi p}{m}) \quad (32)$$

where h, p, and ε_p are defined as before.

The phase relationship is the quadrature spectrum. The program BMD02T calculates this as:

$$QS_{xy}(h) = \frac{\Delta t}{\pi} \sum_{p=o}^{m} \varepsilon_p \, (R_{xy}(p) - R_{xy}(-p) \sin(\frac{h\pi p}{m}) \quad (33)$$

The major importance of the cross-spectrum is in the calculation of the transfer function.

2.2.7 System Transfer Function and Coherence Function

The relationship between the input to a system and its corresponding response is known as the transfer function. As with the autocovariance - PSD relationship, the information in the transfer function can be represented in either the time or frequency domain. In the frequency domain the transfer function may also be called the frequency reponse function.

The formal development of the time-domain transfer function comes from the concept of the impulse response[10]. The system's response to a single impulse at $t - \tau$ is defined as:

$$y(t) = h(\tau) \, x(t - \tau) \quad (34)$$

where $h(\tau)$ is the time domain transfer function. The relationship between the impulse and the response is shown in Fig. 5. Note that

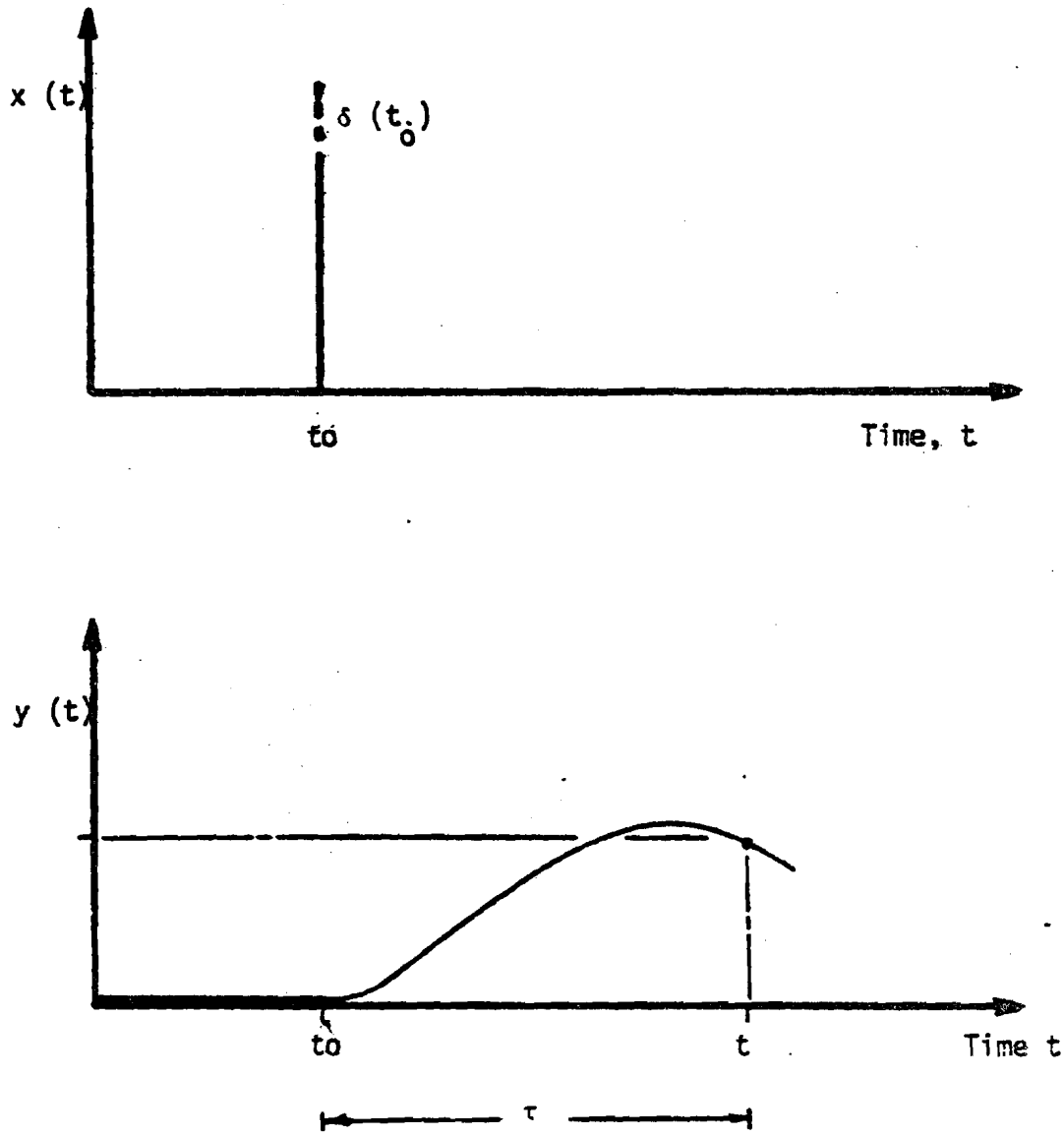

FIGURE 5. IMPULSE RESPONSE OF A LINEAR SYSTEM

the system responds to the impulse after the impulse occurs, so $h(\tau)=0$ for $\tau \leq 0$.

While the concept of an impulse response is somewhat artificial, it is a useful analytical tool. A time history of stochastic variables can be decomposed into a series of impulses. Then assuming that the system is linear, so that the responses to all of these impulses are additive, the system response to the input variable $x(t)$ can be written:

$$y(t) = \int_0^\infty h(\tau)\, x(t - \tau)\, dt \qquad (35)$$

known as the convolution integral.

The information for the response function $y(t)$ can be transformed into the frequency domain by taking the Fourier Transform of both sides in Eq. (35). The result is:

$$Y(n) = X(n)\, H(n) \qquad (36)$$

In the frequency domain, the transfer function is the ratio of the output function to the input at each frequency n.

The Fourier Transform is also useful in developing simple relationships between the PSD, CSD and the transfer function. These are given below:

$$S_{yy}(n) = S_{xx}(n)\, |H(n)|^2 \qquad (37)$$

$$S_{xy}(n) = S_{xx}(n)\, H(n) \qquad (38)$$

The actual computation in BMD20T for the magnitude of the transfer function is made with Eq. (38).

The coherence function is a measure of the linearity of the system, which has been seen to be an important assumption. The ratio of the square of Eq. (38) and Eq. (37) is the coherence function squared:

$$H_{xy}^2(n) = \frac{S_{xy}^2(n)}{S_{xx}(n)\, S_{yy}(n)} \tag{39}$$

The magnitude of the coherence function is bracketed by the inequality

$$0 \leq H_{xy}(n) \leq 1 \tag{40}$$

and is equal to unity in the case of a linear system.

2.3 Integral Scales

Turbulence in the wind field can be considered as three dimensional cells being carried along with the mean wind. As these wind gusts pass by a stationary point, the spatial character of the gust causes fluctuations in the wind speed as measured in the three orthogonal directions. The wind speed velocity is:

$$\underline{u}(t) = \underline{i}\, u(t) + \underline{j}\, v(t) + \underline{k}\, w(t) \tag{41}$$

where $\underline{i}$, $\underline{j}$, and $\underline{k}$ are the downstream, lateral, and vertical unit vectors, respectively. The fluctuating components of the Reynold's decomposition, $u'(t)$, $v'(t)$, and $w'(t)$ can be viewed in either the time domain or frequency domain.

Viewed in the time domain, the turbulence is often characterized with the integral scales of length and time.

The integral length scale can be regarded as average size of the large scale wind gusts. The integral time scale can be regarded as

the time it takes for the average gust to pass a stationary point in the wind field. This can be interpreted as the time required for the fluctuating wind speed signal to become uncorrelated with itself. This time is defined as the area under the autocorrelation curve[11]. Thus the integral time scale is:

$$T = \int_0^\infty Q(\tau)\, d\tau \tag{42}$$

By Eq. (18), it is known that for random signals $Q(\tau)$ will oscillate about zero at large τ. For practical application of Eq. (42) this simplification is made:

$$T = \int_0^{\tau_c} Q(\tau)\, d\tau \tag{43}$$

where τ_c is the time of the first zero cross-over of the autocorrelation function.

The length scale L is related to the time scale by the mean wind speed, U:

$$L = UT \tag{44}$$

The gusts in the downstream direction have the longest length scale. Teunissen[12] found the ratio of length scales at 19.3 m to be:

$$L_u : L_v = 1 : 0.31 \tag{45}$$

Since the largest gusts contain more power than smaller gusts, as indicated by the -5/3 power decay law, the downstream fluctuations should contain significantly more power than the lateral fluctuations. Teunissen also found that the vertical fluctuations to have approximately the same length scales. If this is true at the UMass site, the lateral

and vertical fluctuations can be considered to have the same power. For this site, however, the length scale of the vertical fluctuations was not measured.

C H A P T E R I I I

WIND FIELD/WIND TURBINE DYNAMIC INTERACTION

3.1 Introduction

By treating the wind turbine as a linear "black-box" system, specific design details are not required to obtain the response characteristics of the machine. Instead, the characteristics of the driving (input) and response functions are measured and related through the transfer function.

Even with this simplified approach, important quantitative results are obtained concerning the dynamic response of the wind turbine. These include the "steady-state" operating characteristics, the coefficient of power, C_p, the cut-off frequency, n_c, and the fraction of power extracted from the turbulence. To obtain this information, a careful characterization is required of the driving and response functions. The driving functions are considered to be wind speed and wind direction, characterized by their integral scales and power spectral densities. The response functions are considered to be rotor RPM, generator output current, and machine yaw angle. The wind velocity fluctuations in the vertical direction are not considered.

It is assumed ad hoc that the system is linear and that the yaw response is decoupled from the RPM/current response. The importance of the linearity assumption has already been discussed in Section 2.2.7; the accuracy of the assumption is tested with the coherence function and discussed for each transfer function measured.

The analysis of the dynamic interactions is based on three analog records. Relevant information on these data and their associated digitized records is summarized in Table 1.

The data are analyzed at two sampling rates, Δt = 0.5s and 5.0s. When analyzed using 100 lags, the total resolvable frequency range is calculated from Eq. (2) and (3).

$$\text{Minimum Be} = \frac{1}{2m\Delta t} = 0.001 \quad \text{Hz} \tag{46}$$

$$\text{Maximum Ny} = \frac{1}{2\Delta t} = 1.0 \text{ Hz} \tag{47}$$

This three decade resolution, from 0.001 to 1.0 Hz. has been found to be adequate in measuring most of the important system parameters.

3.2 Characterization of the Driving Function

3.2.1 Wind Speed

The important representation of the wind speed fluctuations is the PSD. This shows the distribution of power in the wind speed gusts by gust frequency. The smoothed PSD is used in the calculation of the transfer function from wind speed to RPM and wind speed to current. By integrating the area under the PSD, the energy in the gusts in any frequency range can be calculated; this allows the calculation of the turbulent energy extracted by the wind turbine.

The wind speed PSD for each of the three analog records is plotted in Figs. 6, 7 and 8. Note that the PSD represents the combined results from the analysis of two digital records.

ANALOG WIND FIELD RECORD	DIGITAL WIND FIELD RECORD	SAMPLING INTERVAL, Δt, s	DIGITAL WFR LENGTH, s	ANALYZED FREQUENCY RANGE, Hz	AVERAGE WIND SPEED, U, m/s	AVERAGE* GENERATOR CURRENT, I, AMPS	AVERAGE ROTOR SPEED, RPM	YAW MODE
Tape 9	3	5.0	1750.	0.001-0.10	6.35	16.1	79.3	DAMPED
	5	0.5	500.	0.01-1.0	4.58	13.6	80.2	
Tape 11	17	0.5	500.	0.01-1.0	6.96	17.9	116.7	UNDAMPED
	21	5.0	5000.	0.001-0.10	7.00	19.3	115.9	
Tape 10	18	0.5	500.	0.01-1.0	4.57	--	67.7	DAMPED
	22	5.0	5000.	0.001-0.10	6.05	--	71.6	

*No Current Signal Recorded for Tape 10.

TABLE 1. WIND FIELD RECORD DATA SHEET

FOR WFR 3, 5, 18, 18, 21, and 22

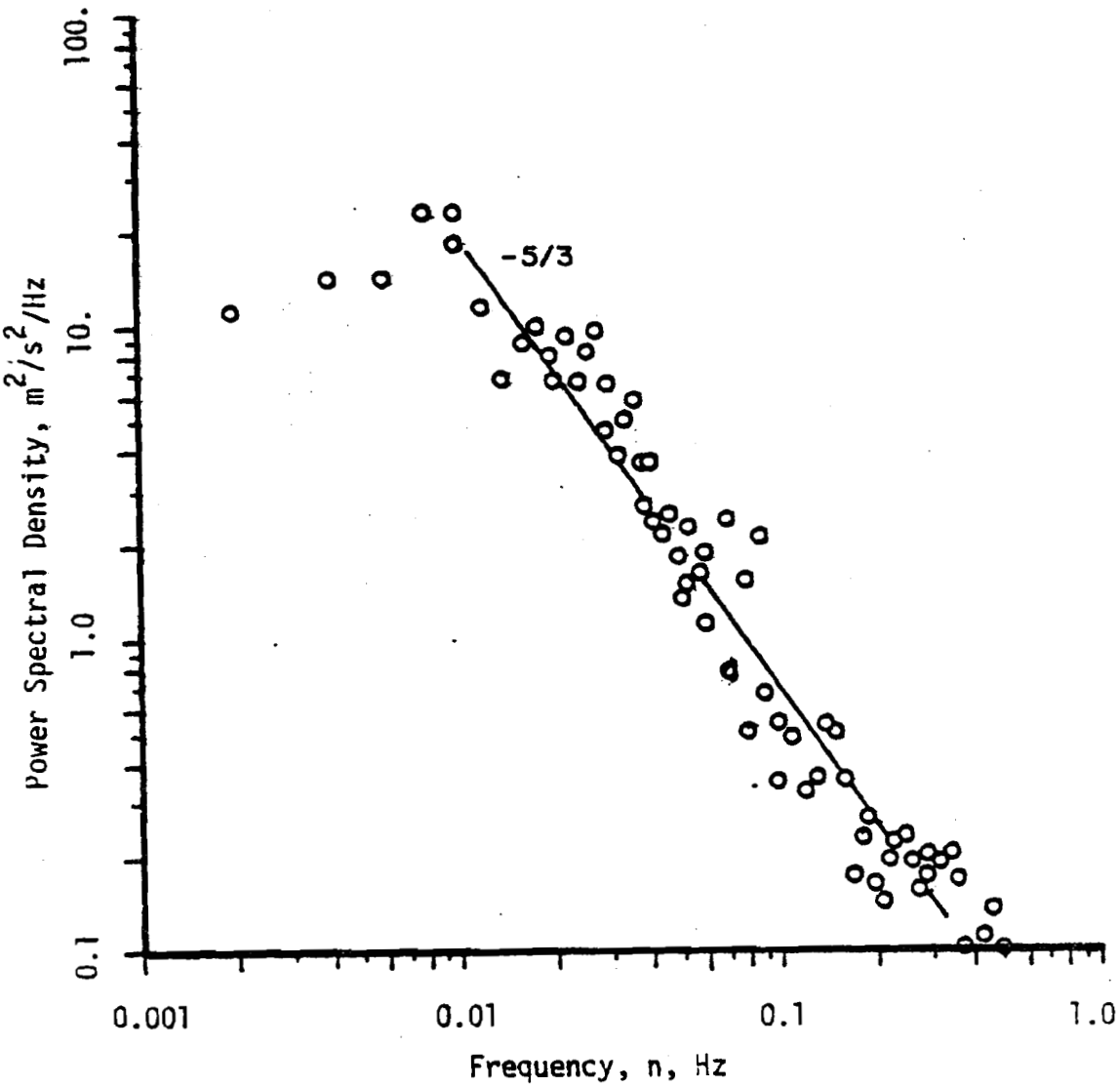

FIGURE 6. WIND SPEED POWER SPECTRAL DENSITY

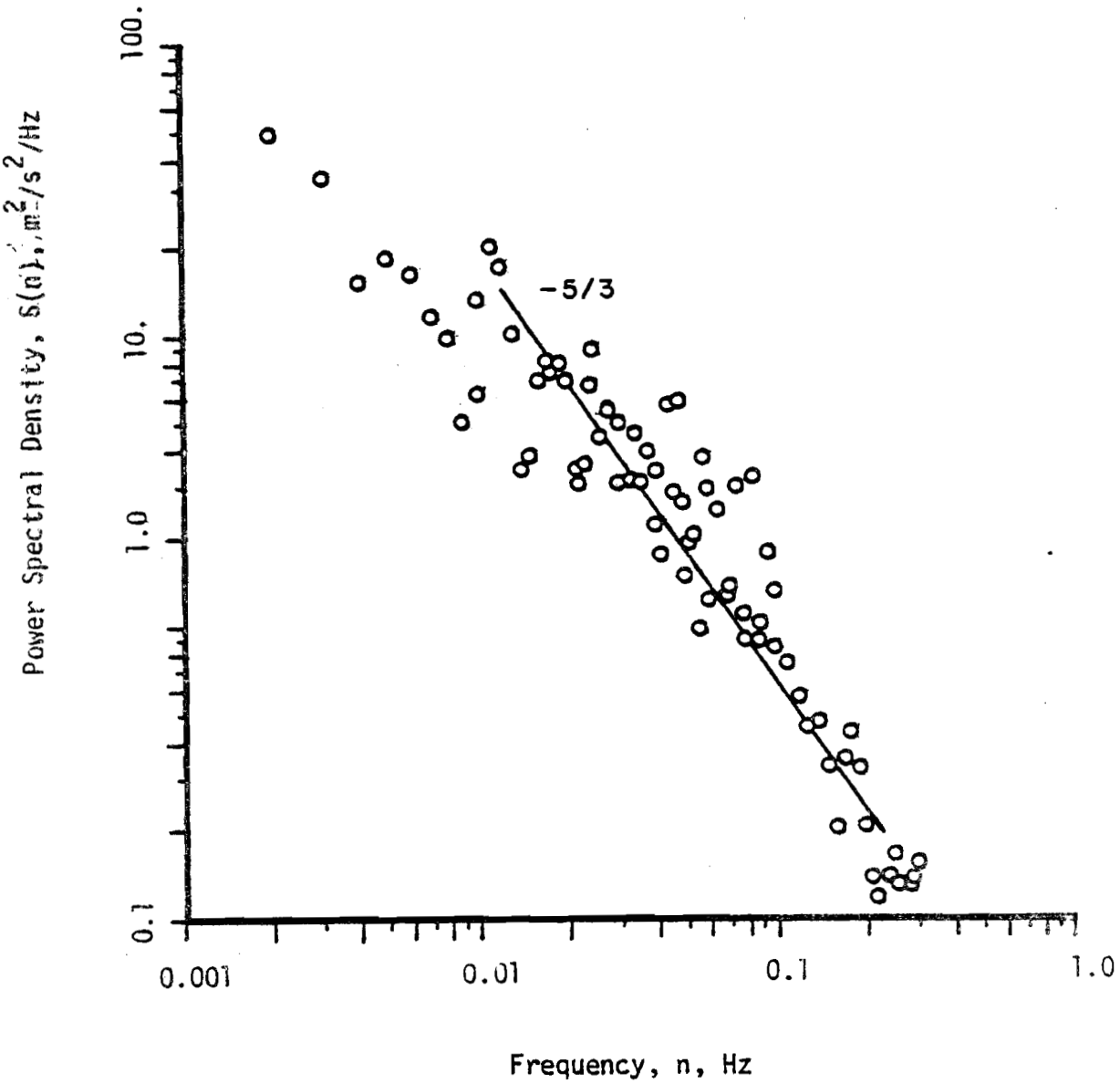

FIGURE 7. WIND SPEED POWER SPECTRAL DENSITY

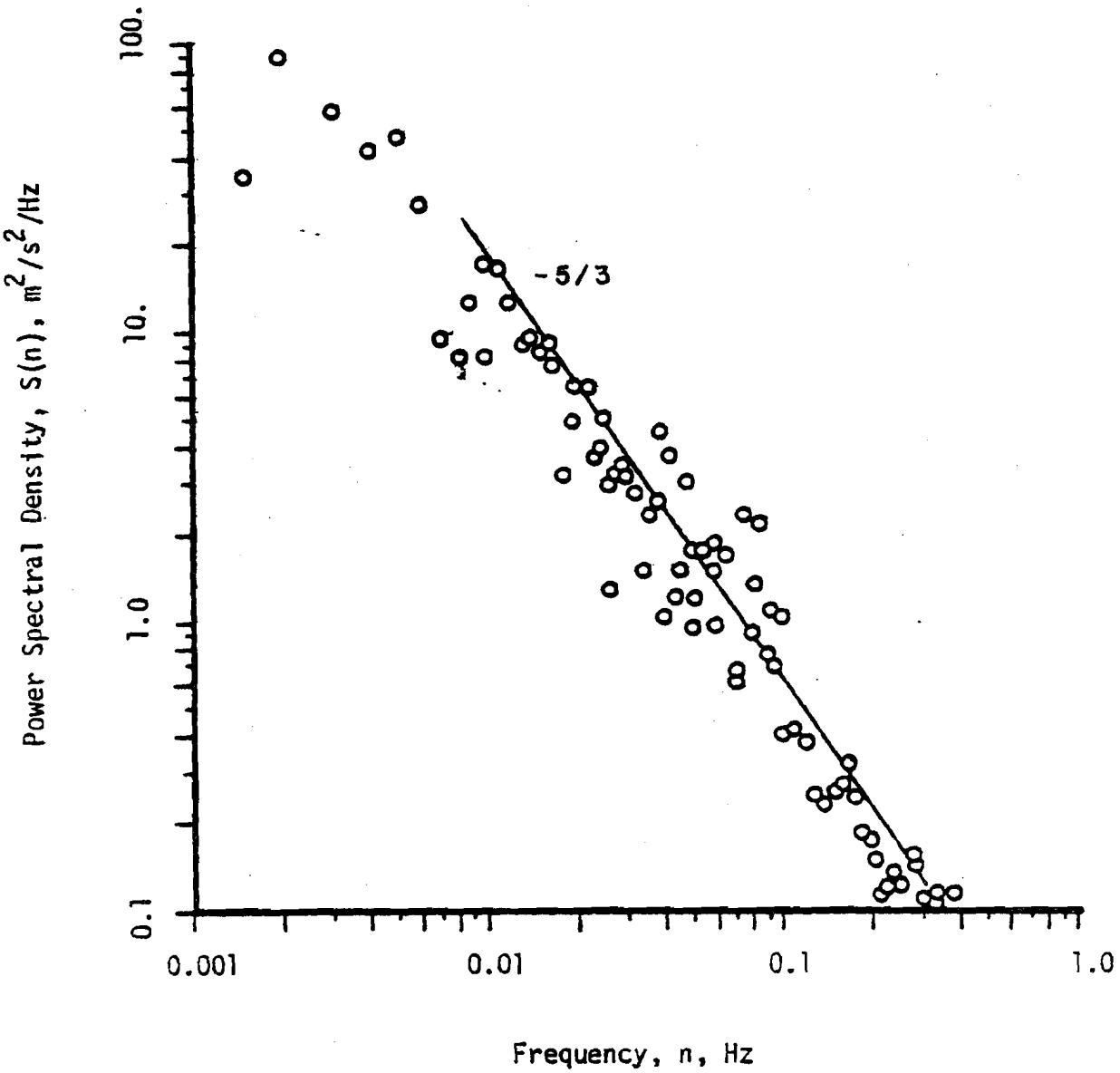

FIGURE 8. WIND SPEED POWER SPECTRAL DENSITY

Davenport[13] gives an empirical fit for the PSD of the u'(t) component in atmospheric turbulence:

$$S(n) = 4.0 \frac{U_*^2}{n} \frac{x^2}{(1 + x^2)^{4/3}} \qquad (48)$$

where $x = 1200\ n/U$ and U_* is the friction velocity. To find the peaks in the PSD curves in Fig. 6, 7 and 8, Eq. (48) is fitted to the data.

The friction velocity, U_*, was not measured for any of the data records. Using a best fit straight line to the linear portion of the PSD, U_* is calculated using Eq. (48).

The calculated values for U_* are shown in Table 2. Values for U_* measured by Murphy and Kirchhoff[14] under similar conditions are shown for comparison. The similarity of the values for U_* gives confidence in the results. These values for U_* are then used in Eq. (48) to extrapolate the PSD into the frequency range below 0.01 Hz. The fitted power spectral densities for the data are shown in Fig. 9.

Comparing the data with their respective fits, each PSD is seen to closely follow the -5/3 power decay law above approximately 0.01 Hz, as do the fitted curves. The apparent peak in the power spectrum for WFR3, Fig. 6, is at approximately 0.008 Hz, whereas the peak in the fitted curve is lower, at approximately 0.005 Hz. A similar comparison can be made for WFR21, Fig. 7 which shows an apparent peak around 0.002 Hz, compared to the peak in the fitted curve at 0.0045 Hz. The fits for WFR18/22, is quite good. The apparent peak and the peak in the fitted curve are both close to 0.004 Hz.

To characterize the turbulence in a different manner, the average gust size is estimated with the integral length scale. Two approaches

DIGITAL WFR	GROUND CONDITIONS	AVERAGE WIND VELOCITY U, m/s	FRICTION VELOCITY, U_*, m/s CALCULATED FROM EQ. 48	FRICTION VELOCITY FROM MURPHY & KIRCHHOFF	MURPHY & KIRCHHOFF PROFILE NUMBER	GROUND CONDITIONS FROM MURPHY & KIRCHHOFF
3/5	BARE	6.35	0.366	0.361	4	BARE
17/21	SMOOTH	7.00	0.330	0.338	5	SNOW
18/21	SMOOTH ICE CRUSTED SNOW	6.05	0.324	0.323	7	SNOW

TABLE 2. COMPARISON OF CALCULATED FRICTION VELOCITIES WITH PREVIOUS RESULTS

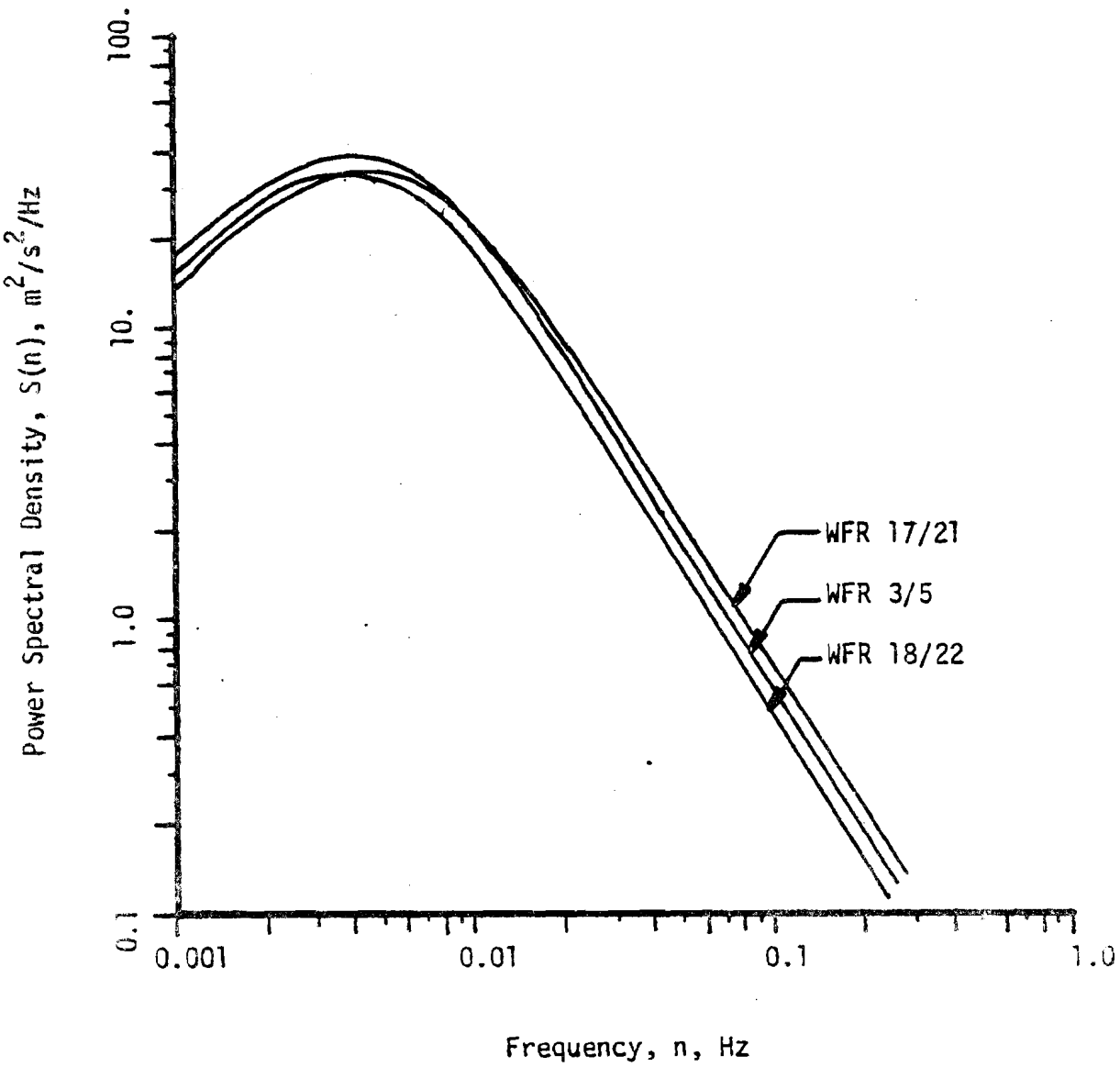

FIGURE 9. FITTED WIND SPEED POWER SPECTRAL DENSITY

to this calculation are made: integrating under the autocorrelation to the first zero crossing, and using Teunissen's[15] relation to interpret the peak in the power spectra.

Teunissen's relation for calculating the integral length scale from PS(n) is:

$$L_u = \frac{0.146 \quad U}{n_p} \tag{49}$$

where PS(n) is the power spectra, and n_p is the peak frequency in PS(n). The calculation of the integral scales from the autocorrelation and power spectra techniques are shown in Table 3. The autocorrelations and the power spectra from which these are calculated are shown in Figs. 10 through 15 and Figs. 16 through 21, respectively.

Difficulties arise in both techniques for establishing the integral scales. For example, the power spectra for WFR3 (Fig. 16) and WFR5 (Fig. 17) both peak at approximately 0.010 Hz. However, the difference in mean wind speed results in a difference in gust length when the gust frequency is converted to gust length.

In addition, multiple peaks of comparable magnitude occur at significantly different frequencies in the power spectra. This occurs, for example, in the power spectra of WFR22 (Fig. 21). The comparison with the integral scales calculated from the autocorrelation for WFR22 (Table 3), is interesting. While the magnitude of the peak at 0.012 Hz for WFR22 is significantly smaller than the peak at 0.004 Hz, the corresponding length scale agrees more closely with the autocorrelation results.

A distinct disparity exists for the length scale as calculated by the power spectra and autocorrelations for records with $\Delta t = 0.5s$. Here the higher frequencies are weighted properly by the power spectra, but probably are more dominant in shortening the time before the

WFR	PEAK FREQUENCY IN POWER SPECTRA n_p, Hz	AVERAGE WIND SPEED U,m/s	DOWNSTREAM INTEGRAL LENGTH SCALE, L_u, m FROM PS(n_p)	DOWNSTREAM INTEGRAL LENGTH SCALE, L_u,m FROM AUTOCORRELATION	DOWNSTREAM INTEGRAL TIME SCALE T_u, s FROM PS(n_p)	DOWNSTREAM INTEGRAL TIME SCALE T_u, s FROM AUTOCORRELATION
3	0.028	6.35	33.1	45	5.2	7.1
5	0.020	4.58	33.4	7	7.3	1.5
17	0.020	6.96	50.8	27	7.3	3.9
21*	0.076 (dominant)	7.00	13.4	100	1.9	14.3
	.048		21.3		3.0	
18	0.020	4.57	33.4	30	7.3	6.6
22*	0.004 (dominant)	6.05	221.	88	36.5	14.5
	.074 (next in size)		11.9		2.0	
	.040		22.1		3.7	
	.012		73.6			

*Multiple peaks occur in the power spectra, each of which is represented. The dominant peak is given first.

TABLE 3. DOWNSTREAM INTEGRAL SCALES

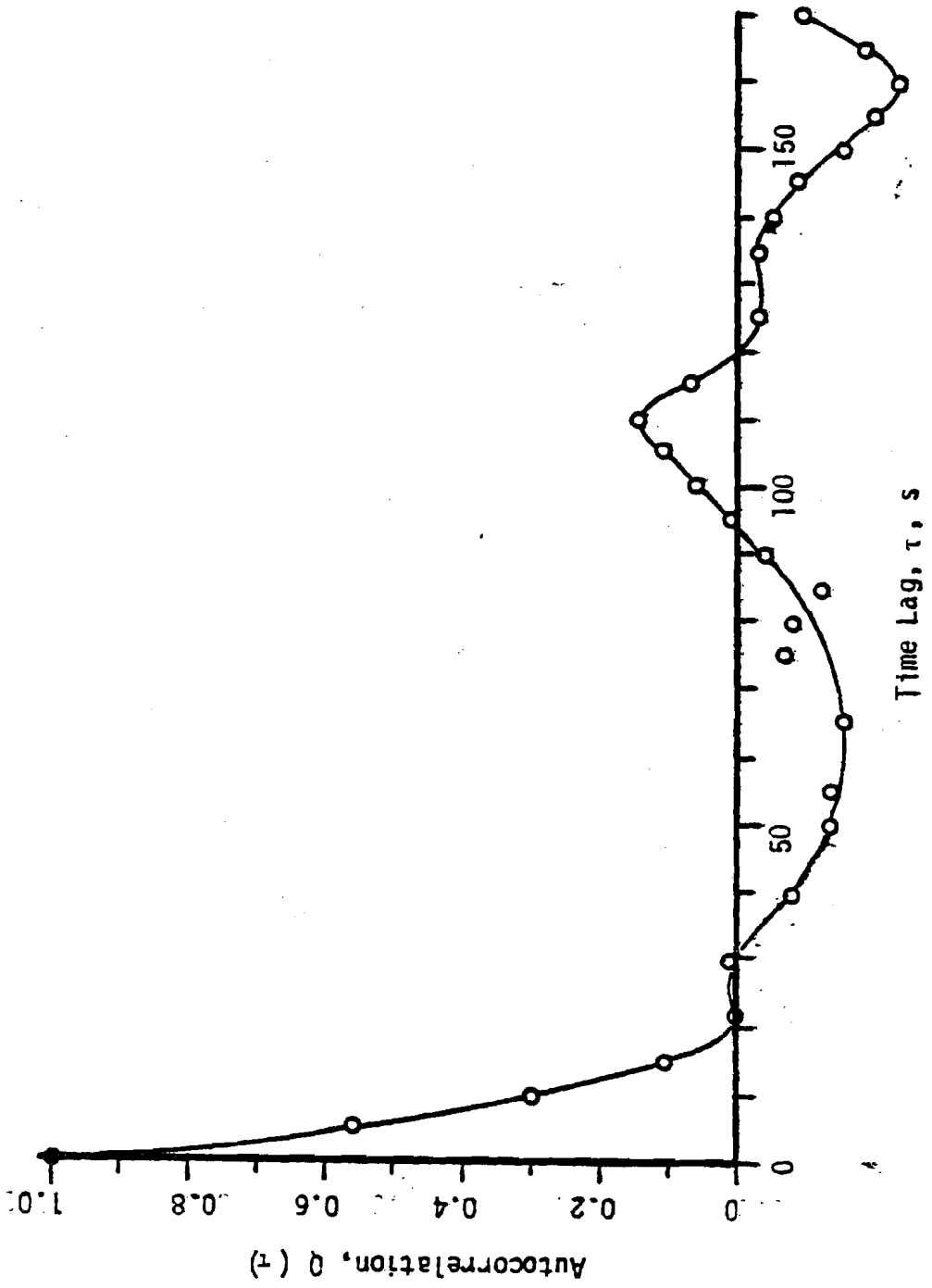

FIGURE 10. WIND SPEED AUTOCORRELATION: WFR 3

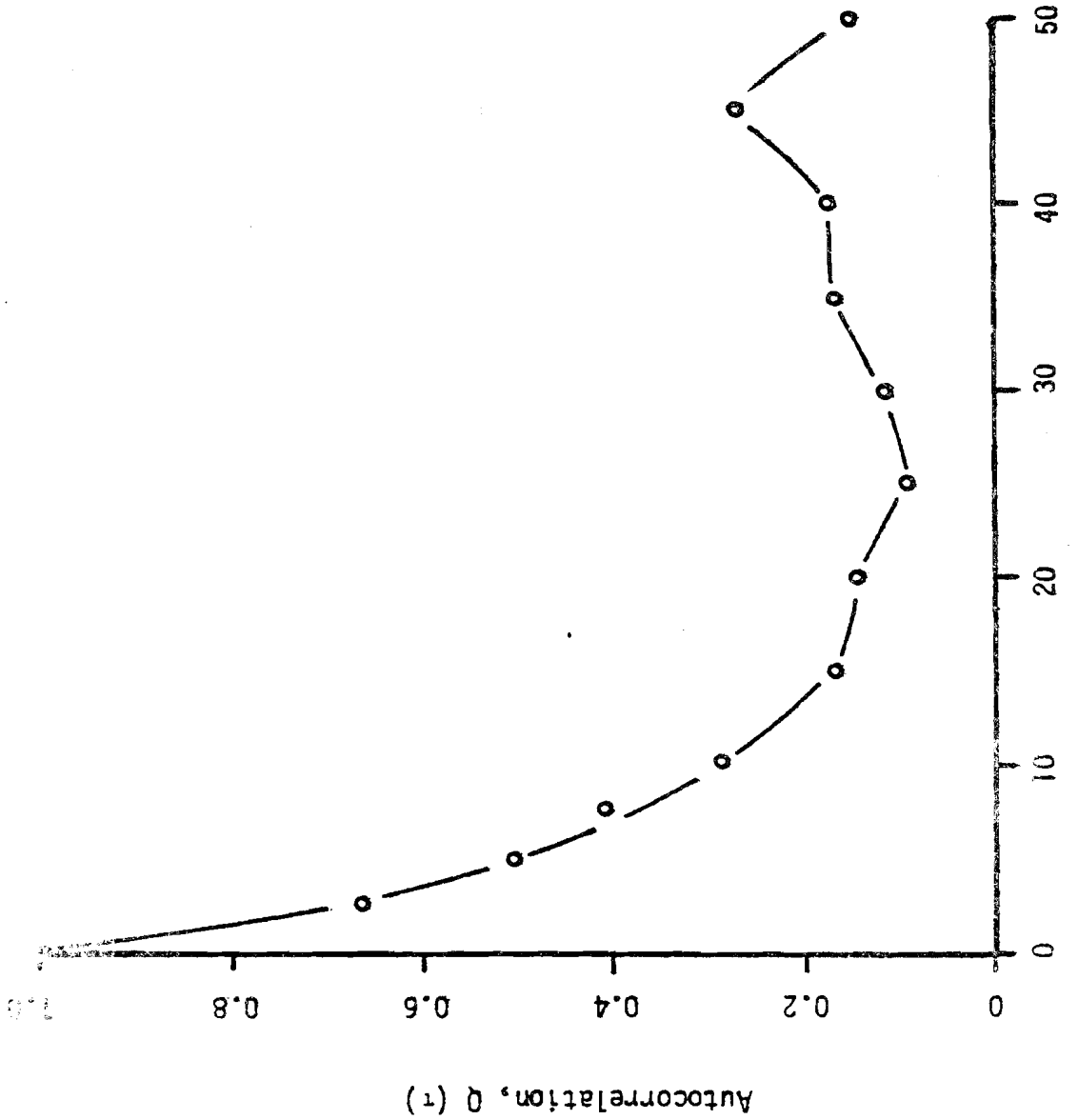

FIGURE 11. WIND SPEED AUTOCORRELATION: WFR 5

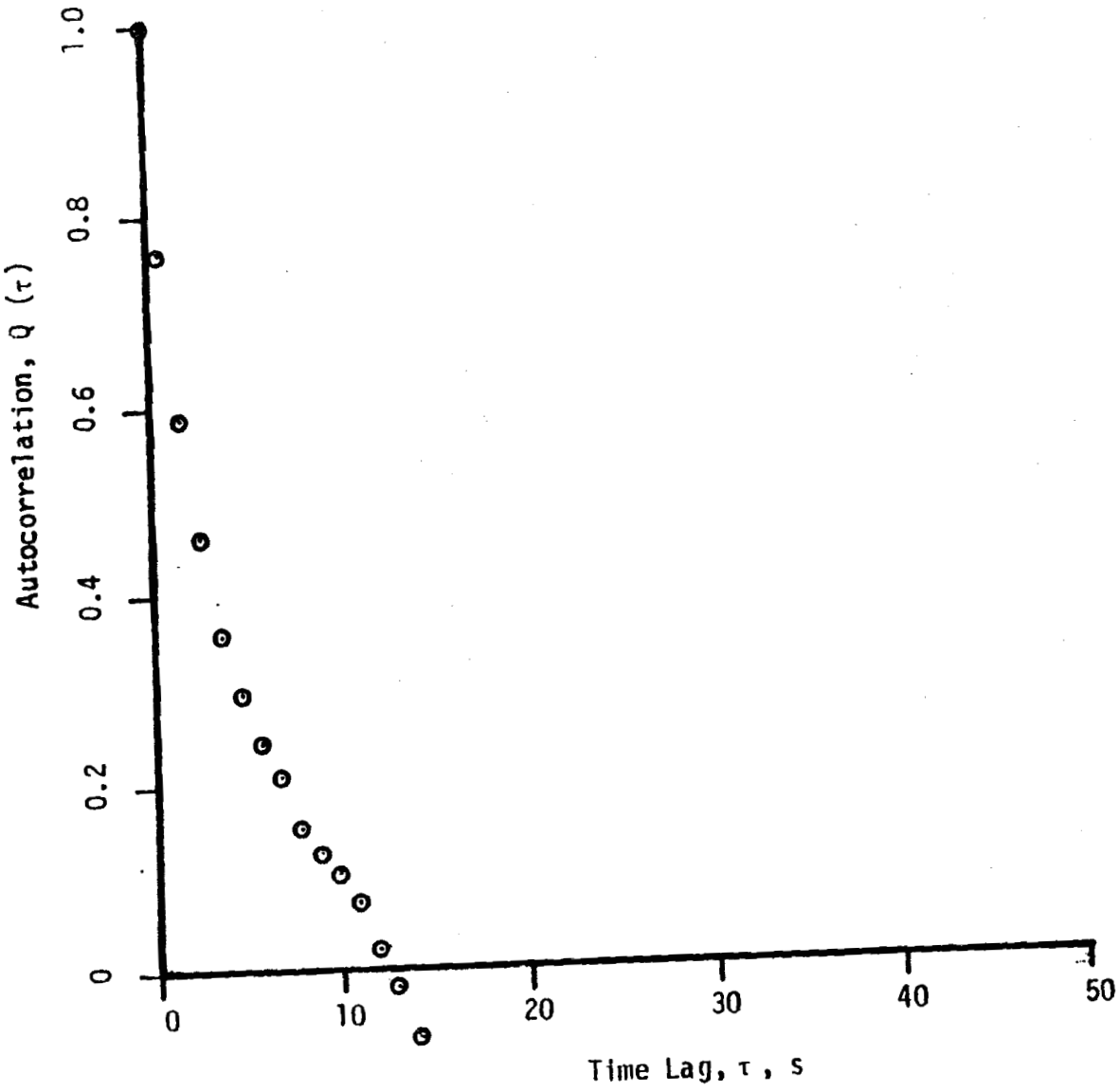

FIGURE 12. WIND SPEED AUTOCORRELATION

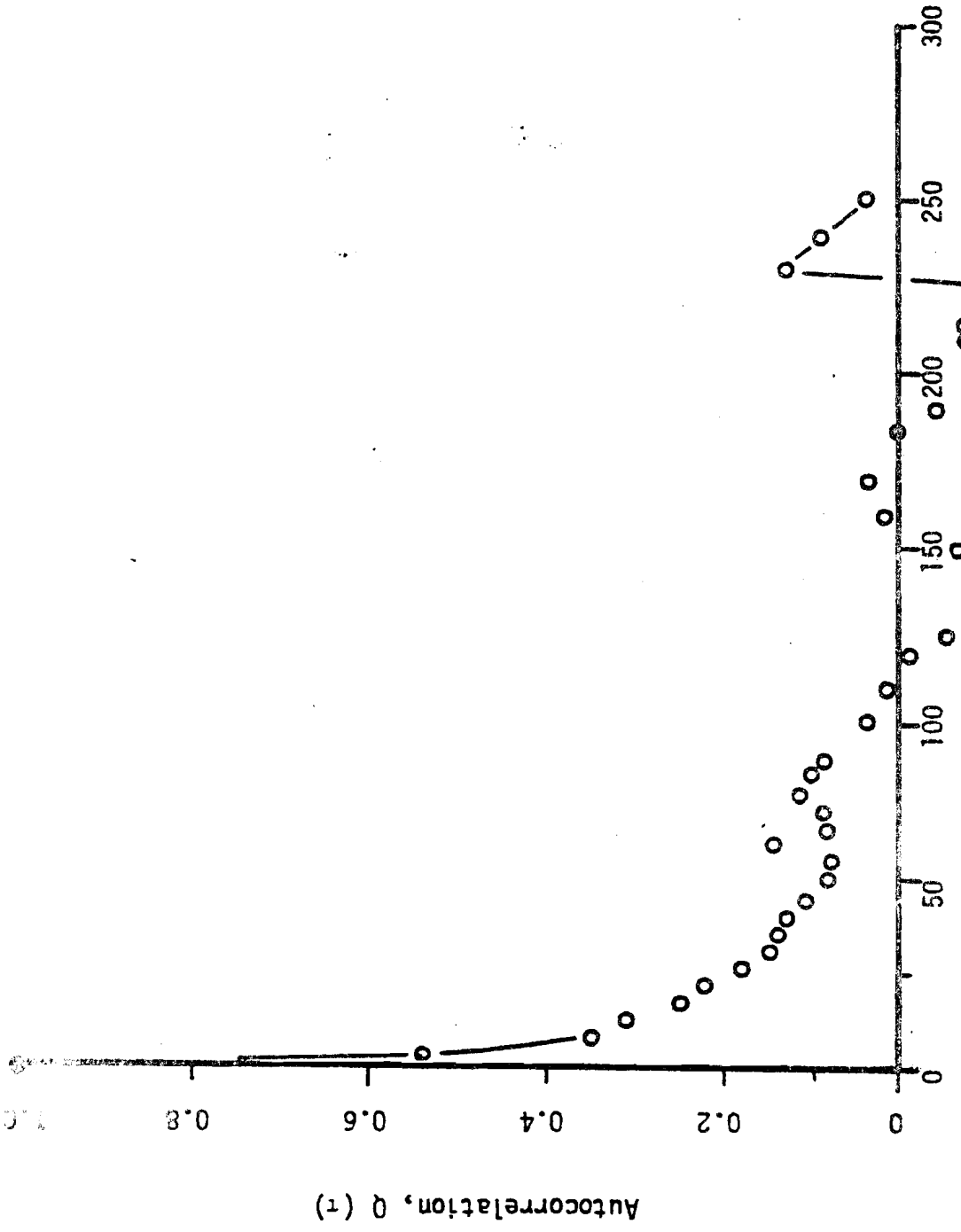

FIGURE 13. WIND SPEED AUTOCORRELATION: WFR 21

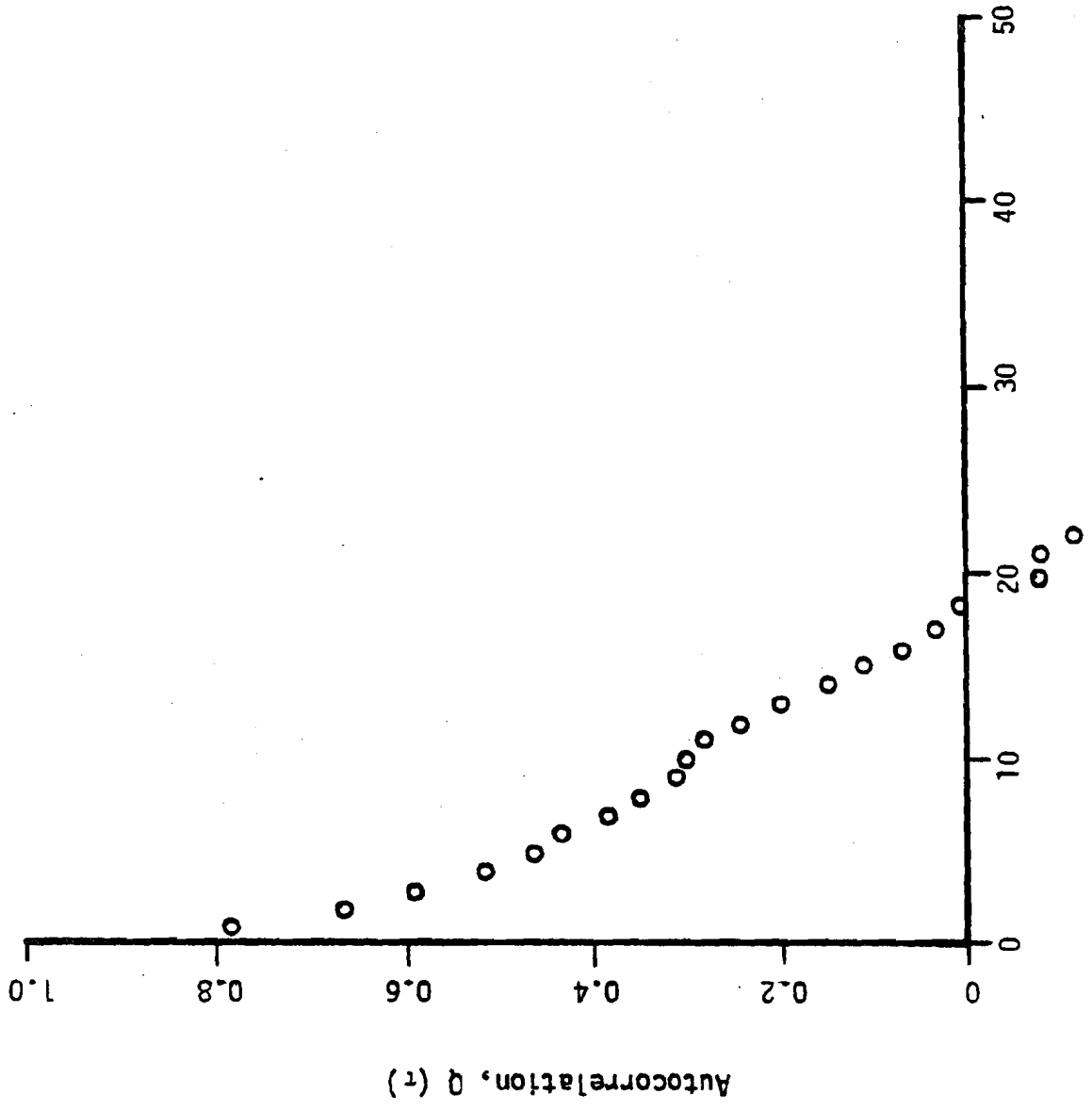

FIGURE 14. WIND SPEED AUTOCORRELATION: WFR 18

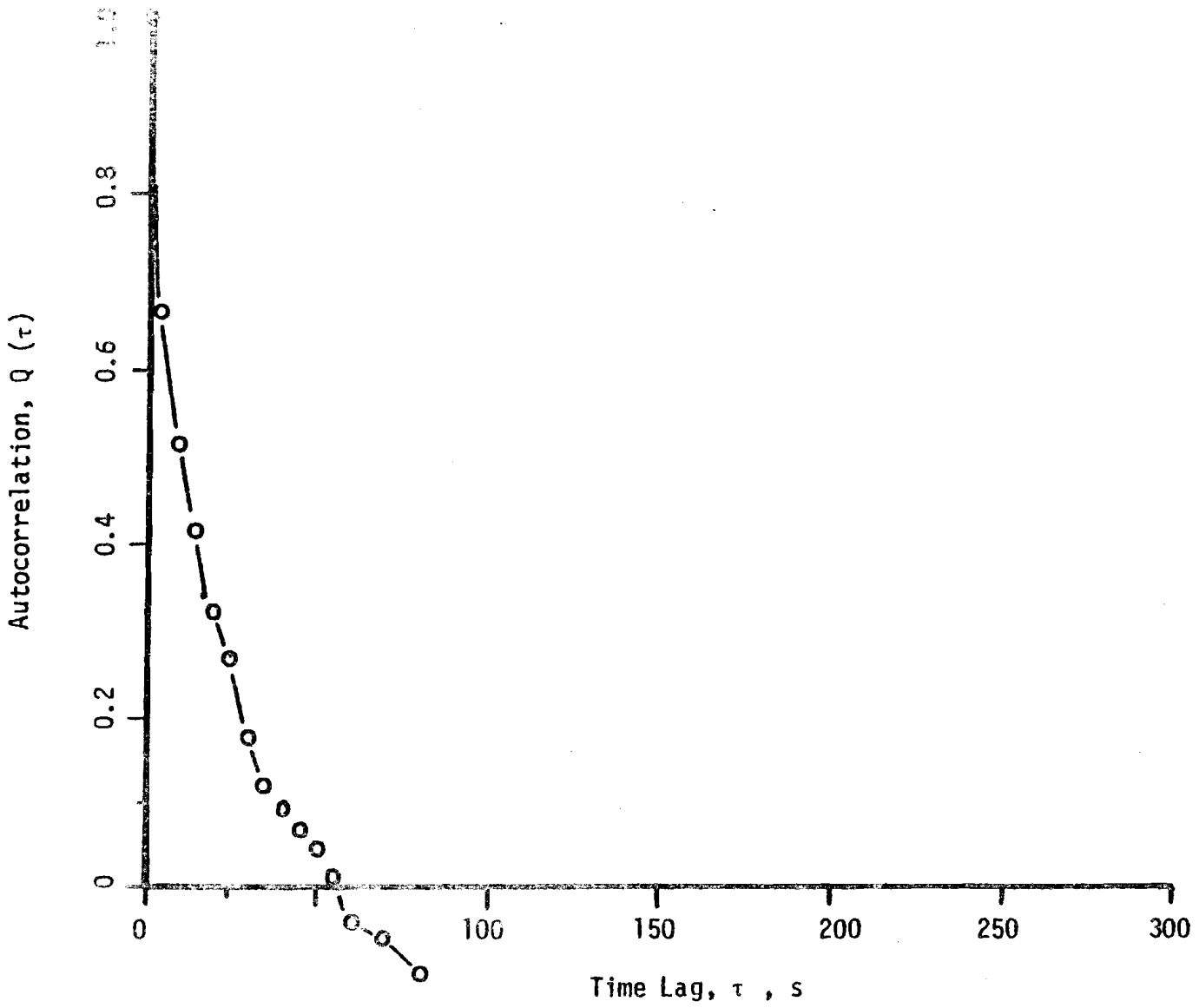

FIGURE 15. WIND SPEED AUTOCORRELATION: WFR 22

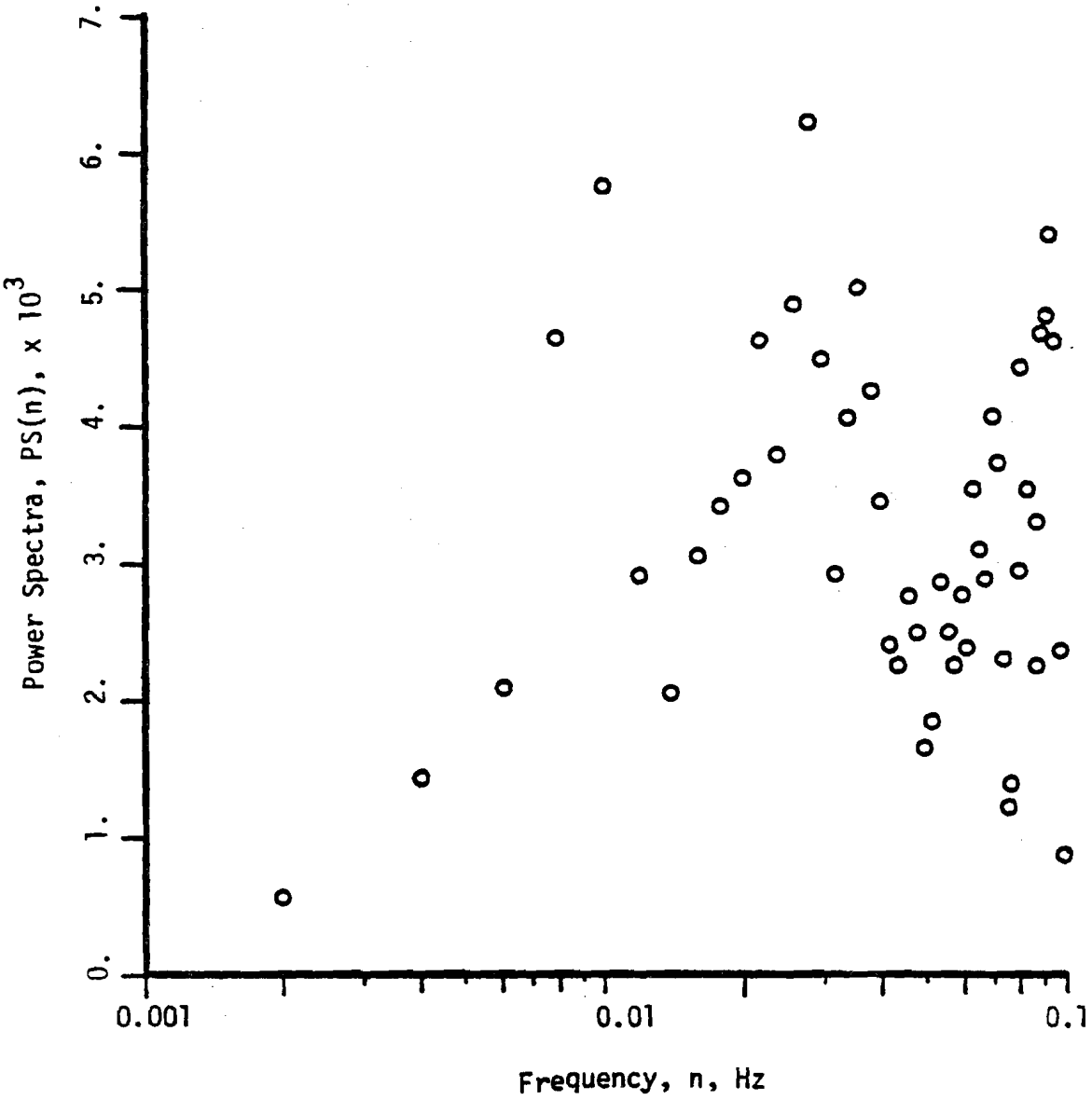

FIGURE 16. WIND SPEED POWER SPECTRA

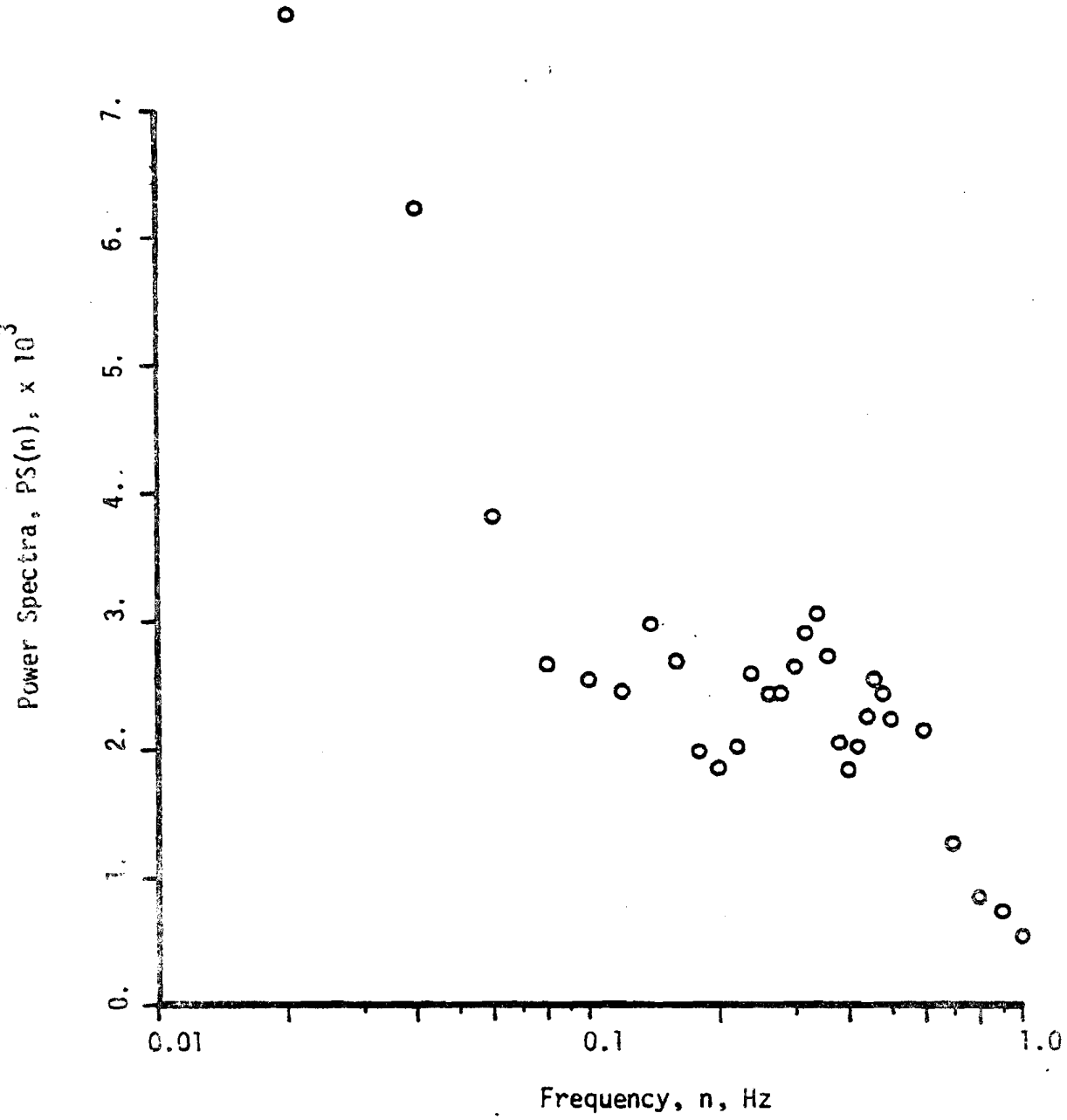

FIGURE 17. WIND SPEED POWER SPECTRA

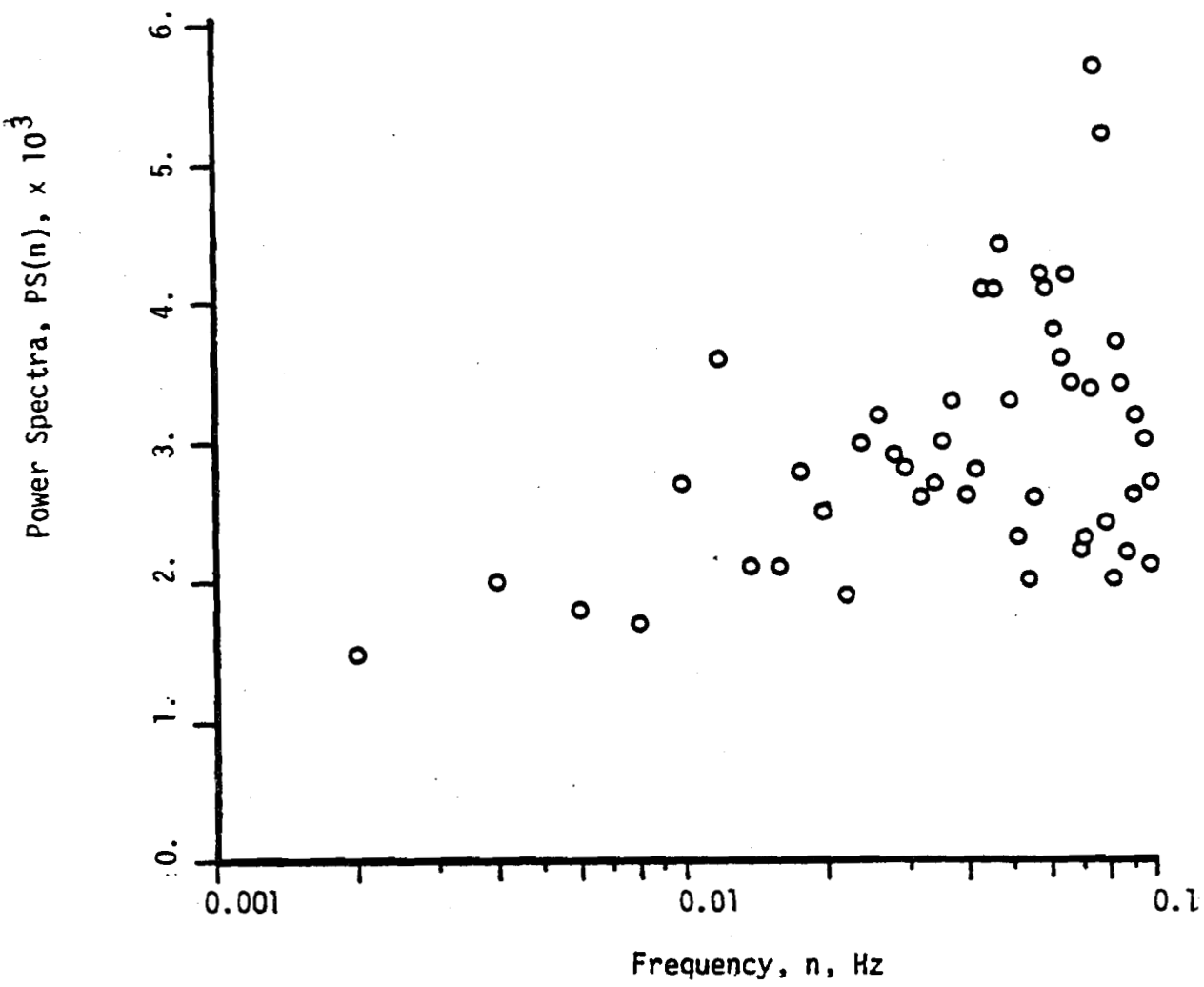

FIGURE 18. WIND SPEED POWER SPECTRA

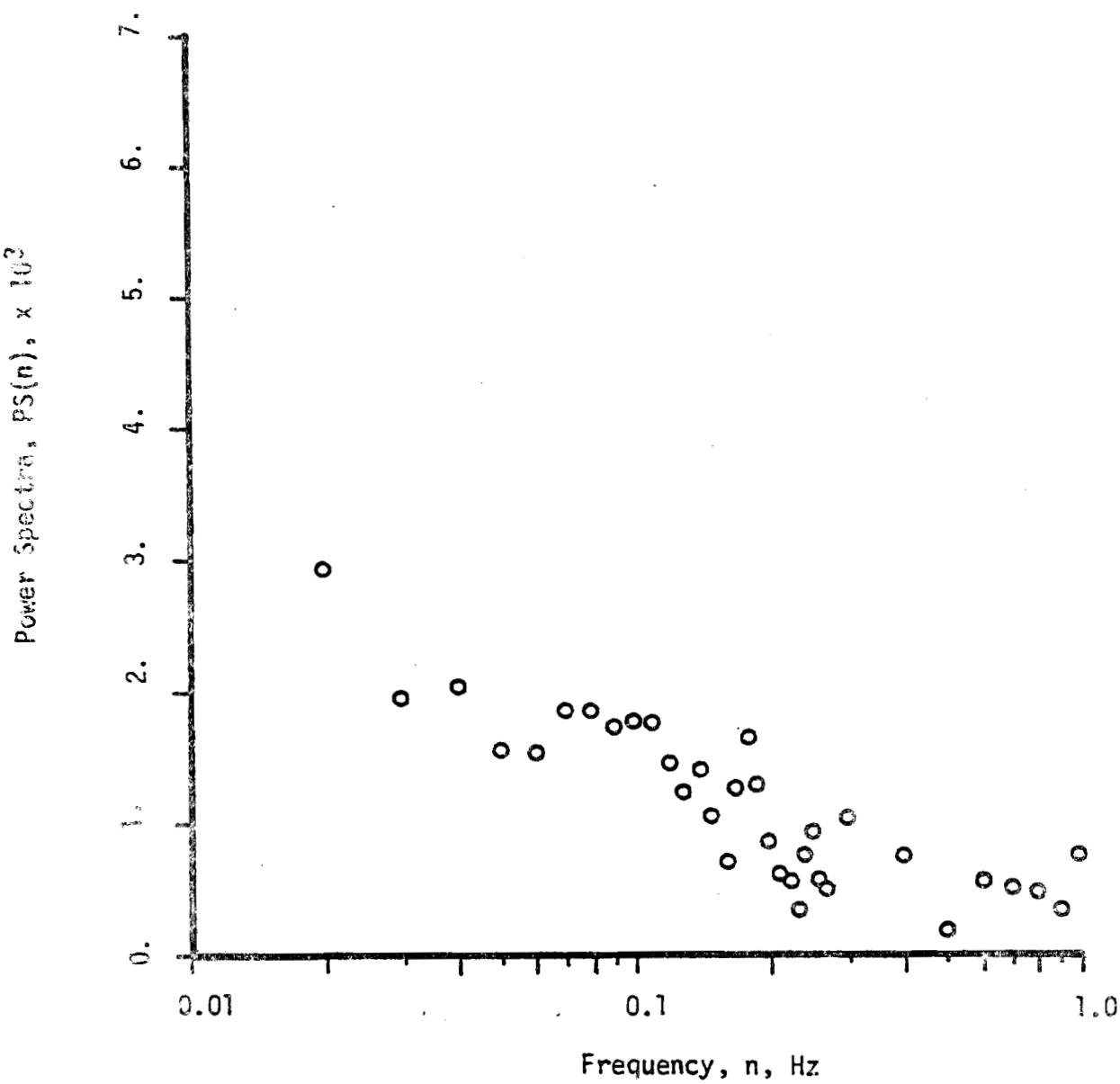

FIGURE 19. WIND SPEED POWER SPECTRA

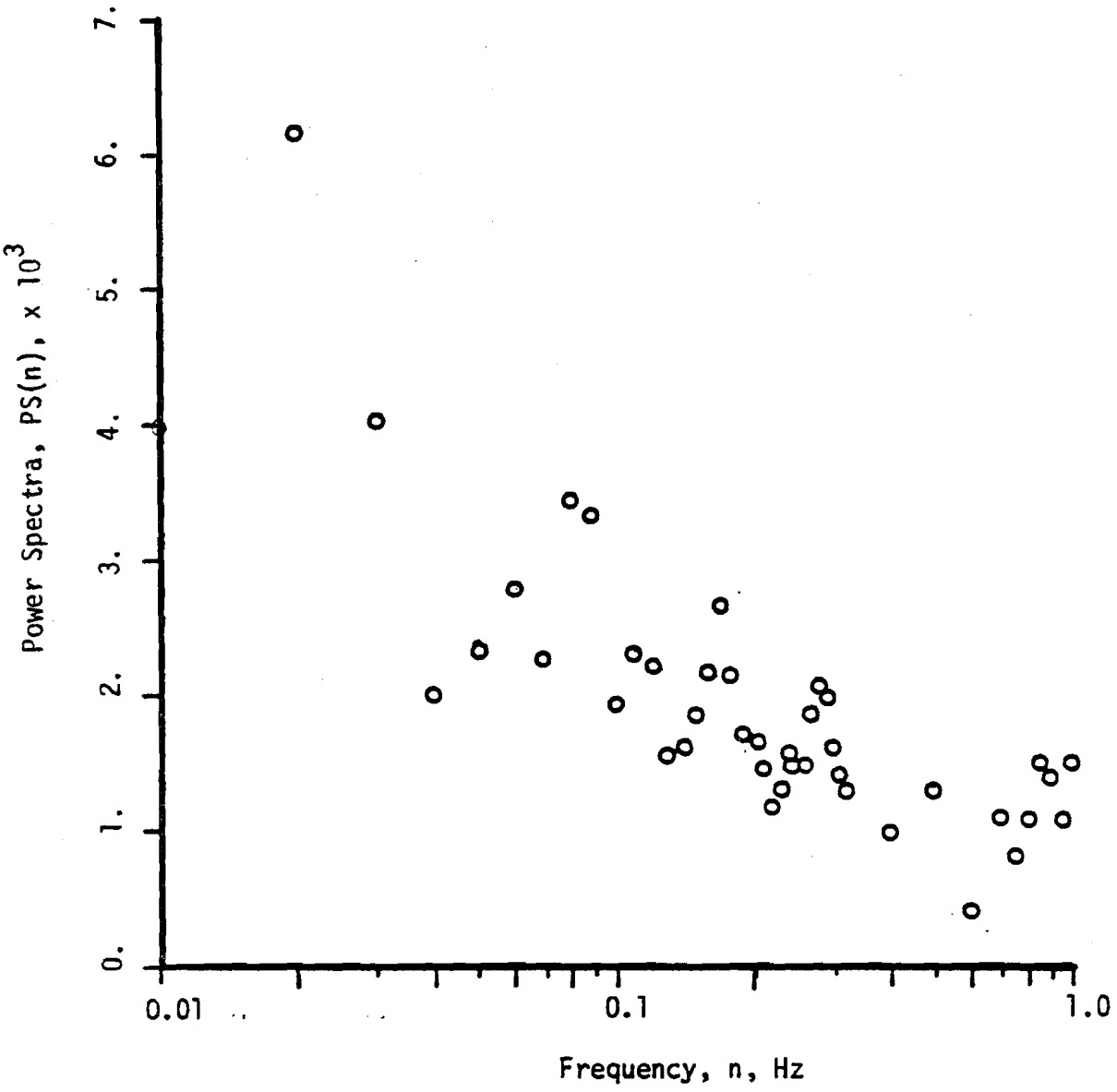

FIGURE 20. WIND SPEED POWER SPECTRA

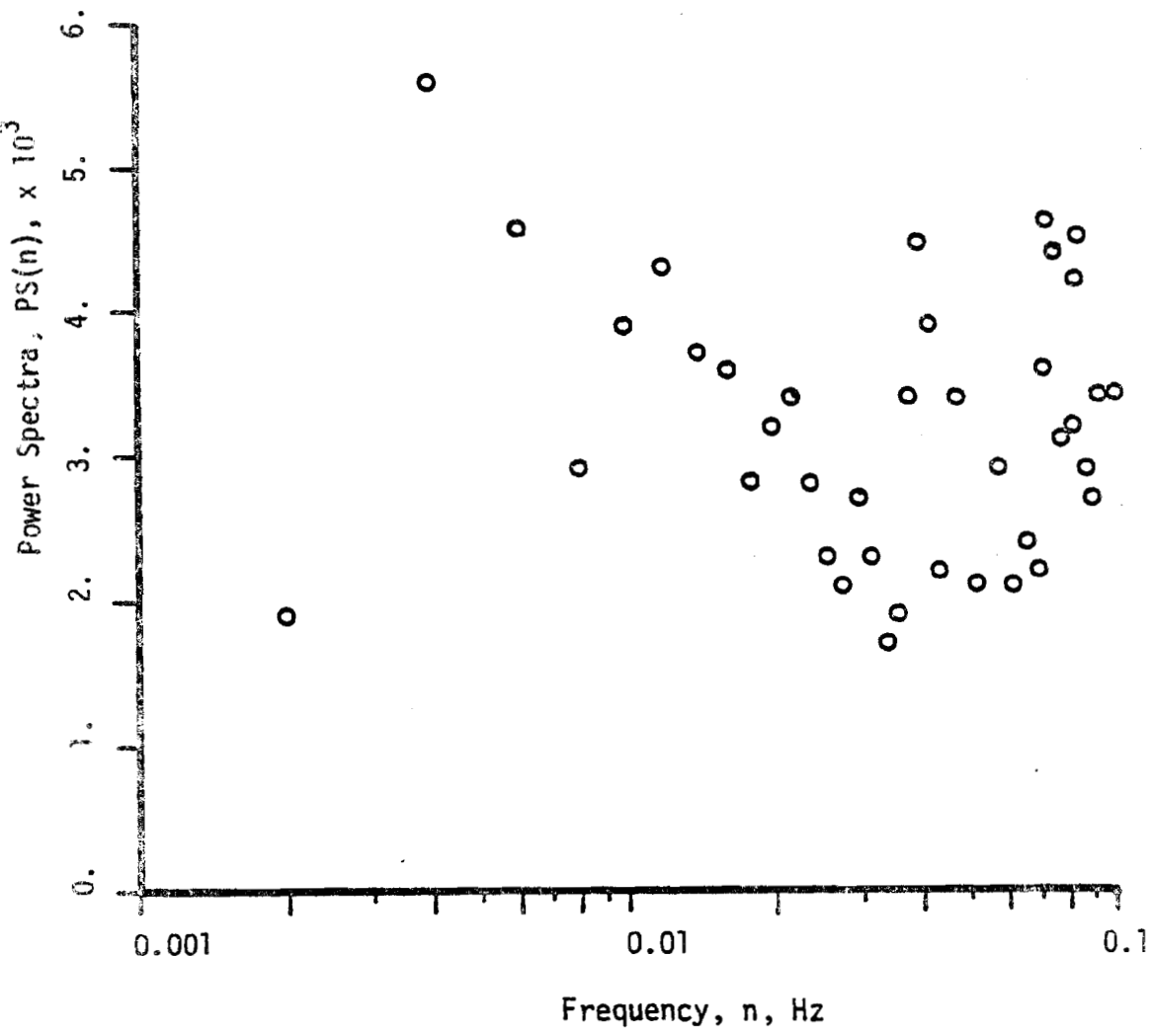

FIGURE 21. WIND SPEED POWER SPECTRA

autocorrelation function becomes uncorrelated. As a consequence, the integral scales are probably useful as an order of magnitude characterization of turbulence in the wind.

The best estimates for the integral length scales are shown in Table 4. As a comparison, data for L_u are computed from Counihan's relation[16]:

$$L_u = C(z)^b \tag{50}$$

where z is the anemometer height and C and b are constants obtained graphically based on the site roughness length, h_o. Murphy and Kirchhoff[17] found h = 0.024 m for the UMass site with no snow cover. Using this roughness length, b and C are approximately 0.18 and 100 respectively. L_u is calculated from Eq. (50) to be 170 m.

The disparity in the integral length scale estimates is not unexpected, because of the large variation in L_u seen in Table 3.

3.2.2 Wind Direction

The characterization of the wind direction fluctuations, v'(t), as a driving function are most usefully described with the PSD. These are shown in Figs. 22 through 24. As with the wind speed fluctuations, the autocorrelation and the power spectra are used to calculate the integral scale. These are shown in Figs. 25 through 36. Data analyzed in this section are taken from the three analog records as summarized in Table 1.

The PSD for wind direction, as with wind speed, closely follows the -5/3 power decay law above approximately 0.02 Hz. Unlike the PSD for u'(t), the PSD for v'(t) shows no clearly defined peak, with the exception of WFR21, Fig. 23, which shows a narrow peak at 0.006 Hz.

ANALOG WFR	DIGITAL WFR	ESTIMATION OF L_u, m
9	3/5	35-84
11	17/21	93-124
10	18/22	56-221

TABLE 4. RANGE ESTIMATION OF DOWNSTREAM INTEGRAL LENGTH SCALES

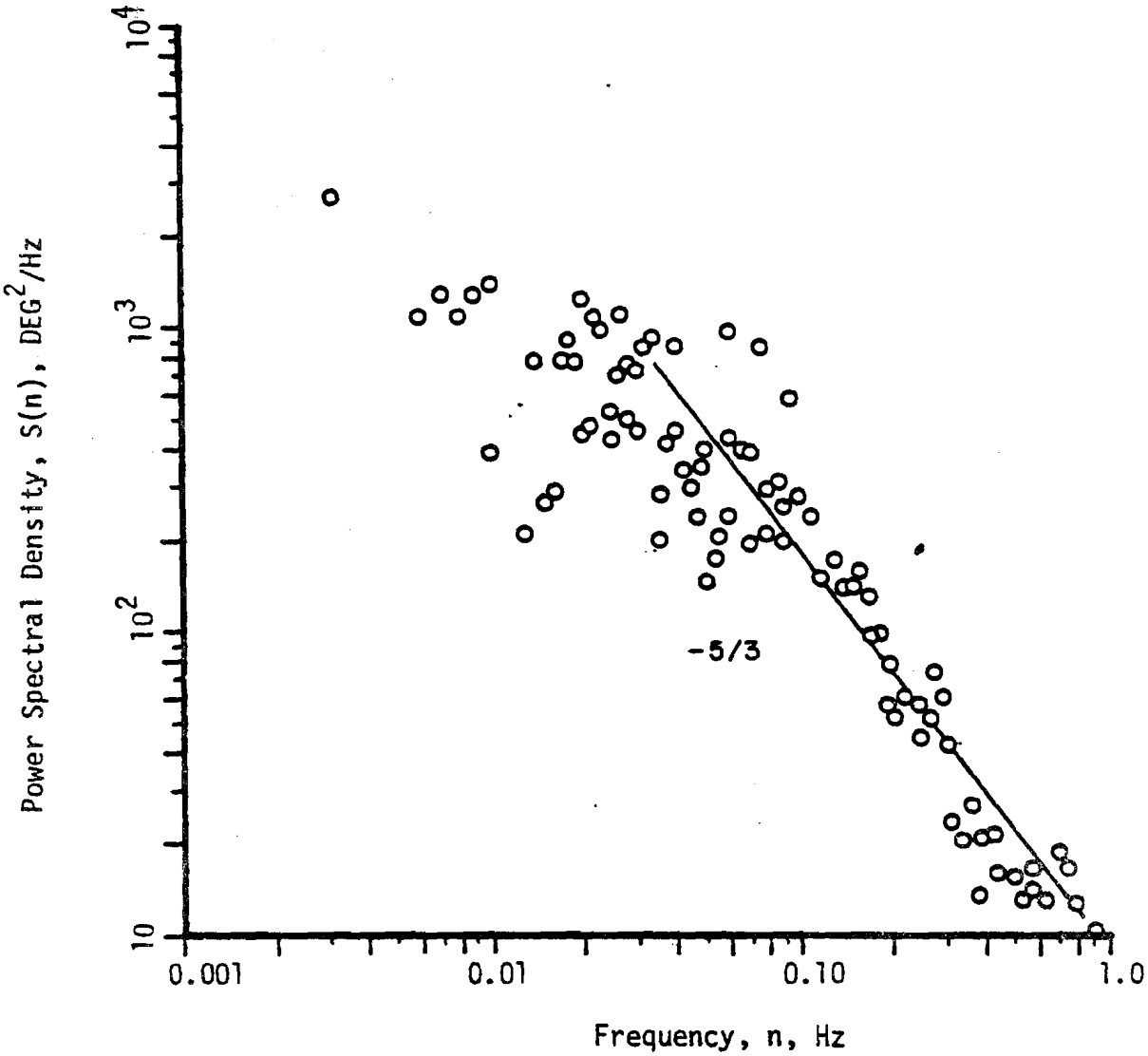

FIGURE 22. WIND DIRECTION POWER SPECTRAL DENSITY: WFR 3/5

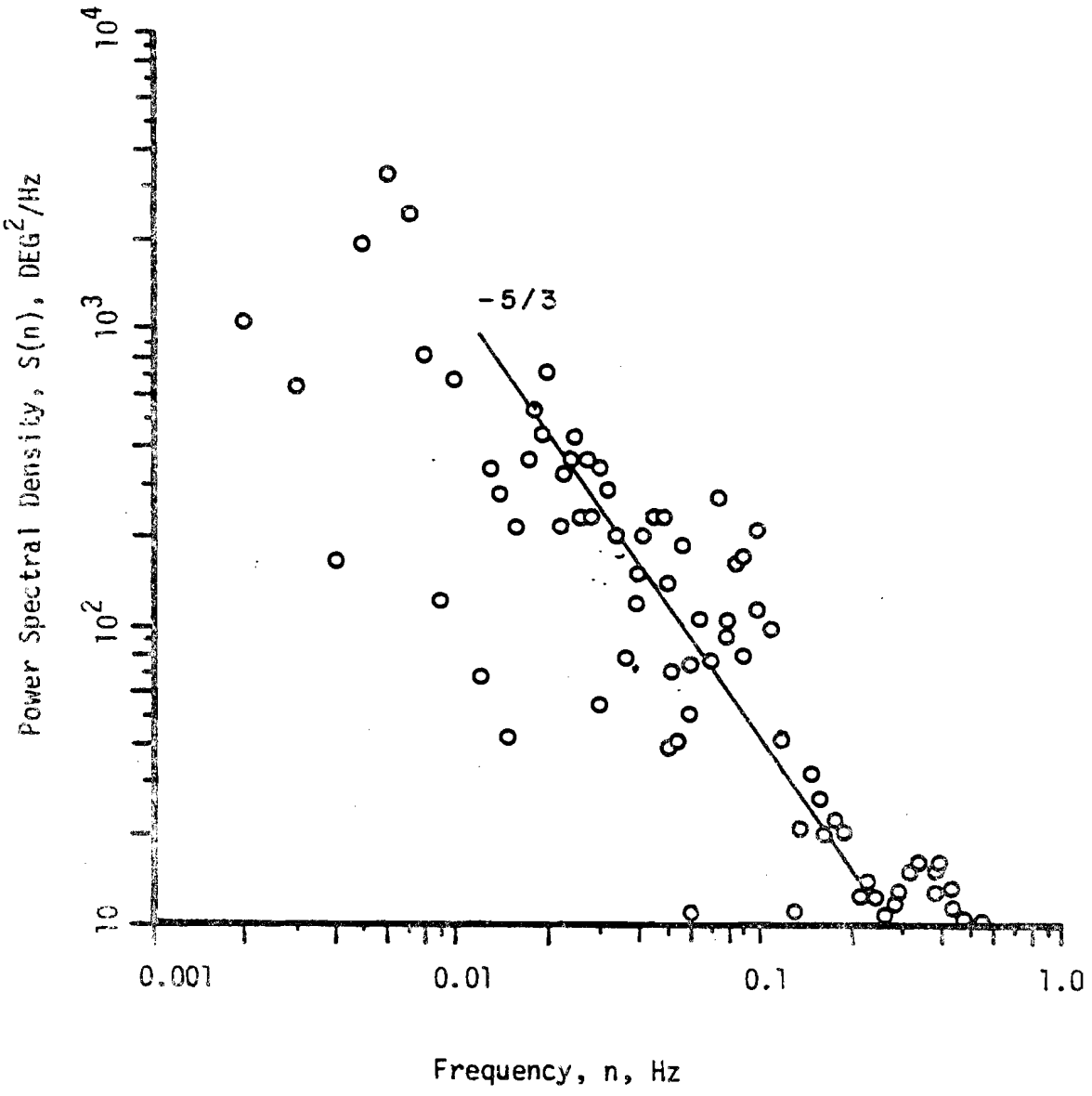

FIGURE 23. WIND DIRECTION POWER SPECTRAL DENSITY: WFR17/21

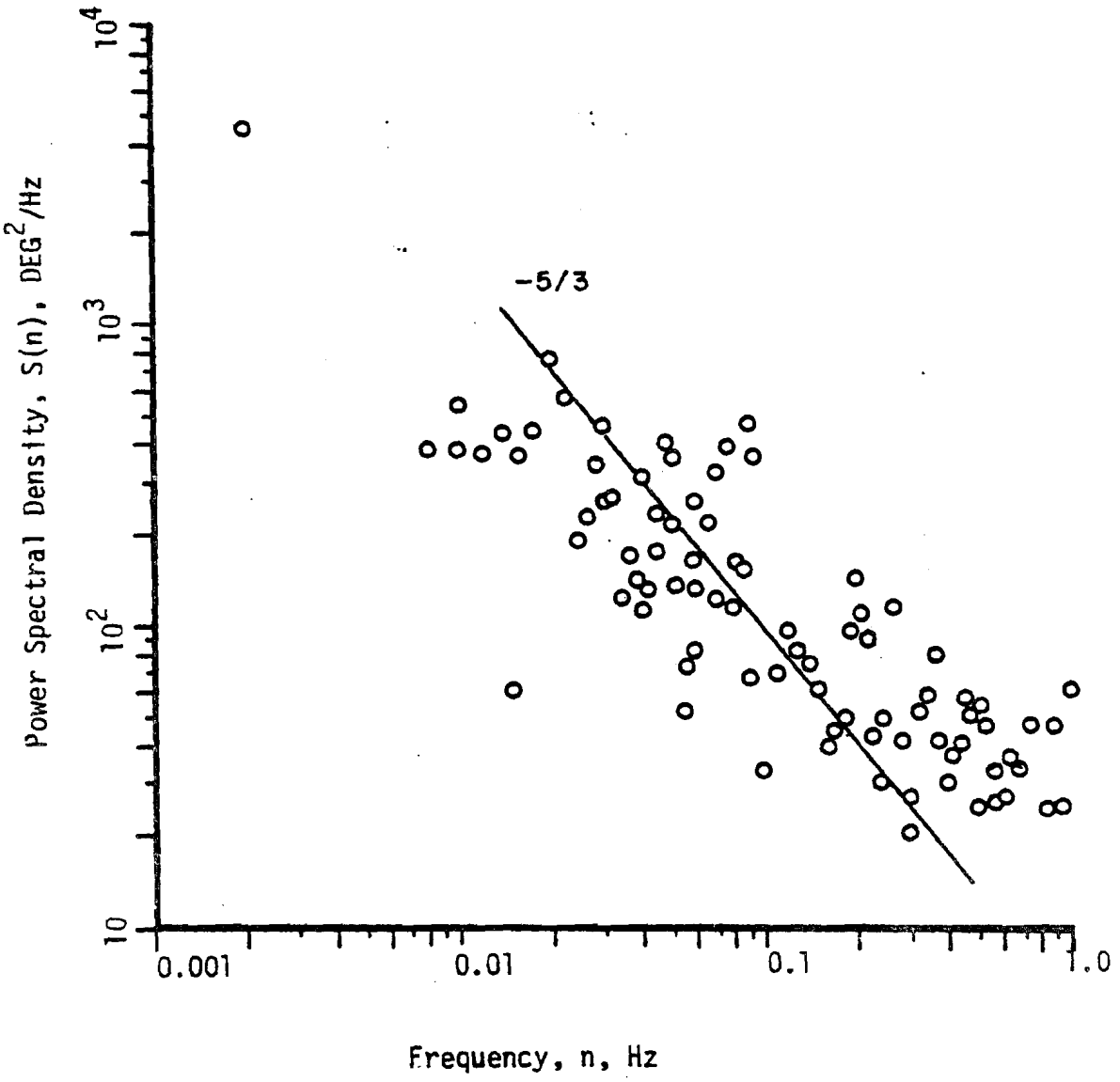

FIGURE 24. WIND DIRECTION POWER SPECTRAL DENSITY: WFR18/22

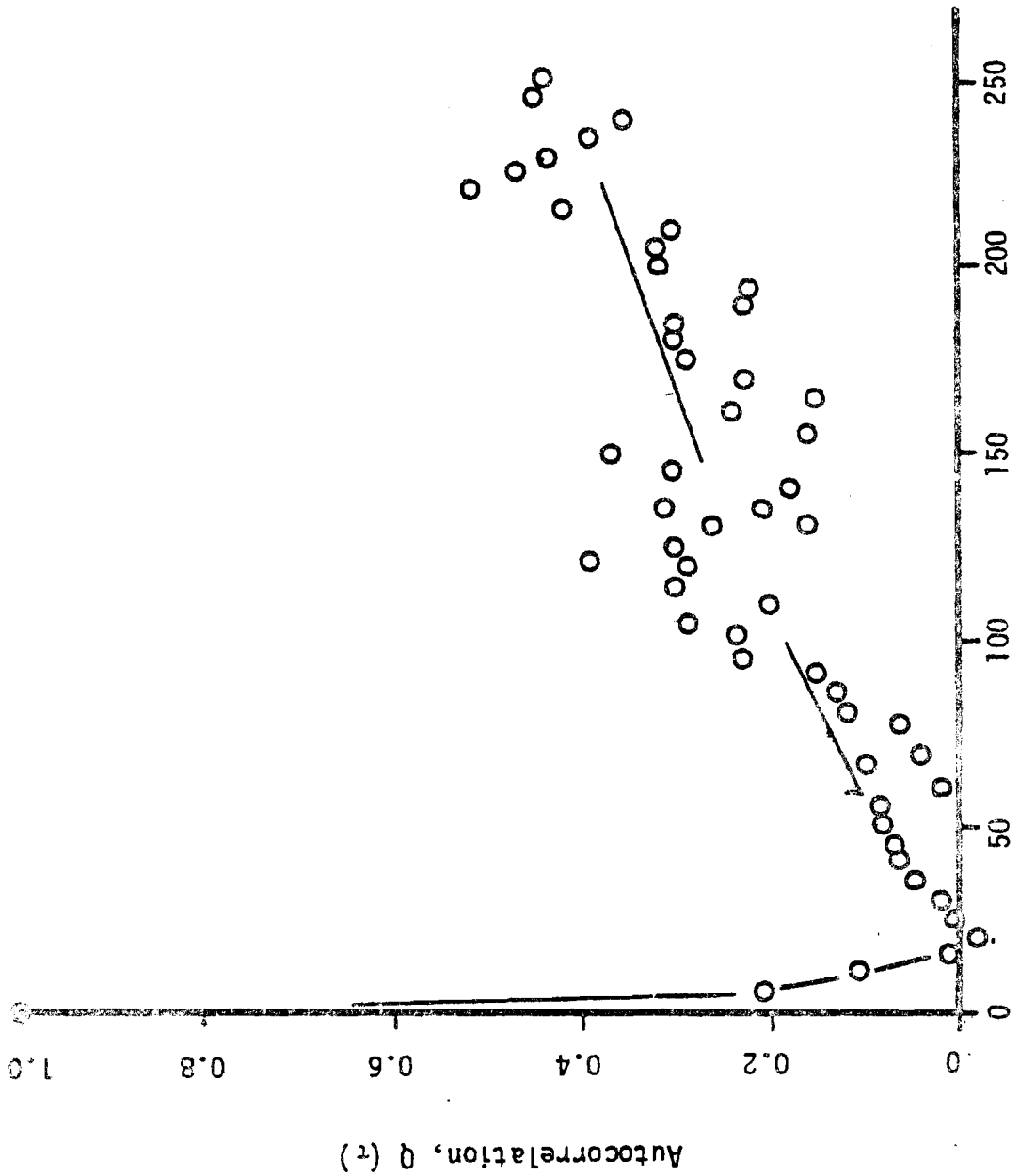

FIGURE 25. WIND DIRECTION AUTOCORRELATION: WFR 3

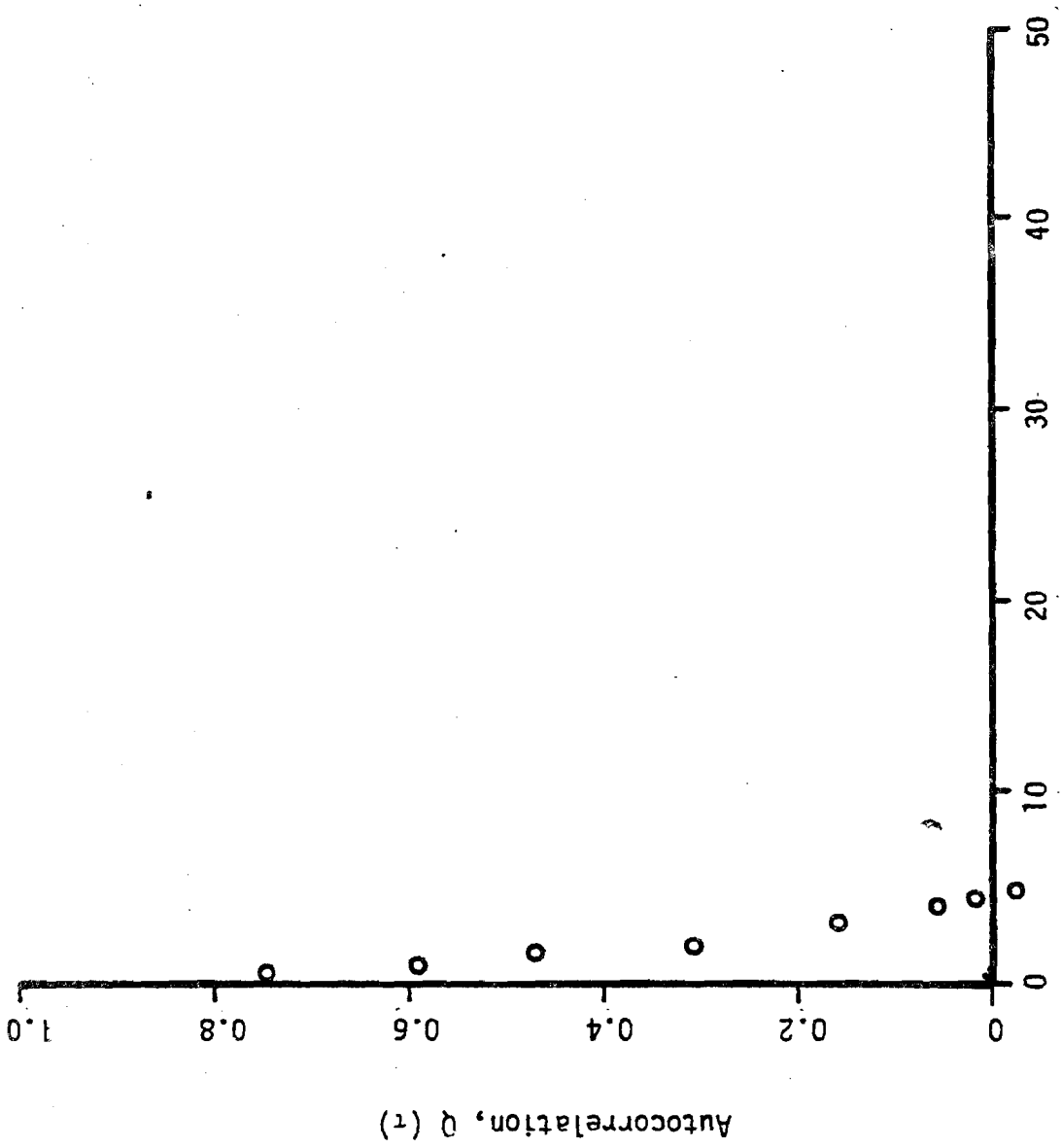

FIGURE 26. WIND DIRECTION AUTOCORRELATION: WFR 5

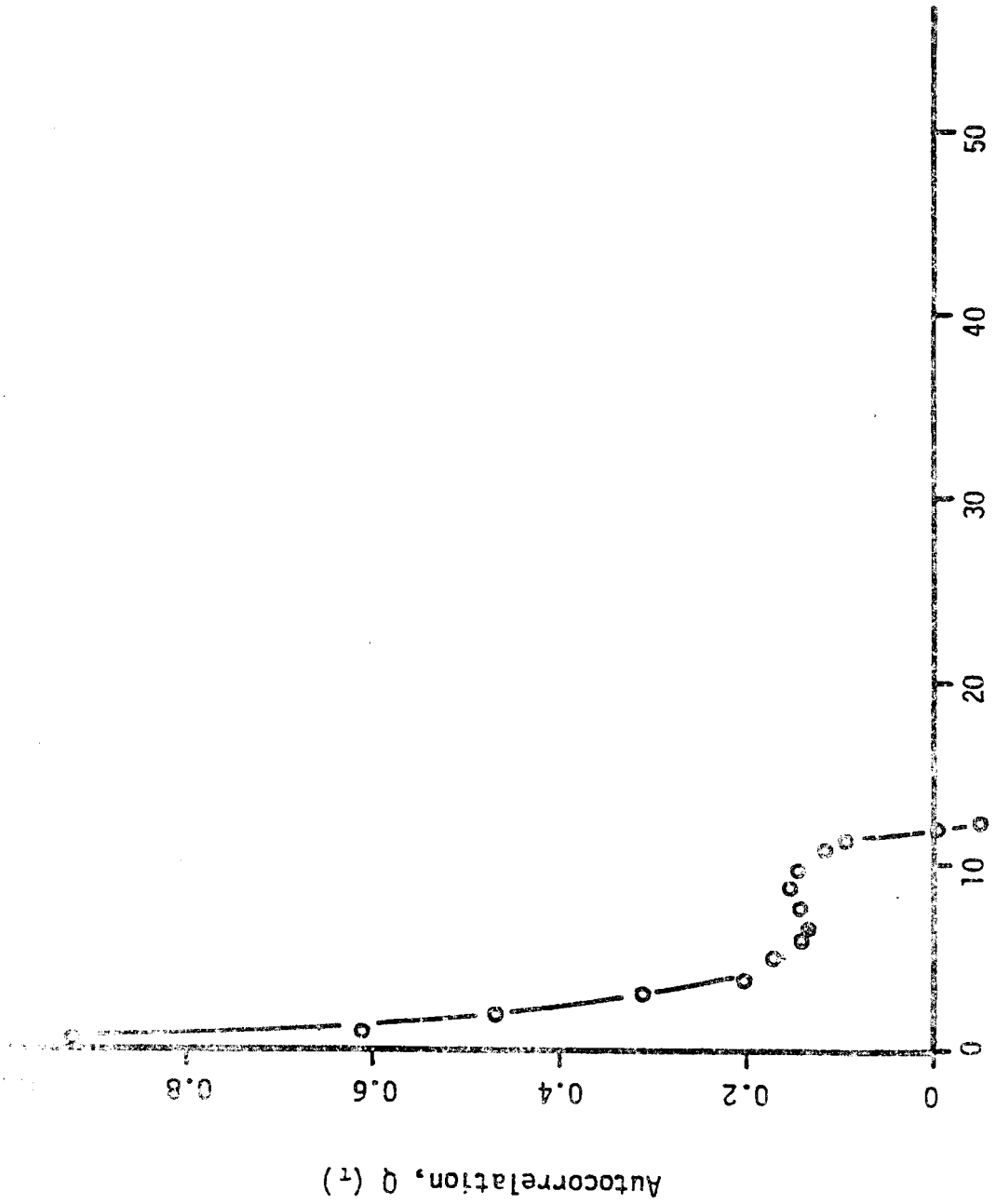

FIGURE 27. WIND DIRECTION AUTOCORRELATION: WFR 17

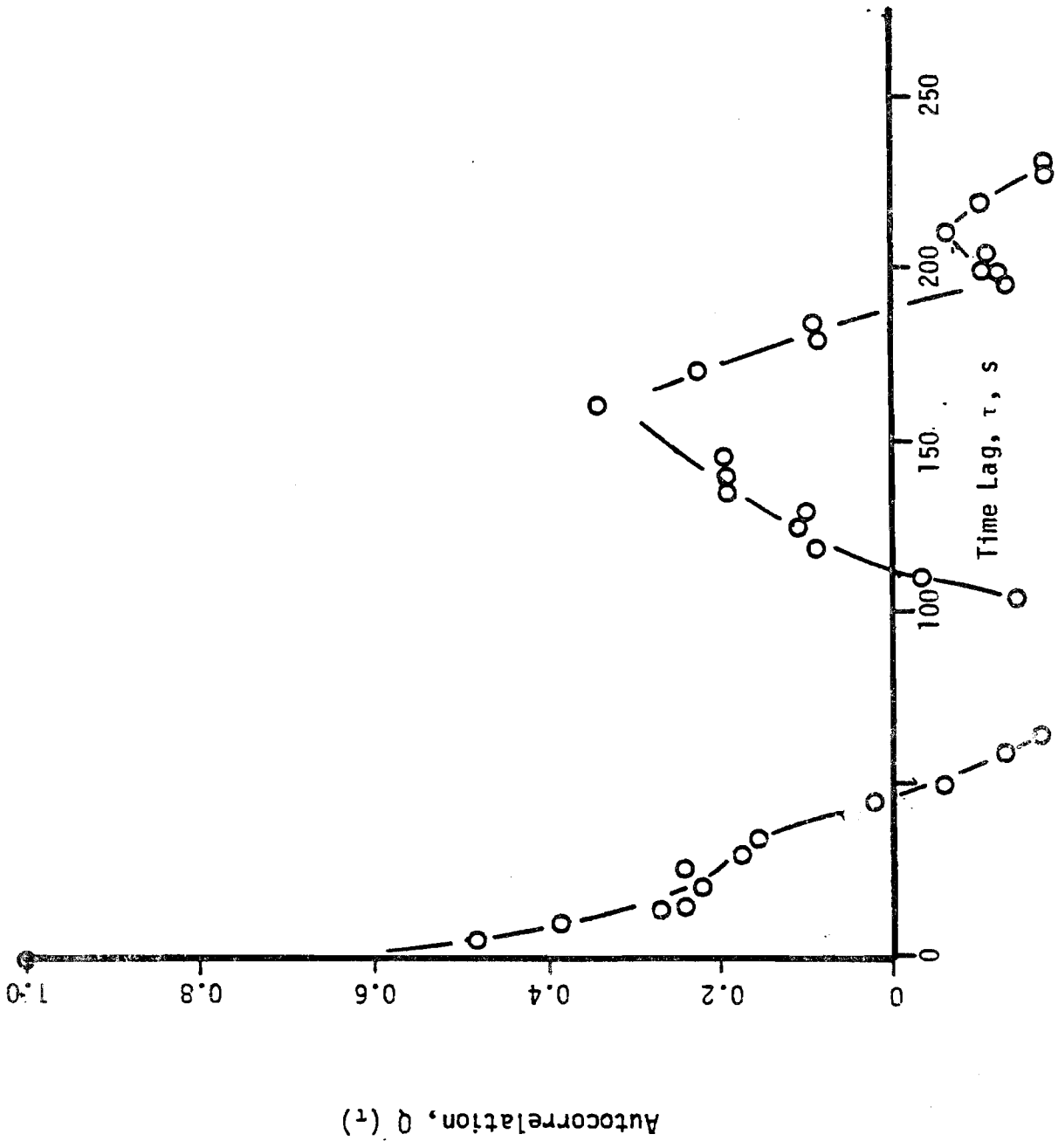

FIGURE 28. WIND DIRECTION AUTOCORRELATION: WFR 21

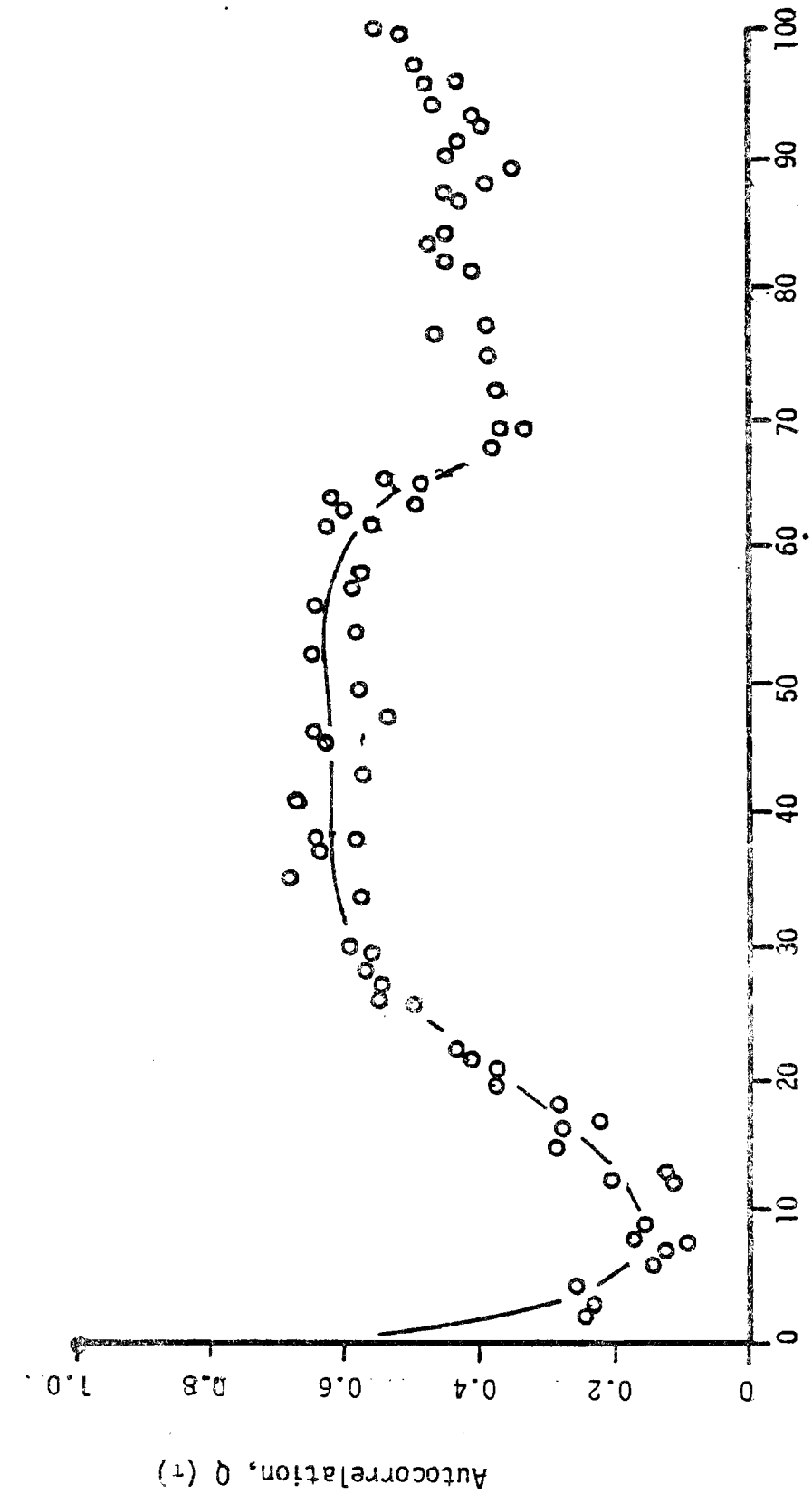

FIGURE 29. WIND DIRECTION AUTOCORRELATION: WFR 18

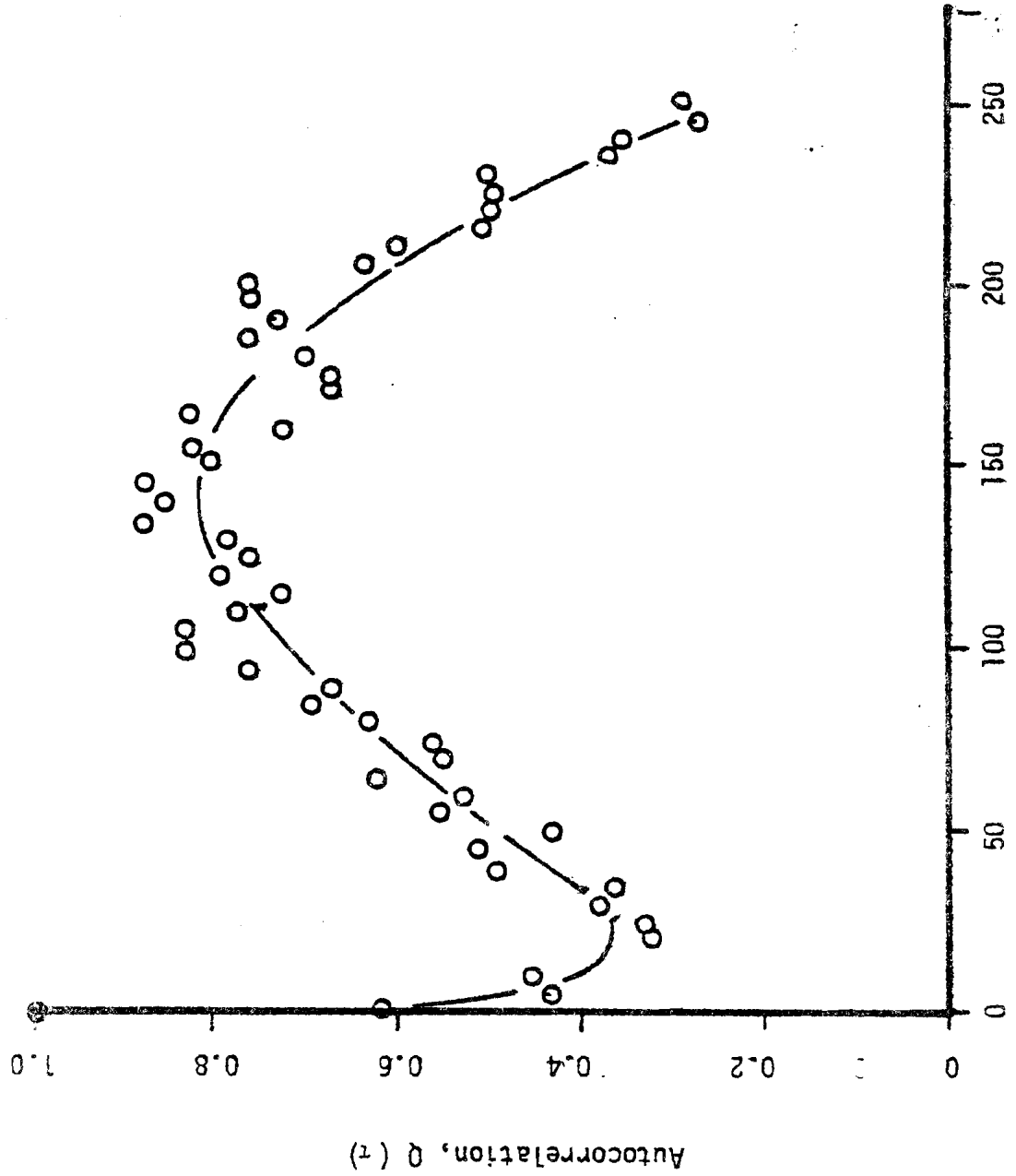

FIGURE 30. WIND DIRECTION AUTOCORRELATION: WFR 22

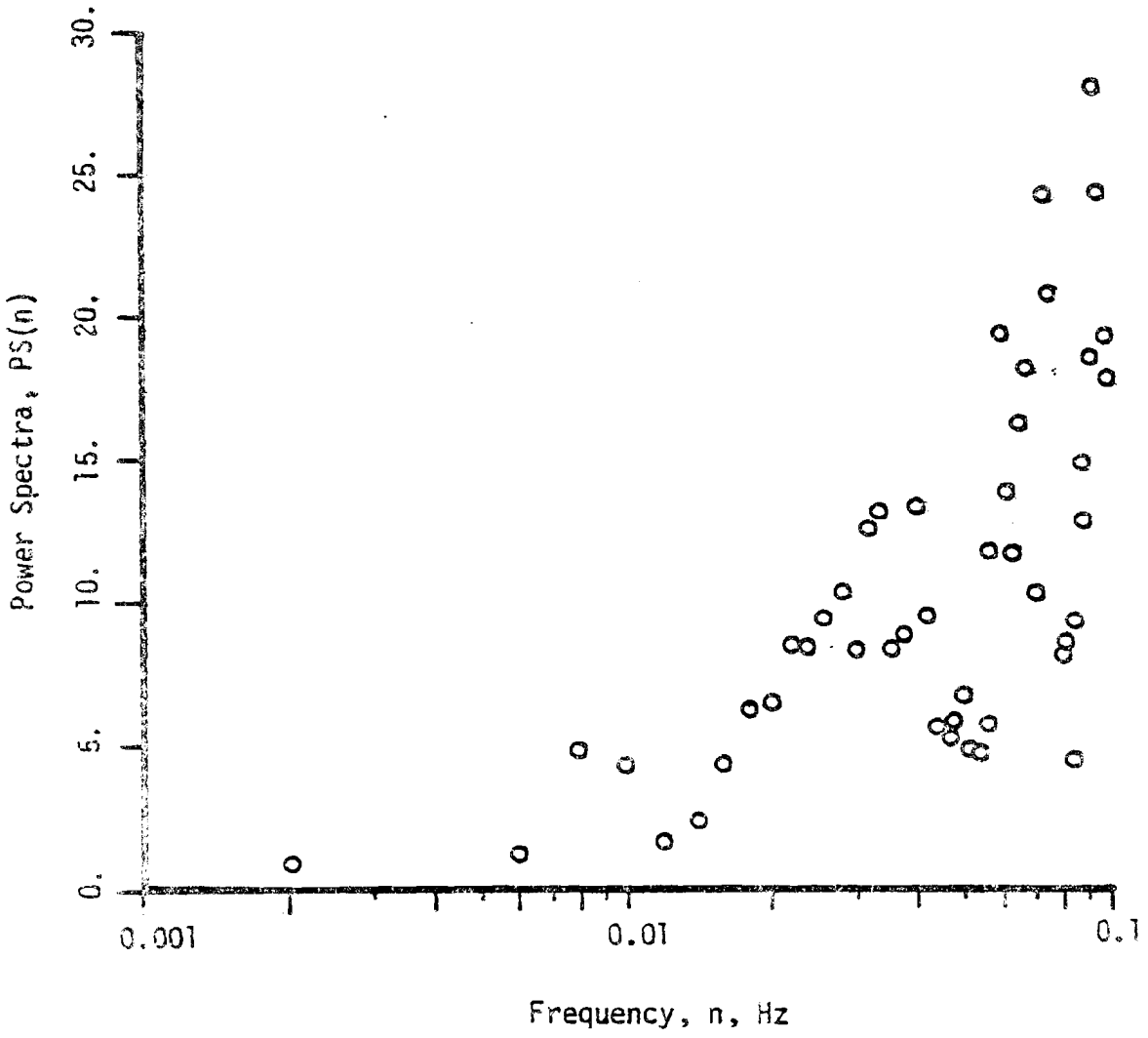

FIGURE 31. WIND DIRECTION POWER SPECTRA : WFR 3

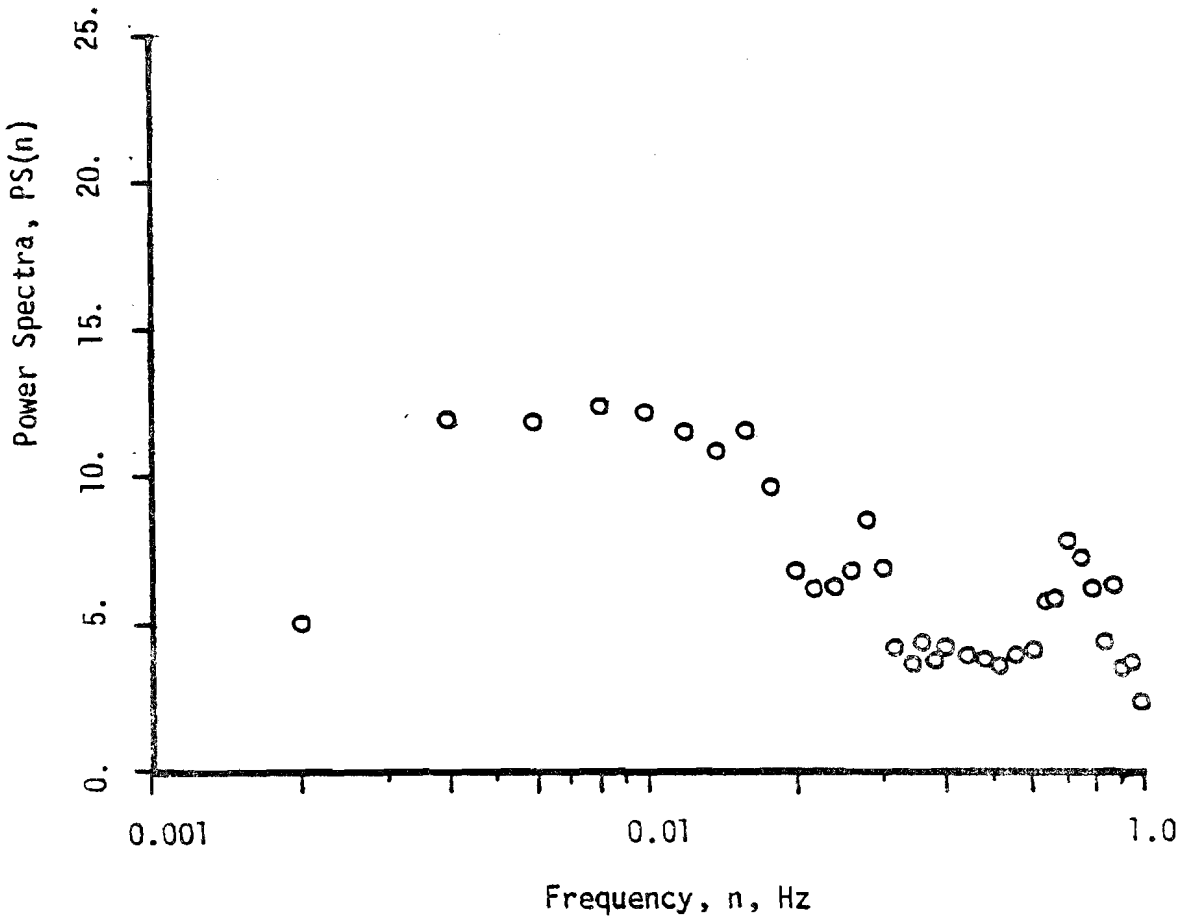

FIGURE 32. WIND DIRECTION POWER SPECTRA: WFR 5

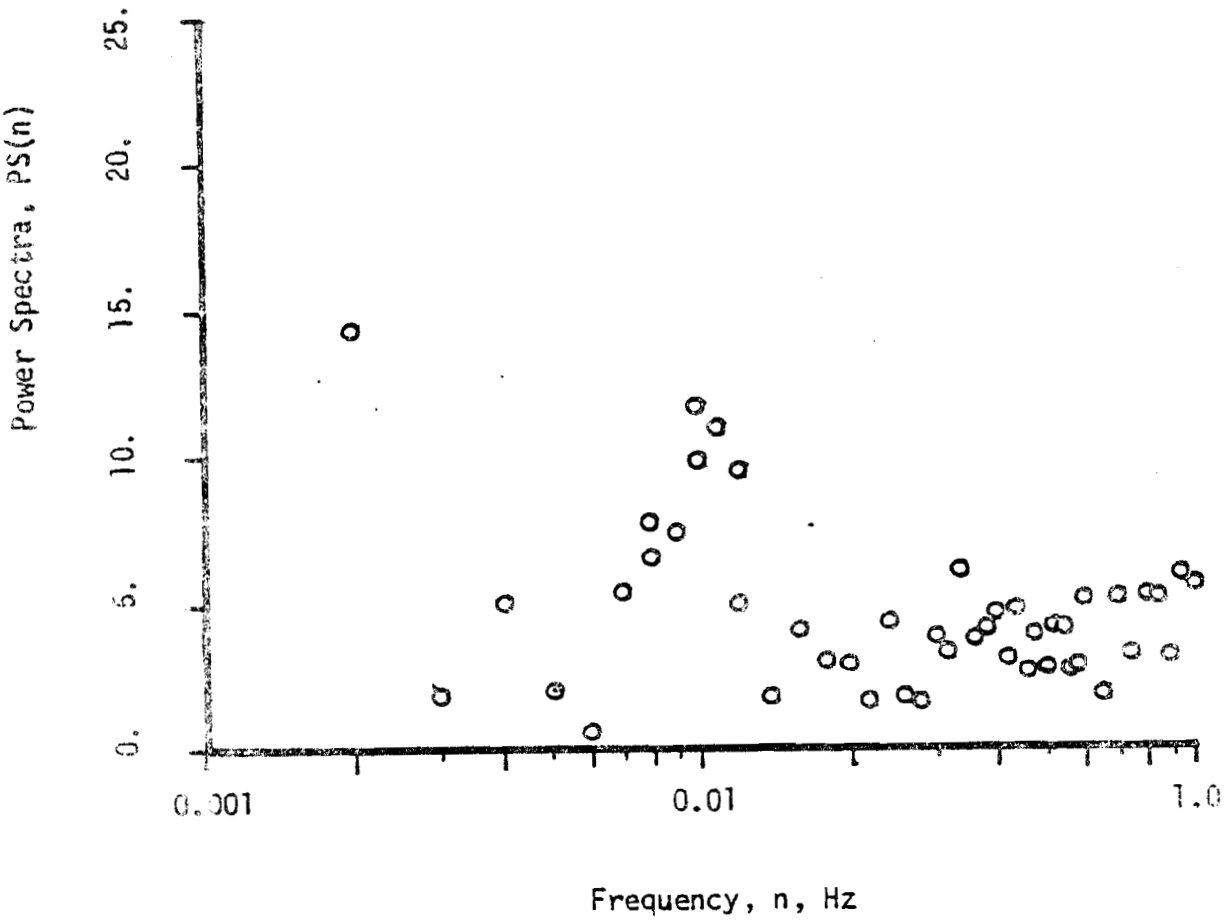

FIGURE 33. WIND DIRECTION POWER SPECTRA: WFR 17

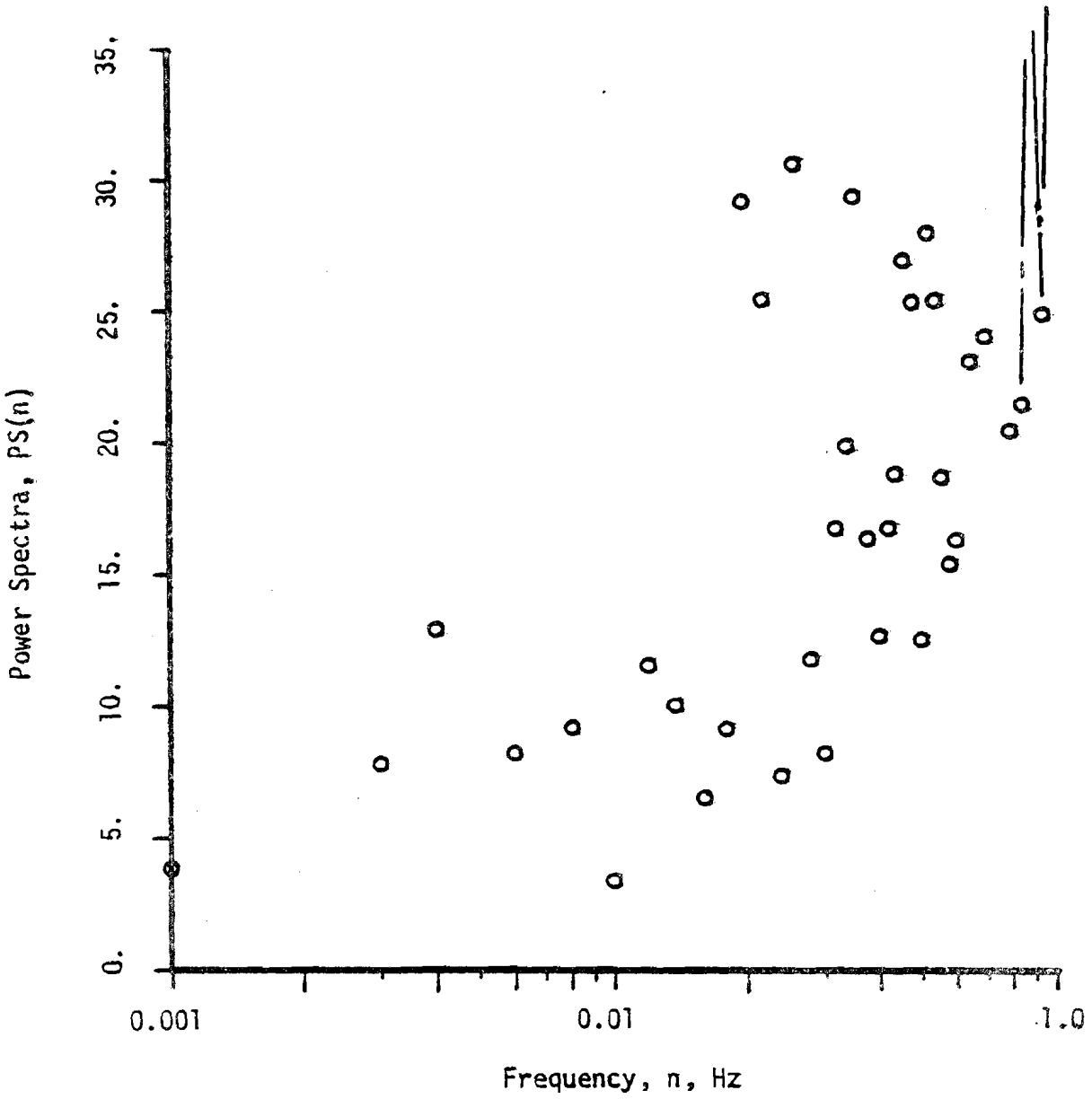

FIGURE 34. WIND DIRECTION POWER SPECTRA : WFR 18

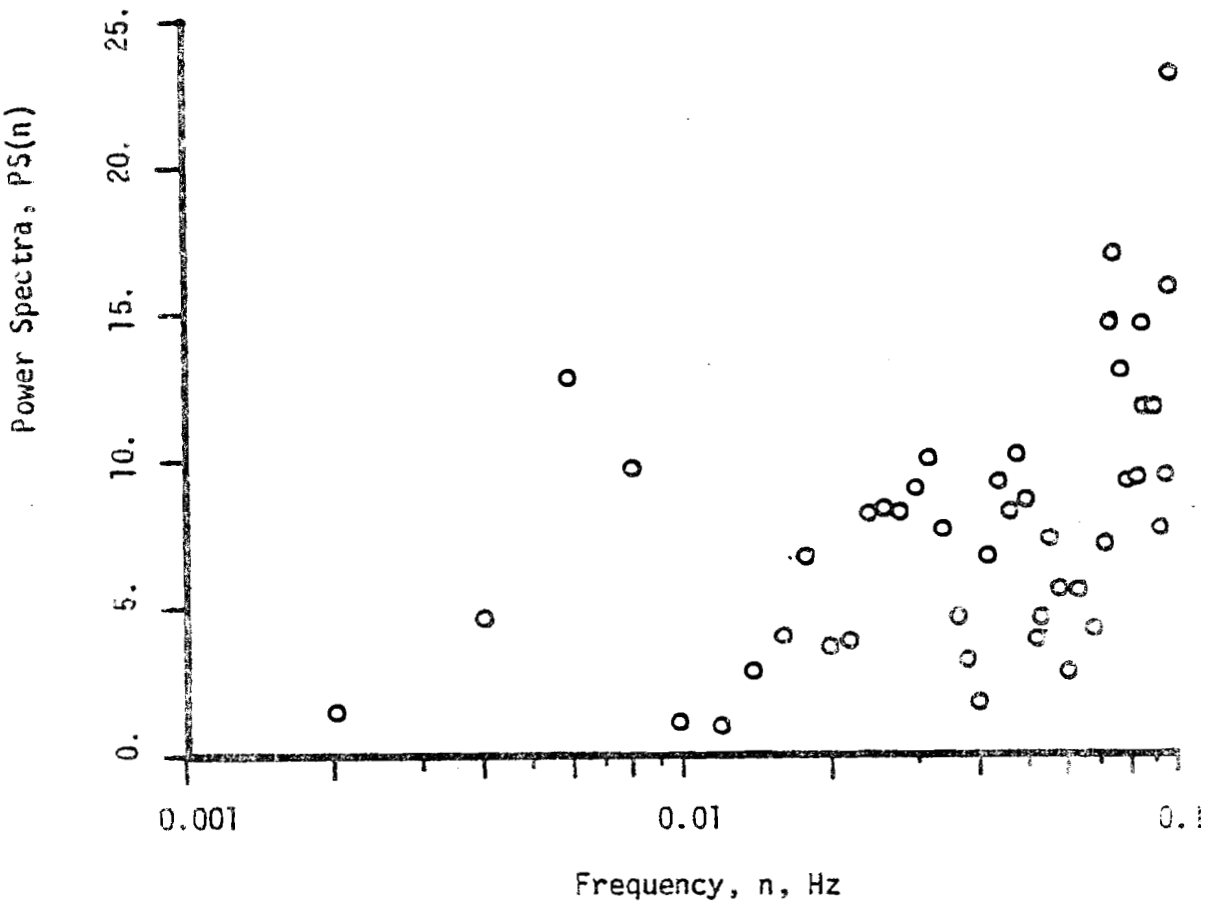

FIGURE 35. WIND DIRECTION POWER SPECTRA: WFR 21

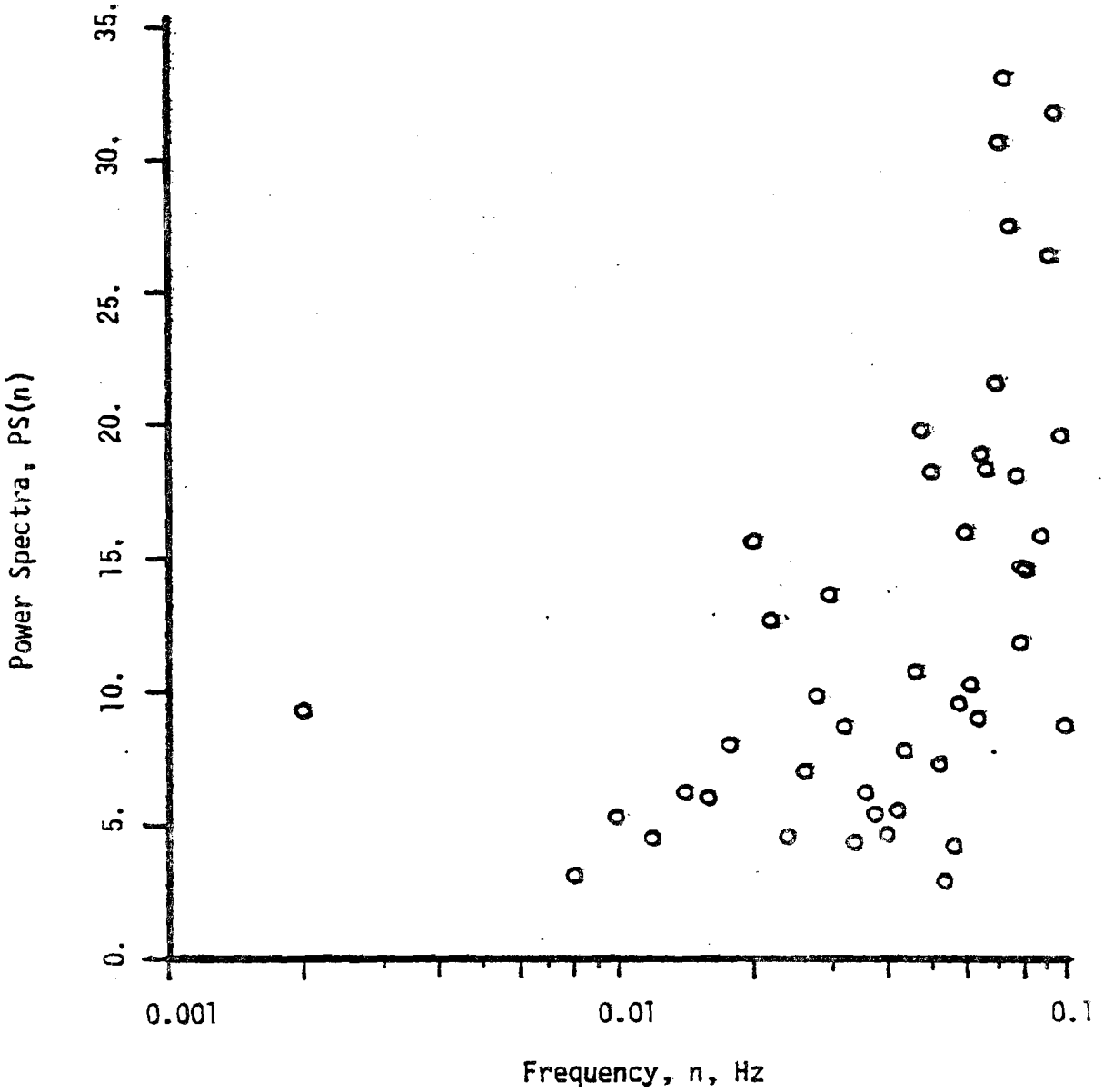

FIGURE 36. WIND DIRECTION POWER SPECTRA : WFR 22

In WFR22, Fig. 24, the only resolved point below 0.008 Hz seems to indicate a continued rise in the PSD with a slope just less than -5/3.

As discussed in Section 2.2.3, the autocorrelation of a harmonic function with superimposed noise has a form similar to Fig. 3b. This type of trend is seen in all of the autocorrelations which resolve frequencies in the 0.001 to 0.01 Hz band (Figs. 25, 28 and 30). An estimate of the frequency and period of these low frequency harmonics can be made from the autocorrelation. For example, in Fig. 28 one cycle of this harmonic is seen to occur between $\tau = 0$ and $\tau = 150s$. The period, T, is estimated to be 150s, and the frequency, n, is approximately 0.0067 Hz. There is close agreement with this result and the associated PSD (Fig. 23), which shows a peak at 0.006 Hz indicating a strong harmonic component at this frequency. The estimates for the period and frequency of these harmonics are shown in Table 5.

Drawing from the analysis of the wind speed fluctuations, it is expected that two different integral length scales will be predicted for the records analyzed with $\Delta t = 0.5s$ and $\Delta t = 5.0s$. This should be particularly evident in the average gust length predicted for $v'(t)$, since the autocorrelations for records sampled at $\Delta t = 0.5s$ cannot resolve the low frequency harmonic components. In addition, these autocorrelations will be dominated by higher frequency noise, tending to shorten the predicted length scale.

The integral scales as calculated from the autocorrelation and from Teunissen[18] are shown in Table 5. Teunissen's relation for calculating the integral length scale is shown below:

$$L_v = \frac{0.106\ U}{n_p} \qquad (51)$$

The integral time scale, of course, is related to the length scale through the mean wind speed.

Comparison of each data record in Table 5 shows that records WFR3, 21, and 22 do show a significantly longer length scale than WFR5, 17, or 18.

It is expected that the disparity between the length scale calculated by records sampled at $\Delta t = 5s$ and those sampled at $\Delta t = 0.5s$ is because the records sampled at $\Delta t = 0.5s$ could not resolve the average gust.

A comparison of the integral length scales calculated by the autocorrelation and power spectra techniques show that a reasonable agreement exists between the two predicted scales, considering the inherent difficulties.

3.3 Characterization of Machine Response

3.3.1 RPM

Fluctuations in the angular velocity of the blade disc are primarily influenced by fluctuations in wind speed. The RPM power spectral density shows how the power in the fluctuations is distributed with frequency. These are shown in Figs. 37 through 39. Each figure is the combined result of the analysis of one analog record with two sampling rates.

Comparison of these power spectral densities shows that the slope of the curve at low frequencies is approximately -5/3. The slope increase in steepness with the frequency, falling off sharply above 0.01 Hz. Above 0.10 Hz, the power in the fluctuations is three

WFR	PEAK FREQUENCY IN POWER SPECTRA n_p, Hz	AVERAGE WIND SPEED, U, m/s	DOWNSTREAM INTEGRAL LENGTH SCALE L_v, m FROM PS(n)	DOWNSTREAM INTEGRAL LENGTH SCALE L_v, m FROM AUTOCORRELATION	DOWNSTREAM INTEGRAL TIME SCALE T_v, s FROM PS(n)	DOWNSTREAM INTEGRAL TIME SCALE FROM AUTO-CORRELATION
3*	.094	6.35	7.2	34.7	1.1	5.47
	.008		84.		13.3	
5	.08	4.58	6.1	7.38	1.3	1.58
17*	.02	6.96	36.9	7.38	5.3	2.3
	0.1		7.4		1.06	
21*	0.1	7.00	7.4	93.1	1.1	13.3
	0.006		124.		17.7	
18*	1.0	4.57	.48	13.7	.11	3.0
	.026		18.6		4.1	
22*	.092	6.05	7.0	56.3	1.2	9.3
	.02		32.1		5.3	
	.002		321.		5.3	

*Multiple peaks occur in these power spectra, each of which is represented. The dominant peak is given first.

TABLE 5. CROSS-STREAM INTEGRAL SCALES

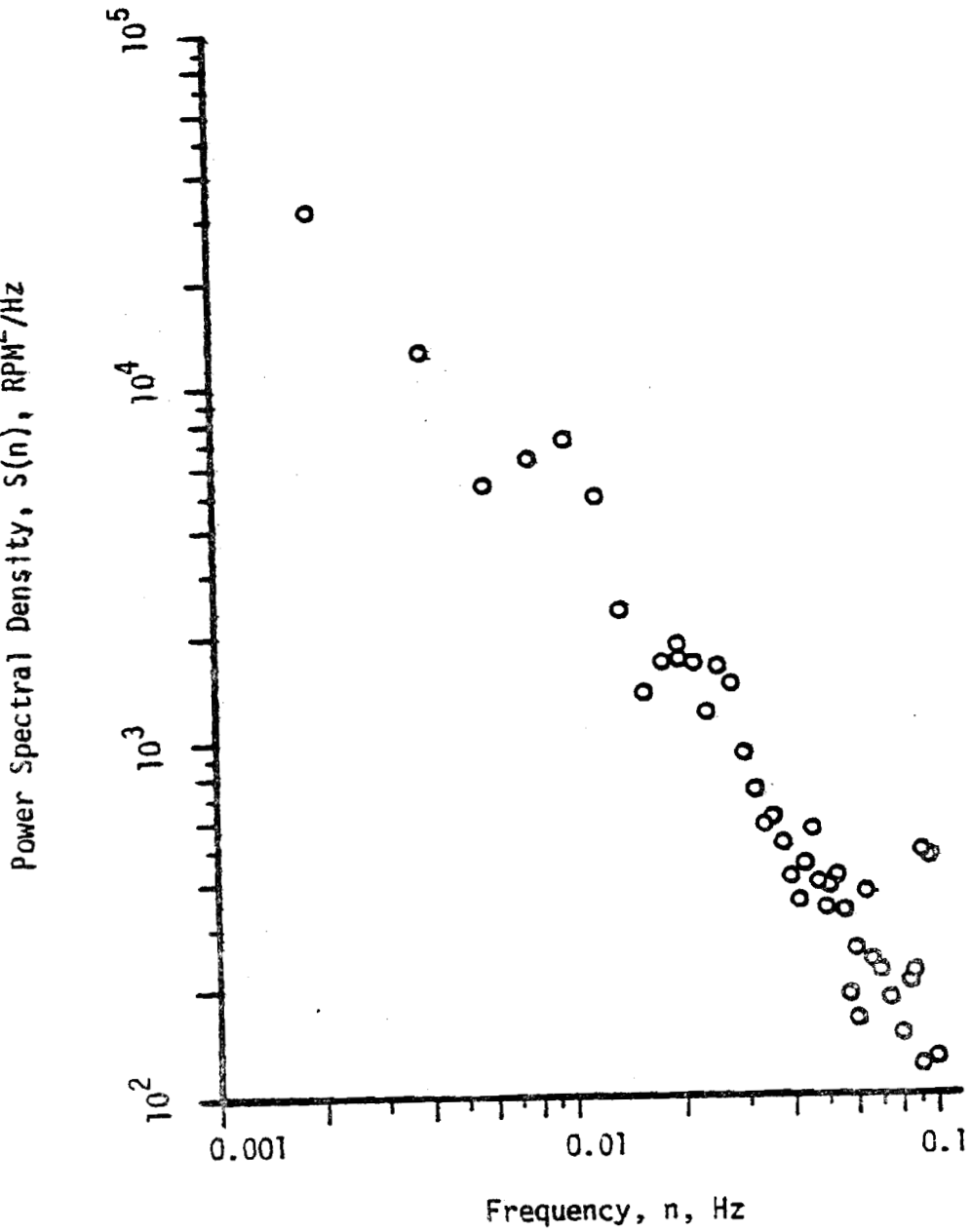

FIGURE 37. RPM POWER SPECTRAL DENSITY: WFR 3/5

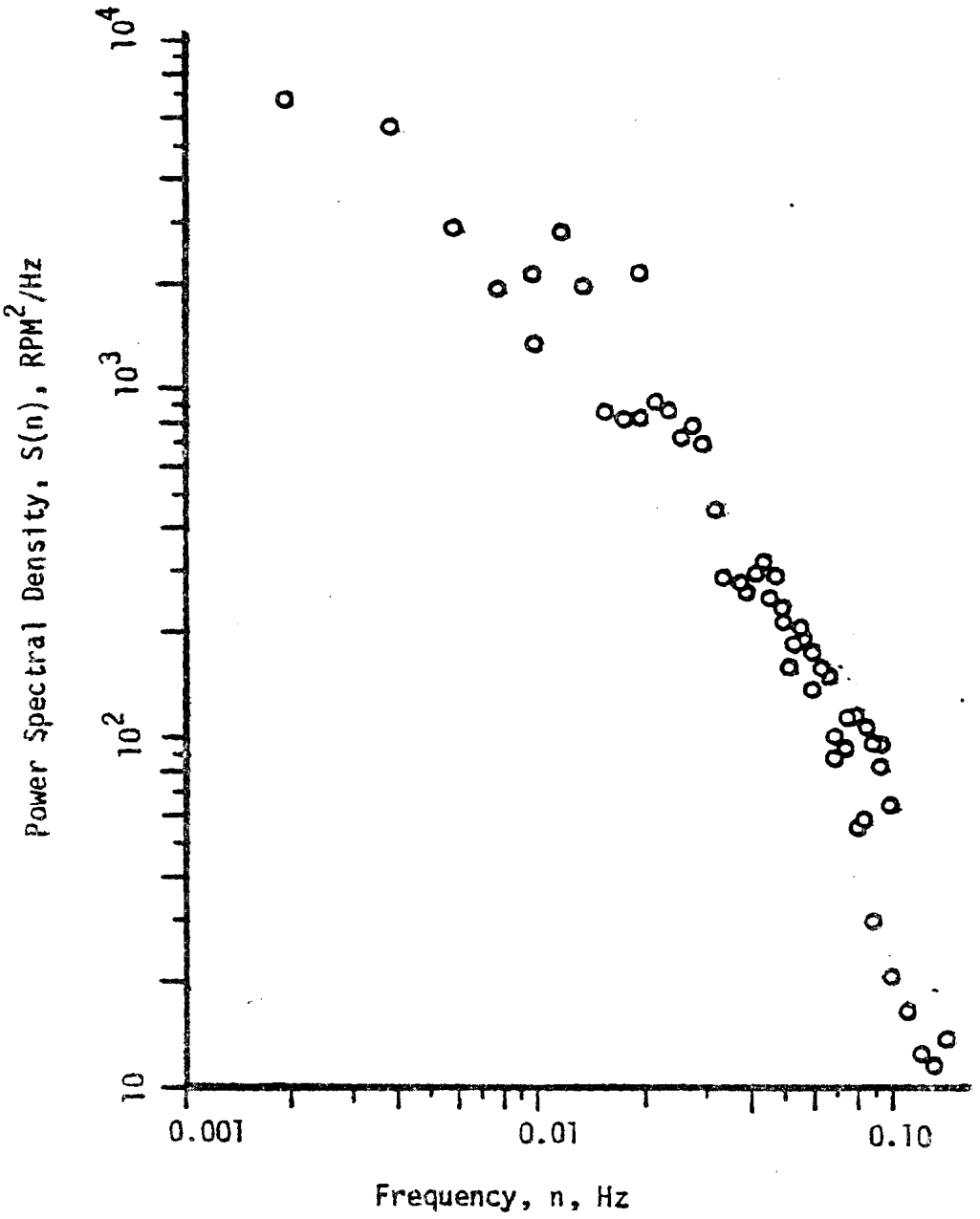

FIGURE 38. RPM POWER SPECTRAL DENSITY: WFR 17/21

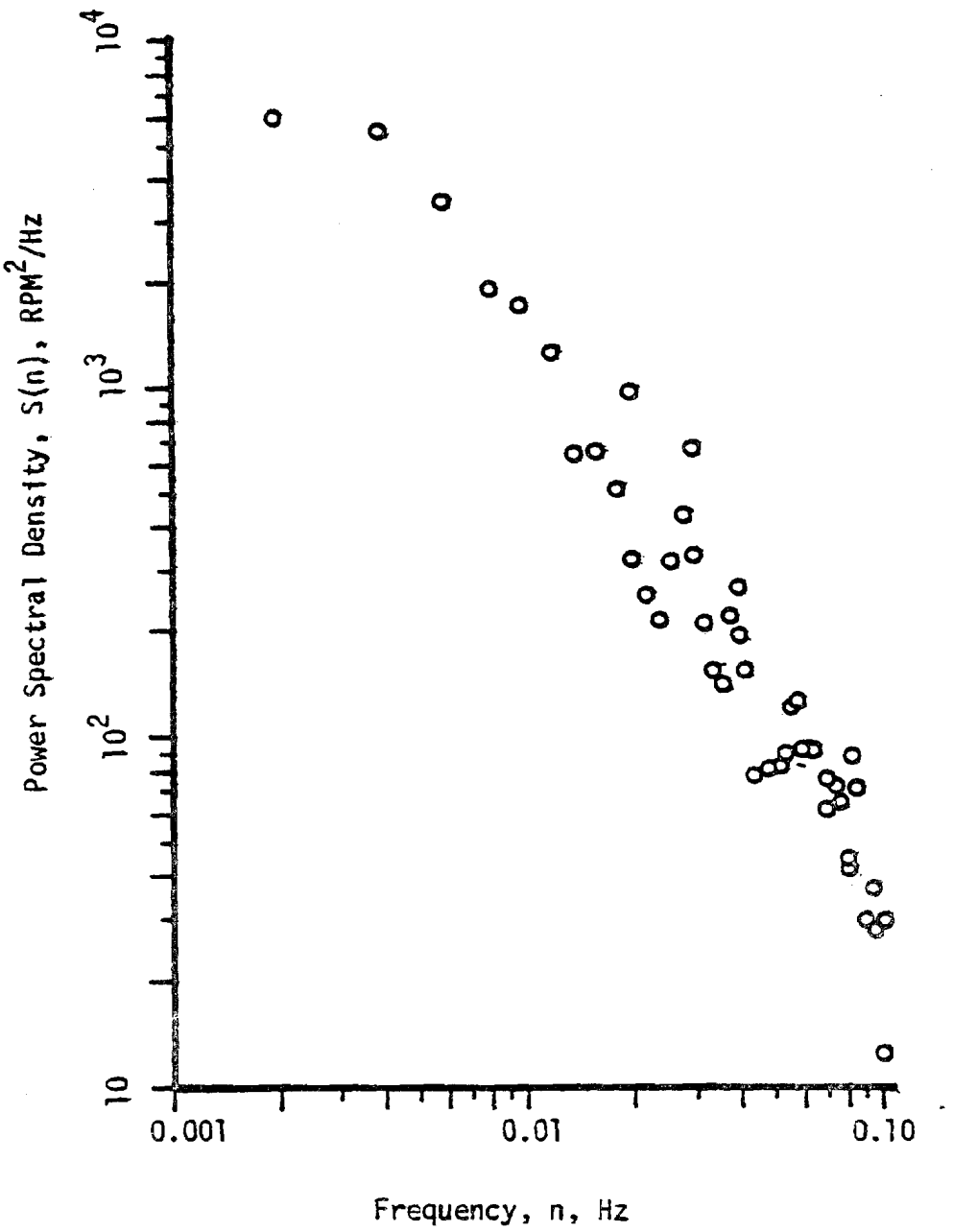

FIGURE 39. RPM POWER SPECTRAL DENSITY: WFR 18/22

orders of magnitude smaller than that at 0.001 Hz.

The PSD in WFR21 (Fig. 38) and WFR22 (Fig. 39) are nearly identical in magnitude over all resolved frequencies, shown in an overlay of the two spectra (Fig. 40). This indicates that although the yaw was undamped in WFR21 (see Section 3.3.3), the fluctuations in the RPM were primarily unchanged in magnitude and frequency. This supports the assumption that yaw/RPM are decoupled responses.

The PSD is only part of the response characterizations. To determine how well power is transferred from the wind speed fluctuations to fluctuations in RPM, the transfer and coherence functions must be analyzed.

3.3.2 Generator Output Current

The analysis of the fluctuations in the generator output current is similar to the RPM. The generator characteristics could be analyzed by studying the interaction between the RPM and current fluctuations, but consistent with the "black-box" system approach, only the wind speed/current interactions are studied. The current time series was not measured for WFR18/22.

Some comparison can be made between records WFR3/5 and WFR17/21, to determine the effect of the undamped yaw on the current fluctuations, but this is difficult because of significantly different experimental conditions. However, since the current fluctuations are directly influenced by RPM fluctuations, which indicate that yaw/RPM are decoupled responses, it is also felt that yaw/current are also decoupled responses.

The power spectral densities for WFR3/5 and 17/21 are shown in Figs. 41 through 42. Both WFR3 and WFR21 show flat peaks in the PSD.

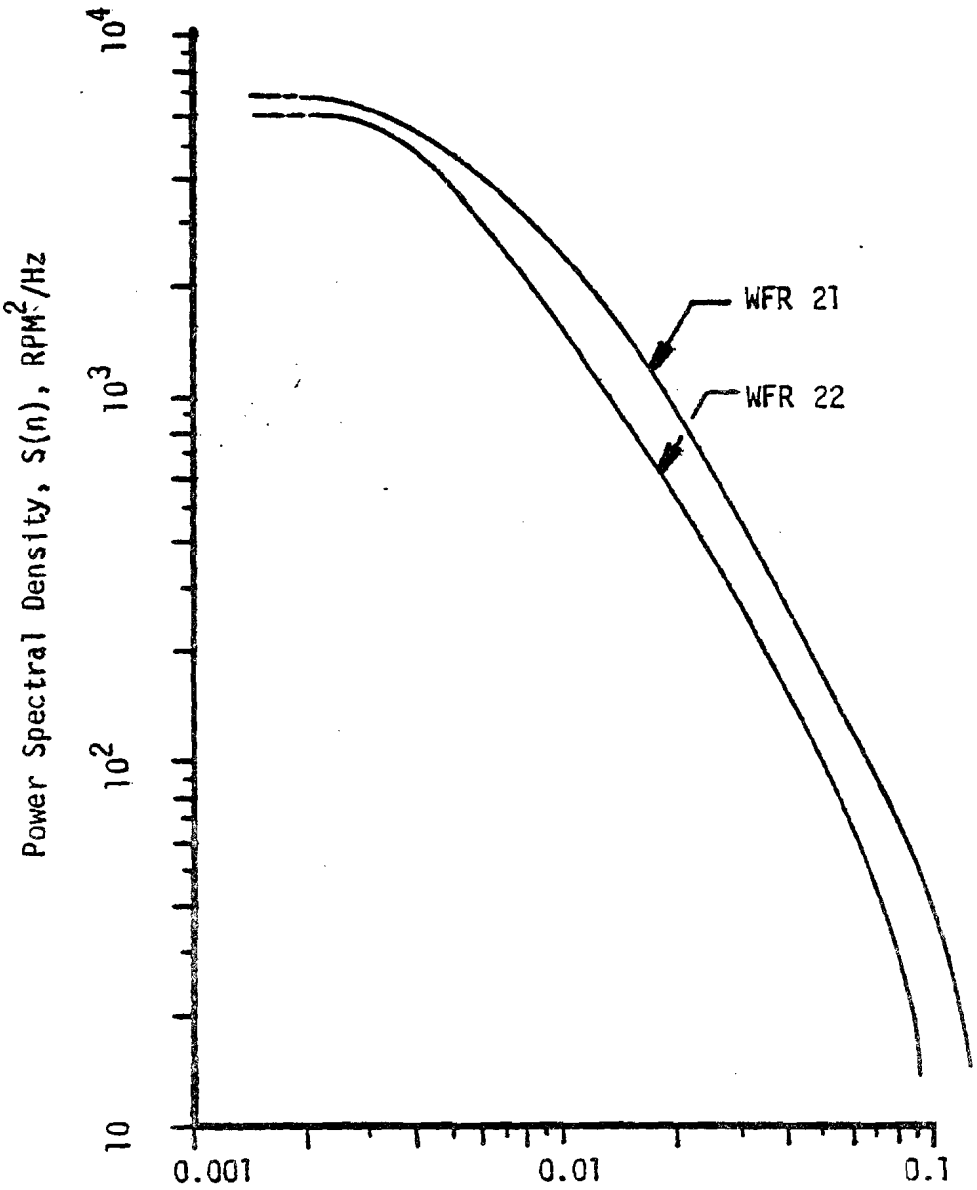

FIGURE 40. RPM POWER SPECTRAL DENSITY OVERLAY

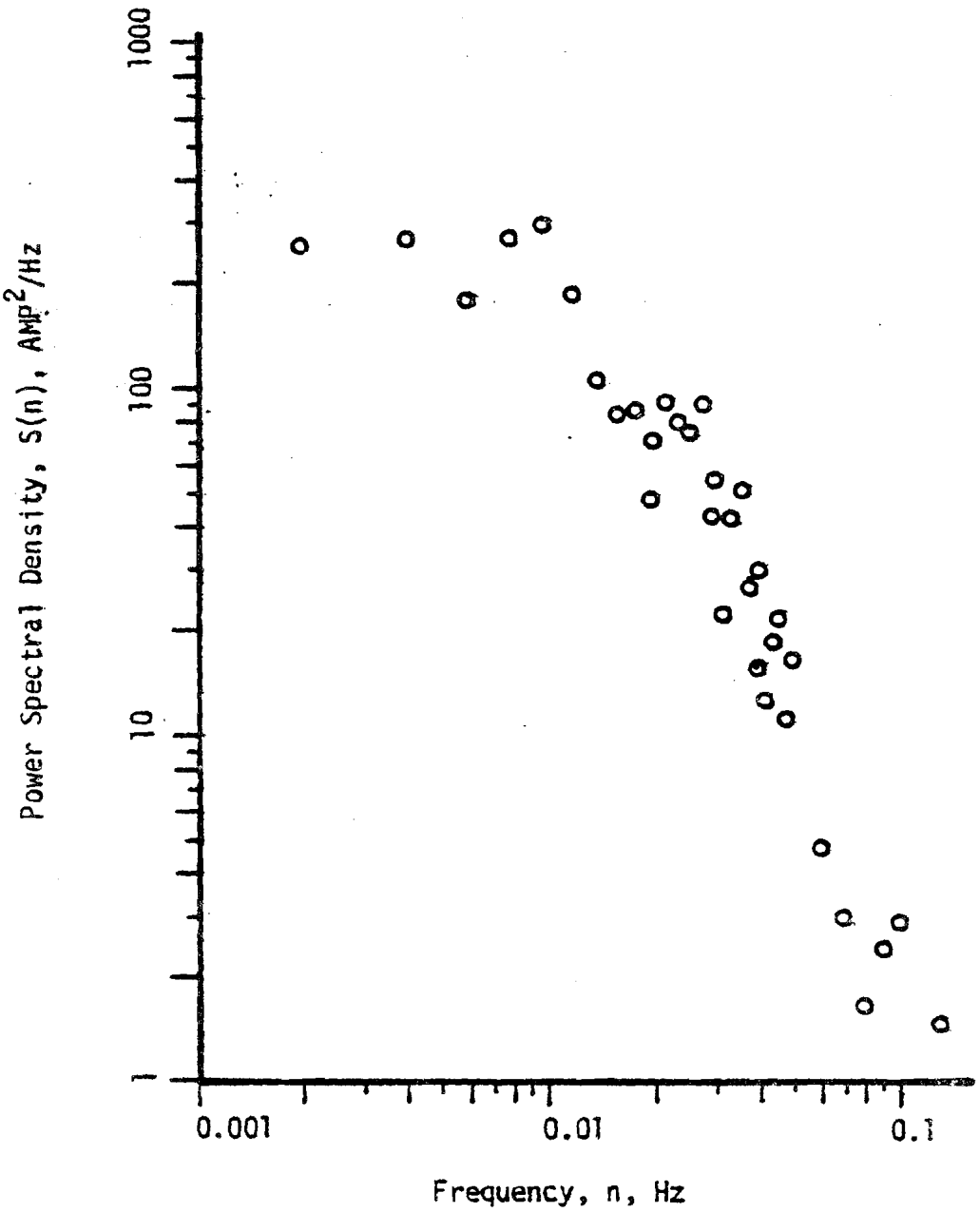

FIGURE 41. CURRENT POWER SPECTRAL DENSITY: WFR 3/5

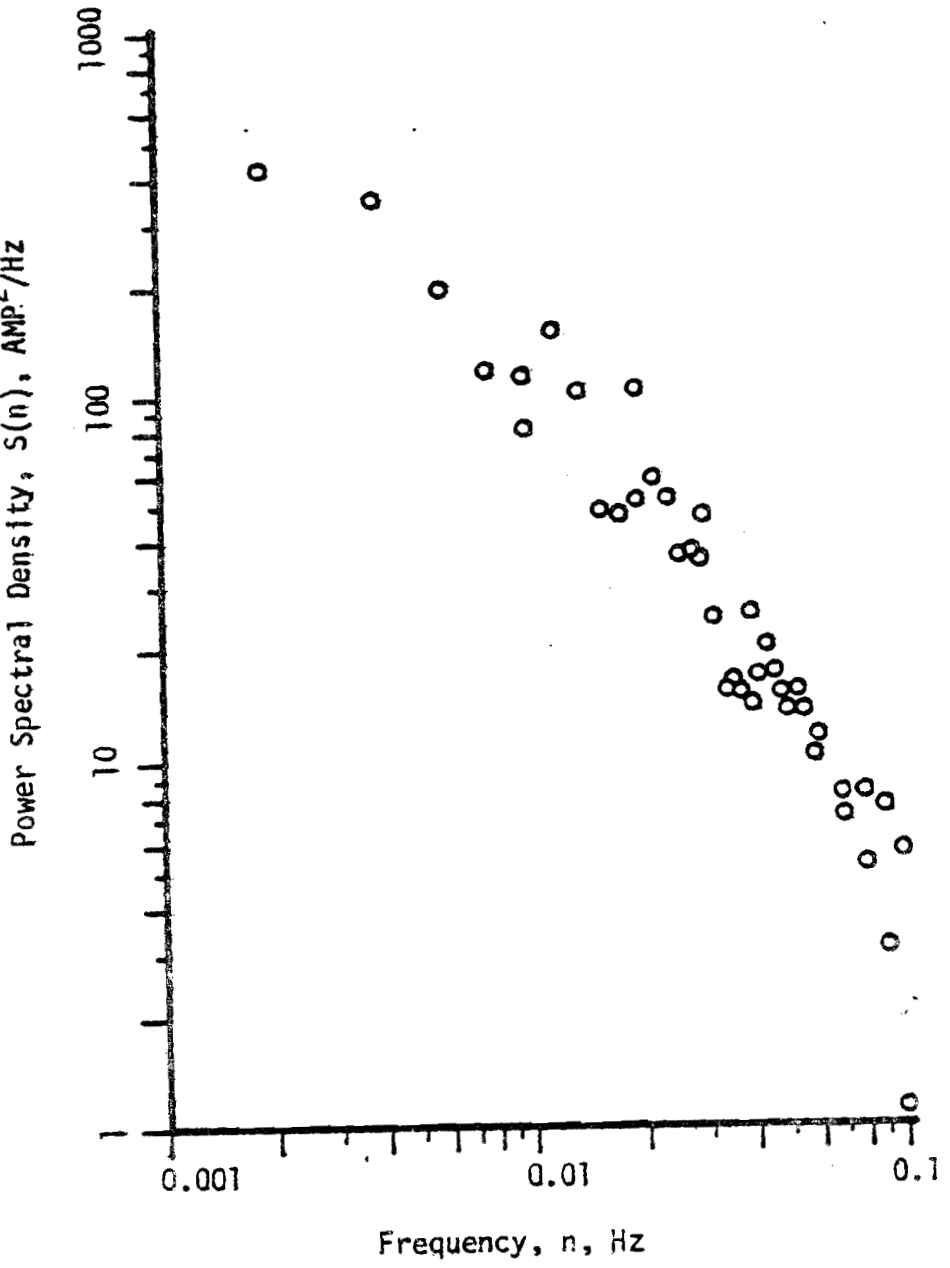

FIGURE 42. CURRENT POWER SPECTRAL DENSITY: WFR 17/21

The peaks in WFR3, though similar in magnitude to the peak in WFR21, occurs at a higher frequency. The peak in WFR3 occurs near 0.01 Hz, compared to WFR21 which has a more clearly defined peak near 0.002 Hz. In both, the PSD falls of approximately to the -5/3 power above 0.01 Hz. They show that the fluctuations contain an insignificant amount of power above 0.2 Hz. In these respects, the PSD for current is similar to the PSD for RPM.

3.3.3 Yaw

The characterization of the yaw angle fluctuations as a response to changing wind directions is important in determining the effectiveness of yaw damping. The machine yaw is damped by shorting the field leads of the yaw driver motor. In this mode, the motor acts as a generator and applies a self-induced restoring torque to the nacelle; this has the tendency to damp out high frequency fluctuations. This should help the machine track the changing wind direction.

WFR3/5 and 18/22 were taken with the yaw damped. WFR17/21 was taken with yaw undamped (i.e., the leads to the yaw driver motor were not shorted). During the recording of WFR17/21, large changes in yaw positions were seen where the wind speed decreased quickly. The nacelle tended to yaw 90° to the west from the NNW mean position. This is attributed to the gryoscopic moments on the nacelle from the changing disc RPM. Cohen[19] has studied this effect analytically.

The power spectral densities for the three analog records is shown in Figs. 43 through 45. Comparison of Figs. 43 and 45 with Fig. 44 shows a sharp constant in power distributions at frequencies above 0.10 Hz. For WFR5 and WFR18, power in the yaw fluctuations above

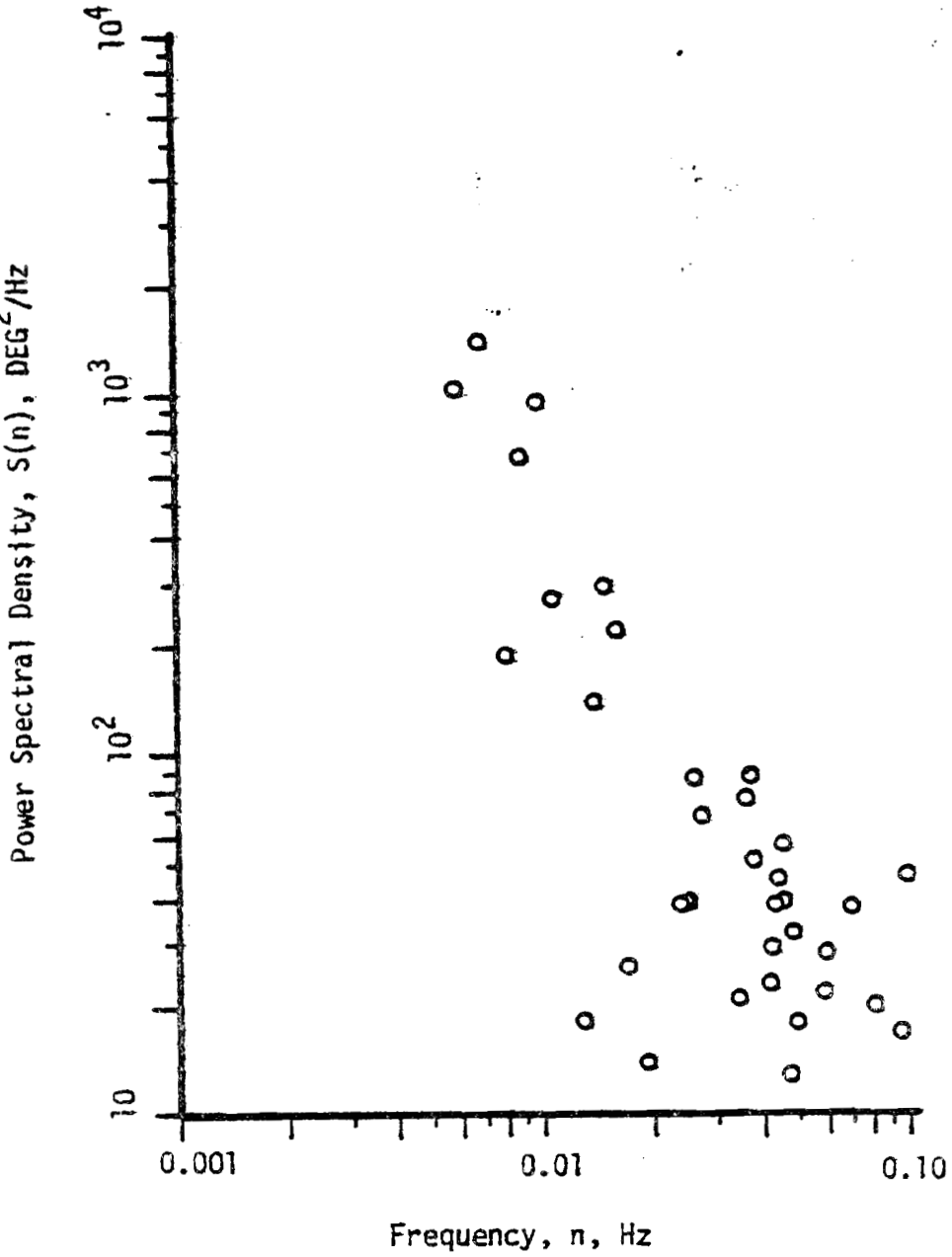

FIGURE 43. YAW POWER SPECTRAL DENSITY: WFR 3/5

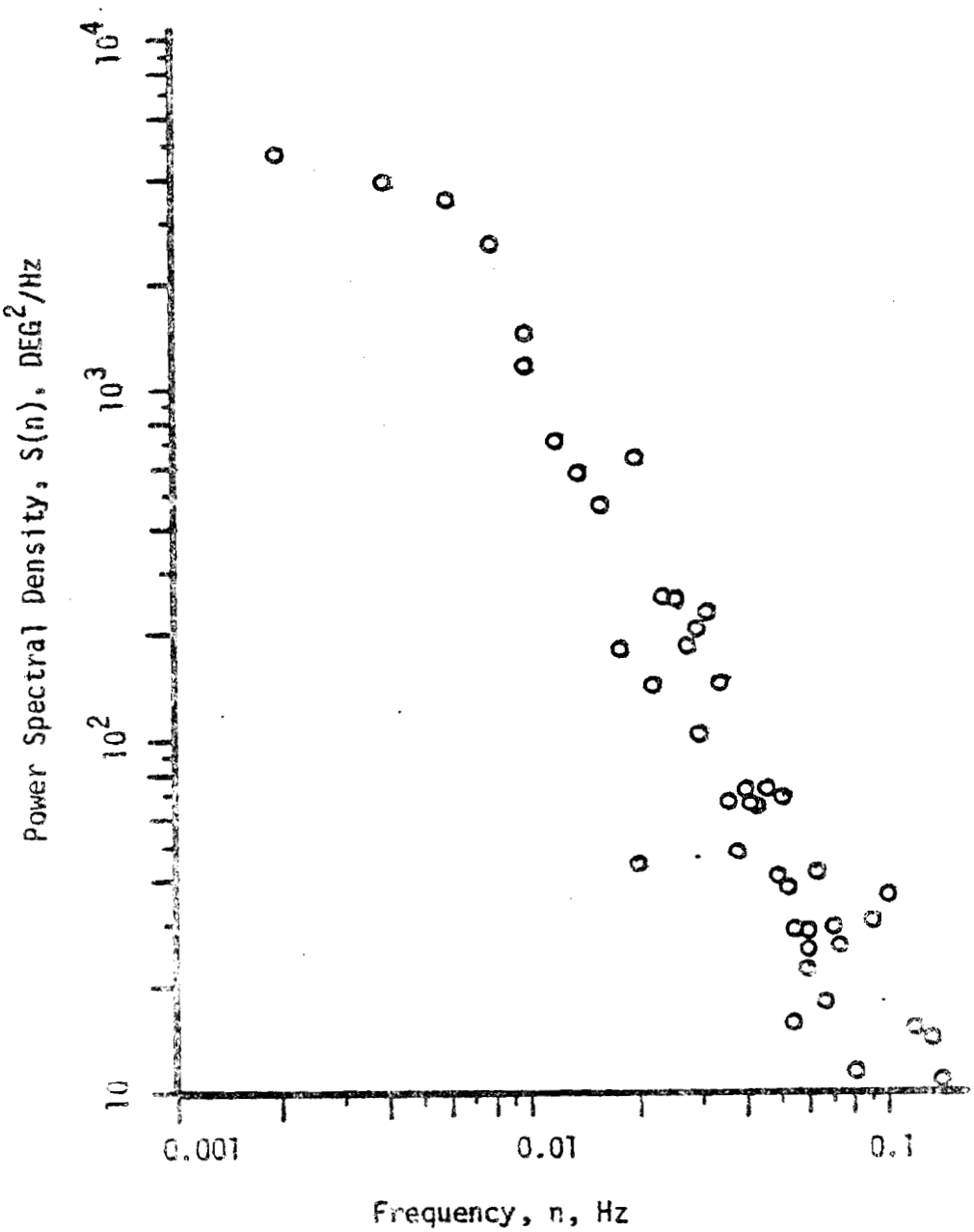

FIGURE 44. YAW POWER SPECTRAL DENSITY: WFR 17/21

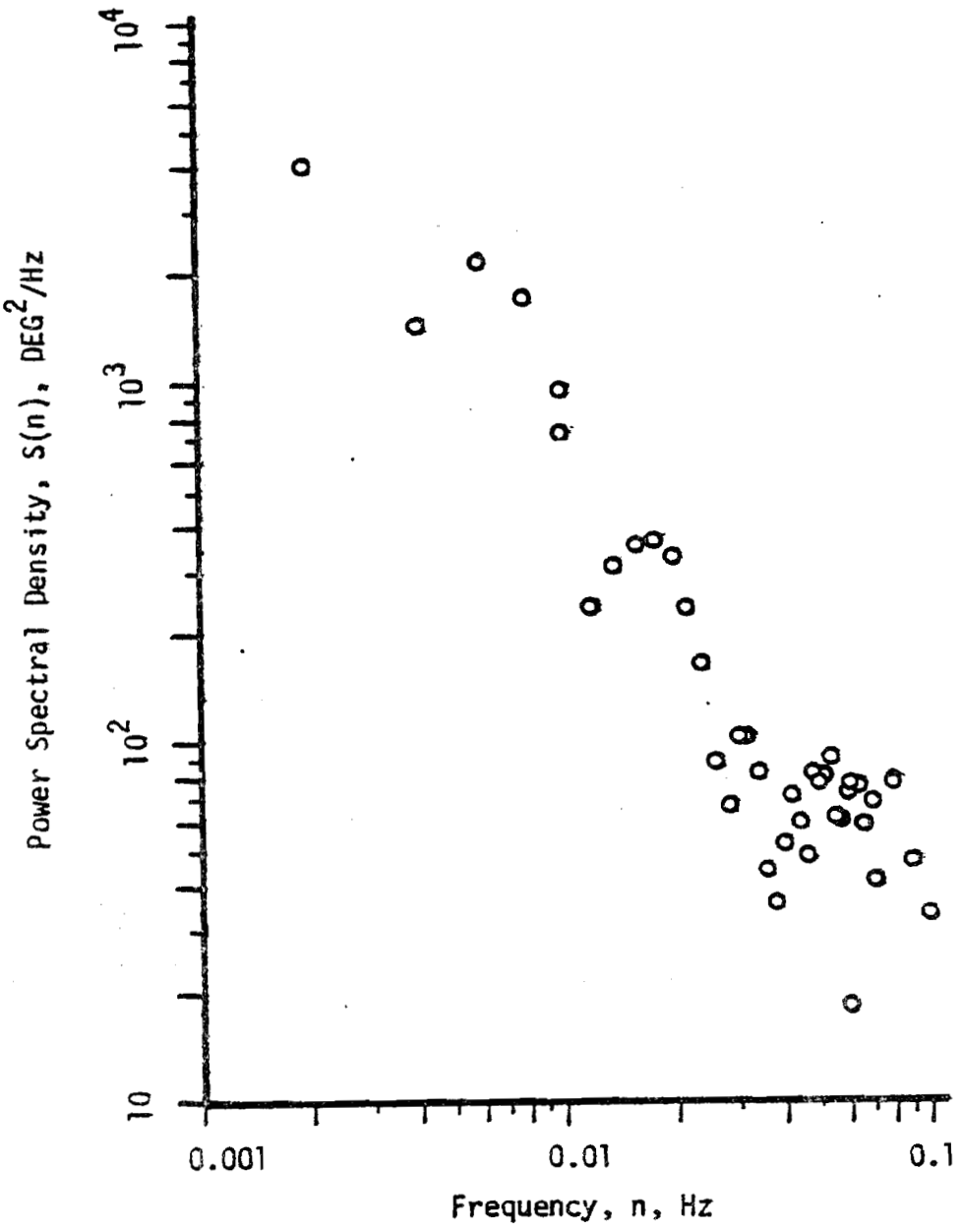

FIGURE 45. YAW POWER SPECTRAL DENSITY: WFR 18/22

0.10 Hz is distributed uniformly to 1.0 Hz, the highest resolved frequency: WFR17 shows almost no power in the fluctuations above 0.02 Hz. The power in the low frequency fluctuations is substantially greater in WFR21 than in either WFR3 or WFR22. At 0.002 Hz in WFR22, however, the PSD peaks at a magnitude comparable with WFR21 at this frequency. But from Fig. 24 it is known that this is the frequency of the low frequency harmonic in the wind direction fluctuations. From this it is concluded that damped or undamped, the nacelle follows closely the lowest frequency components of the changing wind direction.

This can be seen also in the autocorrelations of the nacelle yaw, given in Figs. 46 through 51. The period of the long term fluctuations as estimated from the autocorrelation are shown in Table 6, along with the strong harmonic frequencies from Table 5.

Substantial agreement exists between the frequencies for yaw and wind direction for WFR21 and 22 in Table 6. However, WFR3 shows that the nacelle is tracking a higher frequency component in the wind than the lowest found from the wind direction autocorrelation. By examining the PSD for WFR3 wind direction, it is seen that the PSD peak is at the tracking frequency, 0.008 Hz. This probably means that the 0.008 Hz harmonic contains more power than the 0.0025 Hz component. This cannot be verified directly, since the 0.0025 Hz peak was not resolved in the PSD.

The good comparison of results in Table 6 shows that at the lowest frequencies, the nacelle tracks the wind, whether damped or not.

The presence of sharply defined narrow peaks in the yaw power spectral densities indicates a mechanical resonance at these points.

ANALOG WFR	DIGITAL WFR	PEAK FREQUENCY CROSS-STREAM VELOCITY v(t), Hz	PEAK FREQUENCY* MACHINE YAW FLUCTUATIONS, Hz	YAW PERIOD FROM AUTO-CORRELATION,s
9	3/5	0.008	0.008	130
11	17/21	0.006	0.005	200
10	18/22	0.002	0.002	300

*Based on Longest Integral Length Scale.

TABLE 6. LOW FREQUENCY FLUCTUATIONS IN NACELLE YAW ANGLE IN RELATION TO WIND DIRECTION FLUCTUATIONS

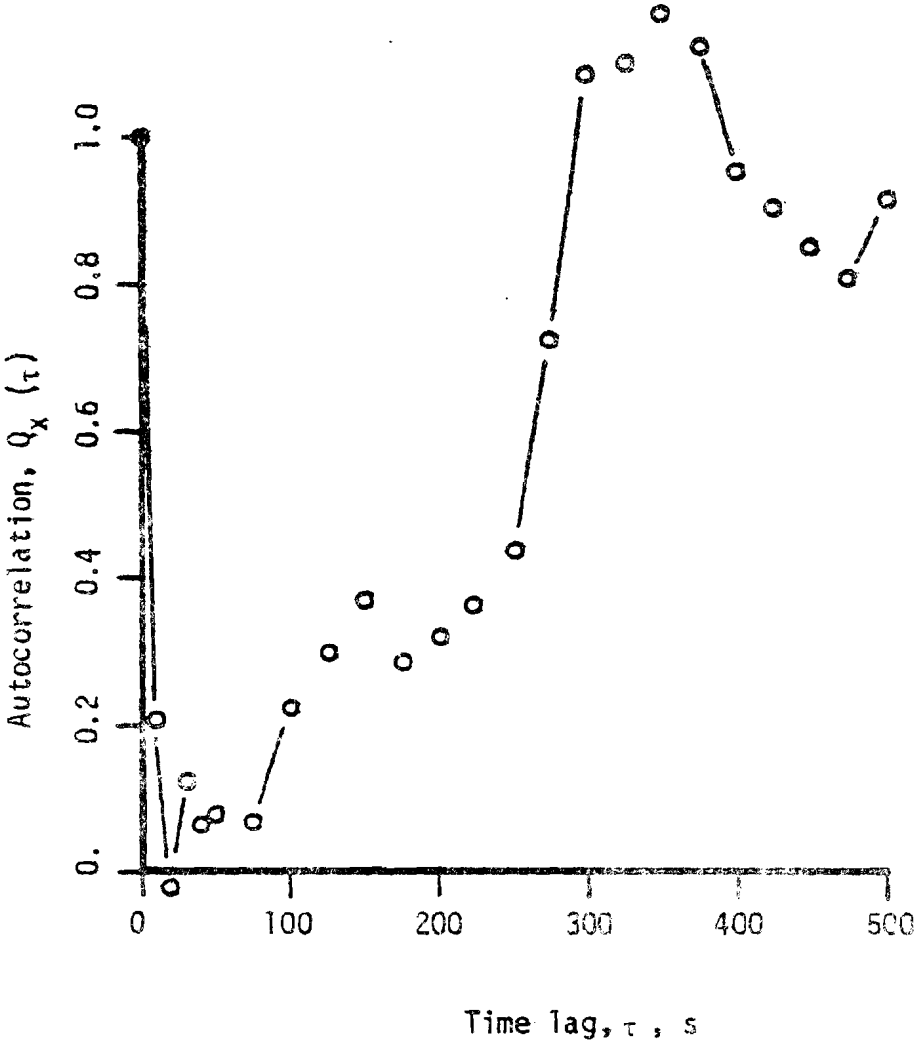

FIGURE 46. YAW AUTOCORRELATION: WFR 3

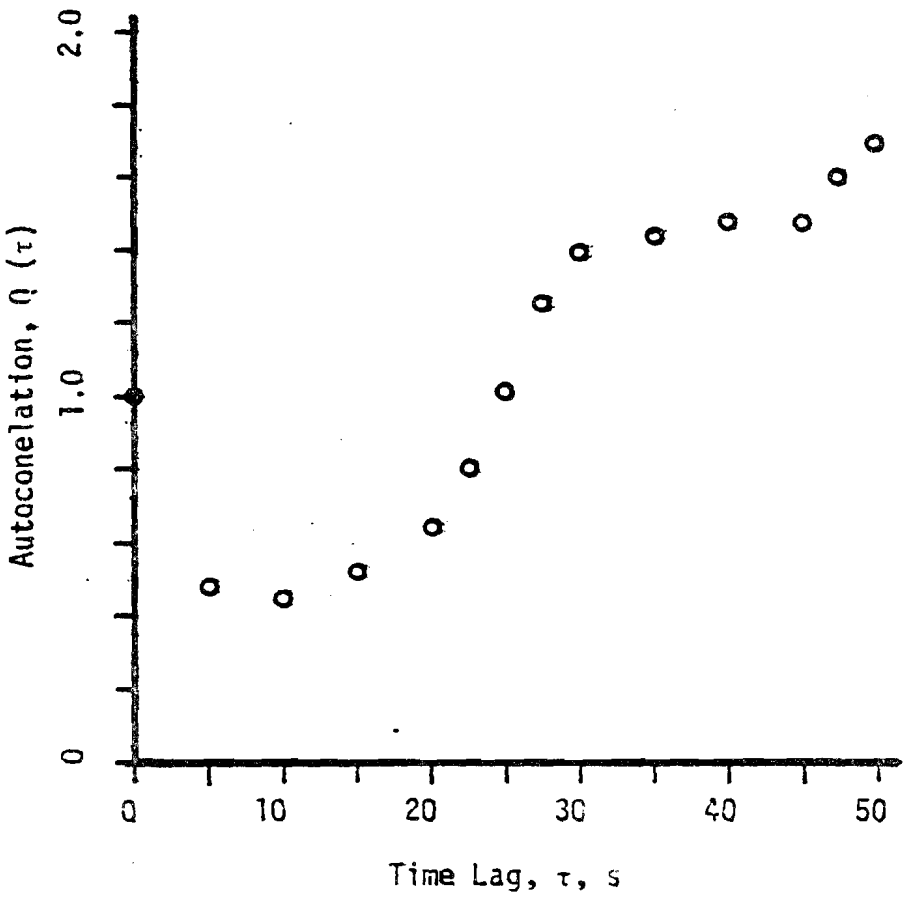

FIGURE 47. YAW AUTOCORRELATION: WFR 5

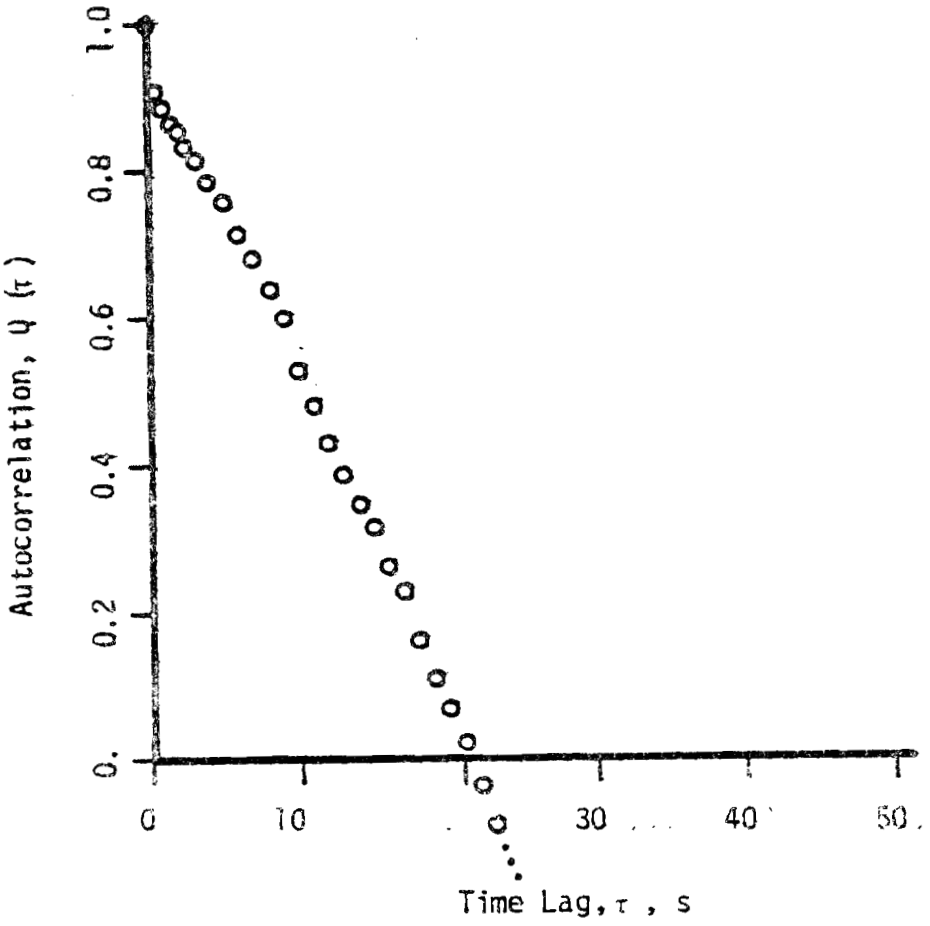

FIGURE 48. YAW AUTOCORRELATION: WFR 17

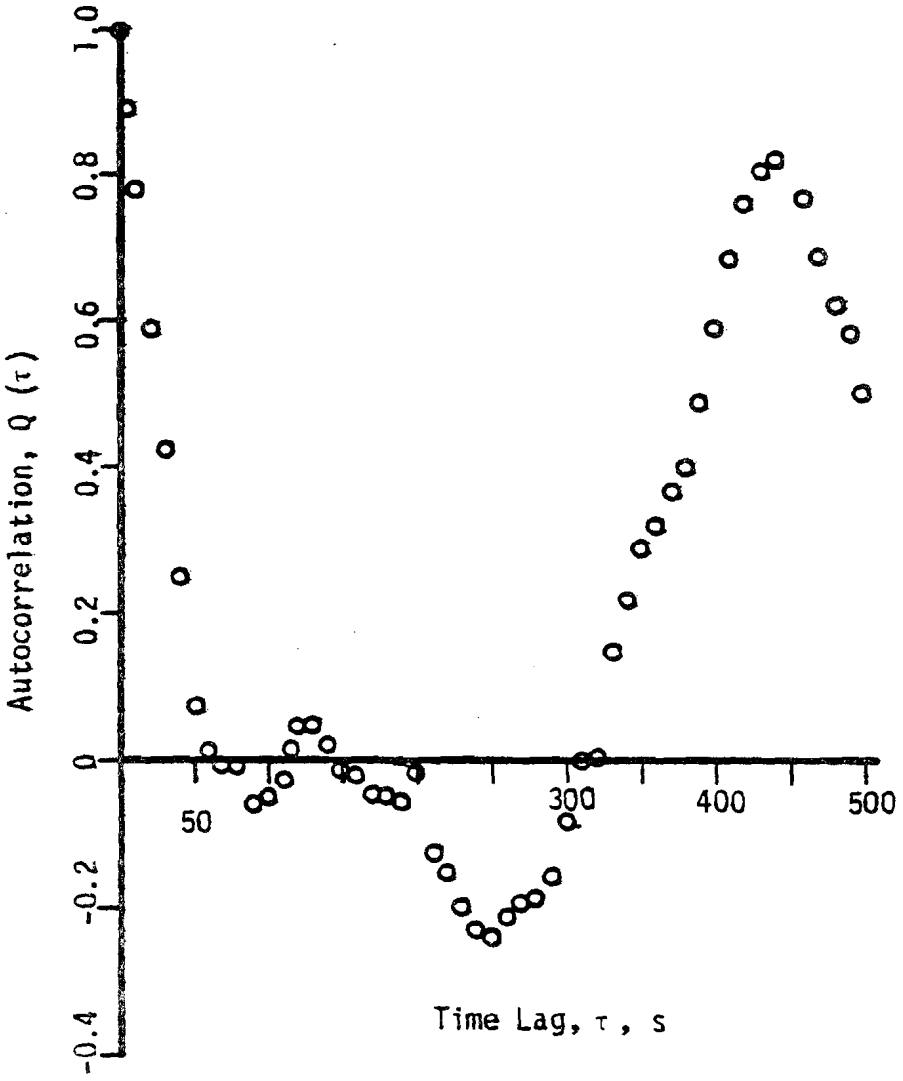

FIGURE 49. YAW AUTOCORRELATION: WFR 21

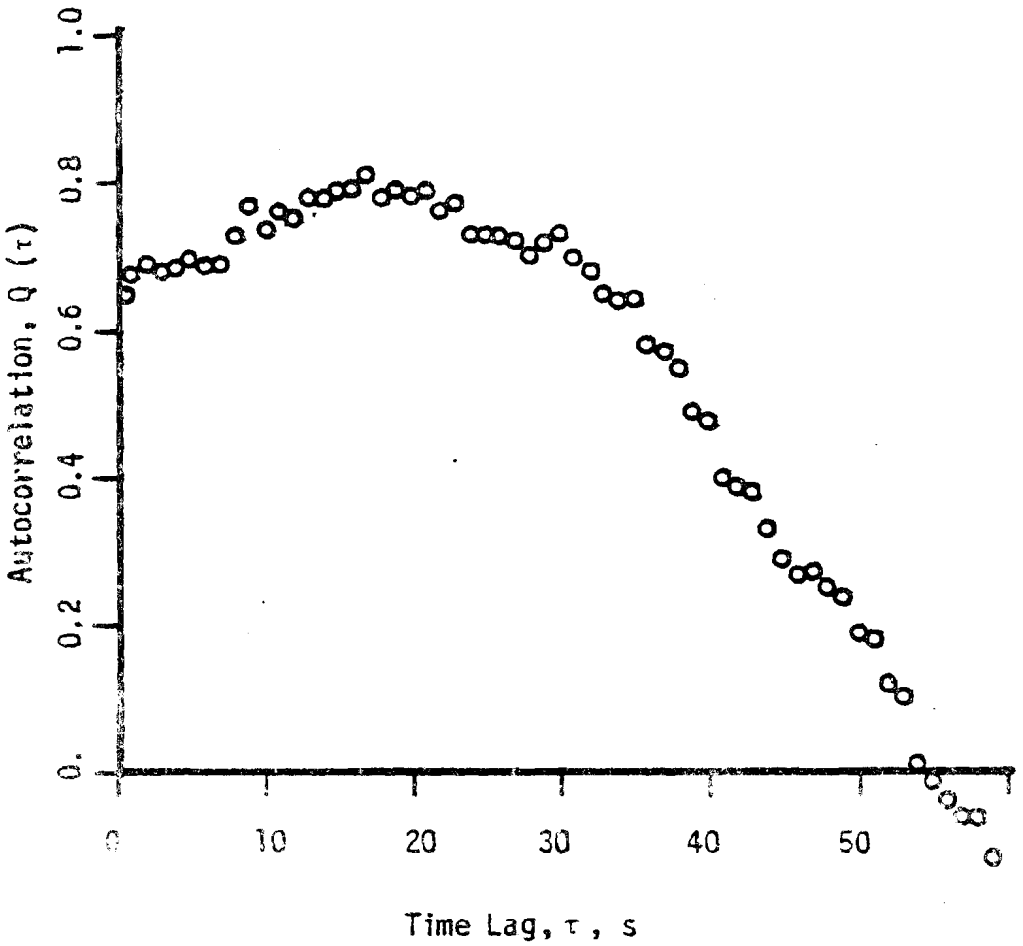

FIGURE 50. YAW AUTOCORRELATION: WFR 18

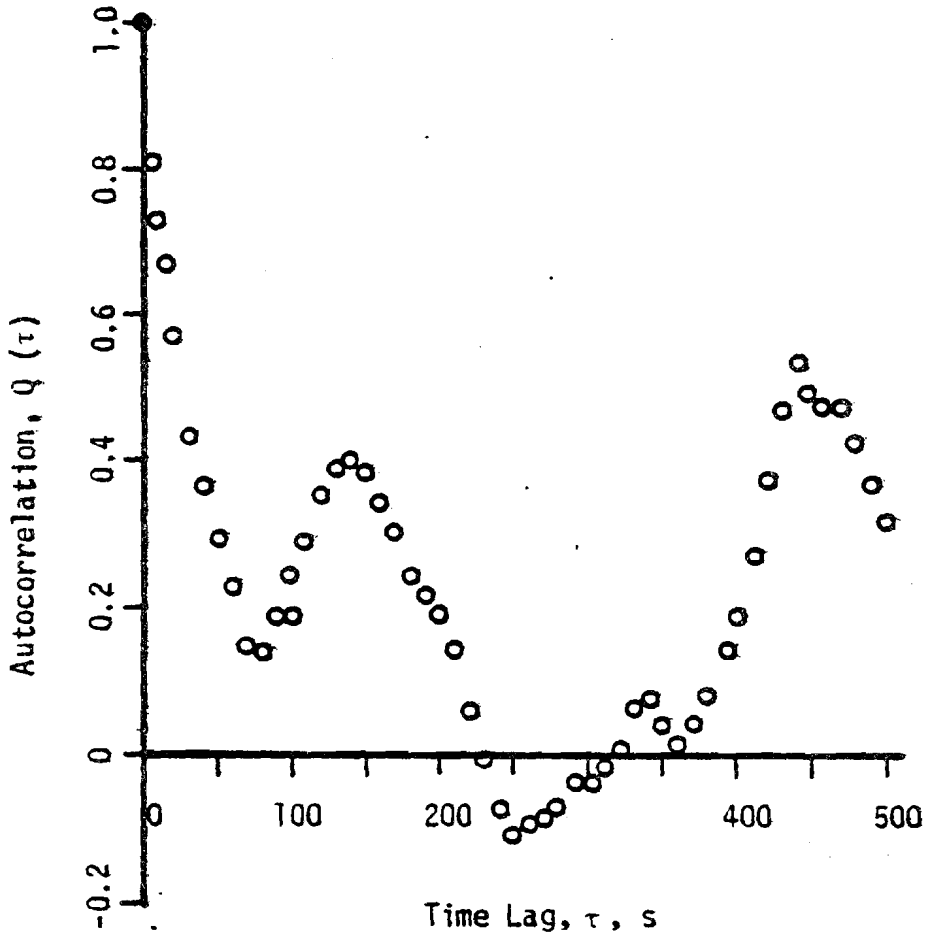

FIGURE 51. YAW AUTOCORRELATION: WFR 22

DIGITAL WFR	AVERAGE ROTOR SPEED, RPM	AVERAGE WIND SPEED, U, m/s	STEADY STATE, RPM-s/m	CUTOFF FREQUENCY* (HALF-POWER POINT) n_c, Hz
3	79.3	6.35	12.5	0.025
5	80.2	4.58	17.5	
17	116.7	6.96	16.8	
21	115.9	7.00	16.6	0.015
18	67.7	4.57	14.8	
22	71.6	6.05	11.8	0.015

*Shown only for records which resolve the 0.001-0.10 Hz frequency band.

TABLE 7. CUTOFF FREQUENCY FOR WIND SPEED TO RPM TRANSFER FUNCTION

For example, a distinct peak exists at 0.035 Hz in the yaw PSD for WFR3, where no distinct peak occurs in the wind direction PSD. This information is more clearly seen in the analysis of the transfer function, and so a detailed discussion is not given here. The nature and location of these peaks is discussed in detail by Cohen[20].

3.4 Characterization of Wind Field/Wind Turbine Interaction

3.4.1 Wind Speed/RPM Interaction

The transfer function and the corresponding coherence function are shown for each data record in Figs. 52 through 63. On each transfer function is marked the "steady-state" response, which is calculated as the ratio of the average RPM to average wind speed.

A comparison of WFR3, 21, and 22, Figs. 52, 58 and 62, shows that in each case the transfer function falls off above 0.01 Hz reaching the half-power point soon after. Table 7 shows the data records with the steady-state and half-power points, n_c. In each case the half-power point or cutoff frequency is taken to be $1/\sqrt{2}$ times the steady state value of the transfer function.

In Fig. 52, the transfer function for WFR3 continues to increase in magnitude below 0.006 Hz, unlike WFR21 and WFR22. Examination of the PSD for wind speed for this record shows that the wind speed does not contain relatively high power at this frequency. The RPM PSD, Fig. 37, continues to increase in magnitude down to 0.002 Hz. This increases the value of the transfer function at these frequencies.

Figs. 53, 59, and 63 show the coherence functions for WFR3, 21,

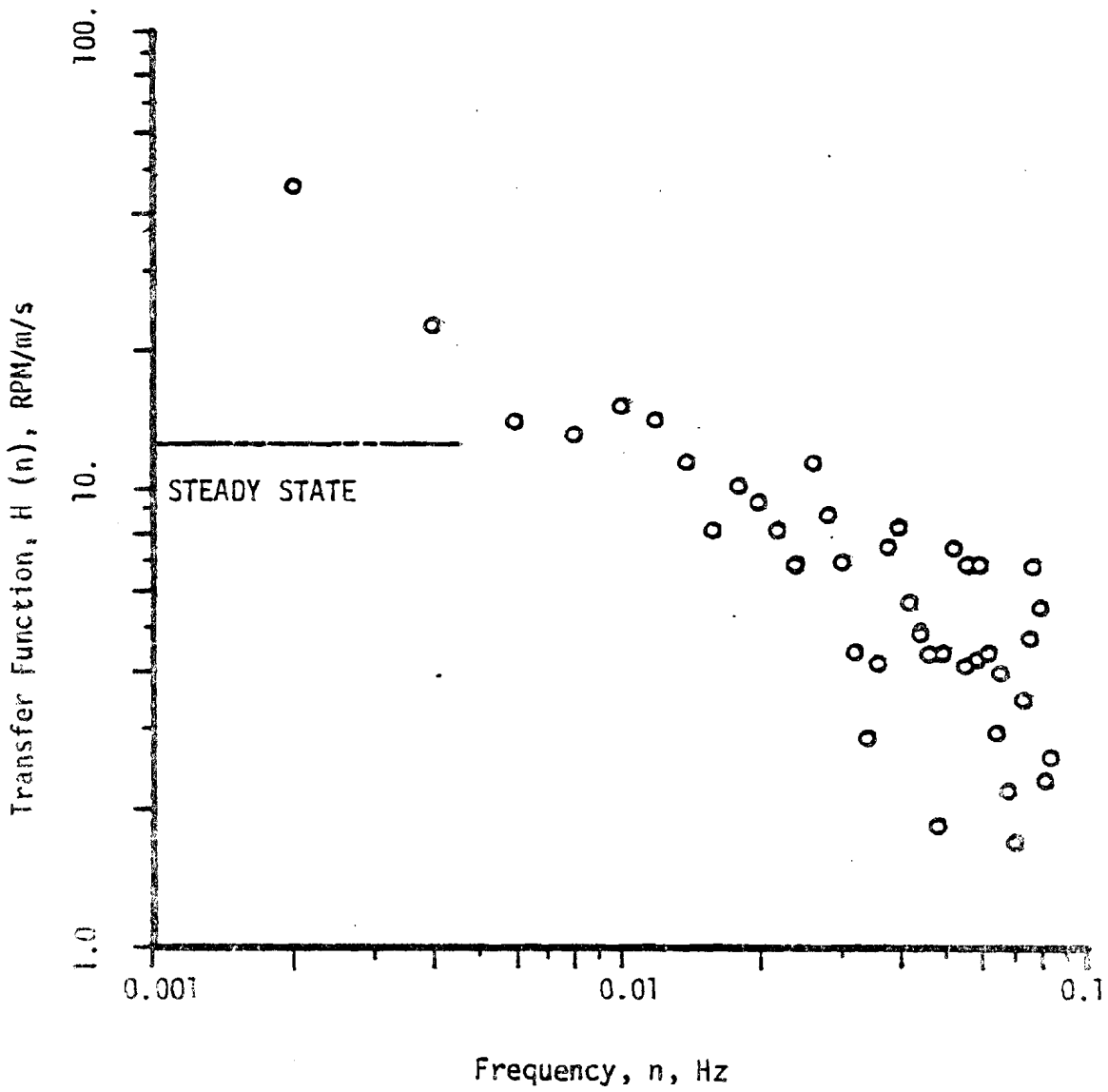

FIGURE 52. WIND SPEED TO RPM TRANSFER FUNCTION : WFR 3

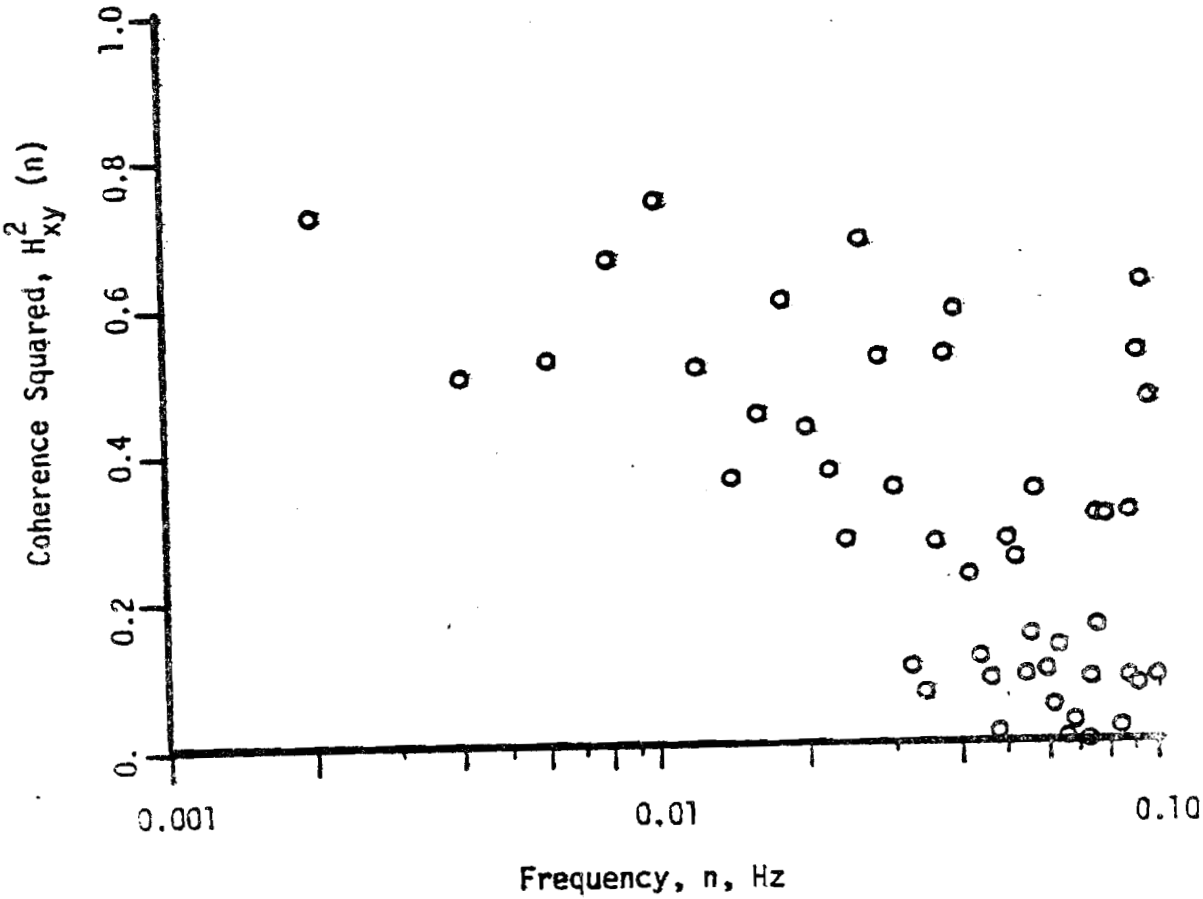

FIGURE 53. WIND SPEED TO RPM COHERENCE FUNCTION: WFR 3

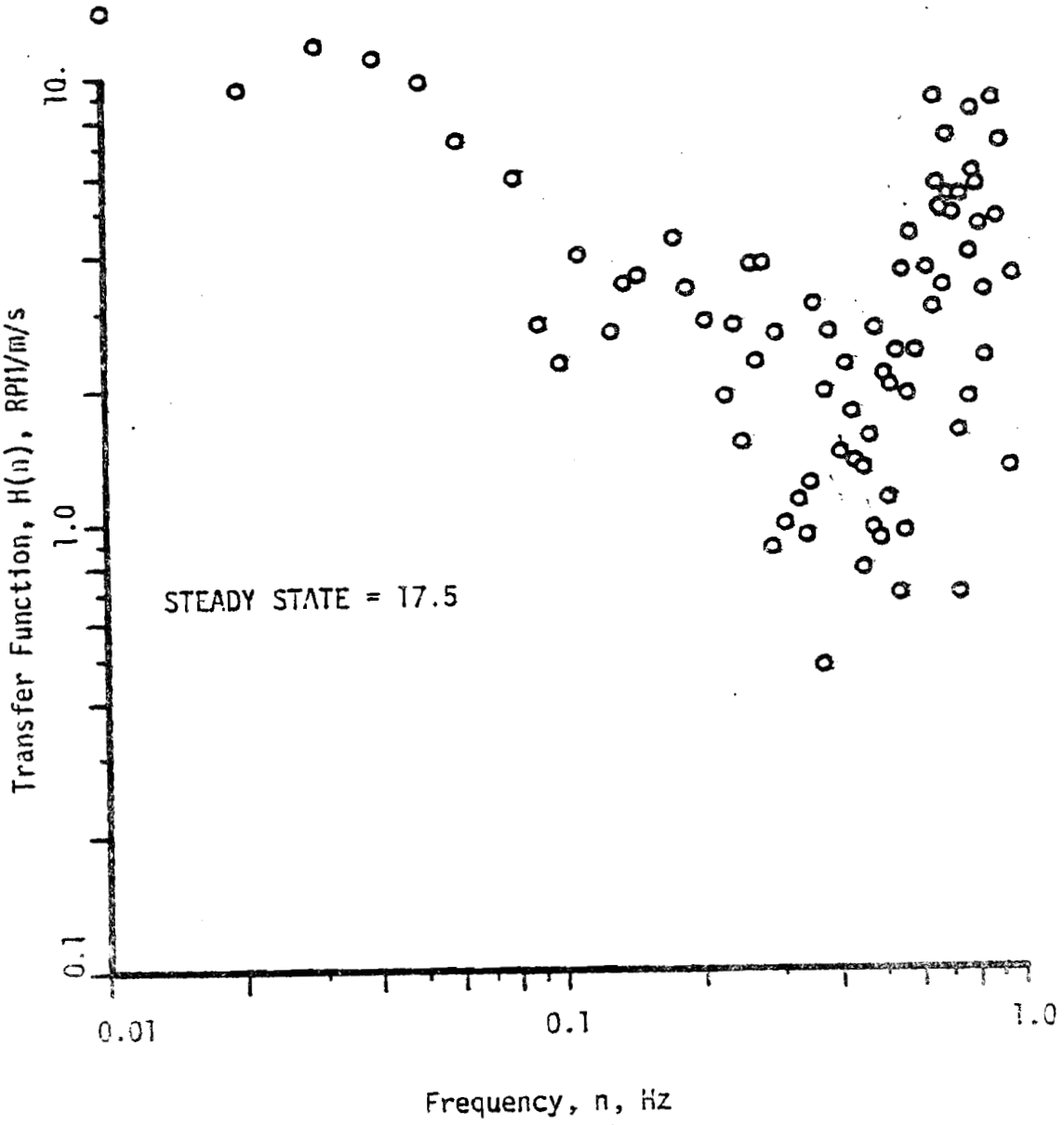

FIGURE 54. WIND SPEED TO RPM TRANSFER FUNCTION: WFR 5

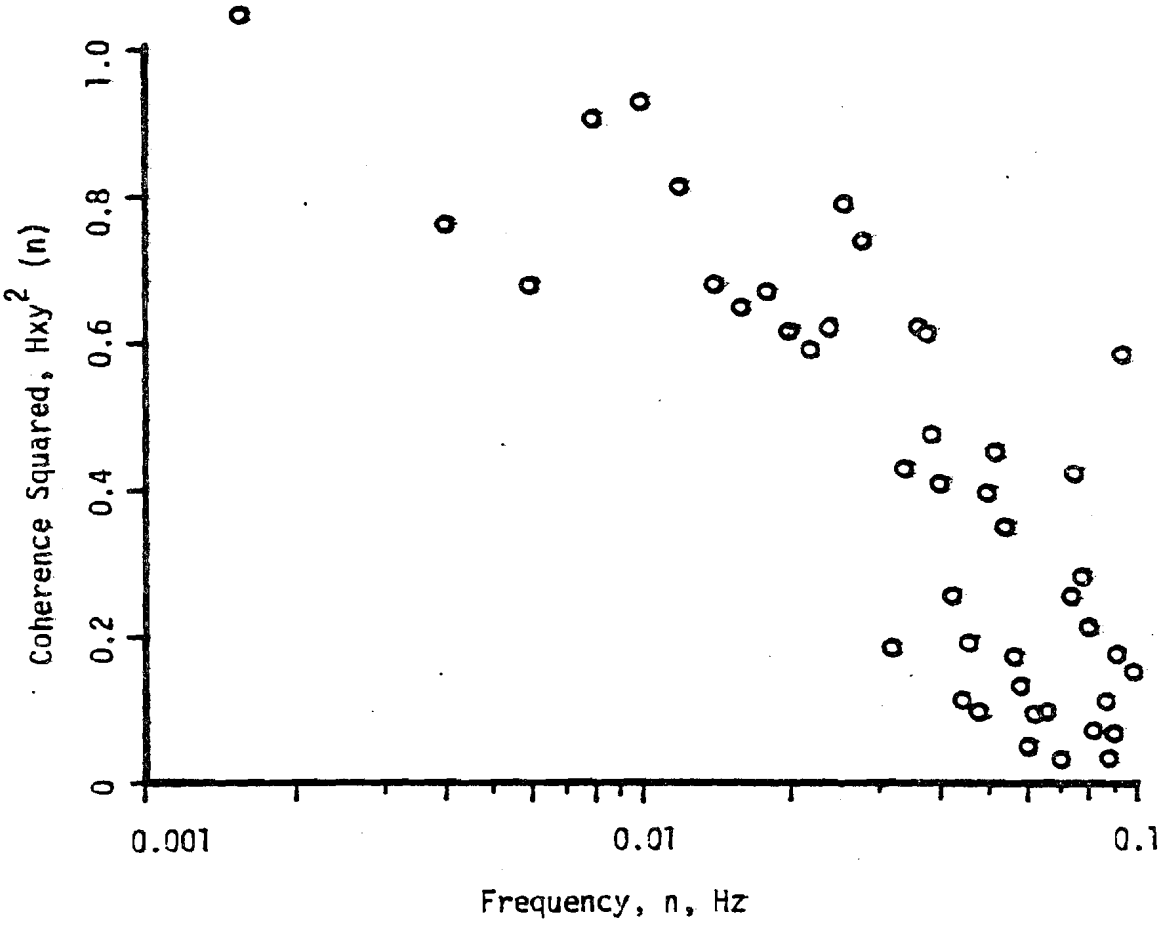

FIGURE 55. WIND SPEED TO RPM COHERENCE SQUARED: WFR 5

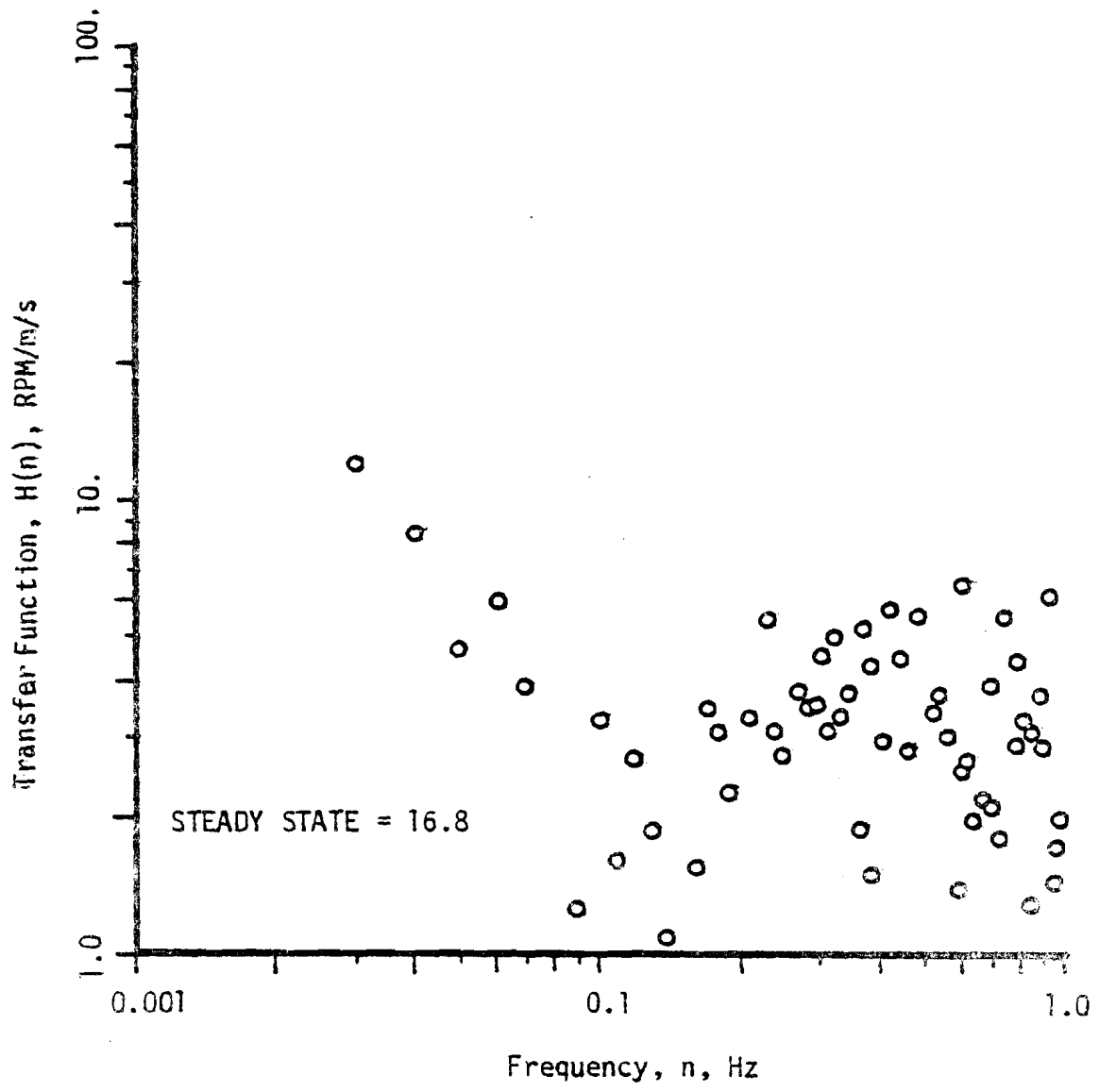

FIGURE 56. WIND SPEED TO RPM TRANSFER FUNCTION : WFR 17

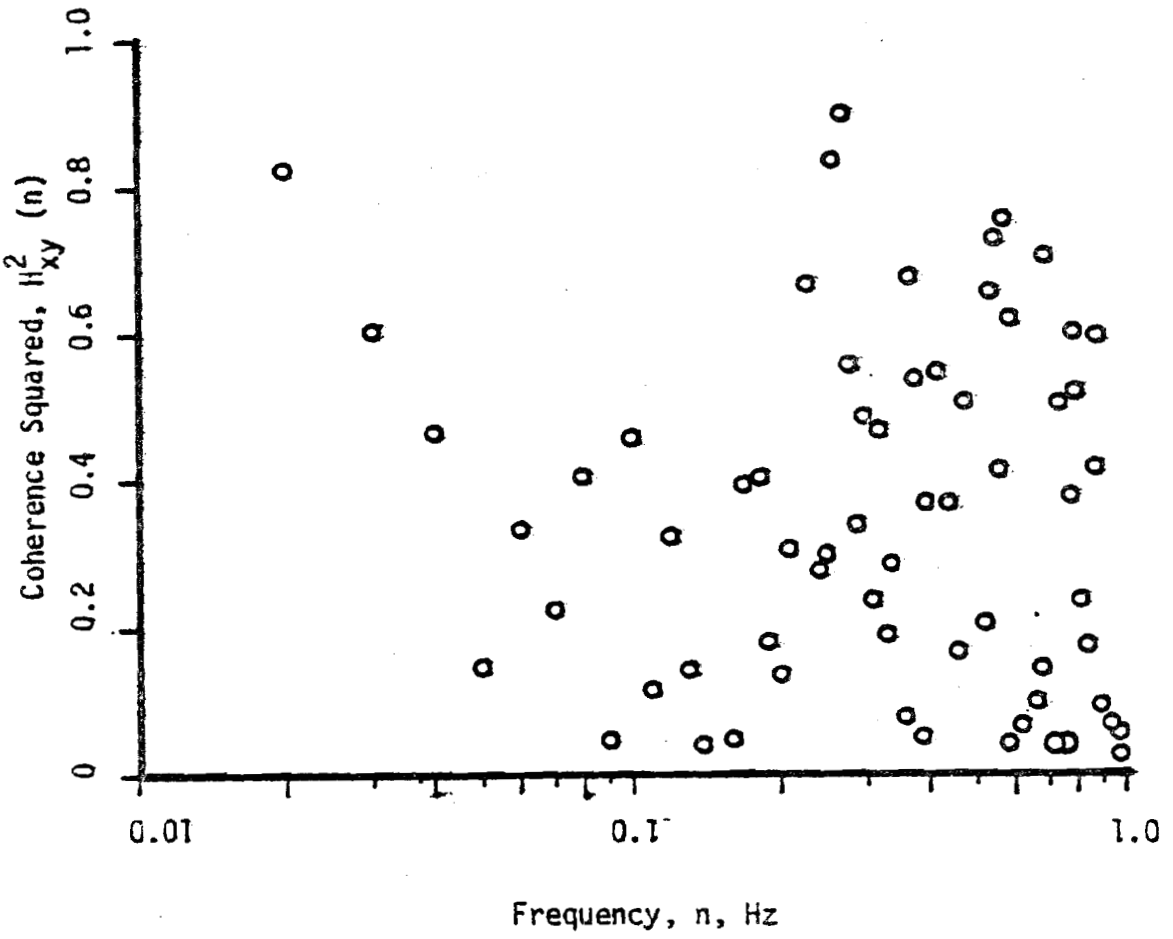

FIGURE 57. WIND SPEED TO RPM COHERENCE SQUARED: WFR 17

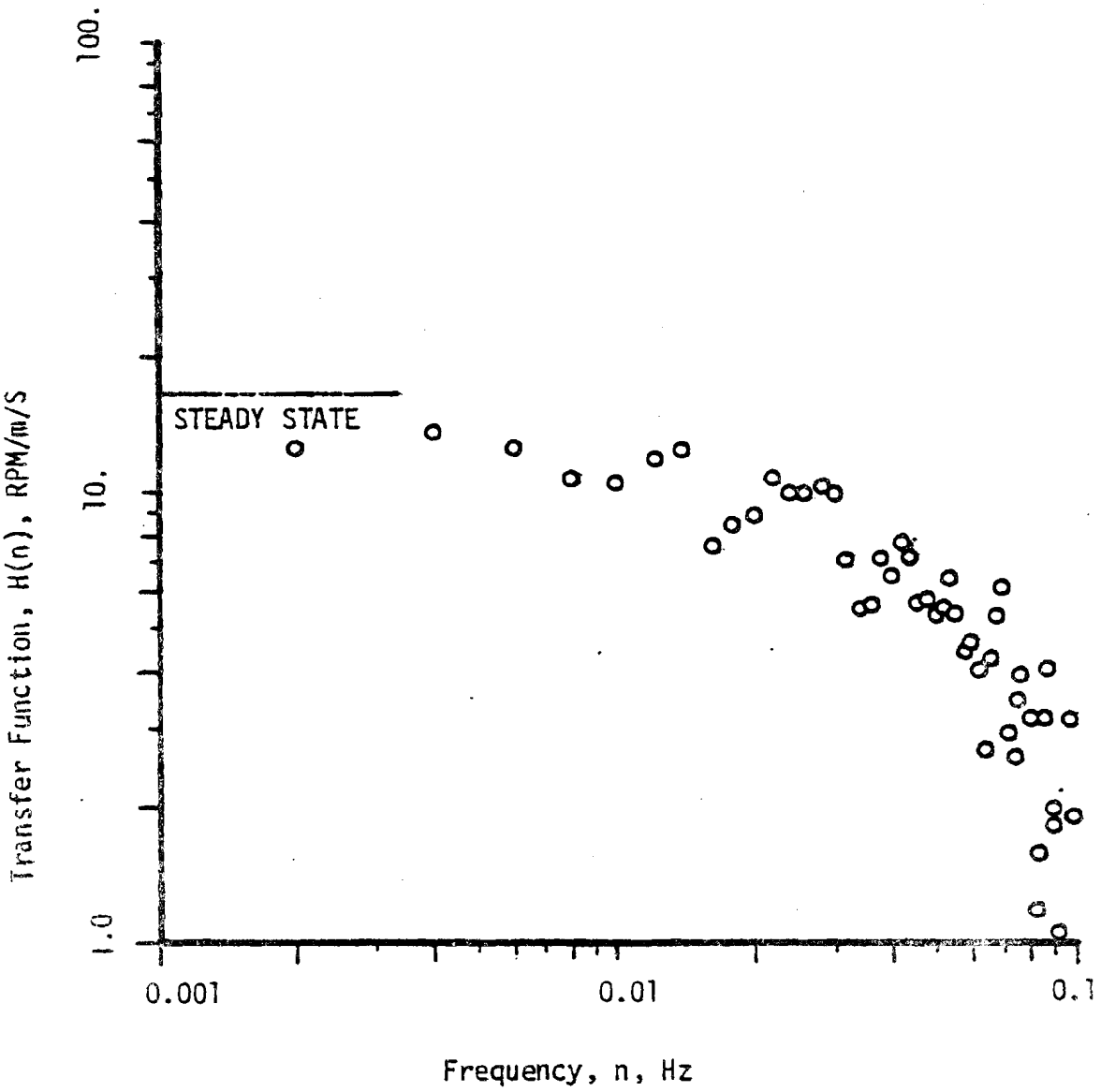

FIGURE 58. WIND SPEED TO RPM TRANSFER FUNCTION: WFR 21

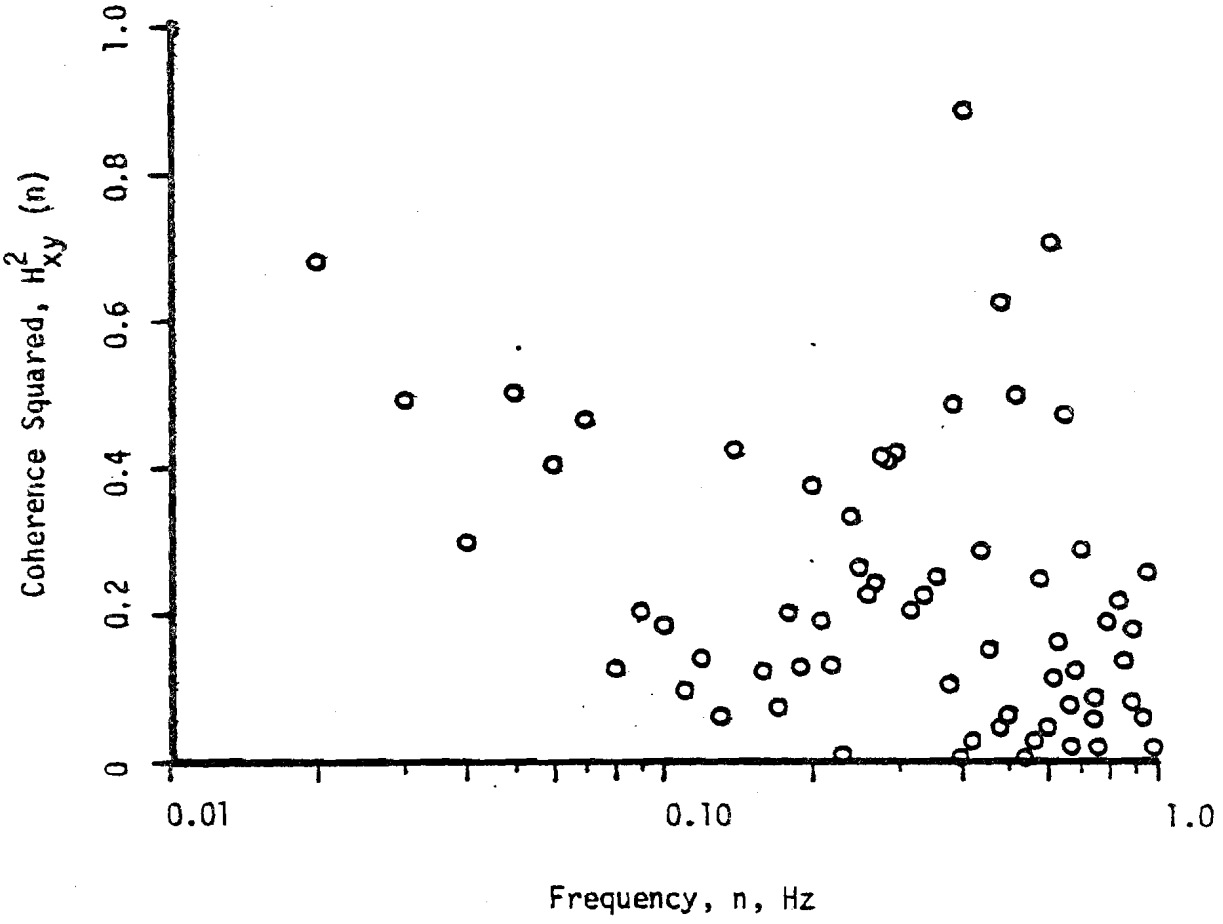

FIGURE 59. WIND SPEED TO RPM COHERENCE SQUARED: WFR 21

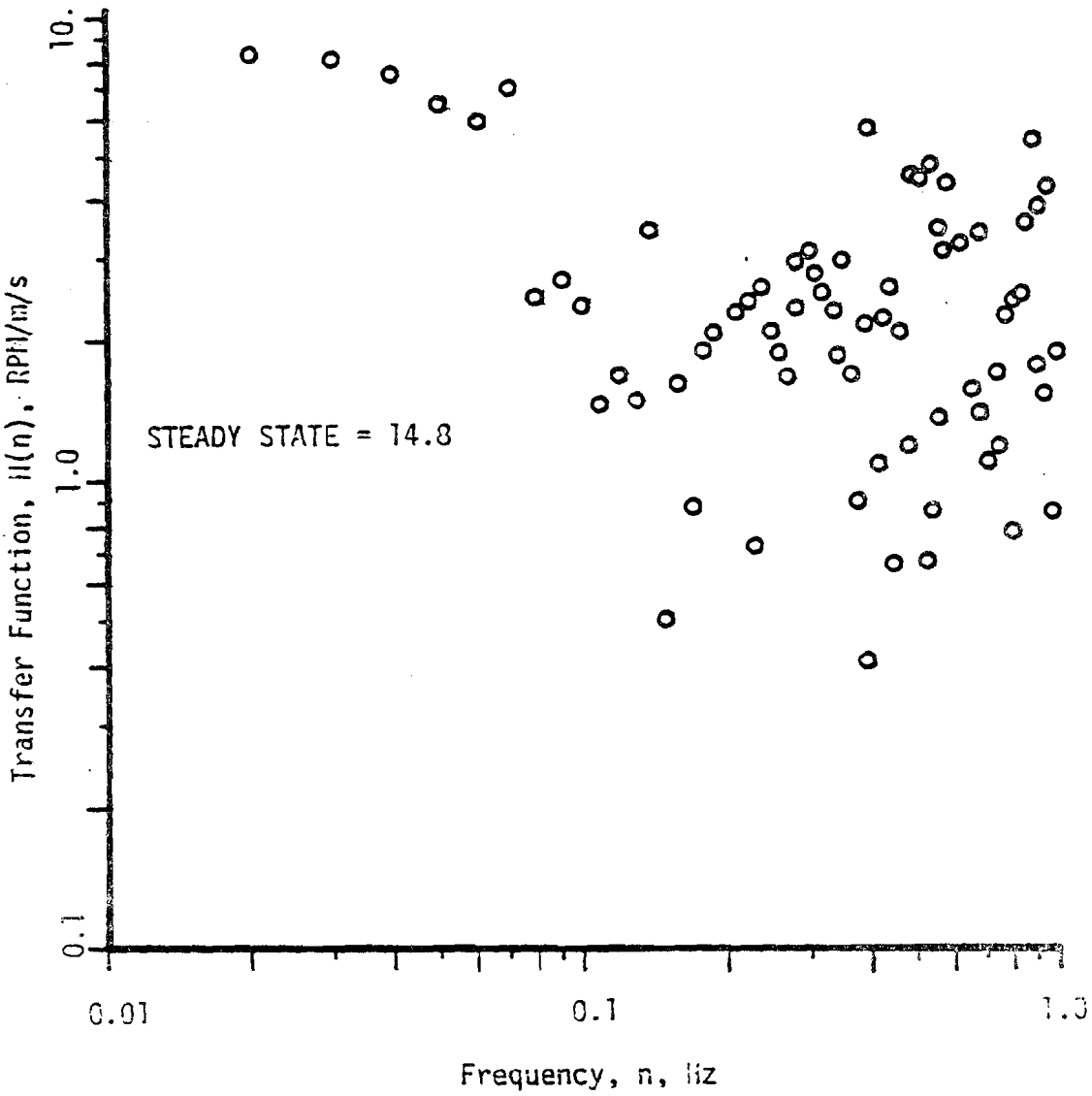

FIGURE 60. WIND SPEED TO RPM TRANSFER FUNCTION: WFR 18

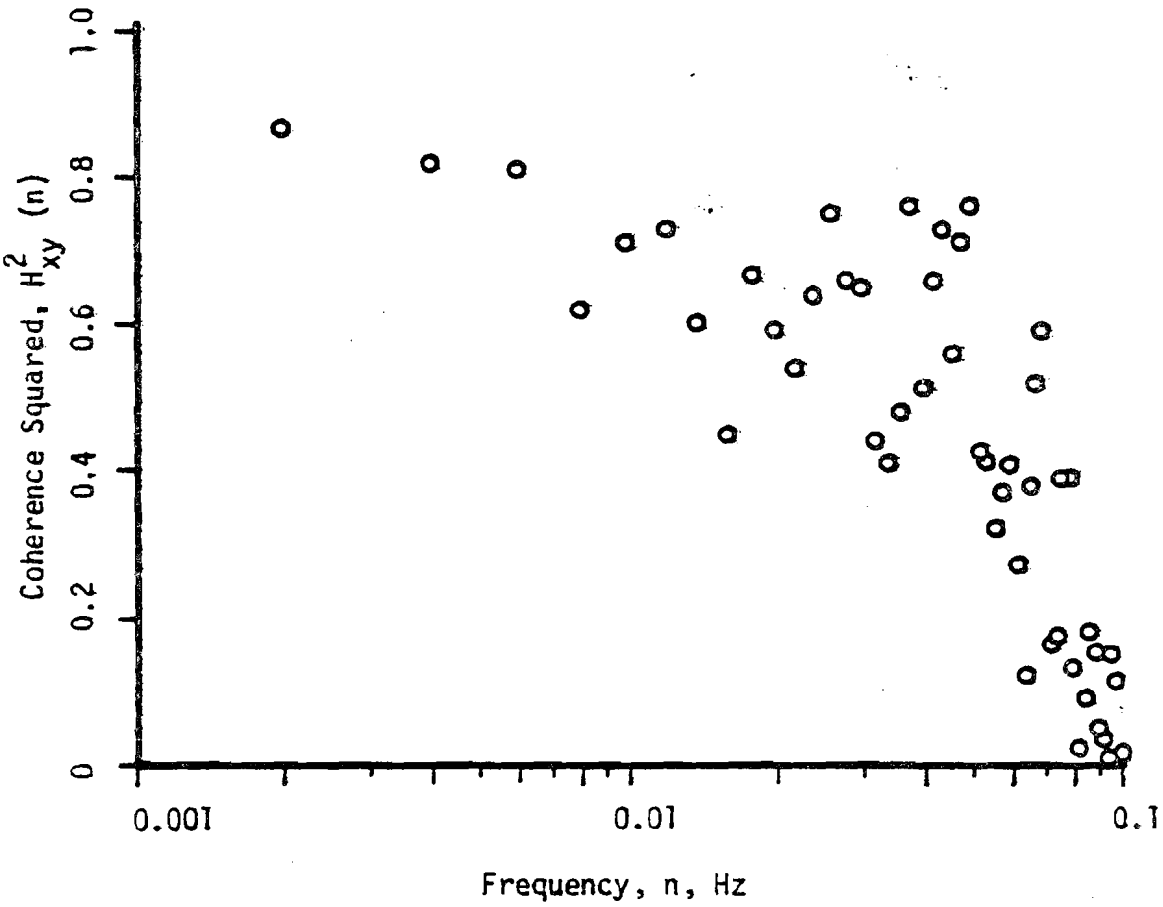

FIGURE 61. WIND SPEED TO RPM COHERENCE SQUARED: WFR 18

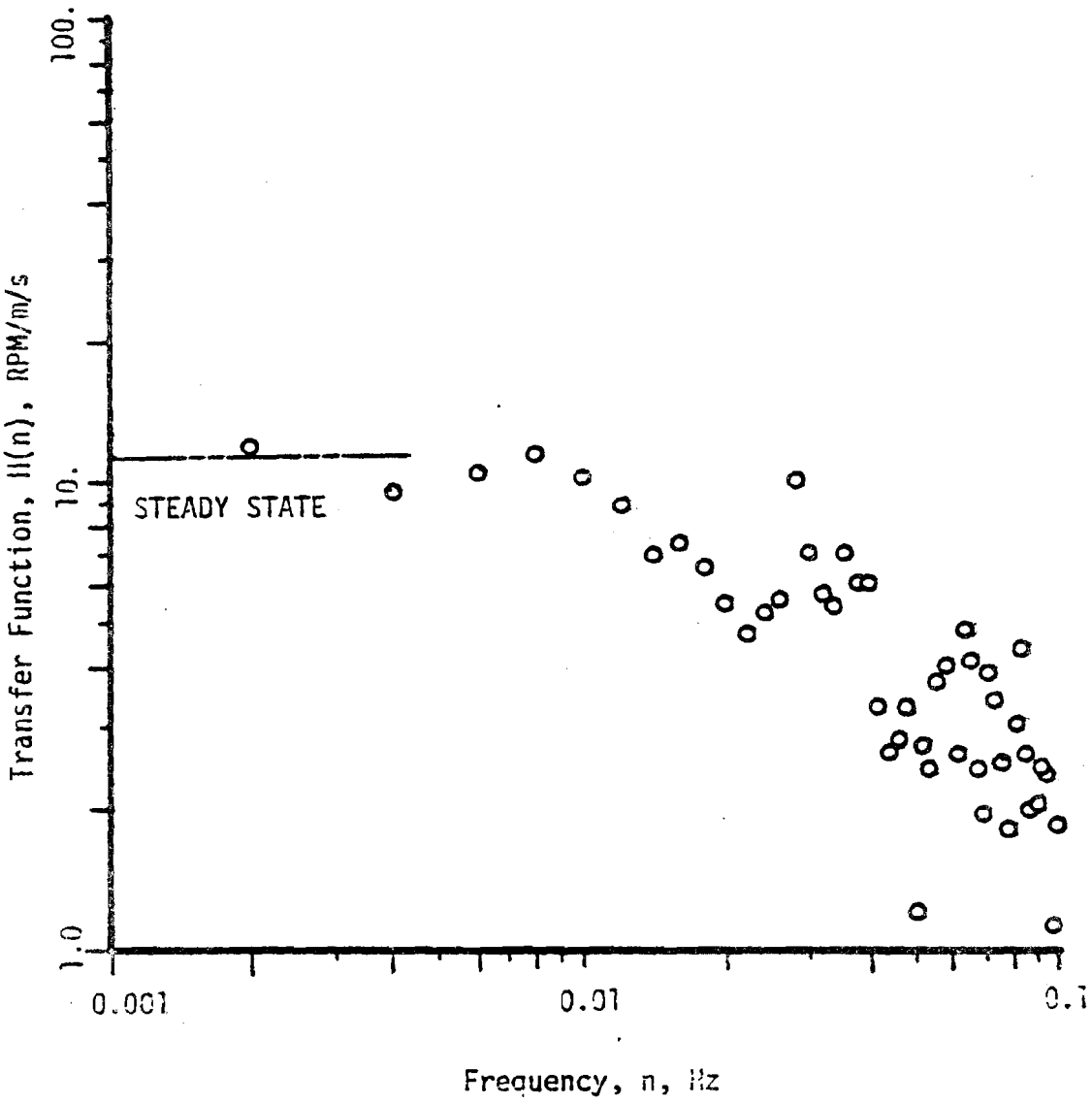

FIGURE 62. WIND SPEED TO RPM TRANSFER FUNCTION: WFR 22

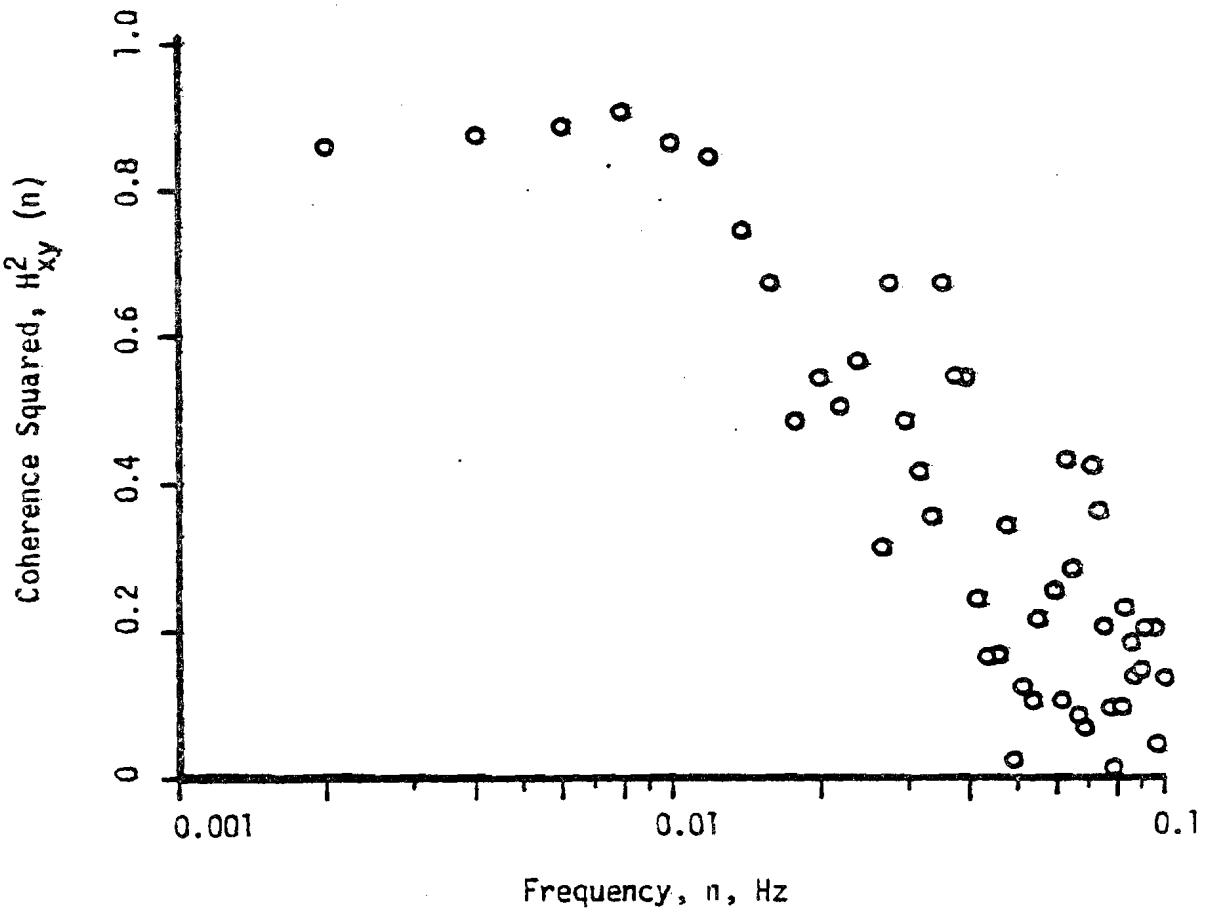

FIGURE 63. WIND SPEED TO RPM COHERENCE SQUARED: WFR 22

and 22. At the frequencies lower than 0.01 Hz, the coherence for WFR21 increases to 0.9; the coherence for WFR22 levels off at this point. In contrast to this, the coherence for WFR3 is never higher than 0.75, and is as low as 0.5.

The coherence function seems to indicate that the RPM response behaved in a highly non-linear fashion during record WFR3. However, it is most probable that the PSD for RPM in WFR3 has been skewed upwards since nearby points were calculated as negative due to statistical "leakage." This would certainly have the effect of raising the magnitude of the transfer function and reducing the coherence.

Above 0.10 Hz, the transfer function for WFR 5, 17, and 18 (Figs. 54, 56, and 60), levels off, and the scatter in the data points becomes more apparent. A comparison of the coherence function for these records, Figs. 55, 57 and 61, shows a marked decrease. It is concluded that the RPM response became highly non-linear above 0.10 Hz, and that conclusions should not be made about the wind speed/RPM interaction in this region without additional work.

For certain specific frequencies, a sharp increase in the coherence function and the transfer function indicate a probable mechanical resonance in the system. The exact frequency where resonance occurs is not clear. Examination of all records, Figs. 52 through 63, brackets the resonance point between 0.4 and 0.8 Hz. A further discussion can be found in Section 3.4.2.

3.4.2 Wind Speed/Current Interaction

The wind turbine response to wind speed fluctuations, as represented in the wind speed to generator output current transfer function, is most important. This is a direct measure of the conversion of energy in the turbulent wind field into electrical power. These transfer functions and their associated coherence functions are shown in Figs. 64 through 71 representing records WFR3, 5, 17, and 21. Generator current was not measured for WFR18/22.

Table 8 shows the calculated steady-state and half-power points for each record. The half-power point or cutoff frequency is defined to be $1/\sqrt{2}$ times the steady state value of the transfer function.

The wind turbine is seen to be a low-pass filter with a half-power point at 0.03 Hz. At higher frequencies the transfer function drops sharply to 0.3 Hz and peaks again at 0.67 Hz for both WFR5 and 17. A corresponding peak in the coherence function indicates that this peak is not a statistical aberation; it most likely represents a mechanical resonance. The peak frequency is well within the range for a resonance in RPM discussed in Section 3.3.1, and while a one-to-one correspondence may not exist between peak resonant frequency in RPM and current, the two frequencies are no doubt close.

The quality of the transfer function for WFR3 and 21 can be considered quite good, since the coherence function for these records is around 0.9, below 0.01 Hz.

Now that the half-power point is known for the wind turbine, an estimation of the turbulent energy extracted by the wind turbine can be made. This calculation is made after a brief introduction to turbulence.

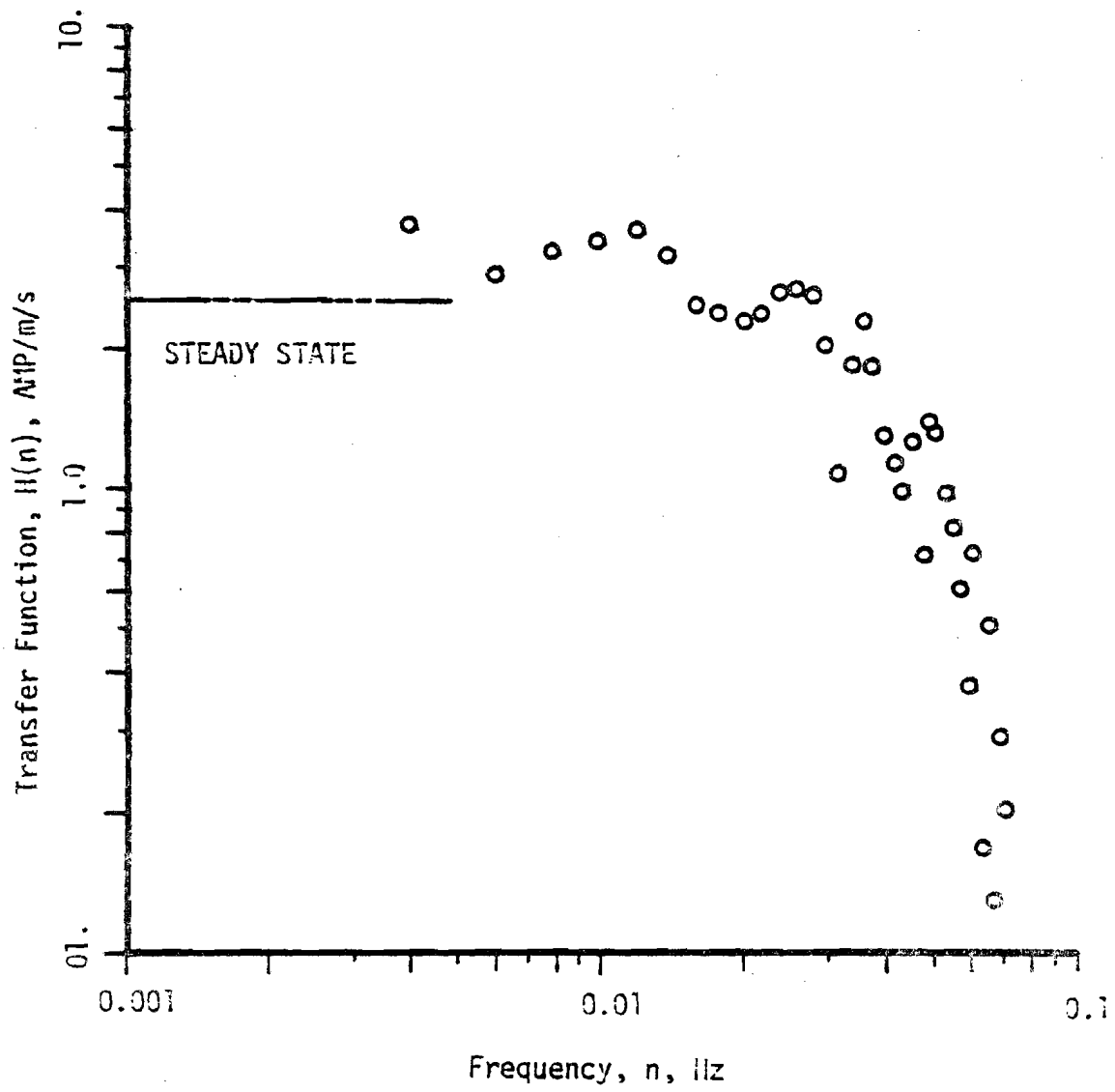

FIGURE 64. WIND SPEED TO CURRENT TRANSFER FUNCTION: WFR 3

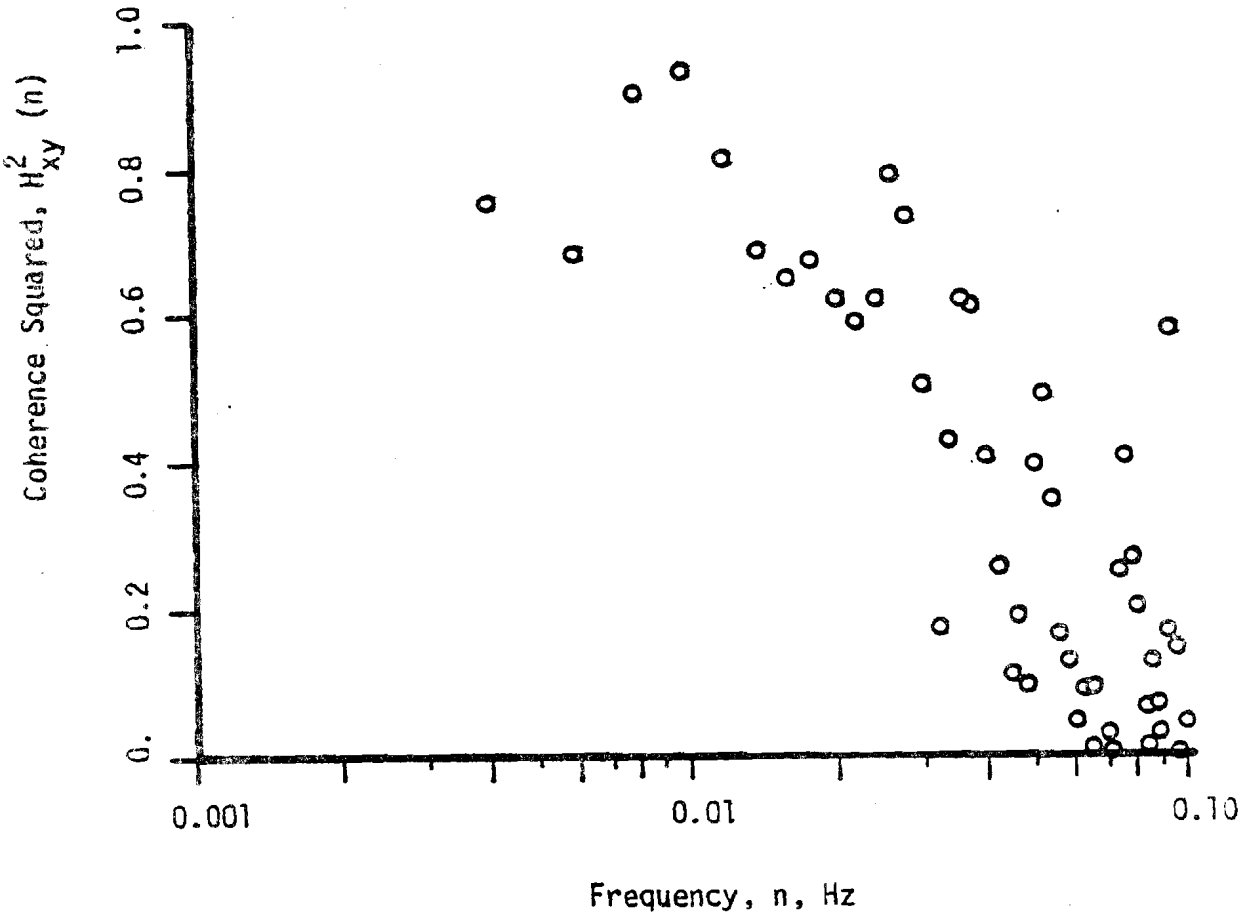

FIGURE 65. WIND SPEED TO CURRENT COHERENCE FUNCTION: WFR 3

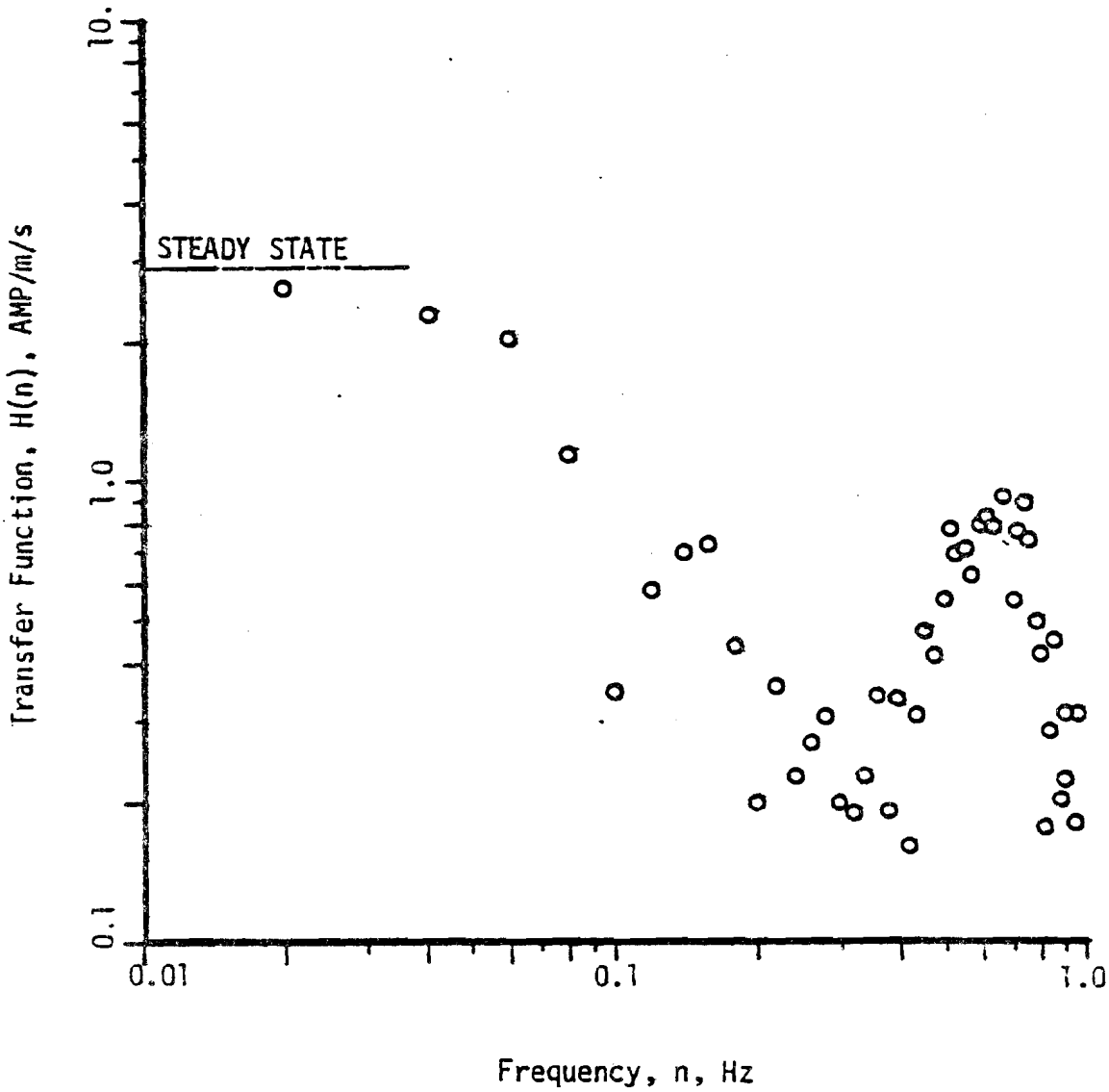

FIGURE 66. WIND SPEED TO CURRENT TRANSFER FUNCTION: WFR 5

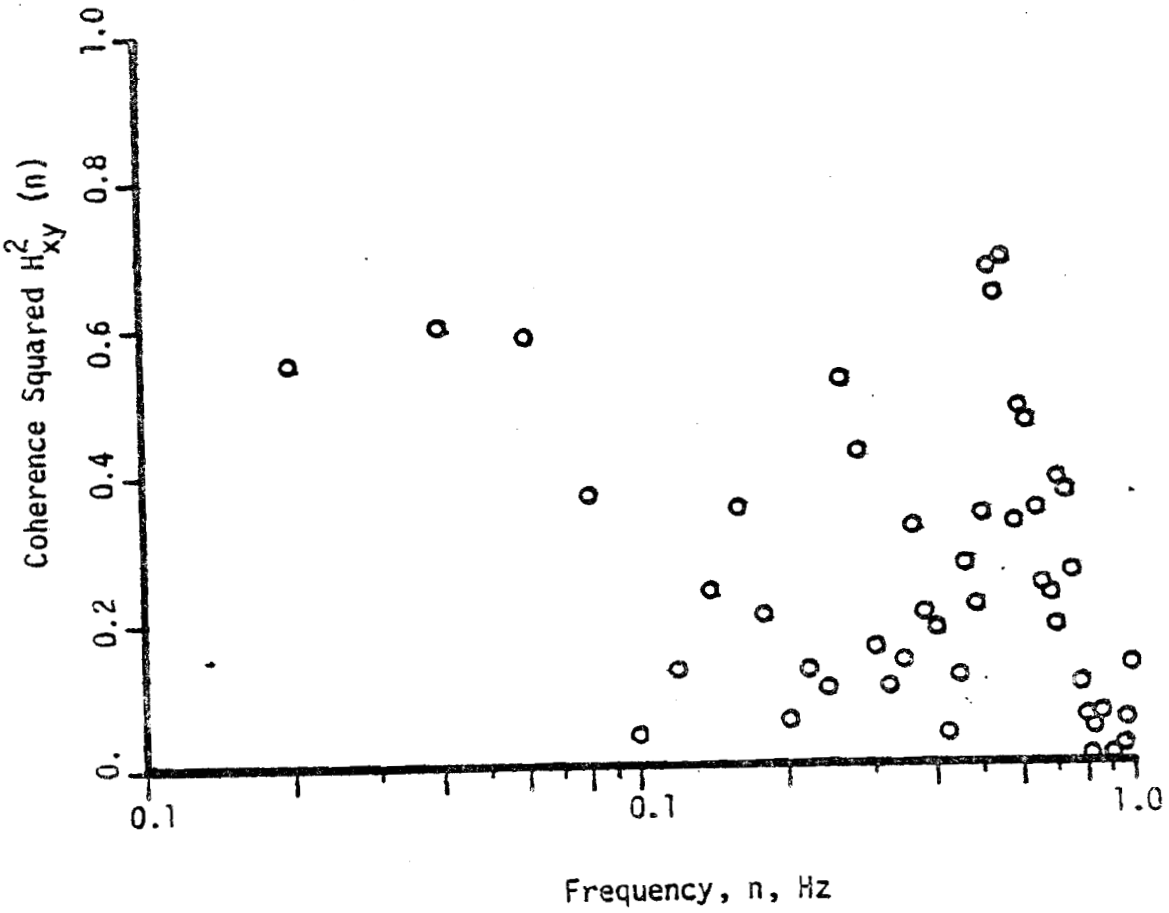

FIGURE 67. WIND SPEED TO CURRENT COHERENCE FUNCTION: NFR 5

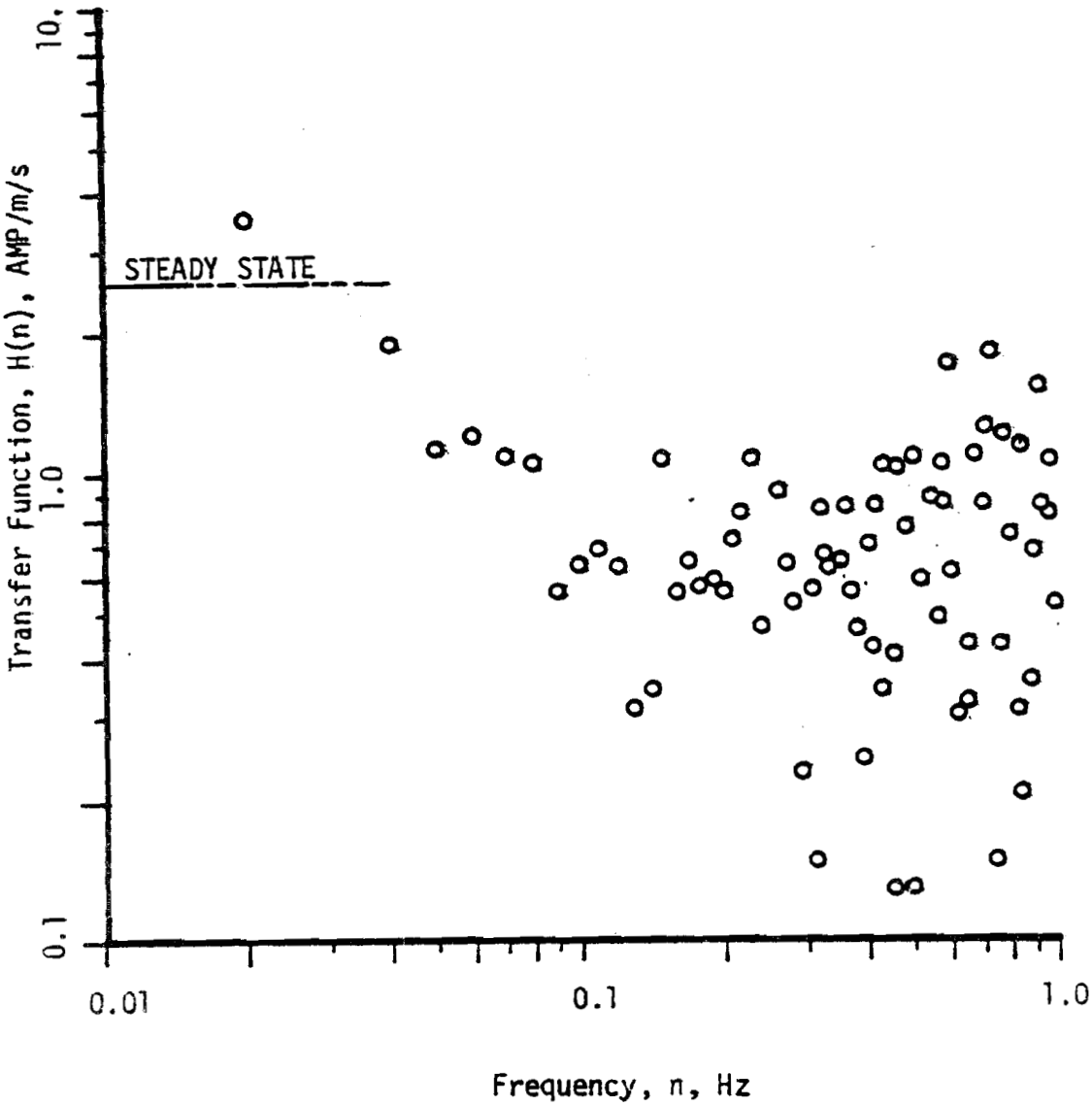

FIGURE 68. WIND SPEED TO CURRENT TRANSFER FUNCTION: WFR 17

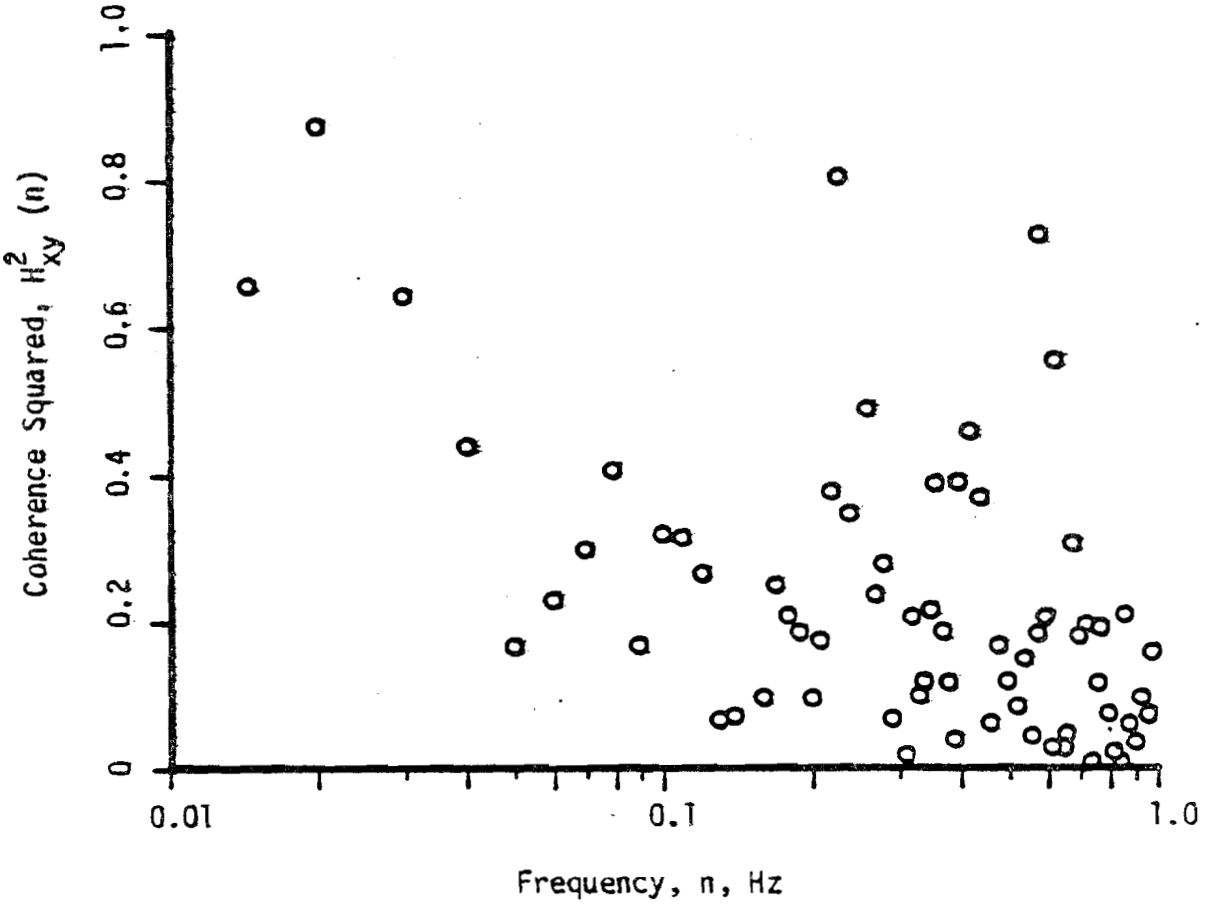

FIGURE 69. WIND SPEED TO CURRENT COHERENCE SQUARED: WFR 17

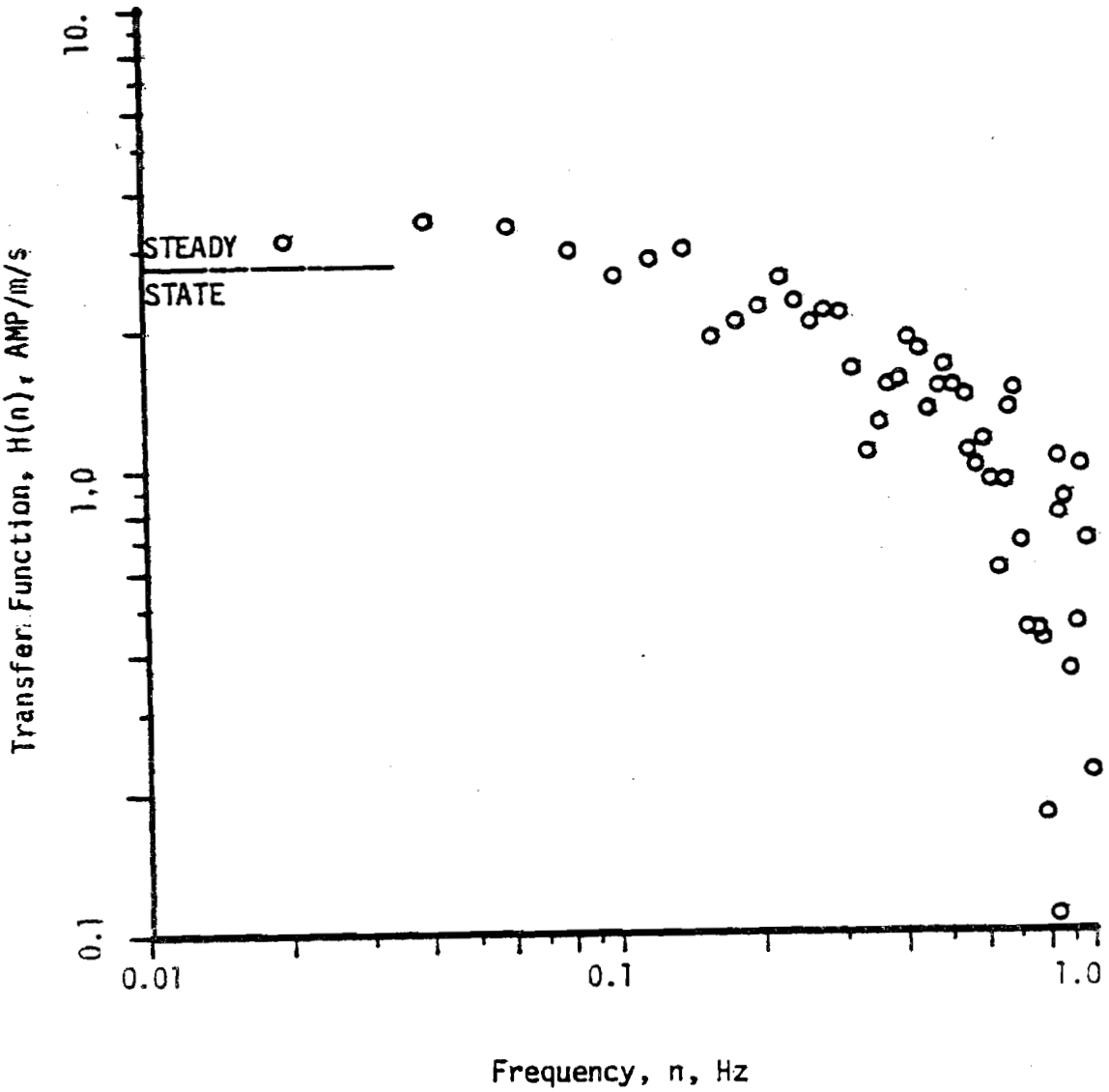

FIGURE 70. WIND SPEED TO CURRENT TRANSFER FUNCTION : WFR 21

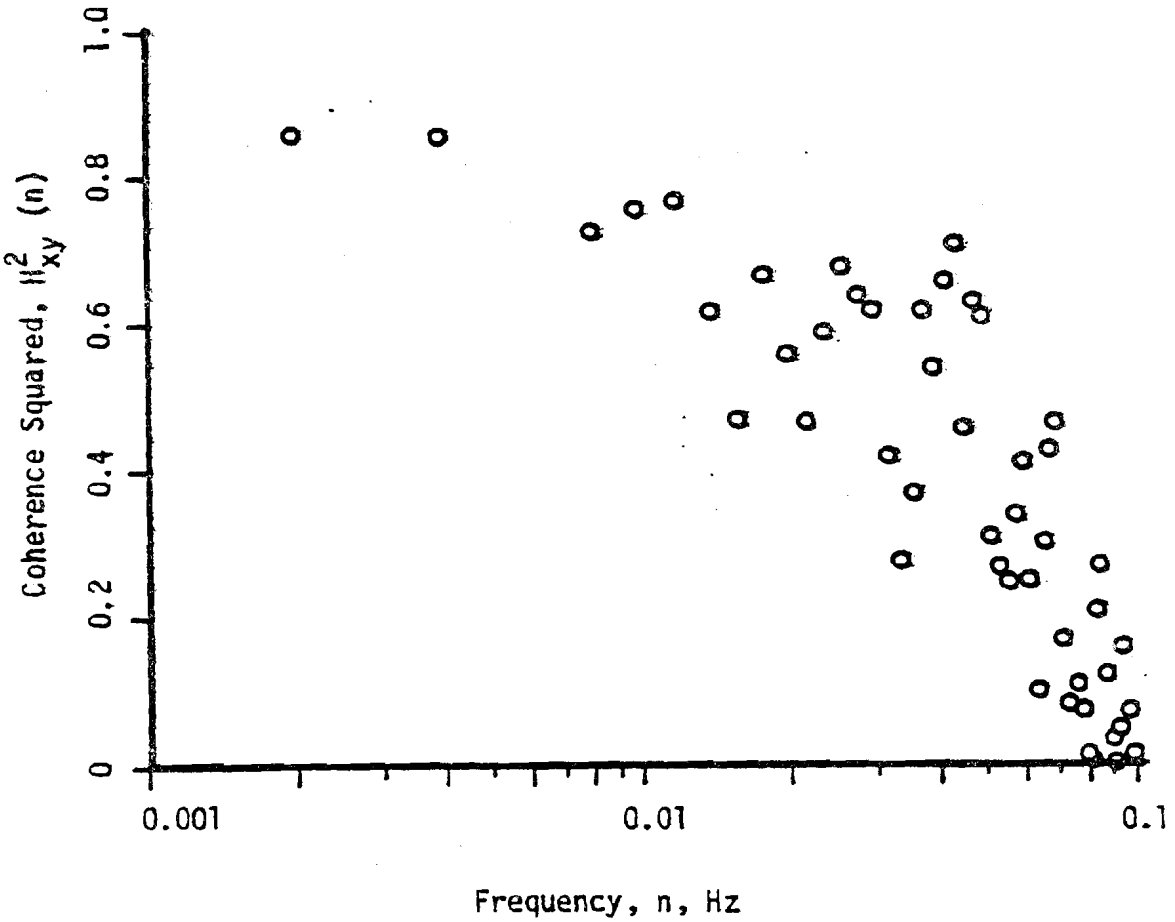

FIGURE 71. WIND SPEED TO CURRENT COHERENCE SQUARED: WFR 21

DIGITAL WFR	AVERAGE GENERATOR CURRENT, I, AMPS	AVERAGE WIND SPEED, U, m/s	STEADY STATE, AMP-s/m	CUTOFF FREQUENCY* (HALF-POWER POINT) n_c, Hz
3	16.1	6.35	2.54	0.03
5	13.6	4.58	2.97	
17	17.9	6.96	2.57	
21	19.3	7.00	2.76	0.03

*Shown only for records which resolve the 0.001-0.10 Hz frequency range.

TABLE 8. CUTOFF FREQUENCY FOR WIND SPEED TO GENERATOR CURRENT TRANSFER FUNCTION

The random fluctuations in wind velocity can be decomposed into the sum of a mean wind velocity, and fluctuations with zero mean. This is Reynold's Decomposition. In the downstream directions, Reynold's decomposition gives:

$$u(t) = U + u'(t) \tag{52}$$

$u'(t)$ is the instantaneous velocity fluctuation and

$$\overline{u'(t)} = \lim_{T\to\infty} \frac{1}{T} \int_0^T u'(t)\, dt \equiv 0 \tag{53}$$

Both the mean wind and the fluctuations contain power which is potentially available to the wind turbine.

The power contained in the mean or "steady-state" wind is given by:

$$P_{ave} = \frac{1}{2} \rho A C_p U^3 \tag{54}$$

where ρ is the density of air, A is the swept area of the disc, and C_p is the coefficient of performance for the particular wind turbine.

The maximum power which can be extracted from the turbulence by a wind turbine is dependent upon how well the machine can respond to the highest frequency gusts. This is the dynamic or frequency response of the machine.

The cutoff frequency is considered to be the highest frequency in the wind to which the machine will strongly respond.

The maximum power in the turbulent wind available to a wind turbine is related to the time average of $u(t)^3$:

$$P_{max} = \frac{1}{2} \rho A C_p \overline{u(t)^3} \tag{55}$$

A relationship between the two power estimates is given by Manwell and Kirchhoff[21]:

$$\frac{P_{max}}{P_{ave}} = 1 + \frac{3\,\overline{u'^2}}{U^2} \tag{56}$$

Comparison of P_{max}/P_{ave} for all data shows that approximately 5% of the total power is tied up in the turbulence (Table 9).

The mean square of the fluctuations, $\overline{u'^2}$, is related through the Fourier Transform to the power spectral density of u'(t):

$$\overline{u'^2} = \int_0^\infty S(n)\, dn \tag{57}$$

Since the real wind turbine cannot respond well to frequencies higher than its cutoff frequency, n_c, only a fraction of the total power in the wind is available. The power fractions extracted from the turbulence is:

$$P_t = \frac{\int_0^{n_c} S(n)\, dn}{\int_0^\infty S(n)\, dn} \tag{58}$$

To obtain P_t for each data record, the equation for the Davenport fit to the PSD is integrated up to the cutoff (half-power) frequency, n_c, and divided by the total area under the Davenport curve. These curves are shown in Fig. 9.

Based on a cutoff frequency of approximately 0.03 Hz, WF-1 is able to extract approximately 70% of the power in the turbulence. A general representation of P_t vs n_c is given by the normalized cumulative PSD integral equation plotted in Fig. 72. This shows that a turbine with a better frequency response (higher cutoff frequency) will extract

TABLE 9. POWER EXTRACTED FROM THE TURBULENCE

WIND FIELD RECORD	U (m/s)	U_* (m/s)	$\int_0^{0.3} s(n)dn$	$\int_0^{\infty} s(n)dn$	$\frac{P_{max}}{P_{ave}}$	$\frac{P_t}{P_{ave}}$	% P_{max} EXTRACTED	TURBULENT CONTRIBUTION TO TOTAL POWER EXTRACTED	TURBULENT POWER LOST DUE TO INERTIA % P_{max}
3/5	6.35	.366	.554	.785	1.058	1.041	70.5	4.1	1.7
17/21	7.00	.330	.436	.638	1.039	1.027	68.5	2.7	1.2
18/22	6.05	.324	.440	.616	1.050	1.036	71.4	3.6	1.4

Average Power Extracted from Turbulence, %: 70

Contribution of Turbulence to Total Extracted Power, %: 3.5

Maximum Possible Contribution from Turbulence to Power Extracted, %: 4.9

NOTE: The mean wind speeds used in calculation for this table are for WFR3, 21 and 22, since the majority of the power is contained within the frequency range these records resolve.

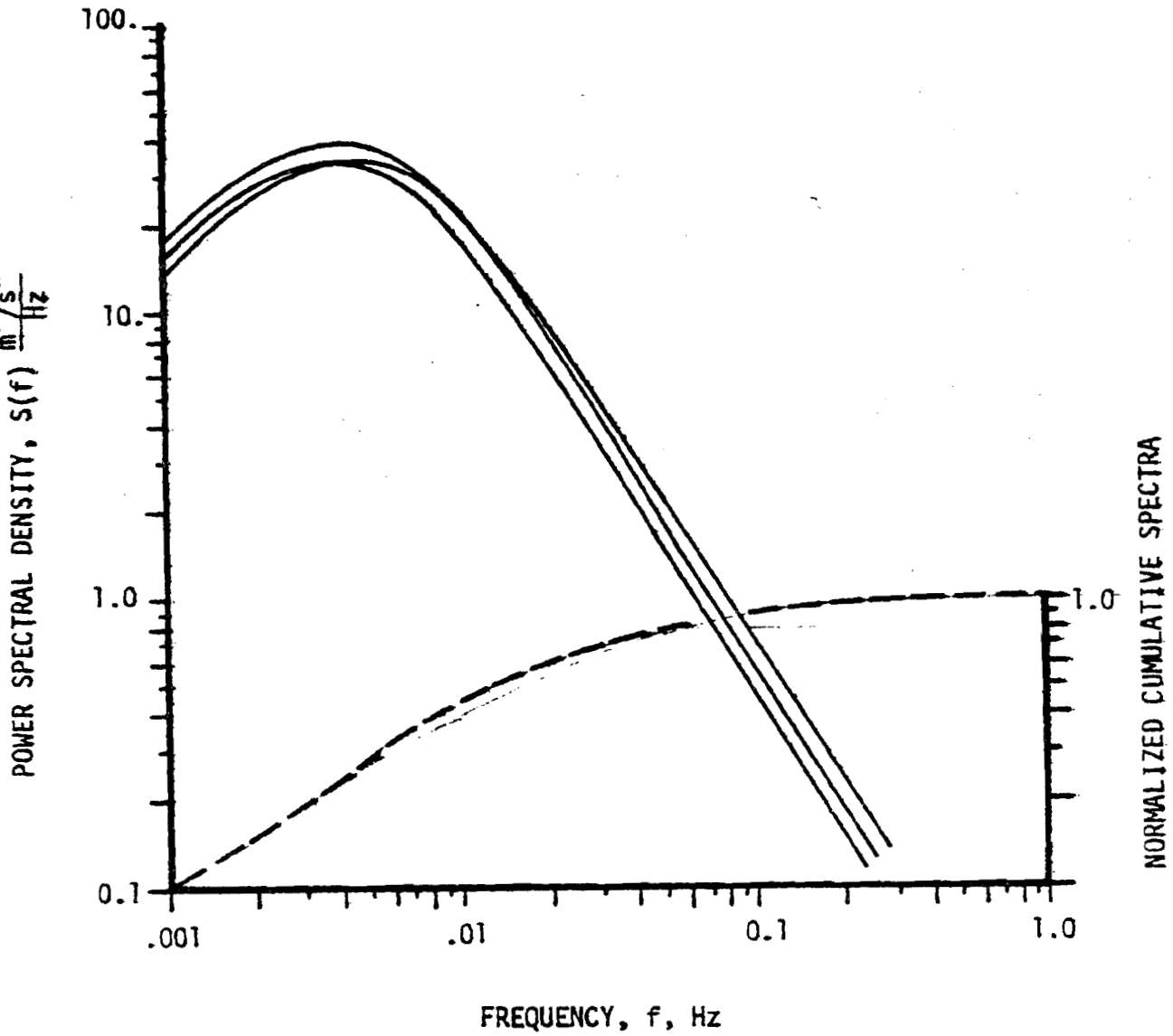

Figure 72. Cumulative Power Spectral Density Integral

more power from the turbulence than an otherwise similar less responsive machine.

3.4.3 Wind Direction/Yaw Interaction

The nacelle yaw is damped in normal operations to help the machine track the changing wind direction. To evaluate the differences in the damped and undamped yaw response, the measured and theoretical wind direction to yaw transfer functions are analyzed. The measured transfer functions and their related coherence functions are shown in Figs. 73 through 76. The damped and undamped theoretical transfer functions are shown in Figs. 77 and 78, respectively. These were calculated by Cohen.[22]

The measured transfer functions are characterized by a wide scatter in the data, with generally poor coherence (see Figs. 74 and 76). As a consequence, comparison with the theoretical transfer functions is somewhat speculative.

In Fig. 73, for undamped yaw, the magnitude of the transfer function seen to decrease with increasing frequency from the steady state value. Three narrow peaks occur at 0.01, 0.04 and 0.06 Hz. The latter two peaks bracket the 0.05 Hz peak shown in the corresponding theoretical curve, Fig. 78. The primary peak in Fig. 73 is lower in frequency than the 0.03 Hz primary peak in Fig. 78. For the damped case, Fig. 77 shows predicted peaks at 0.001 and 0.0045 Hz. The latter peak could correspond to the peak at 0.007 Hz in Fig. 75, but this is not clearly so. In this case, however, the primary peak predicted at 0.001 Hz could well be closer to 0.0025 Hz, a region in the measured transfer function which was not resolved.

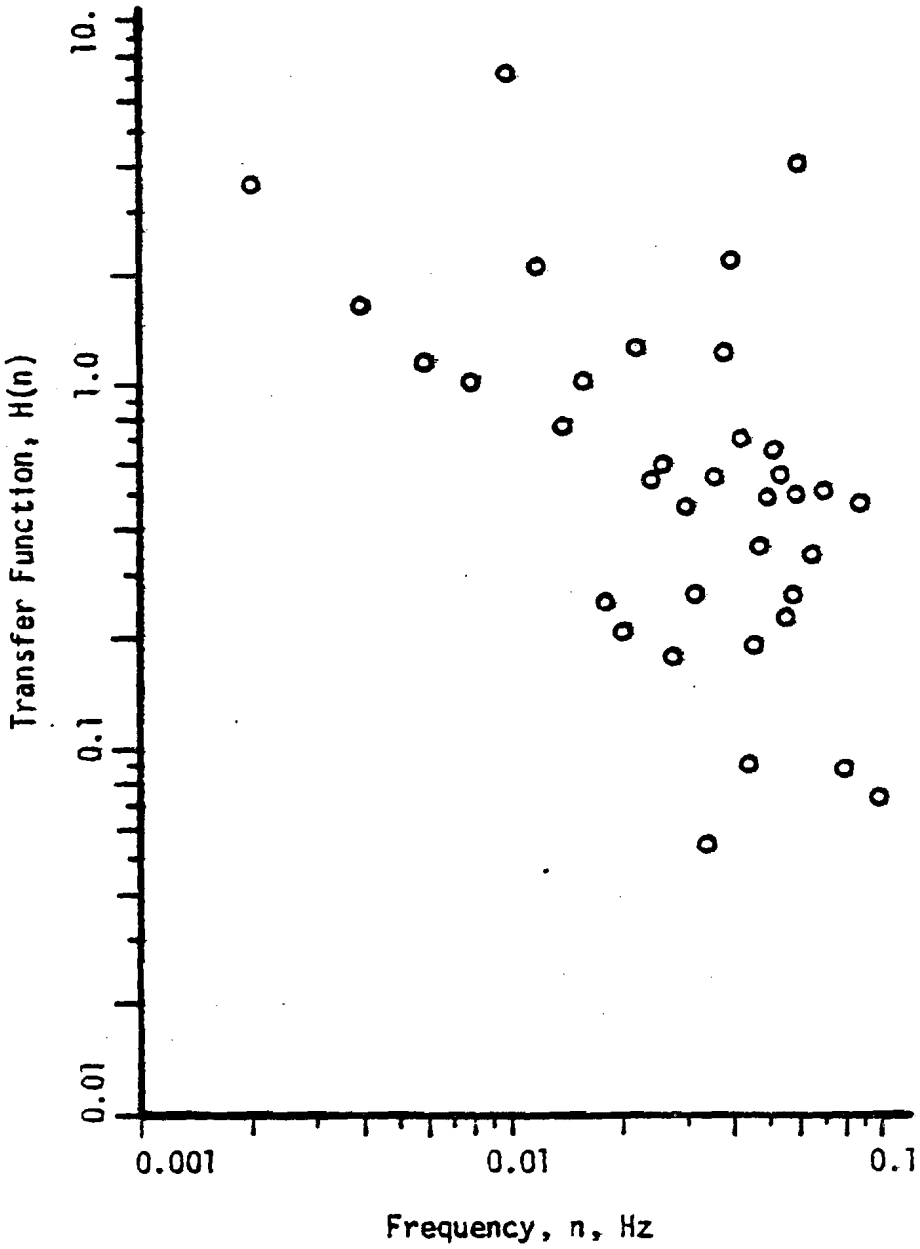

FIGURE 73. WIND DIRECTION TO YAW TRANSFER FUNCTION: WFR 17/21

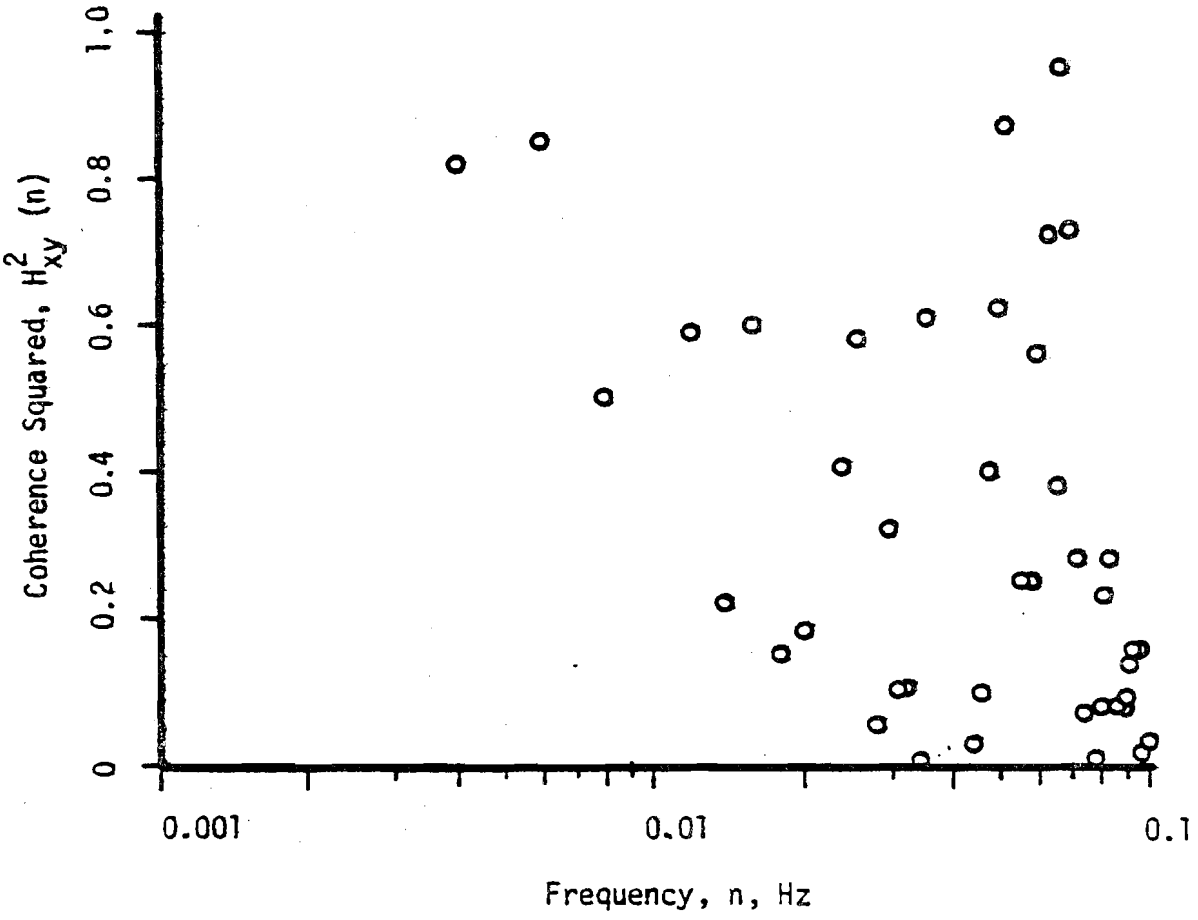

FIGURE 74. WIND SPEED TO YAW COHERENCE SQUARED: WFR 17/21

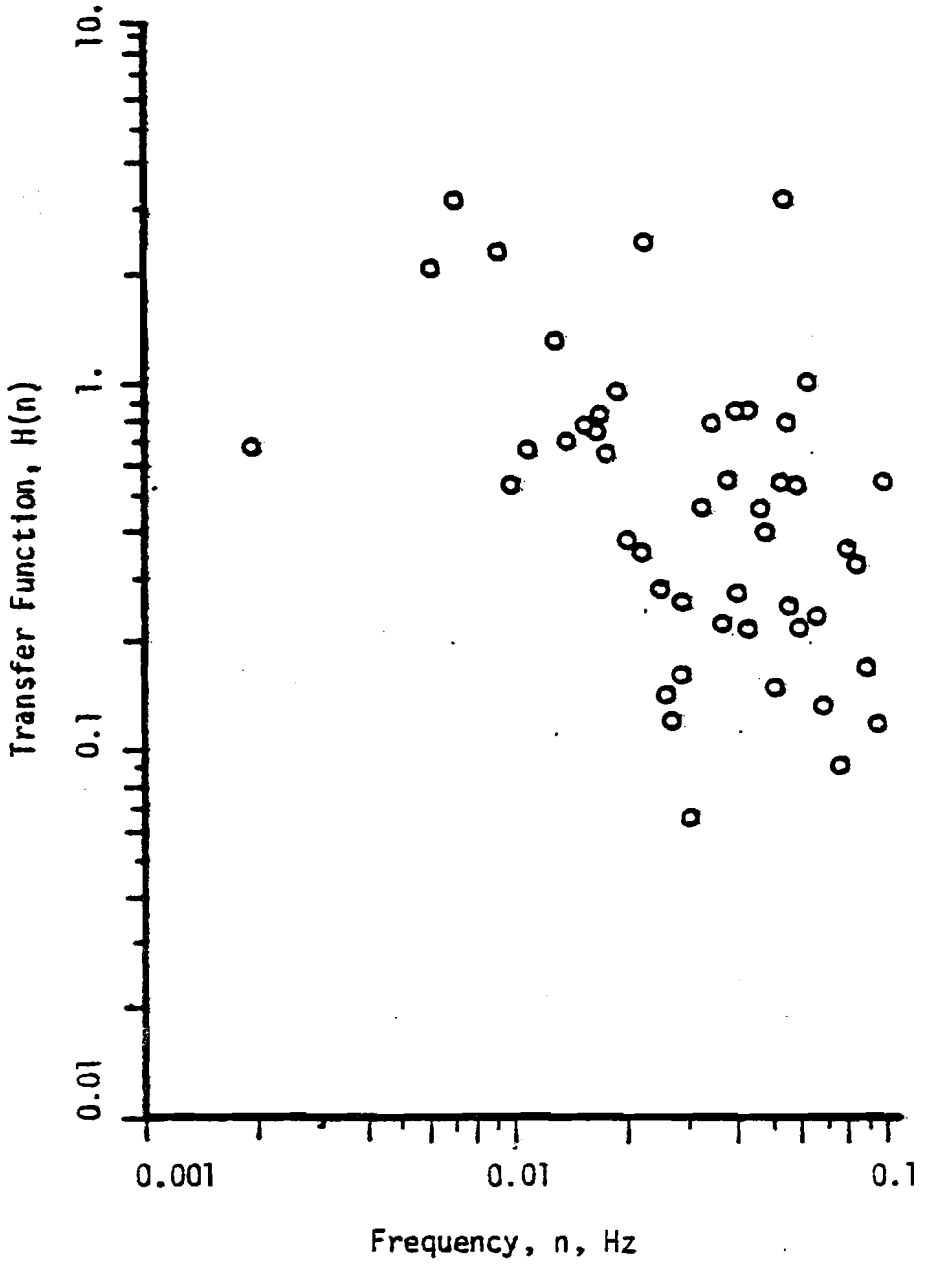

FIGURE 75. WIND DIRECTION TO YAW TRANSFER FUNCTION: WFR 18/22

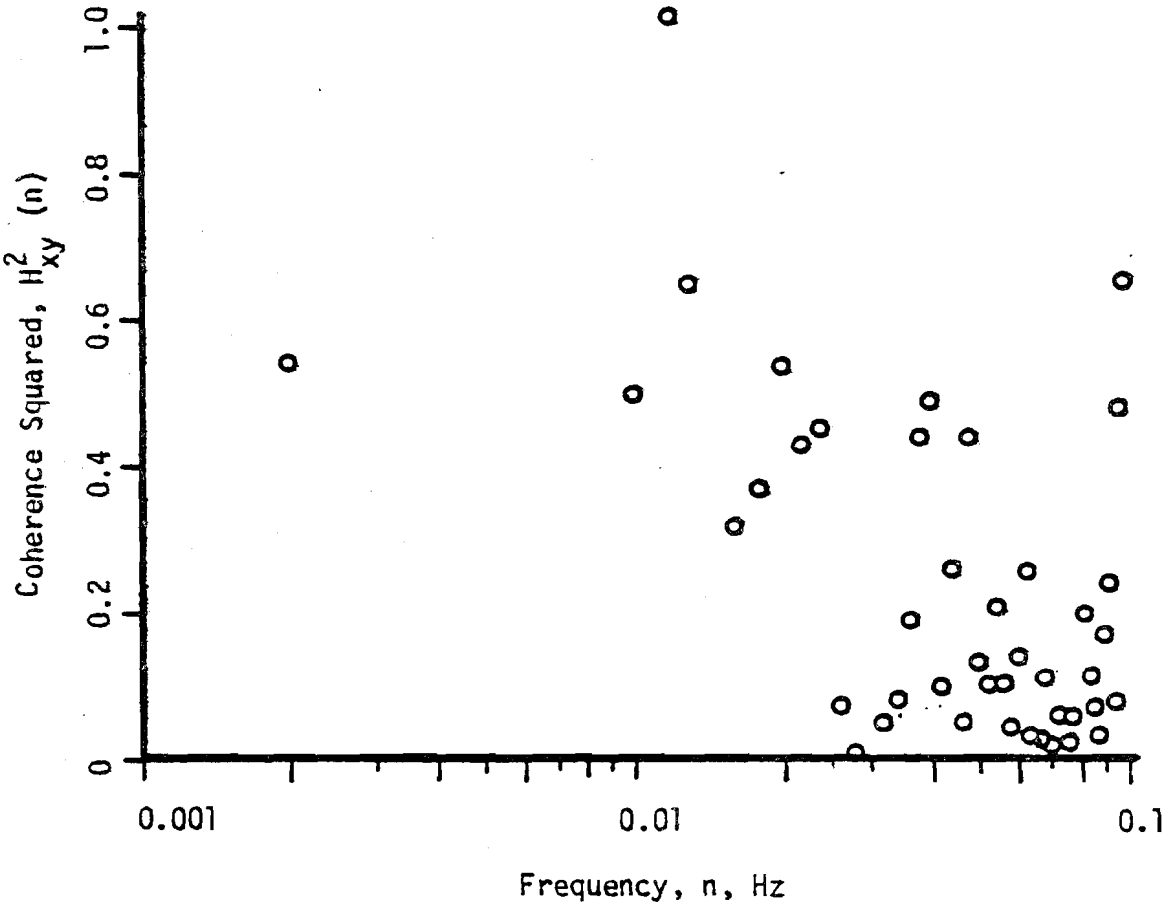

FIGURE 76. WIND DIRECTION TO YAW TRANSFER FUNCTION: WFR 18/22

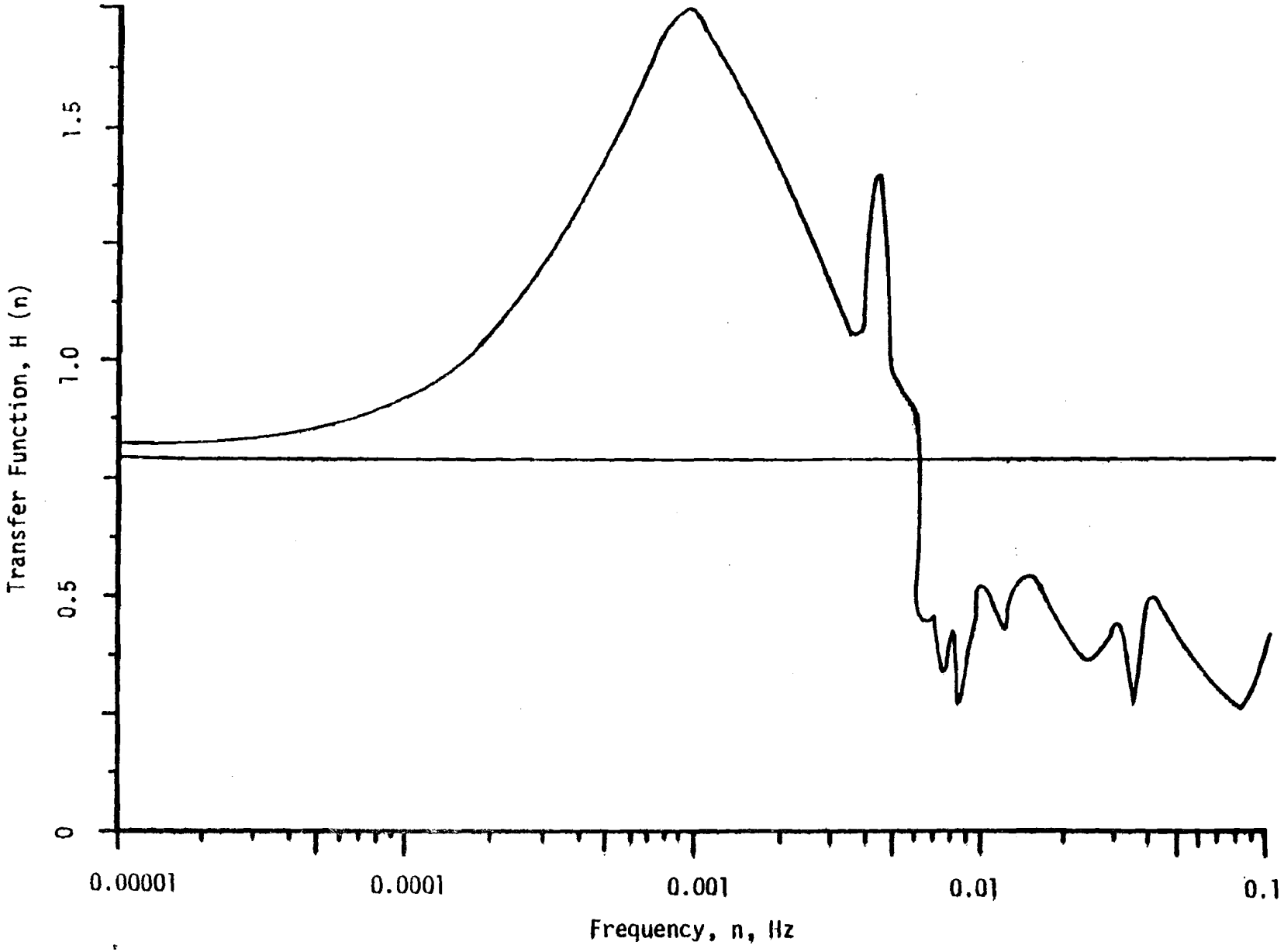

FIGURE 77. DAMPED YAW THEORETICAL TRANSFER FUNCTION

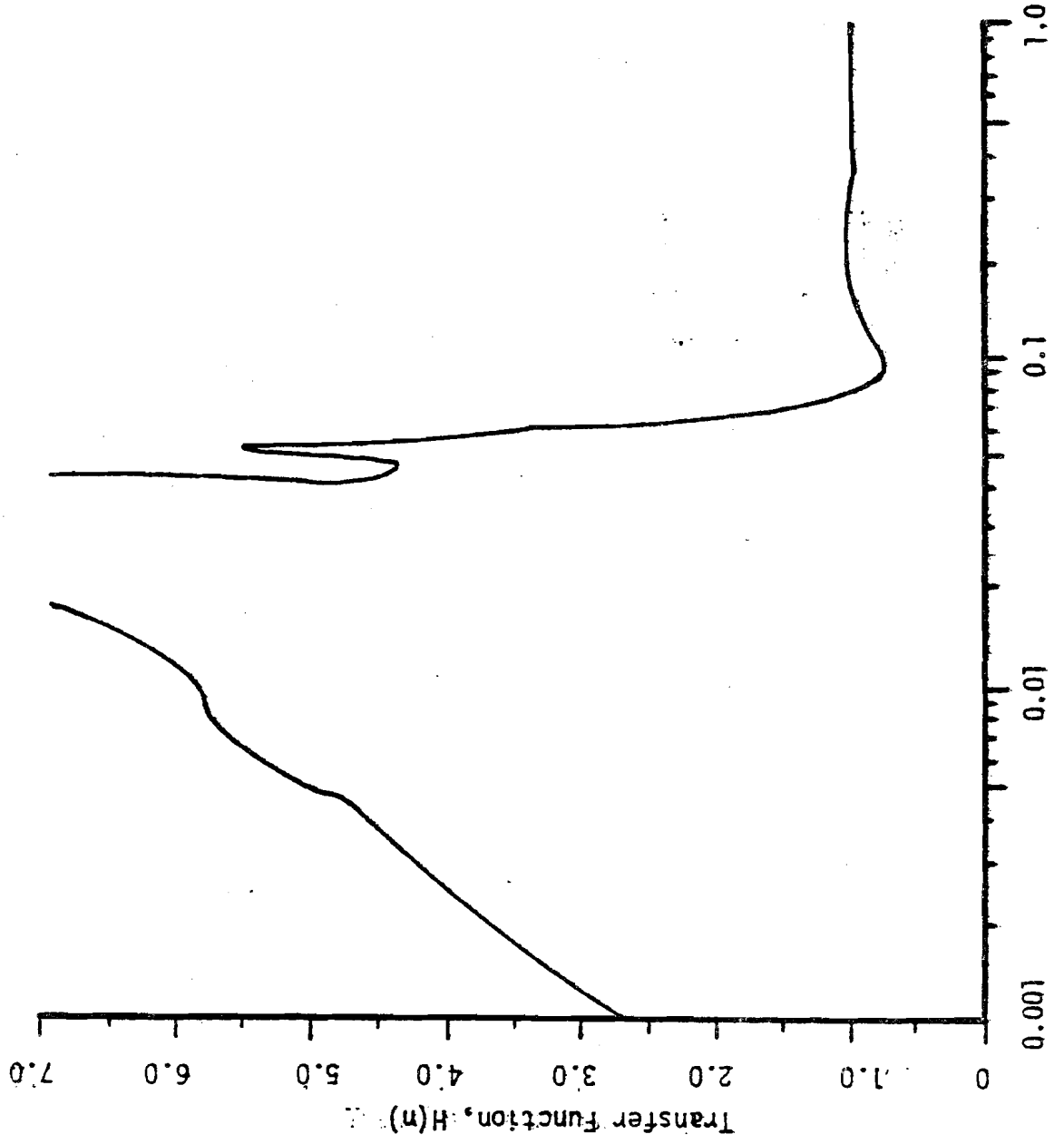

FIGURE 78. UNDAMPED YAW THEORETICAL TRANSFER FUNCTION

Even though the theoretical transfer functions can not be verified directly, it appears that the predicted peaks could well be close in frequency to those of the actual system. Because of the clarity of the theoretical curves, they are most useful in determining the major differences in the damped and undamped yaw response.

The most important difference is that damping severely restricts the magnitude of the resonant oscillations. This is seen in the comparison of Figs. 77 and 78. In Fig. 78, the magnitude of the primary peak is much greater than 7 DEG^2/DEG^2. The corresponding peak in Fig. 77 is much smaller, at 1.75 DEG^2/DEG^2.

Yaw damping also has the effect of attenuating the higher frequency response. In Fig. 77, the damped response is seen to sharply decrease below 0.5 DEG^2/DEG^2 at approximately 0.006 Hz. The undamped nacelle still responds strongly to wind direction fluctuations above 0.05 Hz, and at 1.0 Hz has a level response of 1.0 DEG^2/DEG^2.

Damping of the nacelle yaw response thus attenuates the magnitude and frequency of the resonant oscillations, thereby allowing the nacelle to better track the changing wind direction.

C H A P T E R I V

FAR FIELD MEASUREMENTS

4.1 Introduction

In Chapter III, the response of the wind turbine to the dynamic wind field was investigated. This chapter investigates the effect that the wind turbine has on the wind field.

A single analog record is analyzed to provide this information. In addition to generator current and wind direction, pulses from five anemometers in the wind field were recorded. The layout of the anemometer towers is shown in Fig. 2.

The digitizing of the analog record was done in two different manners, as discussed in Section 4.2. The pertinent information about the analog and digital records is shown in Table 10.

The mean wind direction was along the line of the anemometer towers. This enabled an investigation into the validity of Taylor's Hypothesis, which is discussed in Section 4.3. In this context, the effect of the wind machine on the wind field can be easily discussed.

4.2 Comparison of Data Analysis Techniques

The initial analysis of the far field data used a different wind speed sampling technique from that used for the interaction measurements in Chapter III. The wind speeds in WFR19 were determined using a LSI microprocessor program which counted the number of anemometer pulses over a given time interval, which in this case was 1.25s. These data were than analyzed in the standard manner with BMD02T after translation and scaling with DECODE (see Appendix A).

ANALOG WIND FIELD RECORD	DIGITAL WIND FIELD RECORD	SAMPLING INTERVAL t,s	DIGITAL WFR LENGTH,s	AVERAGE GENERATOR CURRENT, I, AMPS	AVERAGE WIND SPEED, U, m/s BY ANEMOMETER NUMBER				
					1	2	3	4	5
12	19	1.25	1250	21.6	7.30	7.75	7.76	8.44	9.15
	26	1.00	1000	18.9	7.41	9.60	8.56	8.54	9.64

TABLE 10. WIND FIELD RECORD DATA SHEET FOR WFR 19 AND 26

The new sampling technique was necessary to sample all five wind speeds concurrently, since only one anemometer pulse integrator box was available. To check the results, the autocorrelation for the No. 5 anemometer wind speed was computed after sampling in the standard manner. The results are shown in Fig. 81. The integral time scales for No. 5 anemometer, as computed by the two techniques, are significantly different: 11.9s for the pulse integrating (old) technique and 33s for the averaging (new) technique.

As a quick check to determine the validity of this processing technique, the probability density function (PDF) of wind speed was plotted. Speeds for anemometer No. 5 are plotted for WFR19 and WFR21 in Fig. 79. The PDF and WFR19 is strikingly skewed toward higher wind speeds, and the right-hand tail is cut short. The PDF for WFR26 is nearly symmetrical in shape.

Because of these differences, an analytical comparison of the two techniques was made. For this comparison, the signal average over the time interval (the new technique) was approximated as the average of the two interval endpoints. The two techniques used in the analytical comparison are shown in Fig. 80.

The equations developed for the sample mean using the old and new techniques, respectively, are shown below:

$$\bar{x} = \frac{1}{N} \Sigma \, (x_1 + x_2 + \ldots + x_N) \tag{59}$$

$$\bar{y} = \frac{1}{N} \Sigma \, (\frac{1}{2} x_1 + x_2 + \ldots + x_{N-1} + \frac{1}{2} x_N) \tag{60}$$

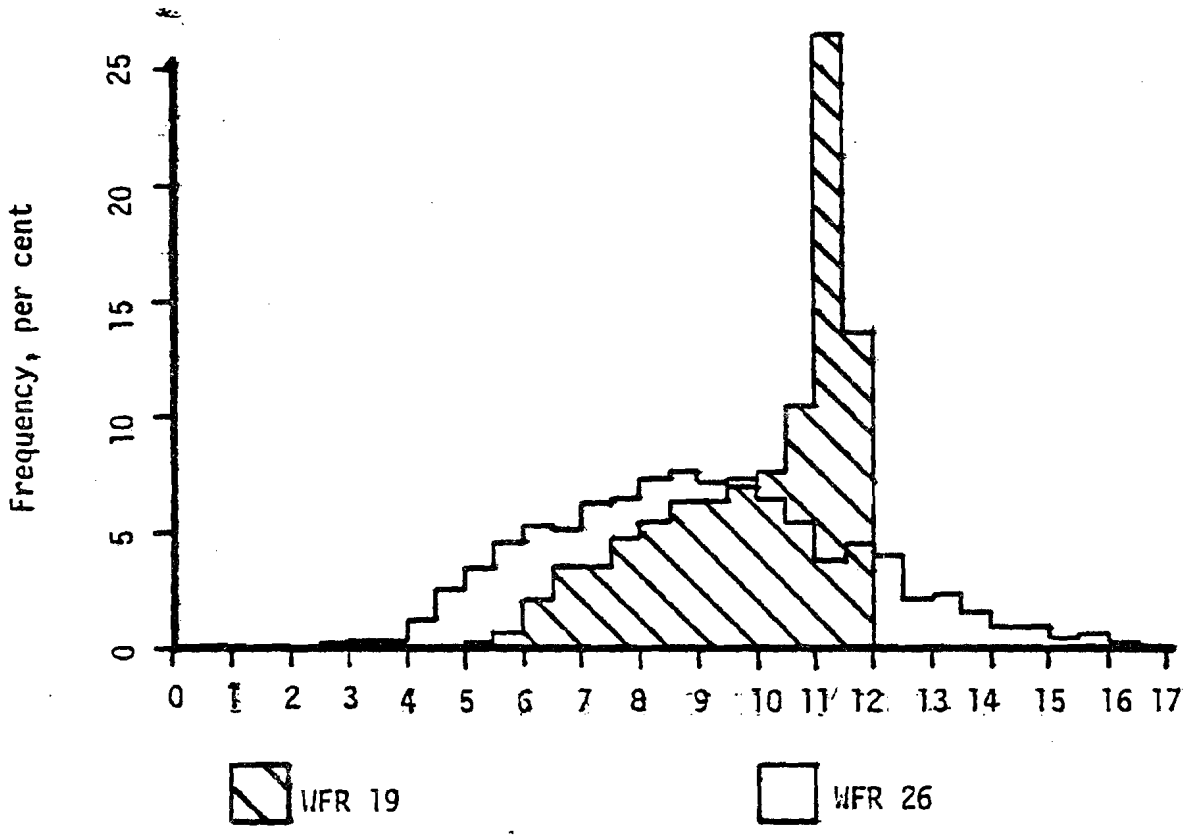

FIGURE 79. WIND SPEED PROBABILITY DENSITY FUNCTION: WFR 19/26

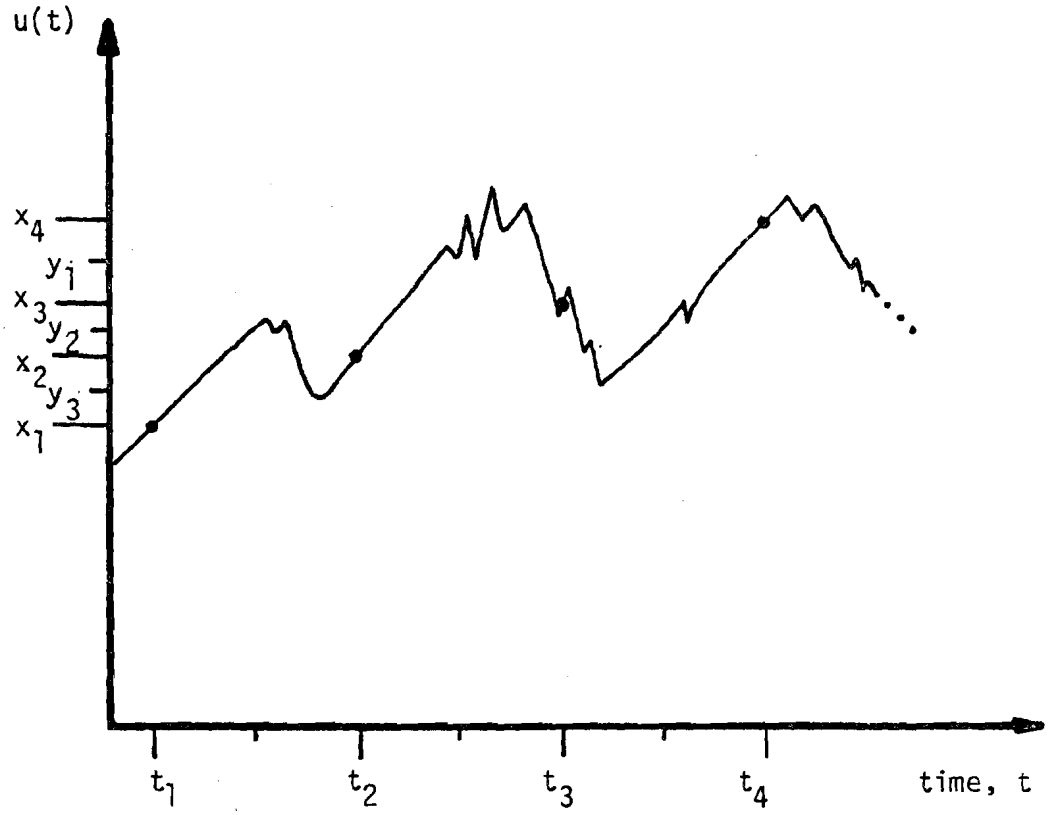

Figure 80. Wind Field Record Sampling Techniques

For a large number of data points, the means for both techniques can be seen to be nearly identical.

Similar equations for the autocorrelation were also developed. For the old and new techniques, respectively, these are:

$$Q_x\ (k) = \frac{N}{N-k} \frac{\Sigma x_i\ x_i\ + k}{x_i^2} \tag{61}$$

$$Q_x\ (k) = \frac{N}{N-k} \frac{\Sigma y_i y_{i+k} + y_i y_{i+k+1} + y_{i+1} y_{i+k} + y_{i+1} y_{i+k+1}}{\Sigma\ (y_i^2 + 2y_i y_{i+1} + y_{i+1}^2)} \tag{62}$$

For a small sampling interval, the instantaneous wind speed should be nearly identical with a time average of wind speeds near that point. Thus for a small Δt, the two sampling techniques should yield similar results. The additional terms seen in Eq. (62) would then be negligible.

The quantitative assessment of the differences in calculated statistical parameters for the two techniques could not be made directly from these equations. For example, it could not easily be seen how the autocorrelation (and hence the integral scales) should be influenced by the change in digitizing technique.

As a result, a more direct approach was taken: each wind speed channel was processed sequentially with the old technique. This new record is WFR26. This approach is more cumbersome than sampling all channels simultaneously, but reliable statistical results are ensured. A direct comparison of the differences in the two digitizing techniques was then made by comparing WFR19 and WFR26.

The autocorrelation of wind speed for WFR19 and 26 are compared for each anemometer in Figs. 81 through 85. In Figs. 81, 82, and 83, the autocorrelation for WFR19 takes significantly longer to become uncorrelated than for WFR26. This is probably because the averaging technique used in WFR19 obscured the high frequency randomness in the wind speed signal. This would cause the autocorrelation function to remain correlated over a longer period.

The idea that the averaging technique used in WFR19 attenuates the high frequencies is supported in the PSD of wind speed for anemometer No. 5. The PSD for WFR19 and 26 are shown in Fig. 86. Both are seen to fall off to the expected -5/3 power, but above 0.005 Hz, the fluctuations in WFR19 contain significantly less power than WFR26. But this idea runs into difficulty in comparing $Q_x(\tau)$ in Figs. 84 and 85. These anemometers are 2-blade radii ahead and behind the WF-1 centerline, respectively. For the anemometers downwind of the disc, high frequency turbulence from the blades is expected. If the averaging technique actually obscures the high frequency components in the turbulence, the autocorrelations for WFR19 and 26 should be further apart, not closer together as they are. This indicates that the high frequency gusts

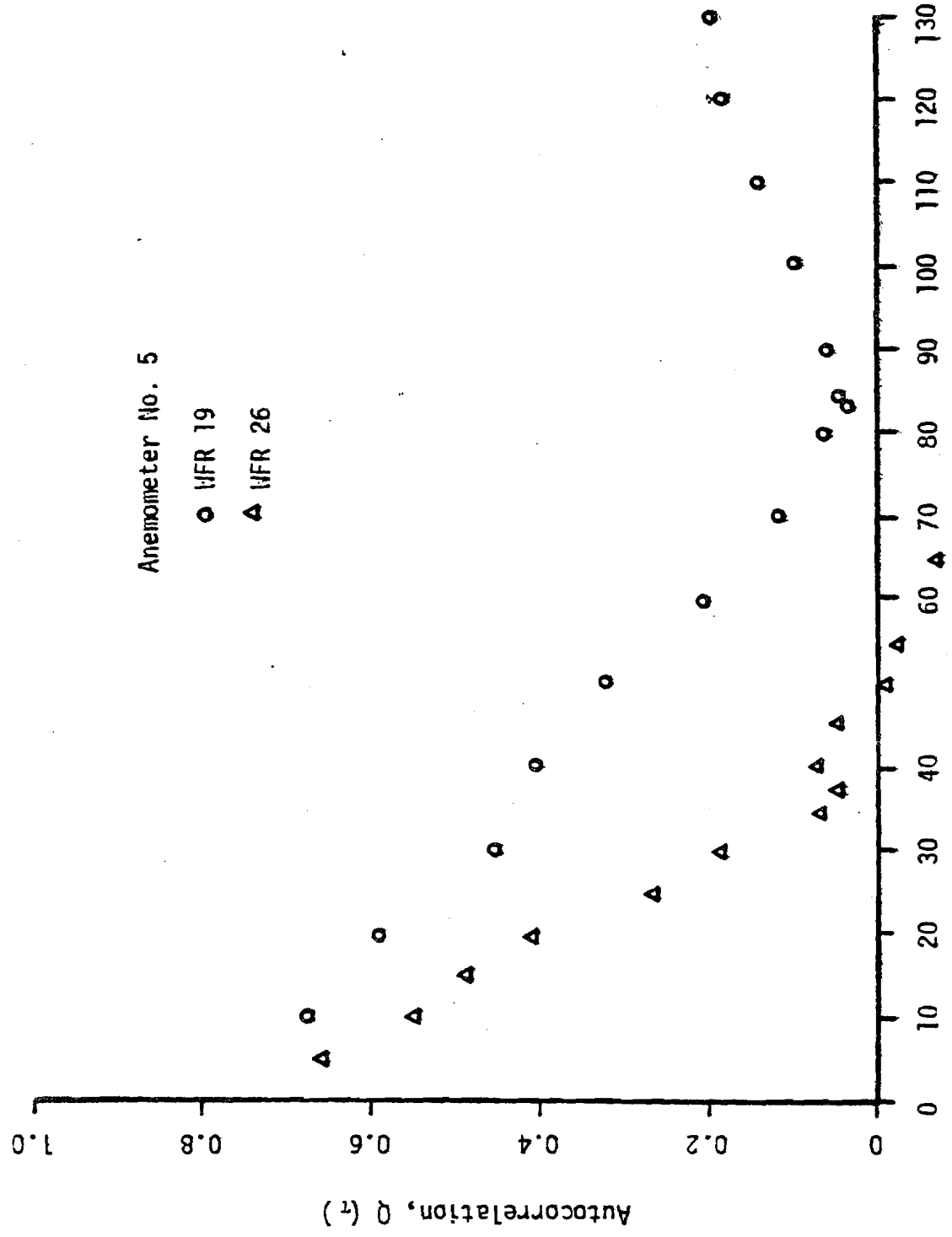

FIGURE 81. WIND SPEED AUTOCORRELATION, ANEMOMETER NO. 5: WFR 19/26

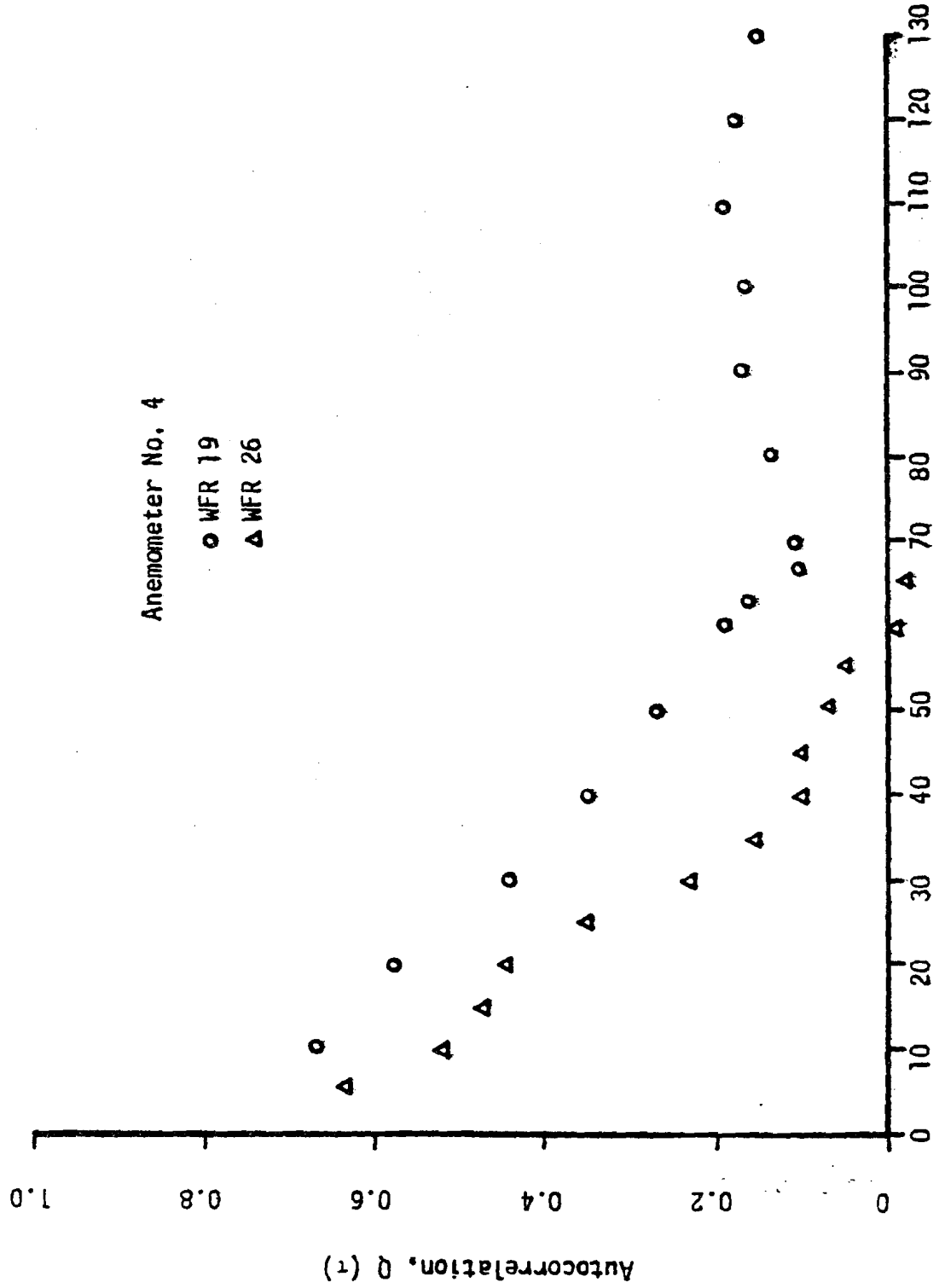

FIGURE 82. WIND SPEED AUTOCORRELATION, ANEMOMETER NO. 4: WFR 19/26

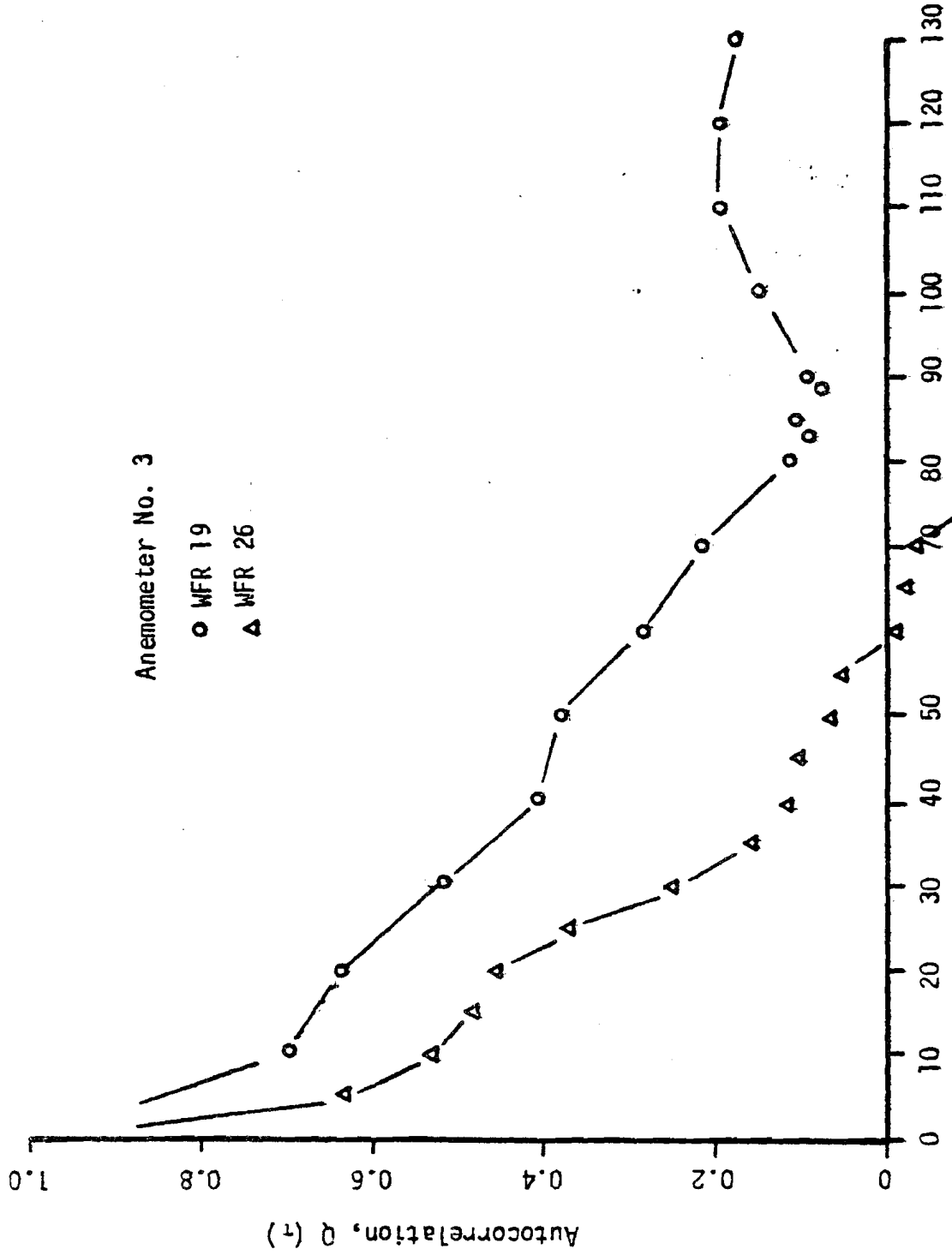

FIGURE 83. WIND SPEED AUTOCORRELATION, ANEMOMETER NO. 3: WFR 19/26

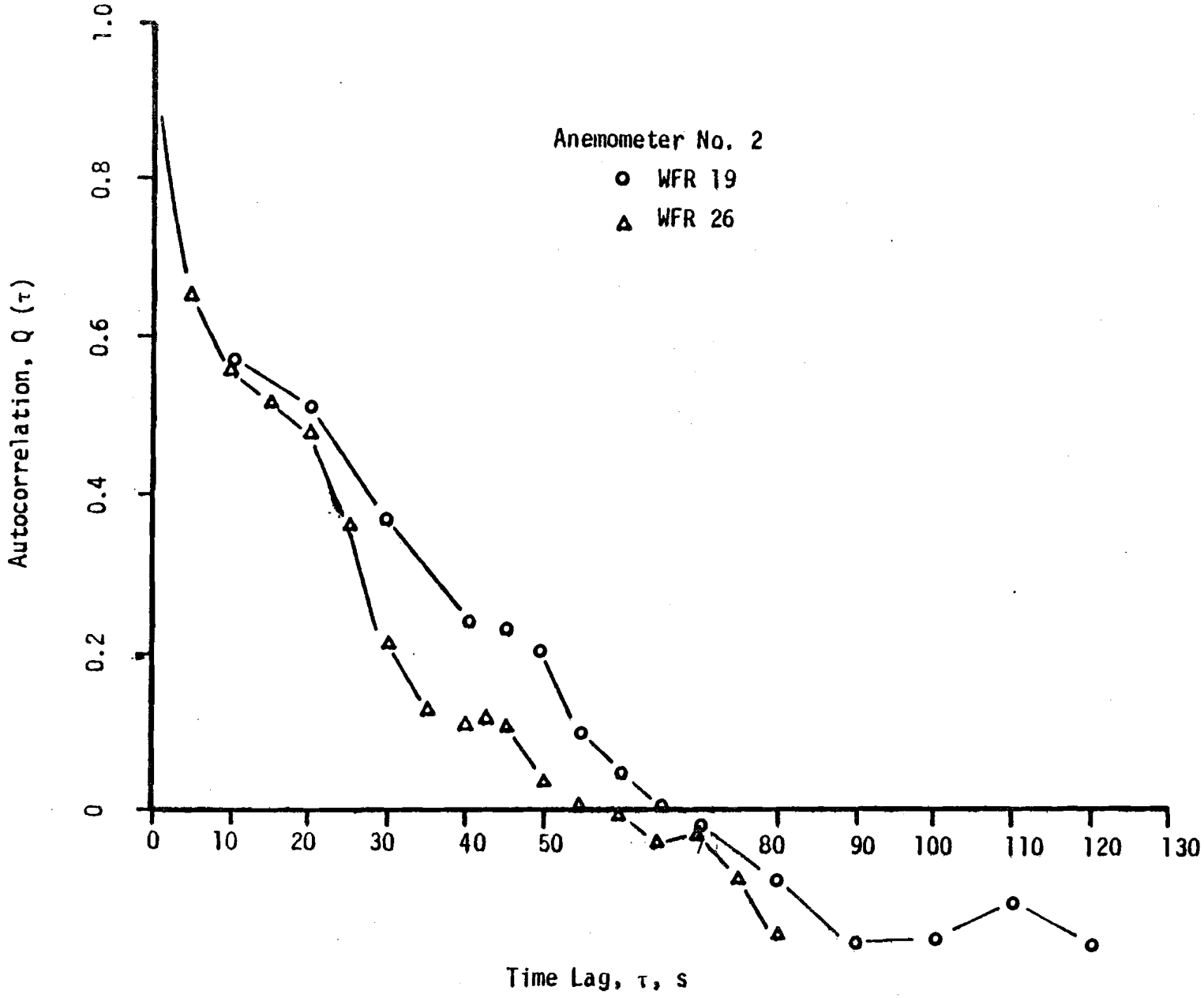

FIGURE 84. WIND SPEED AUTOCORRELATION, ANEMOMETER NO. 2: WFR 19/26

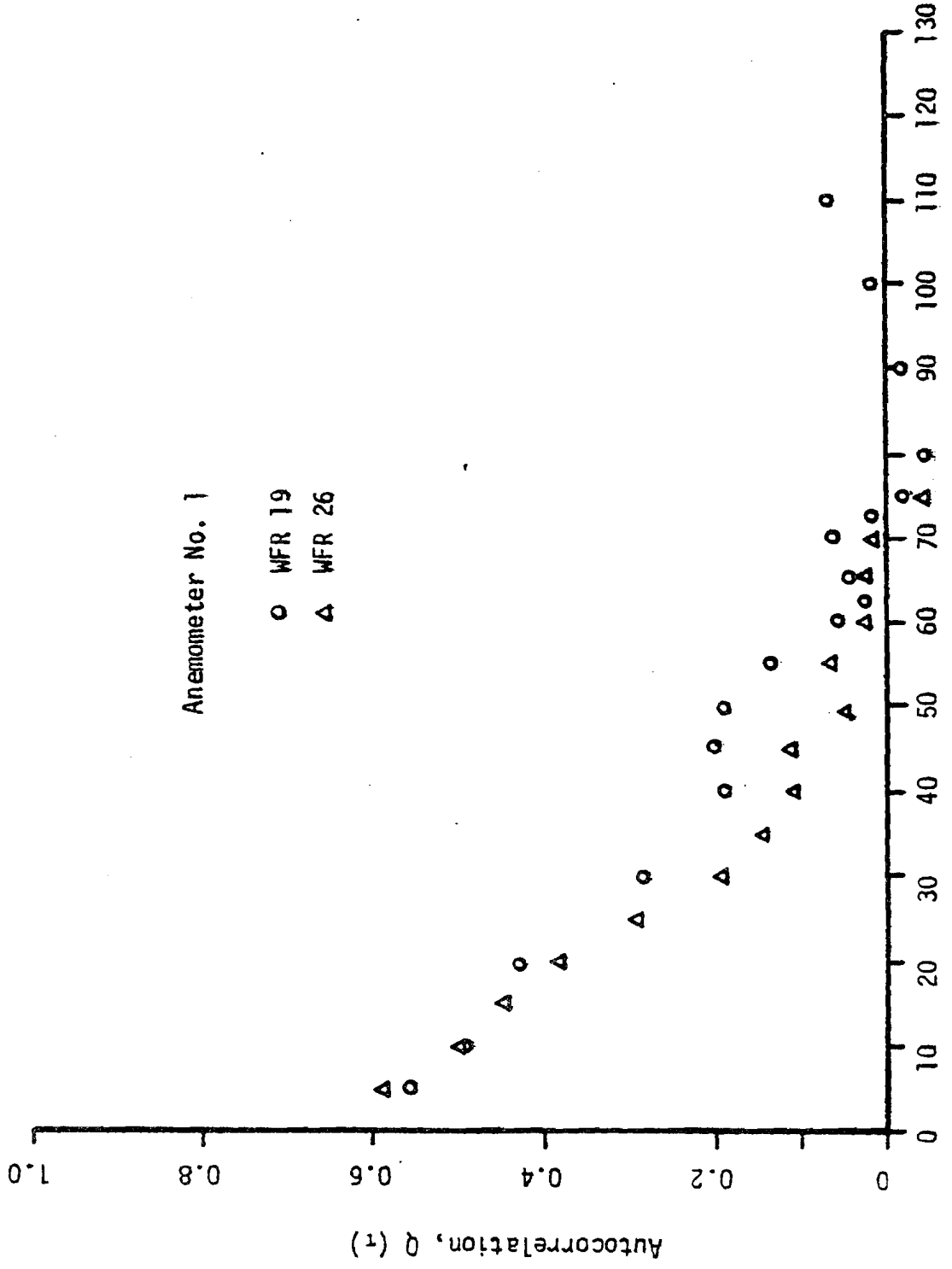

FIGURE 85. WIND SPEED AUTOCORRELATION, ANEMOMETER NO. 1: WFR 19/26

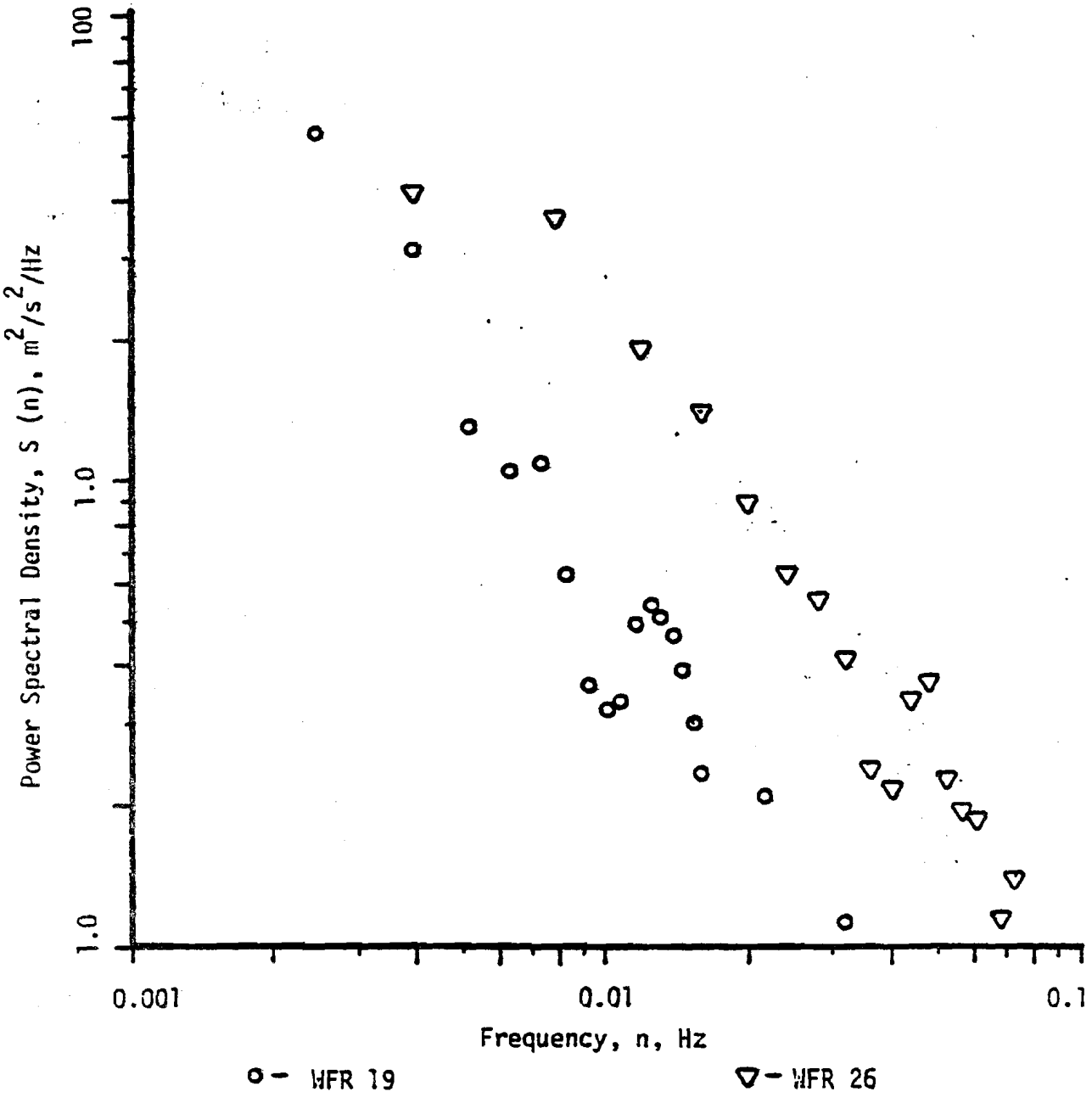

FIGURE 86. WIND SPEED POWER SPECTRAL DENSITY: WFR 19/26

are being attenuated in the wind field close to the blade disc, as expected from theory[23]. This is discussed in Section 4.3.

Additional work is essential before the practical differences in the two sampling techniques can be completely understood. For the remainder of the work, only WFR26 is used. This technique is consistent with the other work already completed.

4.3 Taylor's Hypothesis

Taylor[24] hypothesized that for isotropic turbulence, the turbulent cells were carried along with the mean flow, substantially unchanged in character over large distances. In the downstream direction, this might be summarized as[25]:

$$u(t) = u(t + \frac{x}{U}) \tag{63}$$

where x is the distance between two measuring stations oriented parallel to the flow.

A first examination of Taylor's hypothesis is through the power spectra for each anemometer. These are shown in Figs. 87 through 91.

Examination of each power spectra in turn reveals a general distribution of power in the frequencies above 0.06 Hz downward, building a peak at 0.045 Hz. This peak becomes higher and sharper as the gust travels toward the blade disc. Passing through the disc, the power has again been redistributed into the higher frequencies. Since Figs. 87 through 91 are power spectra and <u>not</u> the PSD for each anemometer, no magnitude variation can be assessed. This is found from the

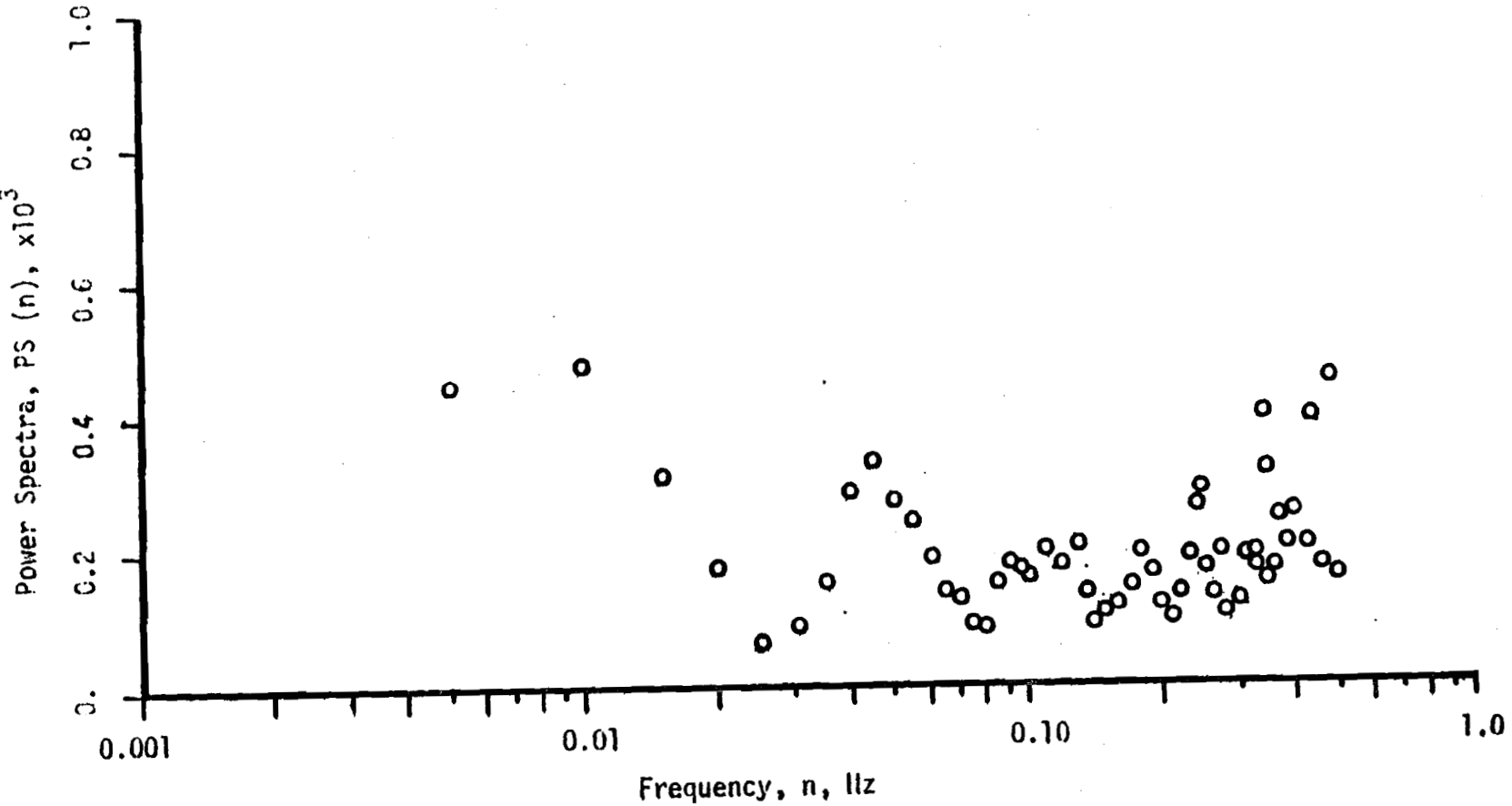

FIGURE 87. WIND SPEED POWER SPECTRA: WFR 26: ANEMOMETER 5

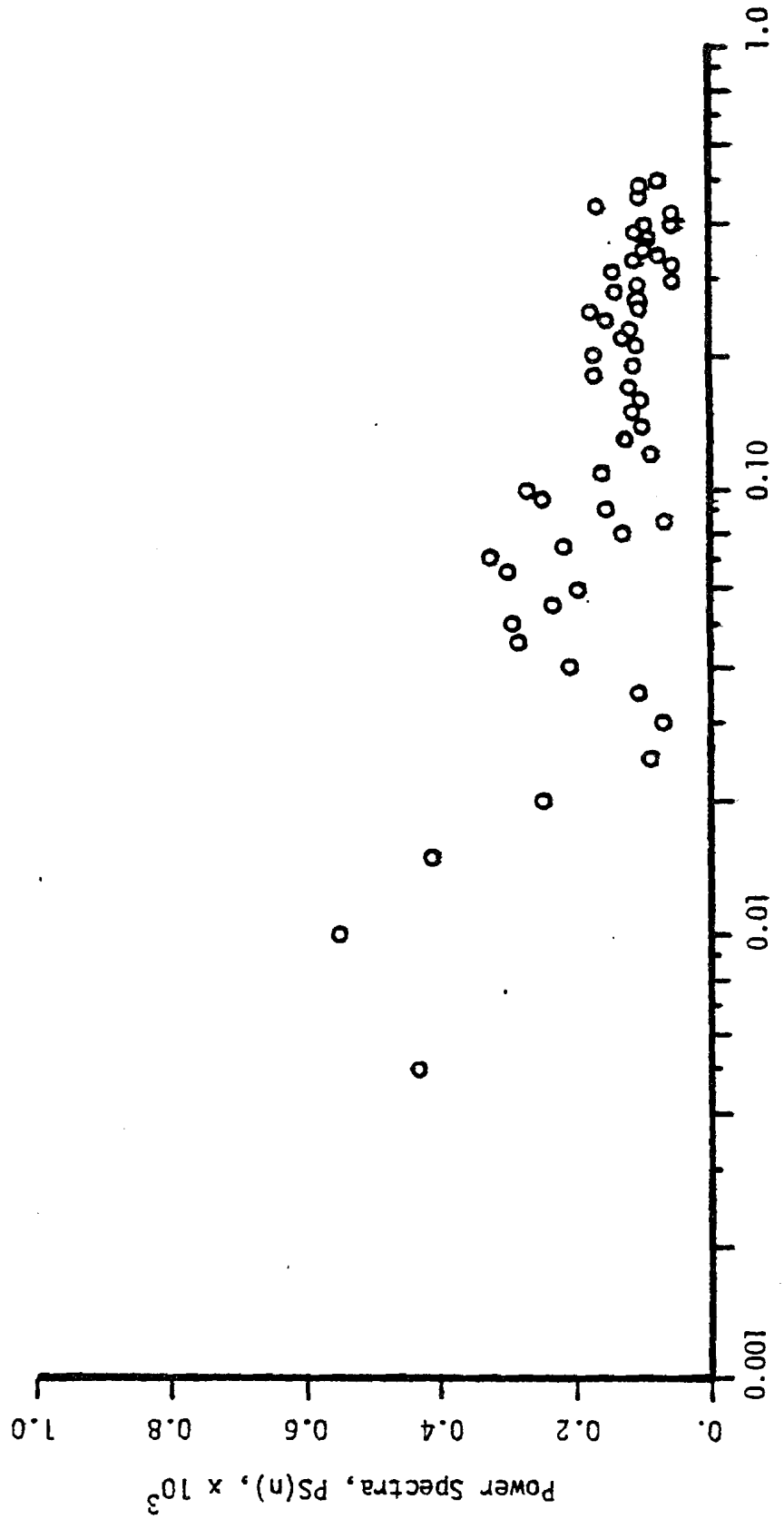

FIGURE 88. WIND SPEED POWER SPECTRA: WFR 26: ANEMOMETER 4

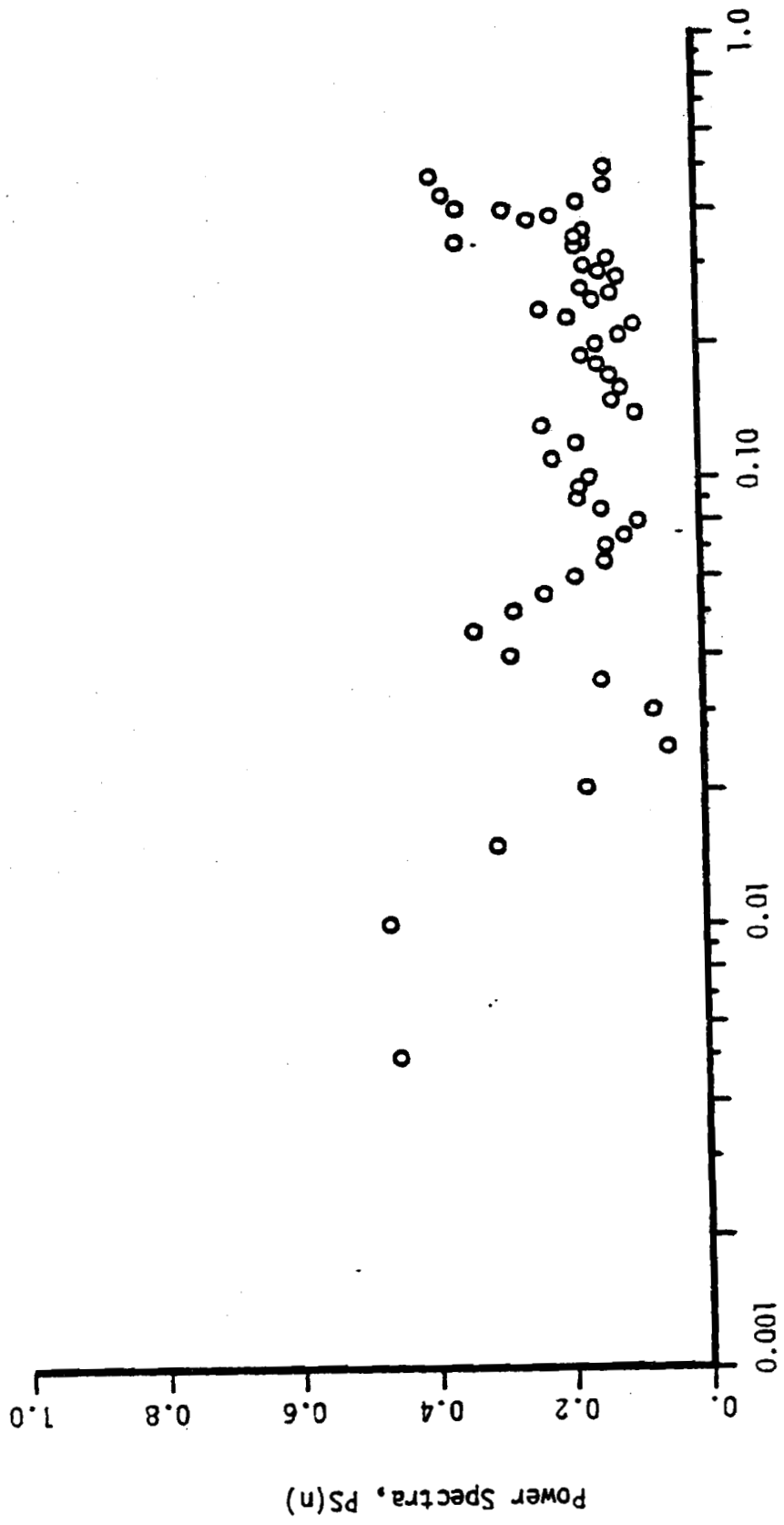

FIGURE 89. WIND SPEED POWER SPECTRA: WFR 26: ANEMOMETER 3

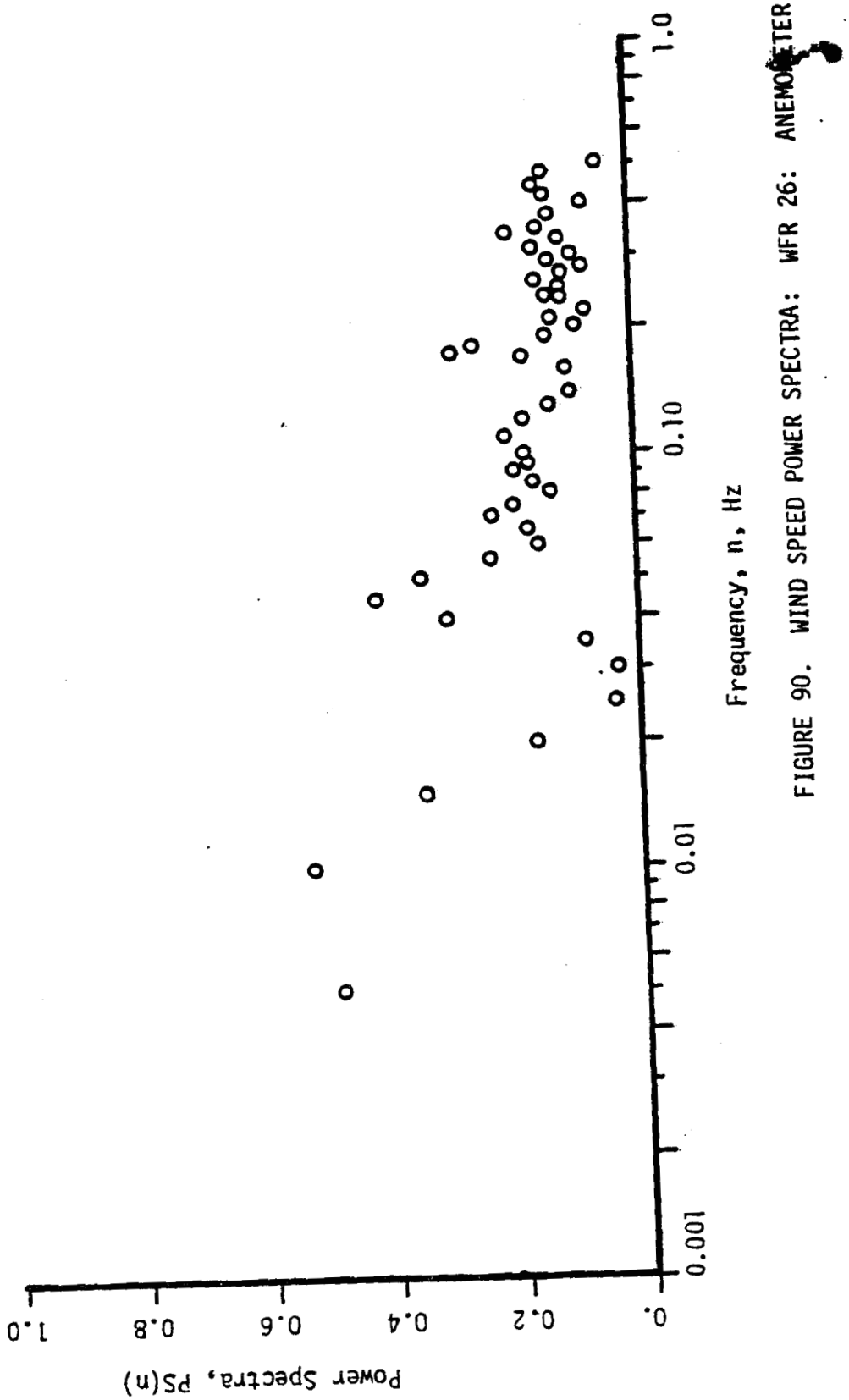

FIGURE 90. WIND SPEED POWER SPECTRA: WFR 26: ANEMOMETER 2

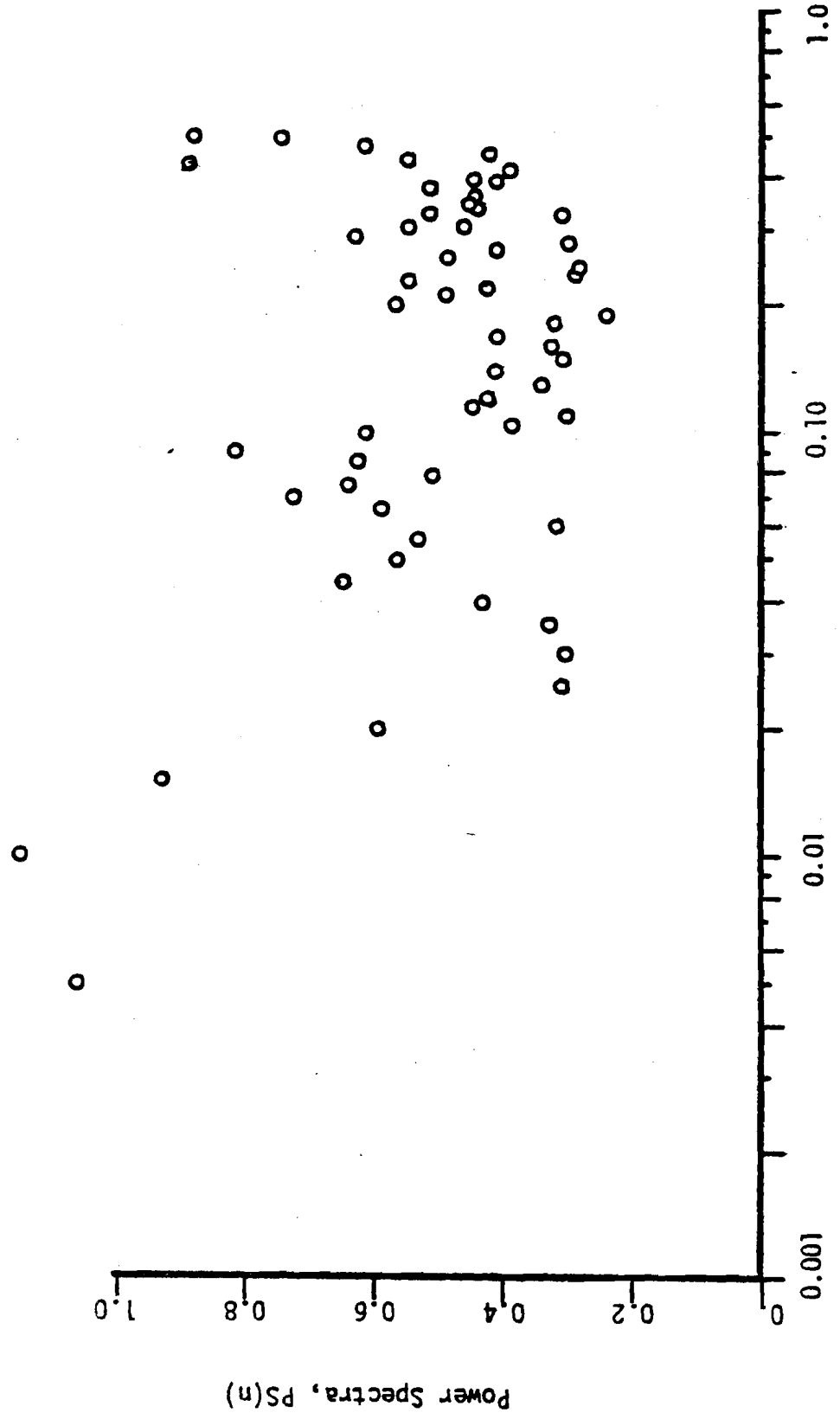

FIGURE 91. WIND SPEED POWER SPECTRA: WFR 26: ANEMOMETER 1

transfer function.

The transfer functions for the upstream anemometer to each downstream anemometer are given in Figs. 92 through 95. Since the transfer function in Figs. 92 and 93 are virtually identical in magnitude and form, it is inferred that no power redistribution with frequency has taken place. A marked change takes place over the interval, within 3 blade radii of the wind turbine (Figs. 93 and 94). The power in the turbulence becomes sharply peaked at 0.045 and 0.085 Hz. This power, as indicated in both the transfer function and power spectra, seems to be redistributed from the higher frequency gusts.

Passing through the blades, a distinct change in the transfer function magnitude indicates significant power extraction from the minimum resolved frequency to about 0.05 Hz. Above this point little power is extracted from the turbulence. For example, the peak seen at 0.085 Hz in Fig. 94, is substantially unattenuated in Fig. 95. This result is of course expected since the half-power point is known to be 0.03 Hz.

A test of Taylor's hypothesis can be made at least in the wind field outside of the known region of influence of the machine. This is probably about 3 blade radii from the machine, as inferred from the transfer functions for wind speeds. For this test, the cross-correlations between anemometers are studied.

A gust which remains unchanged in character and which moves along with the wind speed should be resolved at a downstream anemometer at time T after being resolved at tower five. The peak in the cross-correlation should be at this time deplacement. Based on the mean wind speeds

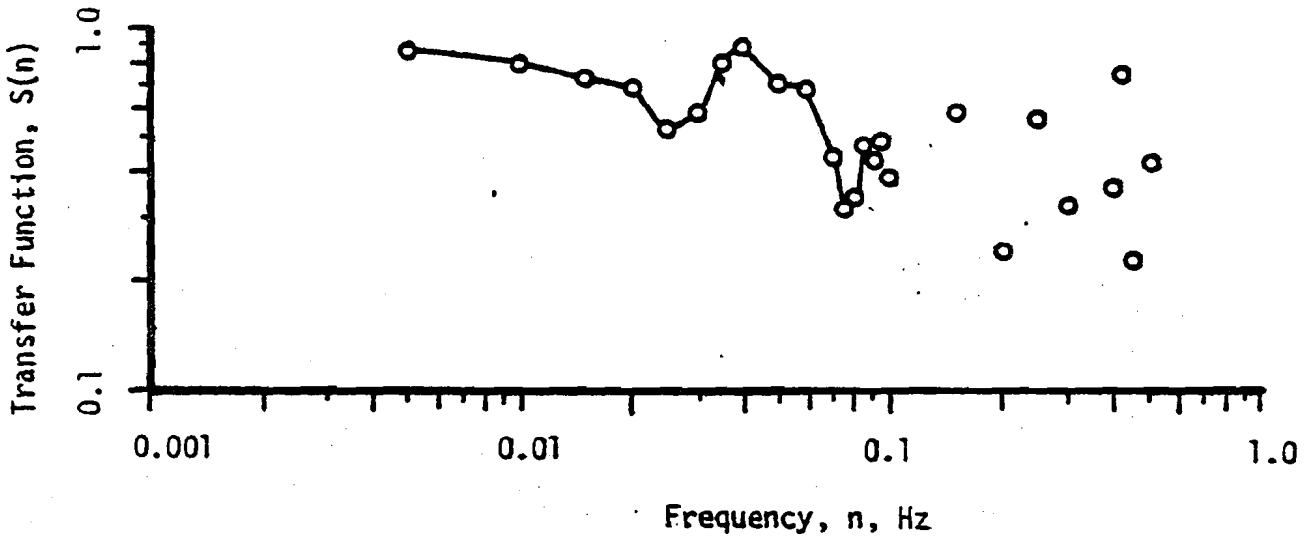

FIGURE 92. TRANSFER FUNCTION: WFR 26 ANEMOMETER NO. 5 to NO. 4

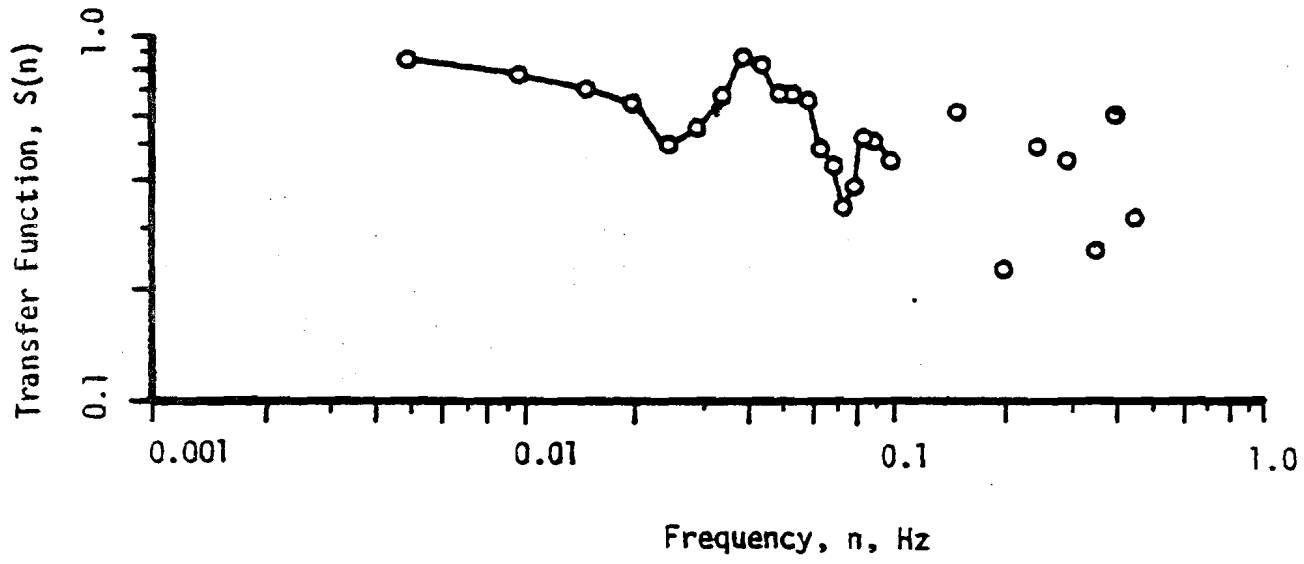

FIGURE 93. TRANSFER FUNCTION: WFR 26 ANEMOMETER NO. 5 to NO. 3

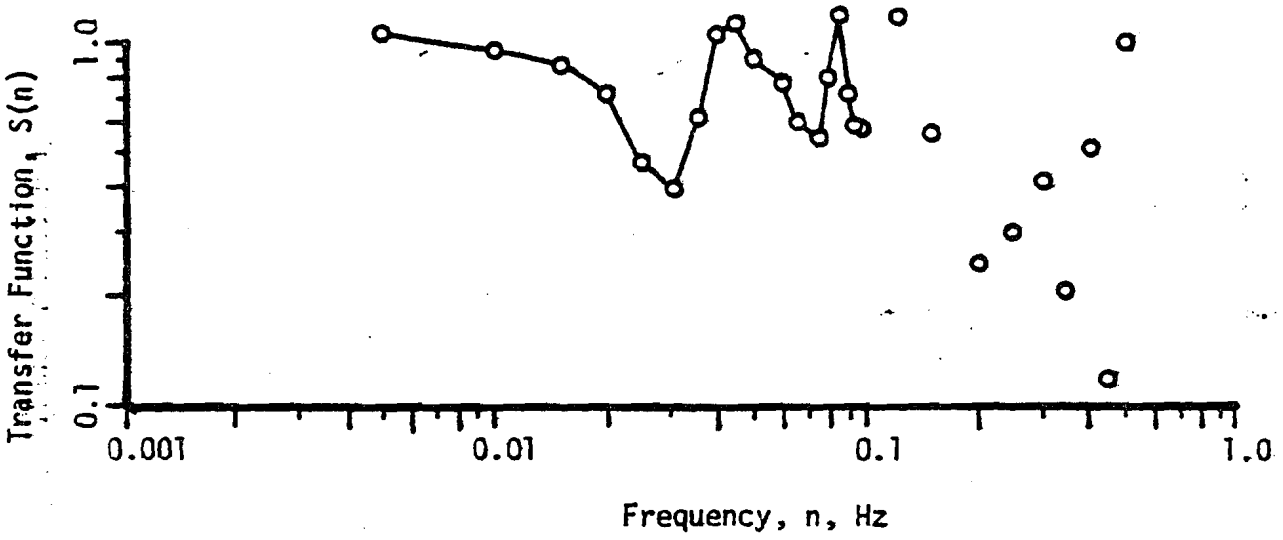

FIGURE 94. TRANSFER FUNCTION: WFR 26 ANEMOMETER NO. 5 to NO. 2

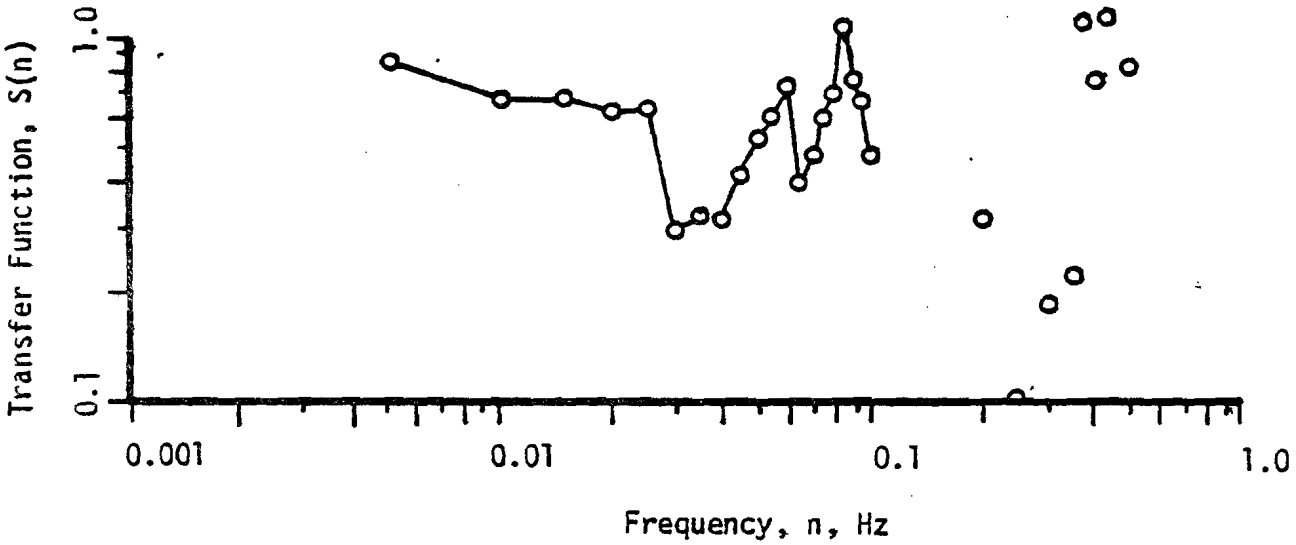

FIGURE 95. TRANSFER FUNCTION: WFR 26 ANEMOMETER NO. 5 to NO. 1

and the distances between towers, the time lag expected for each tower is tabulated in Table 11. For comparison, the cross-correlations are shown in Fig. 96. When time displacement at the peak of each is compared with the expected value, it is found that Taylor's hypothesis is not confirmed.

Taylor originally made this hypothesis regarding isotropic turbulence in wind tunnel tests. The extension as above to the anisotropic wind field is probably not valid. However, while individual gusts may not retain their identify in passing through the wind field, the power distribution with frequency remains substantially unchanged to within 3 blade radii of the machine.

TOWER NUMBERS	AVERAGE WIND SPEED U, ms	DISTANCE BETWEEN TOWERS, m	CALCULATED GUST TRAVERSAL TIME BETWEEN TOWERS, s	ESTIMATED GUST TRAVERSAL TIME FROM CROSS-CORRELATIONS, s
5 4	9.1	24.75	2.7	1
5 3	8.9	34.65	3.9	1
5 2	9.1	39.60	4.4	2
5 1	8.8	59.40	6.8	5

TABLE 11. WIND SPEED GUST TRAVERSAL TIMES BETWEEN ANEMOMETER TOWERS

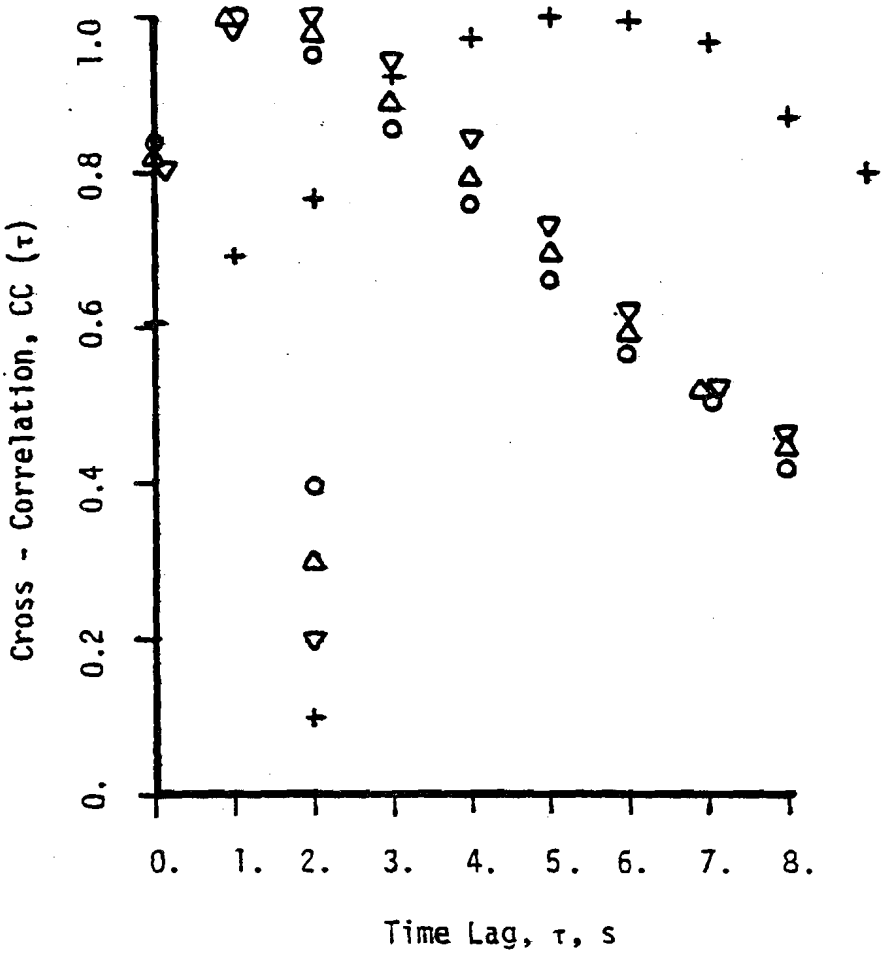

FIGURE 96. WIND SPEED CROSS-CORRELATIONS

CHAPTER V

CONCLUSIONS AND RECOMMENDATIONS FOR FUTURE WORK

The wind field was characterized with the integral scales for wind speed and direction. For wind speed the average gust length was found to be between 40 and 200 m; the average gust in the cross-stream direction has smaller dimensions, between 17 and 100 m. The ratio of these length scales is approximately 1:0.4. This is in agreement with Davenport, who found:

$$L_u:L_v = 1:0.31 \tag{64}$$

The power distribution in the wind turbulence was found to remain substantially unchanged to within 3 blade radii of the disc. Closer to the disc, power at high frequencies was attenuated, while power increased at lower frequencies, particularly at 0.045 and 0.085 Hz.

The power spectral density for both wind speed and wind direction were seen to fall off to the -5/3 power above 0.01 Hz, as expected. The peak in the PSD for wind speed, as found from the fit to the empirical relationship of Davenport, is 0.003 to 0.004 Hz.

The wind turbine was found to behave as a low-pass filter with a half-power point at 0.03 Hz. Above this frequency, the power in the turbulence is attenuated.

The wind turbine captures about 70% of the power available in the turbulence. Such a significant power extraction potential should not be ignored in future designs.

A comparison of the damped and undamped yaw response of the nacelle showed that in both, the machine tracked the low frequency variations in wind direction. In a light, gusty, wind the nacelle was seen to yaw

more than 90° from the steady-state position. This was found by Cohen[26] to be due to the gyroscopic moments exerted on the nacelle by the rotating blades. This was found to be a definite disadvantage in a light wind, since the wind could not always yaw the machine back into position.

This work has been by no means exhaustive. In particular, three projects remain:

1) Wind Field Visualization: smoke bombs released upstream of the wind turbine should provide a visualization of the air flow through and around the blade disc. This would be helpful in confirming the analytical model by Modaressi and Kirchhoff[27]. Preliminary tests are complete but no results have yet been obtained.
2) Near Field Measurements: wind velocity measurements in close proximity to the blade disc are required to confirm the model by Modaressi and Kirchhoff.
3) The statistical relation between the two data analysis techniques discussed in Section 4.2 would be most helpful in the analysis of Far Field data in the future.

The data acquisition system is complete and highly versatile. It is hoped that the system will be used extensively in the future to analyze the dynamic interaction of machine and wind field, and to study the power extraction from the air turbulence by the wind machine.

FOOTNOTES

1. P.A. Murphy and R.H. Kirchhoff, "Measurements of the Dynamic Interaction of the Wind Field with a Horizontal Axix Wind Turbine," Energy Alternatives Program Technical Report UM-WF-TR-78-6, University of Massachusetts, March, 1979, pp. 49-62.

2. W.J. Dixon, ed., "BMD02T," Biomedical Computer Programs, 3rd ed., University of California Press, Los Angeles, 1973, pp. 459-473.

3. J.S. Bendat and A.G. Piersol, Random Data: Analysis and Measurement Procedure, Interscience, New York, 1971, pp. 12-34.

4. R.W. Harris and T.J. Ledwidge, Introduction to Noise Analysis, Pion Ltd., London, 1974, pp. 48-51, 55-66.

5. Bendat and Piersol, op. cit., pp. 17, 21.

6. Ibid., p. 22.

7. A.G. Davenport, "The Spectrum of Horizontal Gustiness Near the Ground in High Winds," Royal Meteorological Society Quarterly Journal, Vol. 87, 1961, p. 199.

8. Bendat and Piersol, op. cit., p. 29.

9. G.I. Taylor, "The Spectrum of Turbulence," Procedures of the Royal Society, A, Vol. 169, 1938, p. 478.

10. Harris and Ledwidge, op. cit., pp. 48, 49.

11. J.O. Hinze, Turbulence, McGraw Hill, New York, 1959.

12. H.W. Teunissen, "Measurements of Planetary Boundary Layer Wind and Turbulence Characteristics Over a Small Suburban Airport," Journal of Industrial Aerodynamics, Vol. 4, 1979, p. 31.

13. Davenport, op. cit., p. 207.

14. Murphy and Kirchhoff, op. cit., p. 20.

15. Teunissen, op. cit., p. 17

16. J. Counihan, "Adiabatic Atmospheric Boundary Layers: A Review and Analysis of Data from the Period 1880-1922," Atmospheric Environment. Vol. 9, 1975, pp. 888.

17. Murphy and Kirchhoff, op. cit., p. 20.

FOOTNOTES (Continued)

18. Teunissen, op. cit., p. 17

19. R. Cohen, D.E. Cromack, and R.H. Kirchhoff, "Yaw Dynamics Analysis of a Horizontal Axis Wind Turbine," Energy Alternatives Program Technical Report UM-WF-TR-79-11, Sept., 1979.

20. Ibid.

21. J. Manwell and R.H. Kirchhoff, "The Turbulent Contribution to Power From the Wind," in preparation.

22. Cohen, op. cit.

23. H. Tennekes and J.L. Lumley, A First Course in Turbulence, MIT Press, Cambridge, Massachusetts, 1972, pp. 75-95.

24. Taylor, op. cit., p. 478.

25. Tennekes and Lumley, op. cit., p. 478.

26. Cohen, Cromack and Kirchhoff, op. cit.

27. K. Modaressi and R.H. Kirchhoff, "The Flow Field Upstream of a Horizontal Axis Wind Turbine," Energy Alternatives Program Technical Report UM-WF-TR-78-5, University of Massachusetts, June, 1978.

28. Murphy and Kirchhoff, op. cit., pp. 49-62.

29. K.A. McElhinney, "The Design of a Microcomputer Based Data Acquisition System," Smith College Honors Thesis, 1979, pp. 2-5.

30. Ibid., pp. 5-8.

31. Dixon, op. cit., p. 459-473.

32. Ibid., pp. 459, 460.

33. Ibid., pp. 462-467.

34. S. Hoogheem, "Magnetic Tape Useage," preliminary release, University Computing Center, University of Massachusetts, 1978.

BIBLIOGRAPHY

1. Bendat, S., and Piersol, A., Random Data: Analysis and Measurement Procedures, Interscience, New York, 1971.

2. Bradshaw, P., An Introduction to Turbulence and Its Measurement, Pergamon Press, Oxford, 1971.

3. Cohen, R., Cromack, D.E., and Kirchhoff, R.H., "Yaw Dynamics Analysis of a Horizontal Axis Wind Turbine," Energy Alternatives Program Technical Report UM-WF-TR-79-11, University of Massachusetts, Sept., 1979.

4. Counihan, J., "Adiabatic Atmospheric Boundary Layers: A Review and Analysis of Data from the Period 1880-1972," Atmospheric Environment, Vol. 9, 1975, pp. 871-905.

5. Davenport, A.G., "The Spectrum of Horizontal Gustiness Near the Ground in High Winds," Royal Meteorological Society Quarterly Journal, Vol. 87, 1961, pp. 194-211.

6. Dixon, W.J., ed., "BMD02T," Biomedical Computer Programs, 3rd ed., University of California Press, Los Angeles, 1973, pp. 517-532.

7. Harris, R.W., and Ledwidge, T.J., Introduction to Noise Analysis, Pion Ltd., London, 1974.

8. Hinze, J.O., Turbulence, McGraw Hill, New York, 1959.

9. Hoogheem, S., Magnetic Tape Useage, preliminary release, University Computing Center, University of Massachusetts.

10. Lumley, J.L., and Panopky, H.A., The Structure of Atmospheric Turbulence, Interscience, New York, 1964.

11. Manwell, J., and Kirchhoff, R.H., "The Turbulent Contribution to Power from the Wind," in preparation.

12. McElhinney, K.A., "The Design of a Microcomputer Based Data Acquisition System," Amith College Honors Thesis, 1979.

13. Moderessi, K., and Kirchhoff, R.H., "The Flow Field Upstream of a Horizontal Axis Wind Turbine," Energy Alternatives Program Technical Report UM-WF-TR-78-5, University of Massachusetts, June 1978.

14. Murphy, P.A., and Kirchhoff, R.H., "Measurement of the Dynamic Interaction of the Wind Field with a Horizontal Axis Wind Turbine," Energy Alternatives Program Technical Report UM=WF-TR-78-6, University of Massachusetts, March, 1979.

BIBLIOGRAPHY (Continued)

15. Taylor, G.I., "The Spectrum of Turbulence," Procedures of the Royal Society, A, Vol. 164, 1938, pp. 476-490.

16. Tennekes, H., and Lumley, J.L., A First Course in Turbulence, MIT Press, Cambridge, Massachusetts, 1972.

17. Teunissen, H.W., "Measurement of the Planetary Boundary Layer Wind and Turbulence Characteristics Over a Small Suburban Airport," Journal of Industrial Aerodynamics, Vol. 4, 1979, pp. 1-34.

A P P E N D I X A

DATA ACQUISITION AND PROCESSING SYSTEM

Introduction

The data acquisition system utilized in this work allows the rapid and efficient collection and transmission to the UMass main-frame computer, the CDC Cyber System for processing. The initial system, described by Murphy and Kirchhoff[28], has been improved by using an LSI/11 microprocessor to digitize analog time series. The microprocessor then oversees direct transmission to Cyber by telephone, instead of handcarrying paper tape as in the original system. Software for the LSI, developed by McElhinney[29], makes the system highly versatile and allows for fairly sophisticated processing.

The LSI sequentially samples and digitizes the multiple analog input signals with a 12-bit A/D converter. In this case the data comes from the seven channel Ampex tape recorder. Twelve-bit binary words are stored in miroprocessor memory.

The entire process of sampling, digitizing, and storing the data requires only a very short time, less than a millisecond. For a relatively short experimental event, this would allow the acquisition of a large number of data points.

Once stored, the information can be transferred to the computer at a rate and in a form which is compatible with the data channel (telephone lines). The clocking, handshaking and coding tasks, are performed by the LSI, and described by McElhinney[30].

The Cyber input buffer is designed to recognize ASCII coded information which is in the form of 8-bit words. For compatability with this data

channel, the LSI breaks down the 12-bit words in memory into two 6-bit bytes, adds two "dummy" bits, and transmits them sequentially to Cyber. Encoded in this manner, the two represent the original 12-bit word as a "high" byte and a "low" Byte.

When received by the computer input buffer, each ASCII word is automatically converted to an alphanumeric character and stored in Text Mode. Two characters now represent the original 12-bit word stored in the LSI.

The following sections describe how this series of characters can be simply converted. By means of the software algorithm, the FORTRAN program DECODE, the characters are converted to a series of base ten decimals representative of the sampled experimental signals.

Editing the Raw Data File

The experimental data, after being transferred to mass storage at Cyber, is in the form of ASCII characters. During translation with DECODE, partial lines of data can be inadvertantly dropped if two colons (:) occur together. To avoid this, the file text is edited and two characters, the colon (:) and the circumflex (^)* are changed into two-character symbols, respectively.

The following sequence illustrates how to edit the raw data file. Responses from the computer are underscored.

```
EDIT
BEGIN TEXT EDITING
? RS:/^/, /^A/;*
        XXX OCCURANCES OF PHRASE FOUND
? RS:/:/,/^B/;*
        XXX OCCURANCES OF PHRASE FOUND
```

? END

END TEXT EDITING

REPLACE

READY

The data file has now been translated and replaced on mass storage, ready for translation with DECODE.

Fig. 97 is the hard copy from an actual time-sharing session where a data file is edited.

*Circumflex (^) is denoted with an up-arrow on TTY terminals.

Decoding the Edited Data File

The translation of the edited data file from a series of ASCII characters to a set of time-series is effected with the FORTRAN program DECODE. The translation is a two-step process, involving the decoding of the ASCII characters and the scaling of the resulting values to the measured levels of the original experimental variable.

The decoding algorithm used by DECODE is based on the one-to-one correspondence between the value of the 6-bit byte transmitted from the LSI and the ASCII representation used by Cyber. The internal display code, of each ASCII character, a two-place octal number, is used to reference a matrix location which contains the decimal equivalent of the 6-bit word the character represents.

The least significant bit (LSB) of the high byte is 64 times the value of the LSB of the low byte. To combine the two translated characters, the high byte decimal representation is multiplied by 64 and added to the low byte. The result is the base ten decimal equivalent of the 12-bit word in LSI memory.

```
003074
@2064/000000 4737
@2066/000000 1000
@R2/003150 4000
@R3/003150 4704
@2064G

 EXIT TEXT MODE.
PACK


 READY.
SAVE


 READY.
EDIT

 BEGIN TEXT EDITING.
? RS:/↑/,/↑A/;*
      34  OCCURRENCES OF PHRASE FOUND.
? RS:/:/,/↑B/;*
      35  OCCURRENCES OF PHRASE FOUND.
? F:/:/
 PHRASE NOT FOUND.
? END
 END TEXT EDITING.

SRU       0.165 UNTS.

 READY.
REP


 READY.
```

Figure 97. Editing Routine

For the special case where a two character representation is required for a 6-bit byte, the DECODE program makes the appropriate equivalence with the decimal value of the colon or circumflex.

As discussed in Chapter I, the experimental information is scaled through the transducer and then through the Ampex tape recorder. Each channel of data may have a different scaling factor. In addition, the analog to digital conversion imposes a scaling on the data. For example, with the A/D board set to receive a 10^V maximum signal, the value of the LSB in the 12-bit word will be:

$$\frac{10^V}{2^{12}} = 2.4414 \times 10^{-3} \tag{65}$$

The value of an input voltage level V_i will be

$$\frac{V_i}{2.44 \times 10^{-3}} = 4096 \quad V_i \tag{66}$$

The development of five typical scaling factors is shown in Table 12. These are not always the scaling factors used for this work because of varying test arrangements, but for each data record, the scaling factors are noted.

DECODE requires information on the length of the edited data file, on the scaling factors, the number of channels of experimental data, and as a reminder, asks the user to name the data file. A typical time-sharing session where the data file is decoded is given in Fig. 98. User supplied information has been underscored.

A general flow diagram of DECODE is presented in Fig. 99. To simplify the presentation, not all of the details of the program are included. It is felt that the details of the program are best explained in the annotated listing, given in Fig. 100.

VARIABLE	TRANSDUCER SCALE	GAIN FOR TAPE RECORDER COMPATABILITY	TAPE RECORDER GAIN	A/D GAIN	A/D DIGITAL SCALE	OVERALL CONVERSION*
ROTOR SPEED	22^{V}/167 RPM	0.406 (voltage divider)	0.112	2	$4095/5^{V}$	$RPM = 0.102 \times NO_{10}$
YAW ANGLE	3.5^{V}/340 DEG	--	0.286	2	$4095/5^{V}$	$YAW = 0.00214 \times NO_{10}$
GENERATOR CURRENT, I,AMPS	5 mv/3 AMPS	10^{V}/67mv (lock-in AMP)	0.100	2	$4095/5^{V}$	$I = 0.0245 \times NO_{10}$
WIND DIRECTION LEG	5^{V}/352 DEG	--	0.200	2	$4095/5^{V}$	$WD = 0.00305 \times NO_{10}$
WIND SPEED, u', m/s	5^{V}/25 m/s	--	0.200	2	$4095/5^{V}$	$u' = 0.0153 \times NO_{10}$

*NO_{10} is the decimal equivalent of the 12-bit binary word stored at Cyber as ASCII Characters, of the two 6-bit words stored in the LSI/11.

TABLE 12. TYPICAL DATA ACQUISITION SYSTEM SCALING FACTORS

```
OLD,DECODE1


 READY.
GET,TAPE1=WFR23


 READY.
RUN

 79/06/07. 09.52.16.
   FILE    DECODE1

NAME DECODED FILE
? WFR23
HOW MANY CHANNELS TO BE DECODED?-I2 FORMAT-
? 5
ENTER NO OF SIX BIT WORDS-I5 FORMAT-
? 10000
 ENTER SCALE FACTOR FOR CHANNEL  1
? .4875
 ENTER SCALE FACTOR FOR CHANNEL  2
? .8302
 ENTER SCALE FACTOR FOR CHANNEL  3
? .09814
 ENTER SCALE FACTOR FOR CHANNEL  4
? .3594
 ENTER SCALE FACTOR FOR CHANNEL  5
? .06104
MEAN OF CHANNEL 1 IS 115.99196
MEAN OF CHANNEL 2 IS 133.30521
MEAN OF CHANNEL 3 IS  19.28706
MEAN OF CHANNEL 4 IS 230.17998
MEAN OF CHANNEL 5 IS   6.99604

SRU       4.147 UNTS.

 RUN COMPLETE.
```

Figure 98. DECODE Time Sharing Session

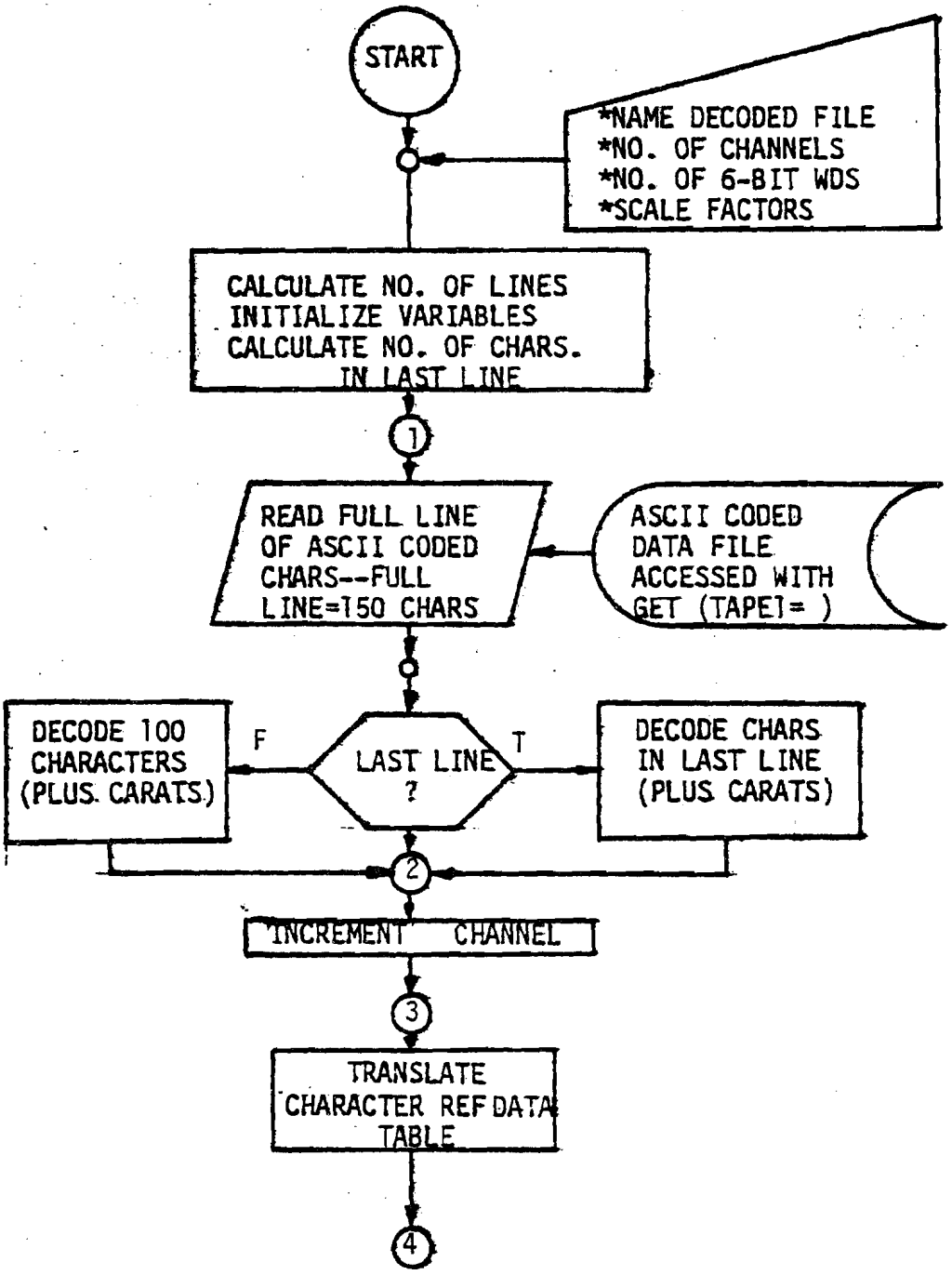

Figure 99. DECODE Information Flow Diagram

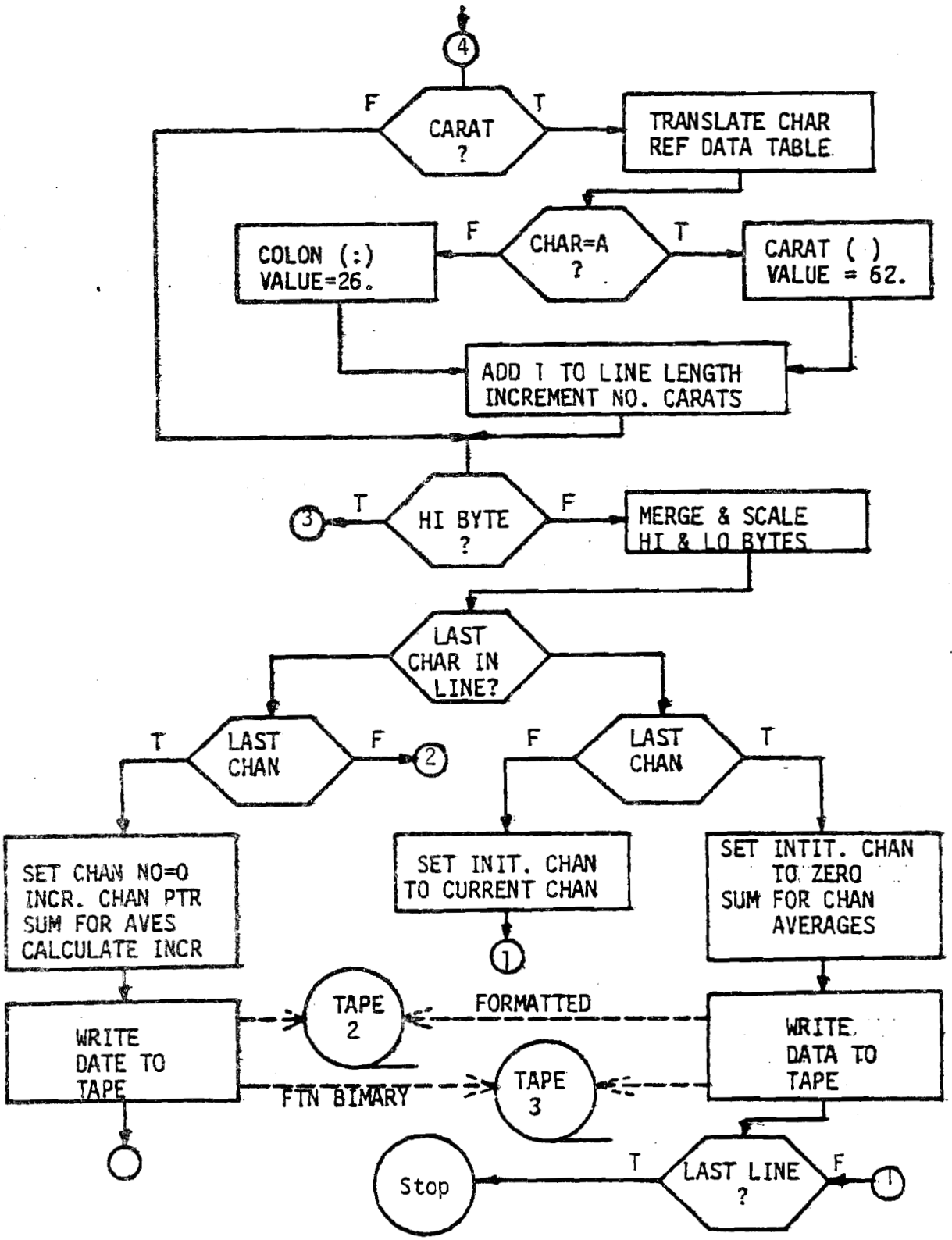

Figure 99. DECODE Information Flow Diagram Continued

```
00230 2 FORMAT(A7)
00250 REWIND 1
00260 REWIND 2
00270 PRINT 3
00280 3 FORMAT(*NAME DECODED FILE*)
00290 READ 4,NEWNAME                  - 1 to 7 alphanumeric character identifies file for reference only
00300 4 FORMAT(A7)                      not used in DECODE
00310 PRINT 5
00320 5 FORMAT(*HOW MANY CHANNELS TO BE DECODED?-I2 FORMAT-*)
00330 READ 6,NCHAN                    - no. of aid channels used in digitizing time series; must be two
00340 6 FORMAT(I2)                      place integer
00350 PRINT 15
00360 15 FORMAT(*ENTER NO OF SIX BIT WORDS-I5 FORMAT-*)
00370 READ 16,NO                      - total no. of characters transmitted from microprocess, less editing
00380 16 FORMAT(I5)                     changes; twice total no. of samples taken
00390 DO 19 K=1,NCHAN
00400 PRINT 17,K
00410 17 FORMAT(* ENTER SCALE FACTOR FOR CHANNEL *,I2)
00420 READ 18,SCALE(K)                - scale factor as determined after table 12, repeats for each channel
00430 18 FORMAT(E12.5)
00440 19 CONTINUE
00450 LINES=(NO+99)/100               - computes no. of lines of coded text present sum of data for each
00460 DO 20 I=1,NCHAN                   channel to zero
00470 20 SUM(I)=0.
00480 INCR=2*NCHAN
00490 CHAN=0
00500 NPERL=100
00510 LAST=MOD(NO,NPERL)
00520 DO 21 L=1,LINES                 - start decoding routine
00530 READ(1,11)(IN(J1),J1=1,150)     - read line of text, R1 format
00540 11 FORMAT(150R1)
00550 NPERL=100                       - nominal no. characters per line (before editing)
00560 IF(L.EQ.LINES.AND.LAST.NE.0) NPERL=LAST - check for end of text, if true characters/line 13 no.
                                               in last line
```

Figure 100. DECODE Annotated Program Listing Continued

```
00100 PROGRAM DECODEB(INPUT,OUTPUT,TAPE1,TAPE2,TAPE3)
00110 INTEGER CHAN,CHAR
00120 REAL MEAN
00130 DIMENSION OUT(2),TAB(63),P(16),IN(150),SCALE(16),SUM(16)
00138C-------------------------------------------------------------
00139C          A    B    C    D    E    F    G    H    I    J
00140 DATA TAB/33.,34.,35.,36.,37.,38.,39.,40.,41.,42.,
00148C
00149C          K    L    M    N    O    P    Q    R    S    T
00150+         43.,44.,45.,46.,47.,48.,49.,50.,51.,52.,
00158C
00159C          U    V    W    X    Y    Z    0    1    2    3
00160+         53.,54.,55.,56.,57.,58.,16.,17.,18.,19.,
00168C
00169C          4    5    6    7    8    9    +    -    *    /
00170+         20.,21.,22.,23.,24.,25.,11.,13.,10.,15.,
00178C
00179C          (    )    $    =         ,    .    #    [    ]
00180+         08.,09.,04.,29.,00.,12.,14.,03.,59.,61.,
00188C
00189C          %    "    _    !    &    '    ?    <    >    @
00190+         05.,02.,63.,01.,06.,07.,31.,28.,30.,32.,
00193C
00194C          \    ^    `
00195+         60.,62.,27./
00196C-------------------------------------------------------------
```

- equivalence table between ASCII characters and decimal values of 6-bit binary words in microprocessor memory

Figure 100. DECODE Annotated Program Listing

```
00570 DO 27 N=1,NPERL,INCR          -decode one data point for each channel (one sampling sequence)
00580 NCI=1
00590 IF(CHAN.LT.NCHAN) NCI=CHAN+1
00600 KARATS=0
00610 INCR=2*NCHAN
00620 KOUNT=0
00630 DO 23 NC=NCI,NCHAN
00640 CHAN=NC
00650 KOUNT=KOUNT+1
00660 DO 24 M=1,2
00670 CHAR=N+2*(KOUNT-1)+M-1+KARATS
00680 K=IN(CHAR)
690 IF(K.LE.0 .OR. K.GE.64) PRINT 676,L,N,KOUNT,KARATS,M,K - safety... will show if text not edited
700 676 FORMAT(5(1X,I3),1X,O20)
00710 OUT(M)=TAB(K) - evaluates decimal equivalent of character thru equivalence table
00720 IF(OUT(M).EQ.62.) 25,24 - checks for carat, if true, go to 25
00730 25   CHAR=CHAR+1
00740      K=IN(CHAR) - read next character on line
00750      OUT(M)=TAB(K) - evaluate character
00760      IF(OUT(M).EQ.34.) OUT(M)=26. - sets character value to that of colon
00765      IF(OUT(M).EQ.33.) OUT(M)=62. - sets character value to that of carat
00770      KARATS=KARATS+1  - counter tracks no. of carats in sampling sequence
00780      NPERL=NPERL+1  - adds 1 to characters per line for each carat or colon
00790 24 CONTINUE
00800 P(CHAN)=(64.*OUT(1)+OUT(2))*SCALE(CHAN) - combines and scales two sequential 6 bit words
00820 IF(CHAR.GE.NPERL .AND. CHAN.NE.NCHAN) GOTO 21 - check for end of line
00830 23 CONTINUE
00835 DO 28 NC=1,NCHAN
00836 28 SUM(NC)=SUM(NC)+P(NC)
00840 INCR=INCR+KARATS-2*(NCI-1)          - increase increment size to include colons and carats
00845 WRITE(3)(P(NC),NC=1,NCHAN)          - write formatted data on tape 2
00850 27 WRITE(2,14)(P(NC),NC=1,NCHAN)
00860 14 FORMAT(16(F10.5))
00870 21 CONTINUE
```

Figure 100. DECODE Annotated Program Listing Continued

```
00880 REWIND2
00885 REWIND3
00900 DO 35 I=1,NCHAN
00910 MEAN=2.*SUM(I)*NCHAN/NO
00920 35 PRINT 38,I,MEAN
00930 38 FORMAT(*MEAN OF CHANNEL*,I2,* IS*,F10.5)
00940 IF(CHAN.GE.NCHAN.OR.CHAN.EQ.0)  GO TO 43
00950 40 PRINT 41
00960 41 FORMAT(*---------WARNING---------*) - goes with safety, line 690
00970 PRINT 42,CHAN
00980 42 FORMAT(I2,*CHANNELS ON LAST LINE NOT RECORDED*)
00990 43 CONTINUE
01000 END
```

Figure 100. DECODE Annotated Program Listing Continued

The translated data is written by DECODE onto two local tapes, TAPE1 and TAPE2. TAPE1 contains the formatted data in F10.5 format. This can be copied to a printer for a hard copy record of the data. TAPE2 is an FTN binary form of the data, which is compatible directly with the Biomedical program BMD02T, and is the most efficient form of storing the information as an indirect access permanent file on disc of a magnetic tape.

DECODE is designed to be a highly versatile, efficient software package for the translation of microprocessor acquired data. The flow chart and annotated listing of the program should provide enough information to make the necessary changes for compatibility with other data acquisition systems.

A P P E N D I X B

BIOMEDICAL STATISTICAL PACKAGE BMD02T

The Biomedical Statistical Package BMD02T[31] is a convenient way to statistically analyze digital time series. Relevant parameters for wind field analysis, such as autocovariance, power spectral density, and transfer functions, are simply specified. Extraneous parameters can be deleted from the output.

On the UMass Cyber System, a short card deck is submitted. The deck set up is shown in Fig. 101. By changing the "PROBLEM" and "SELECT" cards, the data analysis is tailored to the needs of the experimenter, within certain limits.

Data Analysis is limited in the following four ways relevant to this work[32]:

(1) number of time series, s: $1 \leq s \leq 20$

(2) number of data points in each series, N: $1 \leq n \leq 1000$

(3) total number of data points: $N \times s \leq 17000$

(4) number of lags, m: $1 \leq m \leq 199$

The actual form of the "PROBLEM" and "SELECT" cards is shown in an excerpt from BMD02T[33], Fig. 102. Preparation of the cards as shown in Fig. 102 is self-explanatory, with one exception: for files in FTN binary form, as obtained from DECODE, TAPE 3, columns 69 and 70 on the "PROBLEM" card must contain the number 10. This is for compatibility on the UMass System. This is noted on the figure.

Sample output from BMD02T is shown in Fig. 103. This includes an autocovariance function, power spectral density, and a sample plot of each, as printed by the program.

FIGURE 101. BMD02T JOB DECK SET-UP

```
JOB,T30.
ACCOUNTNO,USERNO,PSSWRD.
GET(TAPE1=pfn1)
COPYSBF(TAPE1,OUTPUT)
GET(ALTAPE=pfn2)
FINDLIB,OLDBMD.
CALL,OLDBMD(PROG=BMD02T)
7/8/9  ---End of Record

PROBLM...Problem Card
SELECT...Select Card
FINISH
6/7/8/9 ---End of File
```

See Fig. 102 for Card Preparation

Figure 102. BMD02T Card Preparation

Preparation of the cards listed below is specific for this program. All other cards listed in the preceding section are prepared according to instructions in the Introduction.

b. Problem Card (One Problem Card for each problem)

Col. 1-6	PRØBLM	(Mandatory)
Col. 7-12	Alphanumeric job code	
Col. 13-15	YES	If original data are to be printed in output; otherwise, leave blank.
Col. 16-18	YES	If input series is to be plotted; otherwise, leave blank.
Col. 19-21	YES	If detrending of the input series is called for; otherwise, leave blank.
Col. 22-24	YES	If prewhitening is used; otherwise, leave blank. (Recoloring will also be performed.)
Col. 25-29	C	Constant value, $\|C\| < 1.0$ as in 1(f) (punch decimal). Leave blank if prewhitening is not used.
Col. 30, 31	Number of time series ($1 \leq s \leq 20$)	
Col. 32-35	Number of points in each series ($1 \leq n \leq 1000$)	
Col. 36-38	Number of lags ($1 \leq m \leq 199$)	
Col. 39, 40	Number of selection cards ($1 \leq q \leq 99$)	
Col. 41, 42	-1	If the power spectrum is to be plotted in linear scale.
	00	If the power spectrum is to be plotted in $\log_e$ scale.
	01	If the power spectrum is to be plotted in both scales.
Col. 43-47	Constant time interval (punch decimal, e.g., .01 seconds)	

Col. 48-53 Punch the time unit, e.g., SECOND or MINUTE or other units.

Col. 54-56 YES If reprocessing of data is desired, i.e., the input data for the second problem is the same as that for the first problem and any transformations performed remain; otherwise leave blank.

Note: Selection Cards are the only control cards necessary for reprocessing. Special Transgeneration Cards may also be used.

Col. 57-68 Blank

Col. 69,70 -1 If the data are read in according to d(1) of this section.
00 According to d(2).
T+70 T is the logical tape number for input data from tape in the form d(1) in binary.
T T is the logical tape number for input data from tape in the form d(2) in binary.

~~Mass~~ System: 10 ETN Binary Data

e. ~~Selection Card(s)~~

Col. 1-6 SELECT (Mandatory)

Col. 7 Blank

Col. 8-10 YES If the autocovariance and power spectrum are to be calculated; otherwise, leave blank.

Col. 11 Blank

Col. 12-14 YES If the cross-covariance and cross-spectrum are to be computed; otherwise, leave blank.

Note: Cross-spectrum cannot be computed if prewhitening is performed on the series.

Col. 15 Blank

Col. 16-18 YES If the coherence square and transfer functions are to be computed; otherwise, leave blank.

Figure 102. BMD02T Card Preparation, Continued

Note: Coherence square and transfer functions cannot be computed if the power spectrum was not computed, i.e., Columns 8-10 must contain YES also.

Col. 19 Blank

Col. 20, 21 Number designation of the base series.

Col. 22
- A If the autocovariance of the base series is to be plotted.
- P If the power spectral estimates of the base series are to be plotted.
- B If both of the above are to be plotted. Otherwise, leave blank.

Col. 23, 24 Number designation of the base series if transformation is to be performed on it.

Col. 25-26 The number of series to be crossed with the base series (≤ 19).

Note: This should equal 01 if only a single series is being processed.

Col. 27 Blank

Col. 28, 29 Number designation of the 1st series to cross with the base series.

Note: This should be the designation of the base series if only a single series is being processed.

Col. 30
- A If the autocovariance of the series is to be plotted.
- P If the power spectral estimates of this series are to be plotted.
- B If both of the above are to be plotted. Otherwise, leave blank.

Col. 31
- C If the cross-covariance of this series and the base series is to be plotted.
- S If the cross-spectrum and phase of this series and the base series are to be plotted.
- B If both of the above are to be plotted. Otherwise, leave blank.

Figure 102. BMD02T Card Preparation, Continued

Col. 32	H	If the coherence square of this series and the base series is to be plotted.
	T	If the transfer functions of this series and the base series are to be plotted.
	B	If both of the above are to be plotted. Otherwise, leave blank.
Col. 33, 34		Number designation of the 1st series to cross with the base series if transformation is to be performed on it.
	Note:	Columns 30-34 should be left blank if only one series is being processed.
Col. 35, 36		Number designation of the 2nd series to cross with the base series.
...		
Col. 68, 69		Number designation of the 6th series to cross with the base series if transformation is to be performed on it.

Figure 102. BMD02T Card Preparation, Continued

```
BMD02T-AUTOCOVARIANCE AND POWER SPECTRAL ANALYSIS - VERSION OF MAR. 16, 1965
HEALTH SCIENCES COMPUTING FACILITY, UCLA

                    P R O B L E M  N U M B E R     WFDR3

 INPUT DATA TO BE PRINTED OUT---
 INPUT SERIES TO BE PLOTTED OUT---
 DETRENDING---YES
 PREWHITENING---
 VALUE OF CONSTANT C USED IN THE PREWHITENING TRANSFORMATION Z(T)=X(T+1)-CX(T) ---    0.00000
 NUMBER OF SERIES =  5
 NUMBER OF DATA POINTS =  350
 NUMBER OF LAGS CHOSEN =  50
 NUMBER OF SELECTION CARDS =  2
 USE PREVIOUS DATA---

 CONSTANT TIME INTERVAL =     5.00000 SECOND

 NUMBER OF VARIABLE FORMAT CARDS =  0
```

Figure 103. BMD02T Sample Output

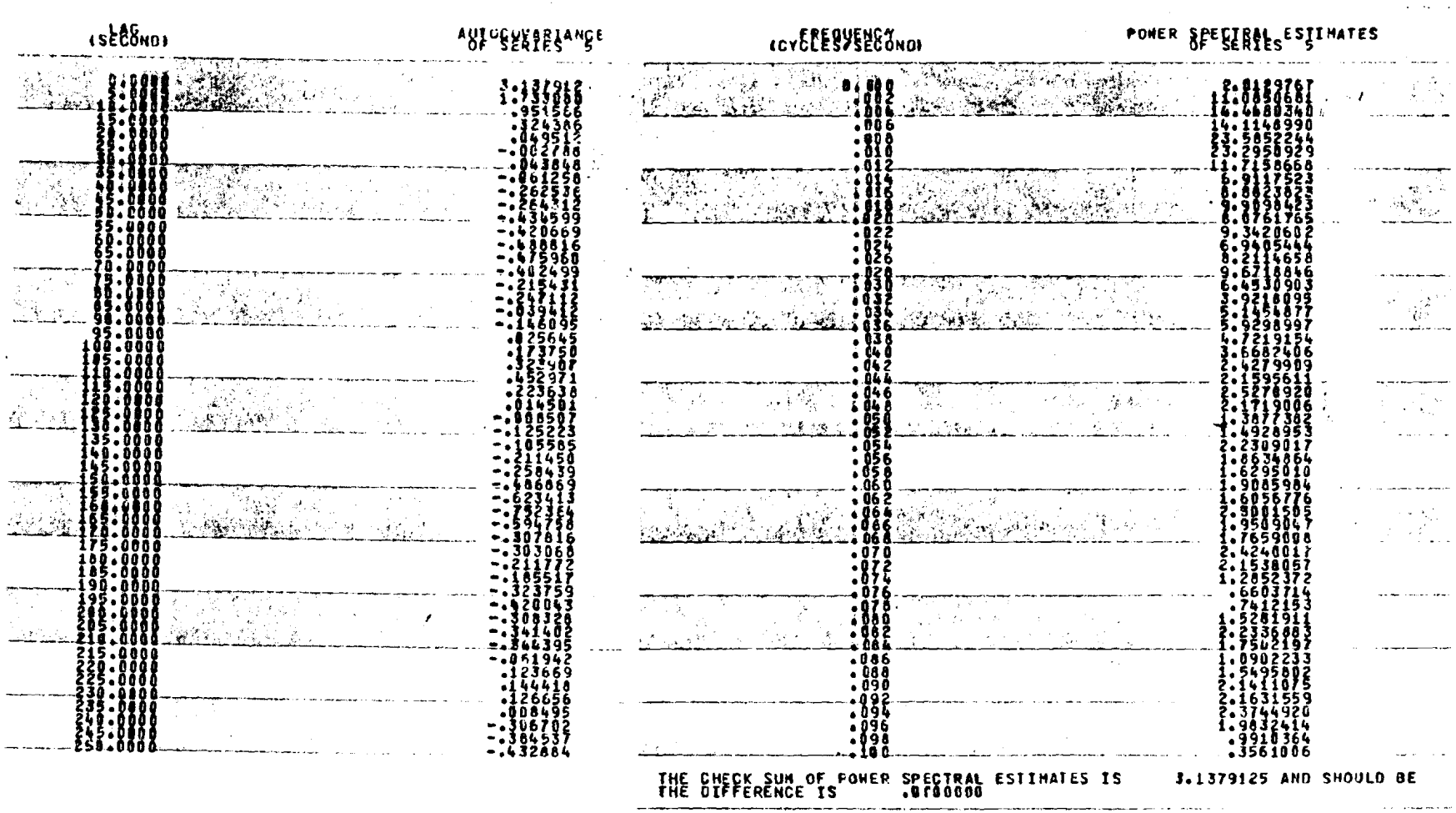

Figure 103. BMD02T Sample Output, Continued

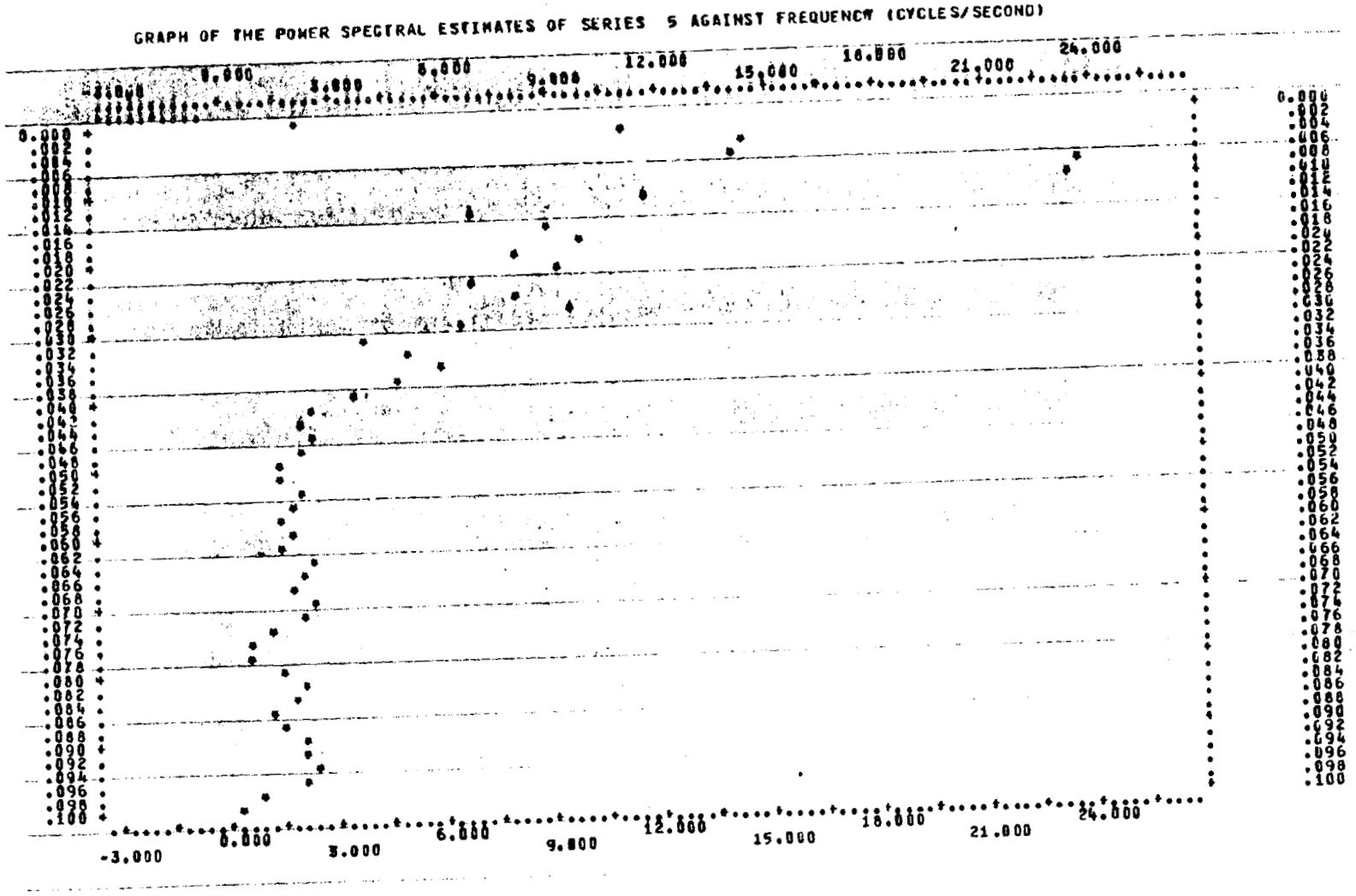

Figure 103. BMD02T Sample Output, Continued

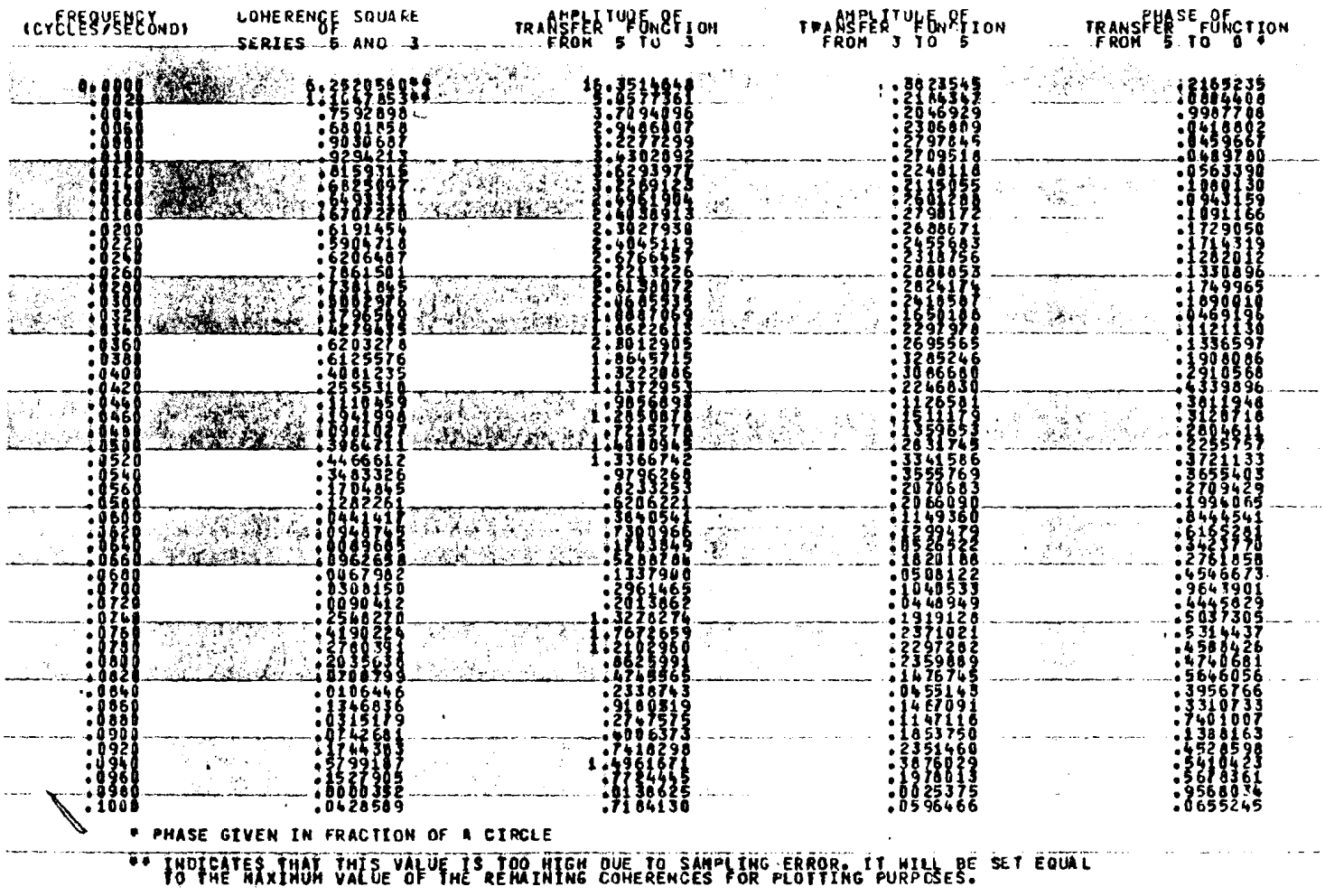

FREQUENCY (CYCLES/SECOND)	COHERENCE SQUARE OF SERIES 5 AND 3	AMPLITUDE OF TRANSFER FUNCTION FROM 5 TO 3	AMPLITUDE OF TRANSFER FUNCTION FROM 3 TO 5	PHASE OF TRANSFER FUNCTION FROM 5 TO 0 *
0.0000	6.2620584**	16.3514448	.8023545	.2165235
.0020	1.1047853**	5.0577361	.2144342	.0884408
.0040	.7592898	3.7094096	.2046929	.9987708
.0060	.6801858	2.9466407	.2306809	.0418002
.0080	.9030607	3.2277299	.2797645	.8459667
.0100	.9294213	3.4302892	.2709516	.0489780
.0120	.8159315	3.6293977	.2240118	.0563390
.0140	.6825097	3.2269123	.2115055	.1000130
.0160	.6403311	2.9961904	.2601288	.0943159
.0180	.6707220	2.4038913	.2798172	.1091166
.0200	.6191454	2.3027930	.2688671	.1729050
.0220	.5904718	2.4045119	.2455683	.1714319
.0240	.6206407	2.6766457	.2318756	.1282012
.0260	.7861501	2.1213226	.2088053	.1330896
.0280	.7381845	2.6130072	.2824174	.1749965
.0300	.8002975	2.0685535	.2418587	.1090010
.0320	.7796569	1.9867069	.1650186	.0469196
.0340	.4279495	1.6622613	.2297970	.1121130
.0360	.6203278	2.8012905	.2695565	.1336597
.0380	.6125576	1.8645715	.3285246	.1908086
.0400	.4081235	1.3222006	.3066680	.2910560
.0420	.2555310	1.1372953	.2246830	.4339896
.0440	.1110459	.9056698	.1126581	.3611948
.0460	.1941990	1.2650878	.1511179	.3126718
.0480	.0981027	.7215270	.1359653	.2804611
.0500	.3966711	1.4880945	.2631745	.2255757
.0520	.4466612	1.3366742	.3341586	.3721133
.0540	.3483326	.9796268	.3555769	.3655405
.0560	.1704845	.8233253	.2070683	.2703429
.0580	.1282261	.6206221	.2066090	.1994065
.0600	.0441417	.3640541	.1149360	.8444541
.0620	.0944745	.7300966	.1299479	.6165281
.0640	.0049565	.1703849	.0526522	.3423770
.0660	.0962658	.5266704	.1820188	.2781858
.0680	.0067982	.1337940	.0508122	.4546673
.0700	.0308150	.2961465	.1040533	.9643901
.0720	.0090412	.2013862	.0448949	.4445629
.0740	.2540220	1.3270274	.1919128	.5037305
.0760	.4190224	1.7672659	.2371021	.5314437
.0780	.2760391	1.2102960	.2297282	.4588426
.0800	.2035638	.8625991	.2359889	.4740681
.0820	.0788799	.4749965	.1476745	.5646056
.0840	.0106446	.2338743	.0455143	.3956766
.0860	.1346836	.9100519	.1467091	.3310733
.0880	.0315179	.2747575	.1147116	.7401007
.0900	.0742681	.6006373	.1853750	.1388163
.0920	.1744303	.7410298	.2351460	.4526598
.0940	.5799187	1.4961671	.3876029	.5410423
.0960	.1527905	.7744445	.1978013	.5070361
.0980	.0000352	.0138625	.0025375	.9568034
.1000	.0428589	.7184130	.0596466	.0655245

* PHASE GIVEN IN FRACTION OF A CIRCLE

** INDICATES THAT THIS VALUE IS TOO HIGH DUE TO SAMPLING ERROR. IT WILL BE SET EQUAL TO THE MAXIMUM VALUE OF THE REMAINING COHERENCES FOR PLOTTING PURPOSES.

Figure 103. BMD02T Sample Output, Continued

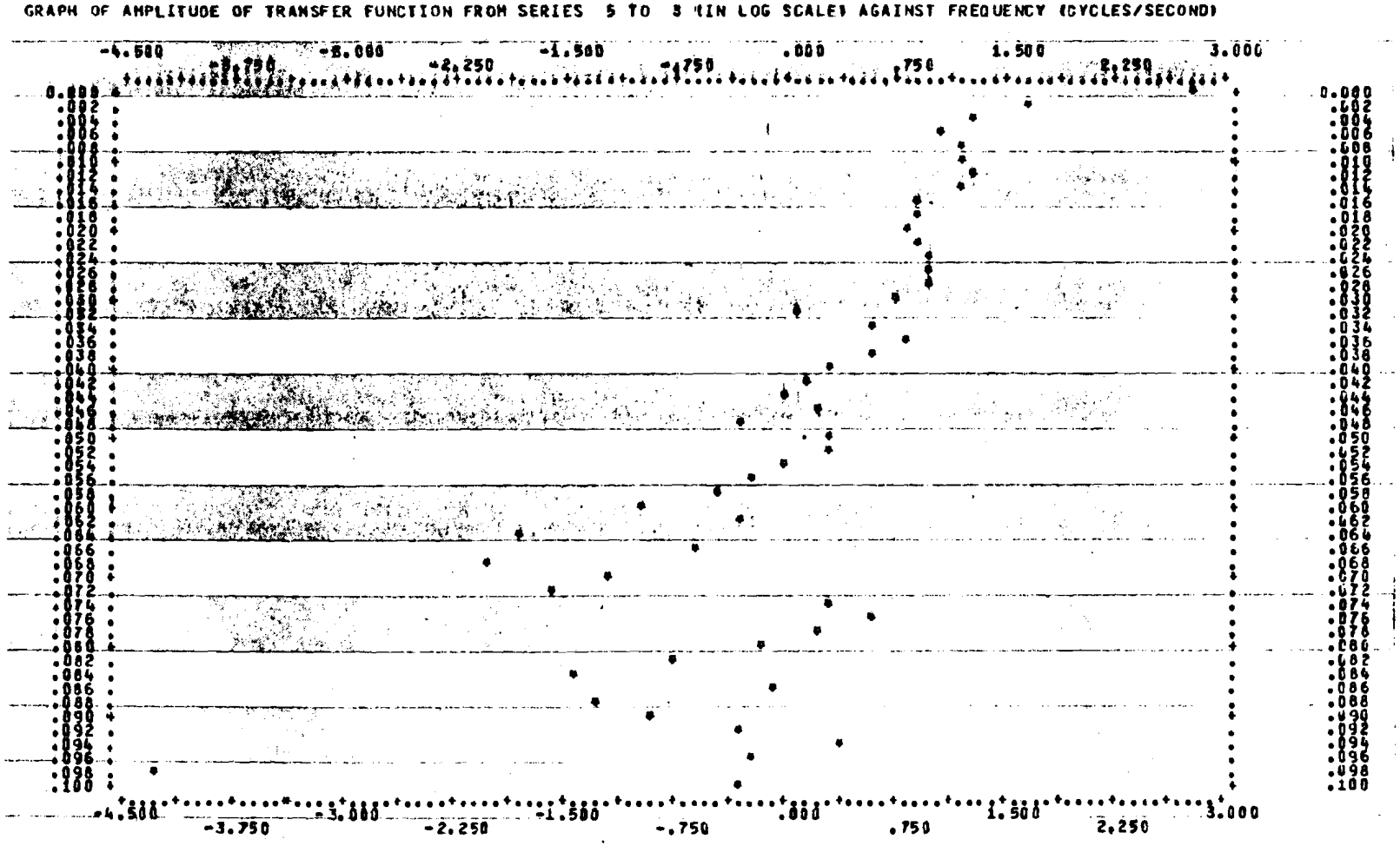

Figure 103. BMD02T Sample Output, Continued

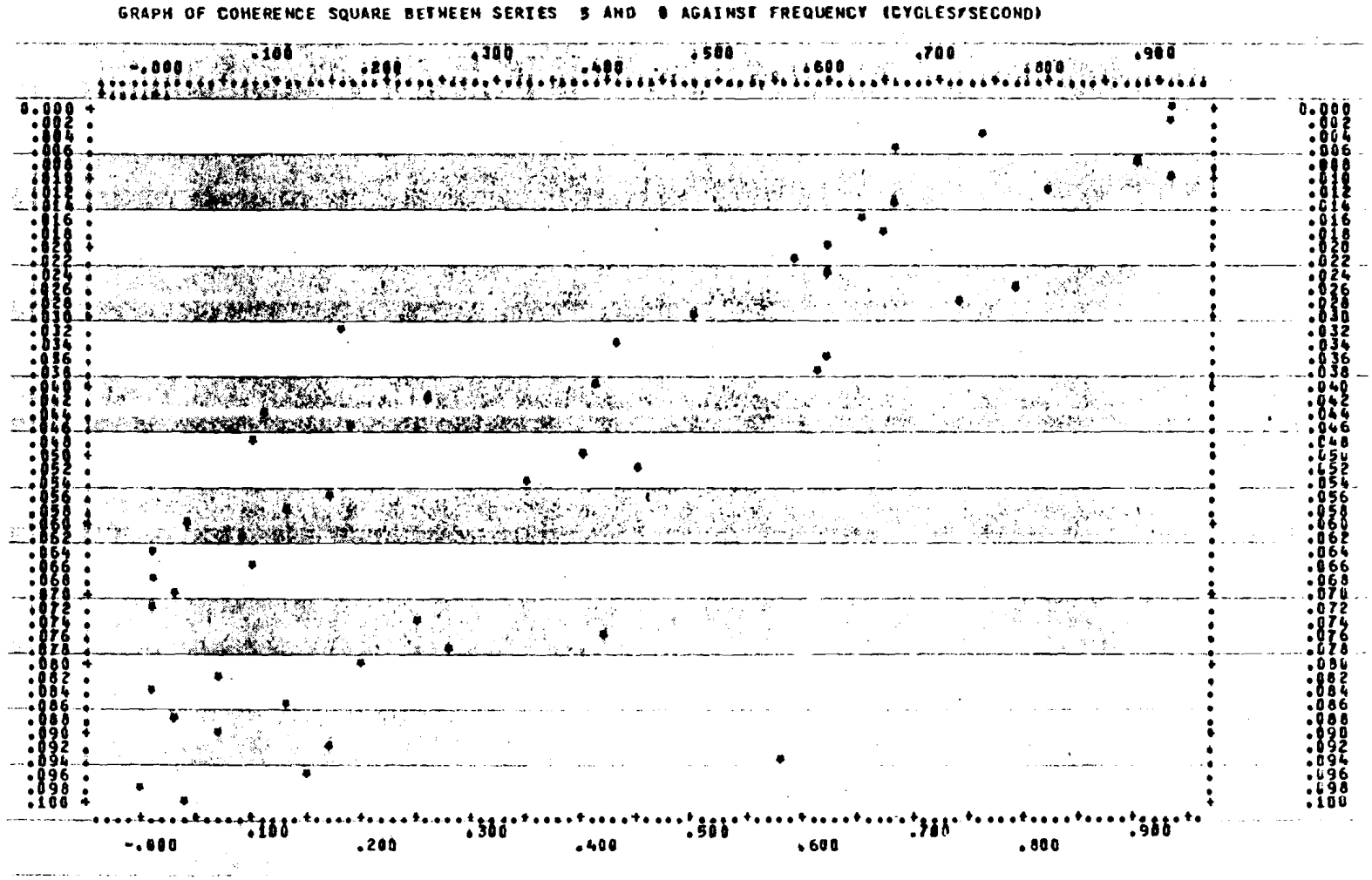

Figure 103. BMD02T Sample Output, Continued

A P P E N D I X C

ARCHIVAL STORAGE OF EXPERIMENTAL DATA

The digital wind field records have been stored on magnetic tape for archival purposes. This appendix details the storage and retrieval system used.

Data Storage

The magnetic tape is a nine-track, 1600 bpi 2600 foot tape. The tape has been labeled intervally, so that each of the many records stored can be retrieved by the previously used identifiers.

The tape is identified first with the volume serial number (VSN), which on this tape is VSN=FANA. A specific file is identified in a LABEL statement first through a file identifier (FI), and then a set identifier (SI). All wind field records, WFR3, 5, 17, 18, 19, 20, 21, 22, and 26 are listed un FI=WFR and a set identifier of the form WFRx, where x is the record number. For example, WFR3 is identified under FI=WFR, SI=WFR3.

Fig. 104 shows a command sequence which might be used to write a new file WFR1 onto tape. A second file, WFR2 is read from the tape and stored on disc for use with BMD02T. Note that Files for use with BMD02T are written in FTN brimary form with the COPYBF statement.

Further details are available on the UMass Cyber Network Operating System manuals on magnetic tape usage[34]. These are not discussed here since they are changed from time to time.

```
JOB, T20.
ACCOUNTNO, USERNO, PASSWORD
VSN(TAPE1=FANA)
GET(TAPE2=WFR30)
LABEL(TAPE1,NT,D=1600,FA=D,SI=WFR,FI=WFR1,PO=W)
COPYBF(TAPE2,TAPE1)
LABEL(TAPE1,  t,D=1600,FA=D,SI=WFR,FI=WFR2,PO=R)
COPYBF(TAPE1,TAPE3)
SAVE(TAPE3=WFR2)
6/7/8/9 -- end of information
```

Figure 104. Magnetic Tape Usage